SEISMIC ASSESSMENT OF THE OUT-OF-PLANE PERFORMANCE OF TRADITIONAL STONE MASONRY WALLS

A Thesis submitted to the Faculty of Engineering of the University of Porto

for the Doctoral Degree in Civil Engineering

by

Alexandre Aníbal Meira Guimarães da Costa

Supervisors:

Prof. António Arêde
Faculty of Engineering, University of Porto

Dr. Andrea Penna
European Centre for Training and Research in Earthquake Engineering
Department of Structural Mechanics, University of Pavia

March 2012

ABSTRACT

The present Thesis focuses on the experimental characterization and numerical study of the out-of-plane behaviour of stone masonry walls for quasi-static and dynamic loads.

Several *in-situ* experiments on existing constructions were performed in order to characterize the quasi-static behaviour of unreinforced and strengthened specimens with techniques commonly used in pre/post-earthquake interventions. For this purposes, a new test setup to perform field tests within reasonable time interval and costs was developed and validated with an extensive tests campaign on damaged constructions after the 1998 Azores earthquake. The efficiency of different strengthening techniques was assessed and compared among them and simple analytical calculations proved to be efficient and conservative solutions when applied to force-based assessment of existing masonry walls.

The dynamic behaviour of masonry walls was also evaluated resorting to shaking table tests as well as numerical simulations. Shaking table tests performed at LNEC (Lisbon, Portugal) on full scale one-storey *sacco* stone masonry façades were made especially devoted to the out-of-plane behaviour, where the selection of the input ground motions revealed to be decisive to trigger the overturning mechanism. The behaviour of the façades was found to be significantly influenced by the presence of the masonry multiple leaves, being the instability achieved by the overturning of the outer leaf and local masonry assemblages' effects.

A novel proposal for simulating the dynamic response of local mechanisms was made resorting to multibody dynamics, where masonry portions (of a given local mechanism) are simulated through kinematic chains (rigid bodies) with concentrated nonlinearity at contact surfaces. The restitution coefficient, an important parameter to correctly describe the dynamic rocking behaviour of rigid bodies, was determined by lab experimental tests of cantilever masonry walls for 2-sided rocking, where the dynamic properties of the wall are reproduced by an equivalent structure based on a proposed methodology named as Equivalent Block Approach (EBA).

Finally, the multibody dynamics approach was validated against two shaking table test results: the shaking table test presented herein and the test performed on a two-storey height double leaf stone masonry façade tested at EUCENTRE (Pavia, Italy). Promising results were obtained and some comments are included regarding static and dynamic analysis of local mechanisms resorting to simplified models. At the end, a proposal for seismic assessment of existing structure is made, where both the in-plane and out-of-plane behaviours are taken into account.

RESUMO

O objetivo da Tese consiste na caracterização experimental e estudo numérico do comportamento fora-do-plano de paredes de alvenaria de pedra sob cargas quasi-estáticas e dinâmicas.

Foram realizados diversos ensaios experimentais *in-situ* para caracterização do comportamento quasi-estático de paredes não reforçadas e reforçadas com técnicas habituais em cenários pré/pós-sísmicos. Foi desenvolvido, testado e validado um novo sistema de ensaio a utilizar em campo, considerando custos e tempo reduzidos para ensaio, tendo sido aplicado em construções danificadas após o sismo do Faial-Pico de 1998. A avaliação da eficiência das técnicas de reforço foi também realizada a partir dos mesmos ensaios. Além disso, cálculos simplificados para previsão da força máxima revelaram-se eficientes e pelo lado da segurança, podendo eventualmente ser aplicados em métodos de avaliação baseados em força.

Após a caracterização para cargas estáticas, o comportamento dinâmico fora-do-plano foi avaliado através de ensaios na mesa sísmica do LNEC (Lisboa, Portugal) em modelos à escala real de alvenaria de duas folhas com enchimento, especialmente focados no comportamento fora-do-plano. A seleção da ação sísmica a introduzir revelou-se decisiva para a correta ativação do mecanismo de colapso. Foi possível verificar através dos ensaios que o comportamento global é bastante influenciado pelas múltiplas folhas, sendo a instabilidade da fachada condicionada pelo derrube parcial da folha externa e arranjo local da alvenaria.

Para simular a resposta dinâmica fora-do-plano de estruturas de alvenaria (mecanismos locais), é proposta uma nova metodologia baseada na dinâmica de sistemas multicorpo, onde porções de alvenaria são modeladas por blocos rígidos, estando a não linearidade concentrada nas zonas de contacto. O coeficiente de restituição, um parâmetro condicionante na modelação do comportamento dinâmico, é determinado através de ensaios experimentais em laboratório onde um novo método denominado como *Equivalent Block Approach* (EBA) é proposto, no qual a parede de alvenaria é simulada através de uma estrutura com propriedades equivalentes.

Na parte final do trabalho, a nova proposta recorrendo à dinâmica de sistemas multicorpo é validada com dois ensaios em mesa sísmica: o ensaio apresentado neste trabalho e o ensaio em mesa sísmica de um edifício em alvenaria de pedra de dois pisos, realizado no EUCENTRE (Pavia, Itália). Os resultados obtidos são muito promissores, apresentando-se alguns comentários relativos a métodos simplificados existentes. Por fim, é apresentada uma proposta para avaliação do comportamento sísmico de estruturas existentes, onde ambos os comportamentos no plano e fora-do-plano são considerados.

ACKNOWLEDGMENTS

As a result of an extensive work, I wish to express my gratitude to several persons and institutions which definitely contributed to the accomplishment of the work:

- First of all, to my supervisor, Professor António Arêde, for its ceaseless help, knowledge, guidance and friendship during all my research and hopefully in the subsequent years;

- To my co-supervisor, Dr. Andrea Penna, assuming the supervision in the same line as in the past, with clear and direct ideas of the work as well as a strong friendship and will demonstrated during my studies in Pavia and along all my work;

- To the Portuguese Foundation of Science and Technology (FCT, Fundação para a Ciência e Tecnologia), which its financial support through a PhD grant is gratefully acknowledged.

- To the Laboratory of Earthquake and Structural Engineering (LESE) and to the Faculty of Engineering of the University of Porto (FEUP), for the support in the experimental activities as well as providing all the necessary conditions to develop my research;

- To the Laboratório Nacional de Engenharia Civil (LNEC), namely the NESDE department, for performing the shaking table tests and all inherent activities. Special acknowledgments are due to Dr. Alfredo Campos Costa for his friendship and guidance on shaking table tests;

- To the European Centre for Training and Research on Earthquake Engineering (EUCENTRE), for providing all required conditions to perform my research at Pavia, and for the shaking table tests experimental data;

- To the Regional Government of Azores, through its Regional Secretariat for Housing and Facilities (SRHE) and the Society in charge of the housing reconstruction after the 1998 Azores earthquake (SPRHI, S.A.) for their support during the field experimental tests performed at Faial. Special acknowledgements are due to Prof. Carlos Sousa Oliveira, Eng. Filipe Neves and Mr. Constantino;

- To all my friends, including everyone met during my working period at Pavia;

- To my family, for their persistent support during my work, and especially to my father for his efforts to make possible the completion of this thesis;

- To my wife Isabel, for her love and happiness, and for all her comprehension and furtherance in all faced difficulties.

TABLE OF CONTENTS

Chapter 5

EXPERIMENTAL AND ANALYTICAL EVALUATION OF THE FREE ROCKING BEHAVIOUR OF A STONE MASONRY WALL THROUGH EQUIVALENT BLOCK APPROACH

Chapter 6

SIMULATION OF THE OUT-OF-PLANE BEHAVIOUR OF EXISTING MASONRY BUILDINGS THROUGH MULTIBODY DYNAMICS

Chapter 7

FINAL REMARKS

Appendix A

LNEC SHAKING TABLE TESTS: GROUND MOTION SELECTION DETAILS AND MONITORING SYSTEM

Appendix B

FREE ROCKING TESTS RESULTS

Appendix C

NUMERICAL SIMULATIONS

LIST OF FIGURES

Chapter 2

IN-SITU CYCLIC TESTS ON EXISTING STONE MASONRY WALLS AND STRENGTHENING SOLUTIONS

Chapter 3

OUT-OF-PLANE BEHAVIOUR OF EXISTING STONE MASONRY BUILDINGS: EXPERIMENTAL EVALUATION

Chapter 4

OUT-OF-PLANE BEHAVIOUR OF A FULL SCALE STONE MASONRY FAÇADE

Chapter 5

EXPERIMENTAL AND ANALYTICAL EVALUATION OF THE FREE ROCKING BEHAVIOUR OF A STONE MASONRY WALL THROUGH EQUIVALENT BLOCK APPROACH

Chapter 6

SIMULATION OF THE OUT-OF-PLANE BEHAVIOUR OF EXISTING MASONRY BUILDINGS THROUGH MULTIBODY DYNAMICS

Appendix A

LNEC SHAKING TABLE TESTS: GROUND MOTION SELECTION DETAILS AND MONITORING SYSTEM

Appendix C

NUMERICAL SIMULATIONS

LIST OF TABLES

Chapter 5

EXPERIMENTAL AND ANALYTICAL EVALUATION OF THE FREE ROCKING BEHAVIOUR OF A STONE MASONRY WALL THROUGH EQUIVALENT BLOCK APPROACH

Chapter 6

SIMULATION OF THE OUT-OF-PLANE BEHAVIOUR OF EXISTING MASONRY BUILDINGS THROUGH MULTIBODY DYNAMICS

Appendix A

LNEC SHAKING TABLE TESTS: GROUND MOTION SELECTION DETAILS AND MONITORING SYSTEM

Appendix B

Chapter 1.

INTRODUCTION

1.1. GENERAL

The human history reveals that stone masonry is one of the most old construction type but, at the same time, its mechanical behaviour and characterization remains uncertain and widely variable. Moreover, history also shows that masonry structures are extremely vulnerable to earthquakes, as evidenced by the collapse of remarkable ancient monuments such as the Rhodes Colossus or the Alexandria lighthouse, two of the seven wonders of the ancient world.

Nowadays, despite significant advances in technology and research, seismic events remain as the most dangerous threat to existing masonry buildings, destroying every year unrepeatable built heritage all around the world with severe losses to human population and economy. To some extent, these earthquake consequences are neither acceptable nor reasonable, considering the scientific, technical and economic investment made on increasing knowledge, supported by adequate analysis tools and measures, which should contribute to the safety and protection of populations.

Recent seismic events around the world have highlighted that earthquake consequences are transversal to the world population regardless of economic, political and ethnical differences. This is clearly evidenced by earthquakes such as those occurred in Umbria-Marche (Italy, 1997), Azores (Portugal, 1998), Kashmir (Pakistan, 2005), Pisco (Peru, 2007), L'Aquila (Italy, 2009), Haiti (2010), Christchurch (New Zealand, 2011), Lorca (Spain, 2011) where numerous collapses are still found occur due to inappropriate interventions on masonry constructions and/or lack of efficient strengthening schemes.

Structural reasons for the bad behaviour of masonry constructions during earthquakes mainly rely on its heterogeneity, anisotropy, negligible tensile strength and poor shear behaviour, which are further aggravated with the decreasing quality of masonry material and its assemblage. The presence of flexible diaphragms and the lack of proper connections between walls and diaphragms and between perpendicular walls are common causes of seismic vulnerability in existing masonry buildings, which tend to exhibit local out-of-plane responses rather than a global behaviour governed by the in-plane wall capacity. In addition, the presence of multiple leaves strongly influences the behaviour, where the main problem is due to the non-monolithic response and to disaggregation of leaves, as frequently observed in post-earthquake surveys. Indeed, "the worst defect of a masonry wall is to be not monolithic in the lateral direction, and this can happen for instance when the wall is made by small pebbles or by two external layers even well ordered but not mutually connected, containing a rubble infill" (Giuffrè 1993; Binda *et al.* 2003). Therefore, interventions should be made to overcome this problem, but as stated by Valluzzi *et al.* (2004), "(...) the knowledge of the mechanical behaviour of multi-leaf masonry walls is still limited, as well as the availability of standards and codes of practice for the proper design and control of the interventions".

Under earthquake action, the out-of-plane performance of existing masonry structures is the most vulnerable issue when no adequate strengthening techniques are provided. In fact, this is a widely known and perceived evidence since Byzantine times (Binda *et al.* 2006) which was early stated in the 15th century by Leonardo da Vinci; since then, it has been suggested that improvements should be made on connections between different leafs and tie rods should be inserted to sustain out-of-plane motions (Milizia 1554; Rondelet 1802). Indeed, the low strength/mass ratio of common masonry structures increases their vulnerability in the out-of-plane direction because inertia forces are not restrained due to reduced stiffness and strength of the masonry walls in that direction. In addition, vulnerable overturning mechanisms are likely to form due to the kinetic energy transmitted by the earthquake.

It is well known that, should the so-called "box behaviour" be ensured on masonry constructions (by effectively connecting horizontal and vertical elements), local collapses can be avoided and the global behaviour may become governed by the in-plane response of the load-bearing walls. By contrast, if no adequate strengthening techniques are applied, the overturning of masonry walls is likely to occur and be further boosted by ineffective retrofit or strengthening solutions commonly used nowadays. Indeed, "the ineffectiveness of these techniques (...) are mostly due to (...) the lack of knowledge on the material and structural behaviour of historic buildings" (Penazzi *et al.* 2000). Therefore, different techniques to be adopted in existing constructions need to be validated concerning their efficiency for preserving both the common masonry construction and the historic built heritage.

Despite being a well known problem, the out-of-plane behaviour of stone masonry structures under static and dynamic actions still needs to be better characterized, in order to provide adequate tools for its seismic assessment and strengthening. In addition, this will potentiate the increase of knowledge and understanding level concerning masonry structures' performance under severe actions, thus protecting populations from constructions' collapse.

1.2. MOTIVATION AND OBJECTIVES

The current methods for the out-of-plane behaviour assessment of masonry façades are mainly based on two distinct strategies: *i)* force-equilibrium formulations, such as those proposed in D'Ayala and Speranza (2003), which rely on more traditional and consolidated perceptions of the response under lateral forces; *ii)* alternative displacement-based formulations, such as that one developed by Doherty *et al.* (2002) or the proposal included in the recent Italian code (NTC 2008). However, the applicability of these procedures for strengthened specimens, as well as for dynamic actions, needs to be validated with consistent experimental data by means of quasi-static and/or dynamic tests.

Due to the lack of realistic experimental data, the out-of-plane behaviour characterization of stone masonry is more relevant if it is made by testing real existing buildings or full-scale physical models which can be considered reliable replicas of real constructions. Moreover, if complementary tests on strengthened specimens can be performed, additional important and relevant information is likely to be delivered to the scientific and technical community, particularly concerning the efficiency of strengthening schemes.

Concerning the overturning of traditional masonry façades, studies carried out over the last decade showed that it may be more correlated to velocity (energy-based parameter) or displacement demands, rather than acceleration values which are more related to developed forces (de Felice and Giannini 2001; Griffith *et al.* 2003; Decanini *et al.* 2006; Sorrentino *et al.* 2008a; Sorrentino *et al.* 2008b). However, with the exception of very recent experiments performed by Al Shawa *et al.* (2011), no other experimental characterization studies can be found in the literature (until the present date) focusing the out-of-plane dynamic response of complete stone masonry façades and involving specific out-of-plane tests.

Within the above described framework, concerning the out-of-plane behaviour of stone masonry walls, the main objectives of the present Thesis can be summarized as follows:

i)   experimental characterization of the quasi-static and dynamic out-of-plane behaviour of stone masonry façades;

ii)   evaluation of the efficiency of strengthening techniques through experimental evidence;

iii)   development and validation of numerical proposals for simplified simulations of the out-of-plane behaviour of masonry façades, considering simple or complex overturning mechanisms, to be implemented on tools for the out-of-plane seismic assessment of existing stone masonry structures.

1.3. OUTLINE AND ORGANIZATION

According to the following paragraphs, the present Thesis is organized in seven chapters and three appendices. Except for the first and the two last chapters, the main document contains published or submitted papers in international peer reviewed journals cited at the end of this section.

Subsequently to this introduction, Chapter 2 describes the development of an experimental test setup for field quasi-static characterization of the out-of-plane behaviour of masonry walls and strengthening solutions. The development and validation of the test setup is presented resorting to *in-situ* experimental campaigns performed on one-storey stone masonry constructions existing in Faial Island, Azores, Portugal. The evaluation of strengthening techniques adopted after the 1998 Azores earthquake is also described, where the main outputs are discussed focusing on parameters such as the ultimate displacement, maximum strength, hysteretic dissipation capacity, among others.

The development of the referred test setup allowed characterizing an existing structure within reasonable time and costs. Taking this into account, Chapter 3 specially focuses on the application of this testing technique on a two-storey stone masonry existing house, also in Faial Island, Azores. A detailed presentation of the experimental campaign is presented, where strengthening techniques were also adopted. The global response is described, supported by all the relevant acquired data that is also presented, as well as the discussion of the efficiency of strengthening techniques based on the experimental characterization of different solutions. At the end, simple analytical predictions for the contribution of the implemented strengthening schemes is presented and validated as a tool for future interventions on existing buildings resorting to force-based procedures.

Since the characterization of the quasi-static hysteretic behaviour of masonry walls was focused in Chapters 2 and 3, the need to characterize the dynamic performance was found important for completeness. Indeed, quasi-static tests are not able to simulate the out-of-plane overturning which is induced in masonry walls due to kinetic energy imparted by dynamic actions.

Bearing this in mind, the remaining chapters (Chapter 4, 5 and 6) are devoted to the dynamic behaviour of stone masonry buildings, starting from simple masonry walls, proceeding with the overturning of a simplified masonry façade and finalizing with a two storey masonry house involving a complex overturning mechanism; all specimens' behaviour was assessed through lab or shaking table tests and complemented with simplified or complex numerical simulations.

Chapter 4 presents a shaking table programme performed at LNEC (Laboratório Nacional de Engenharia Civil, Lisbon, Portugal) on two full scale stone masonry façades. A detailed description of the tested models and monitoring scheme is presented, as well as a brief overview of the shaking table capabilities. Since the out-of-plane overturning was the main goal of the experiments, the procedure to select the input ground motion is presented and discussed, based on several numerical analyses with predefined overturning mechanisms. The core information of this chapter relies on the discussion of the data acquired during the experiments, being presented some recommendations at the end of the chapter for the assessment of the out-of-plane behaviour of stone masonry façades. Finally, the purpose of the shaking table tests was also to provide reliable data to validate a novel proposal for the simulation of nonlinear dynamic behaviour of local mechanisms, as presented in Chapter 6.

Since the numerical simulation scheme described in Chapter 6 requires the so-called restitution coefficient, Chapter 5 is devoted to its experimental characterization for a *sacco* masonry wall (double leaf with poor infill), which is essential for simulating the dynamic out-of-plane behaviour of masonry walls assumed as rigid bodies. Therefore, a brief theoretical background is included concerning the rigid bodies' behaviour under free rocking and earthquake motions, as well as the commonly accepted modelling simplification of out-of-plane behaviour of masonry walls simulated by rigid bodies rocking at the base.

The lack of literature information regarding the restitution coefficient for *sacco* masonry walls, enforced the need for a specific characterization of that parameter. For this purpose, a novel and specially developed experimental test setup is presented in Chapter 5, based on an equivalent block approach (EBA). Details are presented regarding the tests performed on masonry wallettes having characteristics similar to the specimens described in Chapter 4. The experimental data presentation and interpretation is also included in Chapter 5.

The main objective of Chapter 6 is to propose a methodology for simulating the out-of-plane dynamic behaviour of complex local mechanisms, validated with reliable data (shaking table test results), to be used for future seismic assessment of existing masonry buildings. Local mechanisms, constituted by several masonry portions, are divided in different rigid bodies representing kinematic chains with nonlinearity concentrated at the contact regions. The simulation of its dynamic behaviour is made resorting to the dynamics of multibody systems, for

which the MSC Adams™ (Automatic Dynamic Analysis of Mechanical Systems) software (MSC 2012a) was adopted to compute the dynamic response of two different masonry structures.

An overall synopsis of the work is presented in Chapter 7 which summarizes the most relevant results, guidelines and conclusions achieved, including proposals for future research with the developments outlined in the Thesis.

The Appendices section at the end of the Thesis provides extra information to some of the presented material, which may be helpful to clarify statements and/or obtained results. Supplementary material is provided for Chapter 4 (ground motion selection details and shaking table scaled monitoring scheme), Chapter 5 (free rocking test results) and Chapter 6 (numerical simulation details).

As a general comment to the Thesis organization, each chapter contains an initial part with a brief state-of-art description summarizing the most relevant information to the related chapter.

Except for Chapter 1 (Introduction), Chapter 6 and Chapter 7 (Conclusions), the list of publications subjacent to this Thesis is presented in the following paragraphs and referred to the corresponding chapter:

Chapter 2: Costa A.A., Arêde A., Costa A. and Oliveira C.S. (2011). *In-situ* cyclic tests on existing stone masonry walls and strengthening solutions. *Earthquake Engineering and Structural Dynamics*, Volume 40, Issue 4, pp: 449-471. DOI: 10.1002/eqe.1046

Chapter 3: Costa A.A., Arêde A., Costa A. and Oliveira C.S. (2012). Out-of-plane behaviour of existing stone masonry buildings: experimental evaluation. *Bulletin of Earthquake Engineering*, Volume 10, Issue 1, pp: 93-111. DOI: 10.1007/s10518-011-9332-9

Chapter 4: Costa AA, Arêde A, Costa, AC, Penna A and Costa A. Out-of-plane shaking table test of a stone masonry building. Part I: specimen and ground motion selection. *Earthquake Engineering and Structural Dynamics* (submitted).

Costa AA, Arêde A, Costa, AC, Penna A and Costa A. Out-of-plane shaking table test of a stone masonry building. Part II: shaking table tests. *Earthquake Engineering and Structural Dynamics* (submitted).

Chapter 5: Costa AA, Arêde A, Penna A and Costa A. Experimental and analytical evaluation of the free rocking behaviour of a stone masonry wall through equivalent block approach. *Earthquake Engineering and Structural Dynamics* (submitted).

Chapter 2.

IN-SITU CYCLIC TESTS ON EXISTING STONE MASONRY WALLS AND STRENGTHENING SOLUTIONS

SUMMARY

The present work reports on an *in-situ* experimental test campaign carried out on abandoned traditional masonry houses after the 9th July 1998 earthquake that seriously hit the Faial island of Azores. For the testing purposes, an experimental test setup was developed based on a self-equilibrated scheme which is herein described reporting on the advantages and drawbacks of this *in-situ* test setup.

Five specimens were tested aiming at characterizing the out-of-plane behaviour of stone masonry walls and strengthening solutions recommended for post-earthquake interventions. A detailed comparison between solutions' efficiency is presented including a cost *vs.* benefit analysis. In order to assess the efficiency of the developed test setup for other applications on stone masonry walls, an in-plane test on an existing URM panel is also presented. Several related issues are discussed, namely the advantages of dealing with the real boundary conditions and the capacity of providing valuable information of the response, as well as with a detailed analysis of the obtained results.

This work provides increase of knowledge on the seismic behaviour of existing masonry constructions, resulting from the development of an *in-situ* test setup and the efficiency quantification of strengthening solutions. Therefore, the work is thought to positively contribute for the preservation of architectural heritage and for its seismic vulnerability reduction.

2.1. INTRODUCTION

Experimental tests concerning seismic performance currently aim at assessing the behaviour of new/existing buildings by lab experiments on reliable specimens' reproductions. However, the high complexity level associated with these experiments is well known by the scientific community, especially for masonry structures due to difficulties on simulating the original building characteristics such as material properties or boundary conditions among others.

The *in situ* tests, on the other hand, are not a straightforward and easy task to perform due to difficulties on the preparation for and execution of tests in real buildings. That is obviously one of the main reasons why researchers prefer laboratory rather than *in-situ* experiments. However, the difficulties on reproducing the original characteristics of mechanical and boundary conditions (among others) inside the laboratory are very likely to introduce some uncertainty concerning the level of confidence on lab models. Therefore, the need for adequately and realistically reproducing materials and structures on experimental tests is a main issue that enhances the suitability of *in-situ* tests for this purpose.

The development and implementation of an *in-situ* test setup was a key issue of this work with the following objectives: the accomplishment of the requirements previously referred; the assessment of the out-of-plane and in-plane performance of masonry walls in their original conditions and locations; the use of light and reduced equipment. The mentioned points highlight the ability of the test setup to be used elsewhere in order to obtain consistent results.

The conception and development of the testing scheme were made at the Laboratory of Earthquake and Structural Engineering (LESE) of the Faculty of Engineering of the University of Porto (FEUP), in Porto, Portugal. *In-situ* tests were also performed under the responsibility and with staff of LESE.

Taking advantage of the adopted and implemented test setup, three strengthening schemes were used in order to infer the efficiency of different strengthening interventions suitable for use on pre/post-earthquake interventions. The application of strengthening solutions on traditional masonry walls is recommended to improve the seismic behaviour and some of these techniques were tested during the experimental test campaign of this work, leading to a quantitative and qualitative analysis of the efficiency and associated costs.

The quantitative characterization of original masonry walls and strengthening solutions play a major role on the selection of interventions on existing buildings because, as stated by Penazzi *et al.* (2001), " (...) very few research has been carried out on the behaviour of rubble and multiple leaf stone structures before choosing the appropriate repair techniques".

2.2. State of the Art

Several works have been made to date concerning the seismic behaviour of masonry elements and structures, aiming at characterizing their behaviour under horizontal loads by making use of numerical simulation or experimental lab tests and also at assessing their response after strengthening. However the use of lab tests raises other difficulties very common when analysing stone masonry constructions, namely the correct reproduction of the existing materials of the original elements and the conditions the specimen is subjected to *in-situ* (e.g. boundary conditions, acting loads, etc.). Moreover, the majority of the dynamic tests on masonry structures performed on shaking tables are mainly carried out on reduced scale specimens (e.g. Bothara *et al.* (2010)), which may strongly influence the importance of particular issues of their seismic resistance (e.g. the real aggregate interlocking between actual size masonry elements), despite the use of suitable similitude laws on the scale reduction. These comments can be applied also for experiments performed on regular masonry, where tests on masonry panels had been made regarding in-plane or out-of-plane behaviour (Anthoine *et al.* 1995; Magenes *et al.* 1995; Tomazevic *et al.* 1996a; Willis *et al.* 2004; Abrams *et al.* 2007) for which the actual *in-situ* conditions may not have been correctly conveyed.

Concerning the in-plane behaviour of masonry panels, most of the experiments are performed in lab conditions on specimens built as reproductions of new/existing constructions, e.g. Anthoine *et al.* (1995); Magenes *et al.* (2009). However some *in-situ* tests were already carried out on masonry panels in the form of compression, diagonal compression and in-plane shear tests (Corradi *et al.* 2002; 2003). Despite the importance of the performed experiments, the in-plane hysteretic behaviour was not properly identified and cannot be measured and studied, although it is a crucial and important issue concerning earthquake engineering.

As for the out-of-plane behaviour, different test methodologies were developed and are currently used, namely shaking table tests, e.g. Griffith *et al.* (2004); Hamed and Rabinovitch (2008), distributed cyclic loads (Griffith *et al.* 2007; Mosallam 2007), or concentrated loads in terms of point (Maheri *et al.* 2008), or line loads (Willis *et al.* 2004; Mosele *et al.* 2008; Papanicolaou *et al.* 2008), all of them performed in lab conditions. Since the real field conditions are not commonly reproduced and the need for field tests is indeed a major issue, this subject was addressed by Tumialan *et al.* (2003) that have performed out-of-plane field test on brick masonry walls. However the adopted test setup (as used in that mentioned work) was not able to perform increasing cyclic load reversals controlled through hydraulic actuators.

It is worth mentioning that *in-situ* tests reported in the literature refer only to monotonic loads on the tested specimens; this fact further highlights the need for some other testing methods that allow researchers to study the hysteretic characteristics through a feasible and simple manner.

Finally, the improvement of the seismic resistance of historical stone masonry is recognized and worldwide accepted by international committees (e.g. ICOMOS, Penazzi *et al.* (2001)) and assessment codes (e.g. Eurocode 8 – Part 3 (CEN 2005a)). There are several works developed recently on the area using new materials (e.g. FRP (Mosallam 2007) or textile reinforced mortar (Papanicolaou *et al.* 2008)) or traditional ones (Binda *et al.* 1997) and different techniques (a good brief description is presented by ElGawady *et al.* (2004)). However, the main purposes of the present research aim at increasing the knowledge on the seismic behaviour of strengthening/repair techniques recommended by international design/assessment codes (Eurocode 8 – Part 3 (CEN 2005a)) and that can be used for future interventions.

2.3. IN-SITU TEST CAMPAIGN

2.3.1. General overview

The experimental campaign presented in this work aimed at characterizing typical stone masonry walls from Azores, constituted by double leaf basalt stone masonry with poor infill, including some strengthening techniques used on damaged constructions after the 1998 Azores earthquake. However one of the main problems in testing existing masonry is the correct reproduction of materials and assemblages under a laboratory controlled environment. Therefore a key issue of the work consisted on the definition and adoption of a testing scheme which could be used on real constructions (*in-situ*) with three requirements: straightforward implementation; reduced time for each test including a light and portable system; possible to be used on the assessment of existing building under rehabilitation/ strengthening interventions.

The fulfilment of these requirements was achieved (as presented in the following subsection 2.3.2) leading to an adequate testing scheme able to perform in-plane and out-of-plane tests on existing buildings.

2.3.2. Description of the testing scheme

The main support of the test setup herein presented is based on a self-equilibrated action/reaction scheme making use of existing elements in the tested structure. This test setup was adopted especially to assess the out-of-plane behaviour of masonry walls but it is possible to be used also for the assessment of the in-plane behaviour of masonry panels or other elements. The use of self-equilibrating test setup is not new but the way it was developed and applied in this work represents a new step further on the characterization of masonry walls of existing constructions. The great advantage of the proposed method is the absence of a specific external reaction structure because the system is self equilibrated within the tested construc-

tion using existing structural elements to provide the required reaction. Figure 2.1 shows the proposed test setup to assess the out-of-plane performance of masonry walls in order to clarify the implementation of the developed method. The strongest wall serves as reaction structure whereas the other wall (main façade in the presented case) is the tested element; consequently, the system is self equilibrated and provides reaction forces to test the opposite panel without any extra structure. Hydraulic devices are placed at the top of the walls and connected to them through hinged links ensuring well known acting loads and restraint conditions.

This test setup is quite simple and makes use of traditional testing devices, such as hydraulic actuators and displacement transducers; the main innovation relies on the use of a self equili-brated system to perform cyclic tests (mainly, but not exclusively) on existing structures. Obvi-ously, the method can be also applied to new constructions but the destructive nature of the test is very likely to diminish its interest for such type of cases; however it can be applied under rehabilitation interventions on existing constructions if partial demolitions of the structure are prescribed.

(a)   (b)
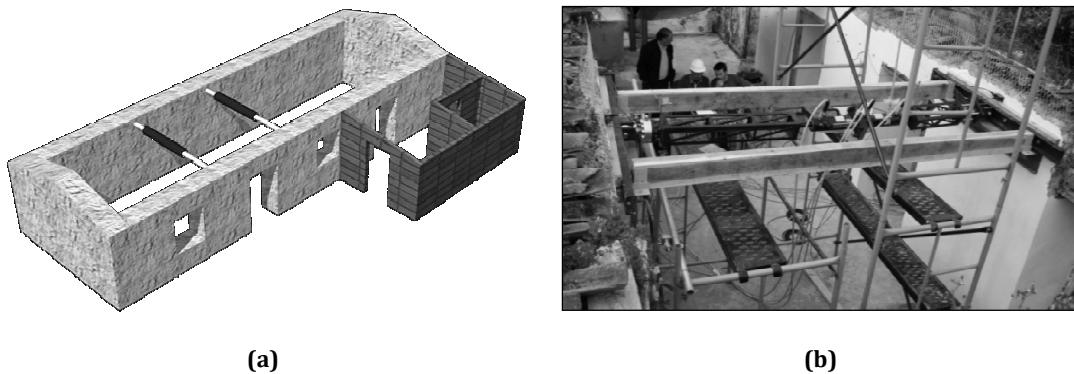
Figure 2.1. Experimental test setup proposal: a) schematic representation for S_01 and S_03 pan-els; b) *in-situ* implementation for tests in S_01 (interior view).

2.3.2.1.   Out-of-plane tests

The first test setup scope was the out-of-plane behaviour assessment of stone masonry walls. Out-of-plane experiments of masonry walls aim at exciting the wall in the direction perpendicu-lar to their strongest axis, leading to simulations of the seismic out-of-plane motions resorting to static loads. In traditional constructions, these motions may lead to a typical collapse mecha-nism due to mass concentration mainly at the walls rather than the floor levels (contrarily to common r.c. frame type structures). Traditional constructions usually have flexible diaphragms (wooden floors) and timber roofs where a top applied load (Figure 2.2 a)) can simulate ap-proximately (through the corresponding deformed shape) both the roof mass excitation and displacement demand due to wall inertia forces, as shown in Figure 2.2, where a typical col-lapse is illustrated.

(a)   **(b)**
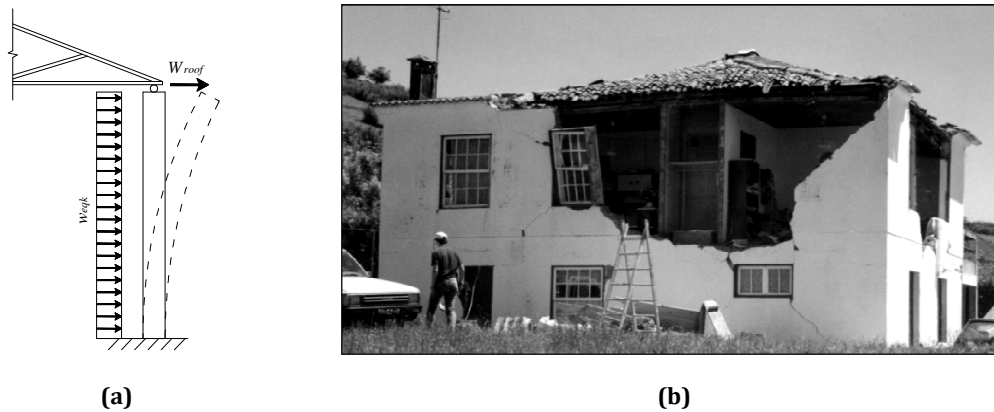
Figure 2.2. Out-of-plane action: a) earthquake loads on a load bearing masonry wall; b) typical out-of-plane collapse (Azores earthquake, 1998)

Collapses of URM walls usually occur due to instability rather than achievement of maximum strength of the material at the compressed section and, consequently, the major objective of the tests should be the simulation of displacements rather than forces.

The adopted loading scheme was set up according to Figure 2.3 a), through which only shear forces V_L are applied to the walls because hinged links are inserted between the loading system and walls. Nevertheless, minor axial loads N_{sw} and bending moments are also involved. The latter are equal to $M_{sw1} = N_{sw} \cdot t_1/2$ and $M_{sw2} = N_{sw} \cdot t_2/2$, respectively, due to the test setup self-weight and to the eccentricity of N_{sw} relatively to the centre of the wall with width t_1 or t_2; the test setup is subjected to its own self weight and to the axial load N_L imposed through the hydraulic units. Figure 2.3 includes a schematic representation of the forces involved in the proposed setup, where the applied out-of-plane loads V_L are equal to N_L. Since the system is self-equilibrated, a load cell inserted between the acting system and the walls is sufficient for monitoring the applied force on both walls.
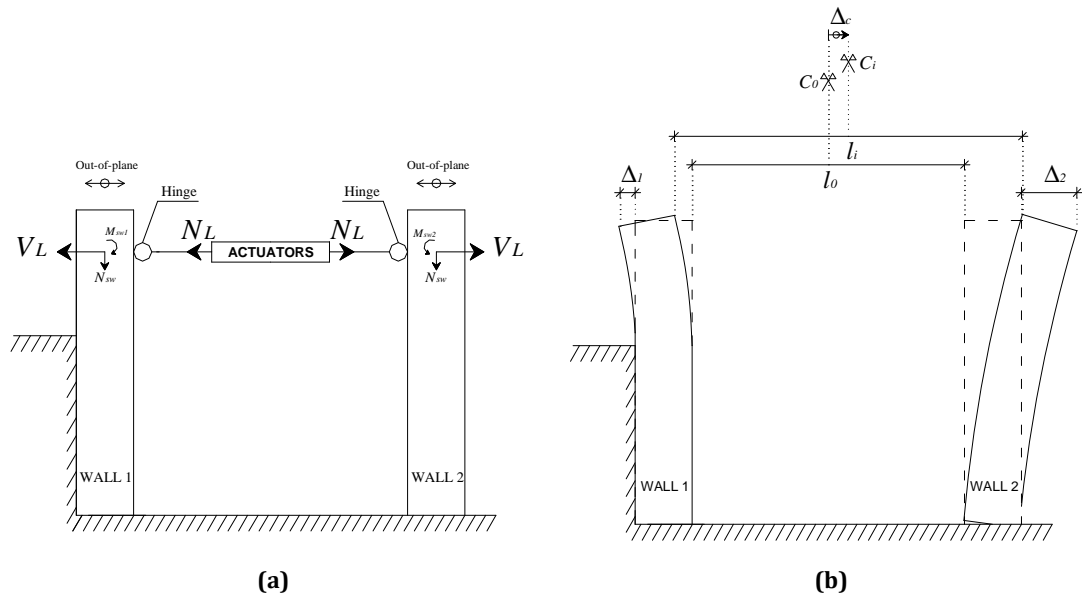
Figure 2.3. Test setup scheme: a) acting forces during the test; b) schematically deformed shapes of the tested panels

The walls will displace differently because the actuators are not attached to a fixed reaction structure, which means that the actuator system centre will be displaced, as represented in Figure 2.3 b). In this figure, l_0 and C_0 are, respectively, the length of the actuation system and its geometric centre at the initial stage of the test (time step 0), while l_i and C_i have similar meaning for the time step i which leads to displacements Δ_1 and Δ_2, respectively, of walls 1 and 2. The difference between C_0 and C_i, represented by Δ_c, is the system centre shift relative to its initial position.

Consequently, the control system of the experiment is better achieved on the basis of external transducers. In the schematic case shown in Figure 2.3 b), the absolute displacement Δ_2 is monitored with a displacement transducer external to the acting system and serves as the reference input for the control system because it is the weaker wall and, therefore, it can be tested up to the collapse.

In fact, wall 1 is stronger due to its reduced effective height and to the continuity along its length and wall 2 represents a façade wall which generally includes significant openings long and heightwise (doors and windows), thus with reduced stiffness and strength when compared to wall 1. However, in other cases, the weaker wall definition may not be so simple and, therefore, the control system should be capable of real-time switching the desired input displacement; this feature was indeed implemented in the control system software developed during this thesis for these applications.

The load application can be controlled either in terms of the load cell measured force or in terms of the displacements read by the external transducers. Therefore, these devices should

be selected according to the properties of the tested walls regarding thickness and expected maximum strength (the later particularly for the case of strengthened specimens) which will define, respectively, the maximum displacement transducer range and load cell capacity.

An important issue that must be taken into account may result from the use of a testing scheme with significant length or a very stiff specimen, because second order effects on the testing system under compression may become a serious problem which might require the adoption of buckling restraining devices.

The use of not very stiff reaction structures is another worth mentioning issue. In fact, since the actuators react against a "flexible" structure (when compared to lab reaction walls which are very stiff and strong), this test setup is not recommended for all kind of experiments and specimens. Actually, this test setup should be used only on test specimens with some flexibility and reduced strength when compared to the reacting structure and always focused on quasi-static tests. This test setup should not be used for dynamic tests because the dynamic proper-ties of the complete system are complex and strongly influenced by the flexibility of the reac-tion structure.

If the requirements mentioned previously are not fulfilled, control problems on the acting sys-tem may arise due to the interaction between the specimen and the reaction structure, such as the difficulty to release the accumulated elastic energy by the reaction wall and the problems on following the post peak behaviour, which, to some extent, will include also the properties of the reaction structure in the response of the tested specimen.

Thus, the test setup proposed in this work may not be applied for all cases and structures but, if due account is taken to the referred restrictions, it may lead to interesting and useful results especially for the characterization of existing masonry constructions as described next.

It is therefore possible, in this way, to have a light and portable system capable of performing out-of-plane cyclic tests under real conditions. The use of measuring devices external to the actuation system allows monitoring and controlling the test independently of any unpredicted behaviour of the actuation system; in addition it permits testing simultaneously two walls wherein the weaker wall will be the only one tested up to the collapse under real displacement control system.

2.3.2.2.   In-plane tests

For the in-plane behaviour assessment of masonry panels, the testing devices should be placed at doors or windows to obtain two wall panels in the same alignment where the ac-tion/reaction system can be applied. The weaker element selection should be done according to the specimen position in the building and to the provision of sufficient reaction by the other

tested ("reacting") element. Thus, it might be necessary to introduce some type of reinforcement or connection of the (expected) reaction element to the global structure in order to minimize its deformability and damage.

After the selection of the elements for testing and hydraulic units' positioning, the spandrel beam (elements above the door/window, Figure 2.4 a)) can be removed (Figure 2.4 b)), leading to a test setup as commonly found on lab experimental tests to assess the in-plane behaviour of masonry panels. On the one hand, this operation affects the actual boundary conditions of the specimen because the spandrels may impose some moment restriction at the top of the wall, as commonly assumed for unreinforced regular masonry (equivalent frame approach). On the other hand, the quality of the spandrel beams of these constructions is usually very weak (Figure 2.4 a)) which may lead to unknown boundary conditions. If the spandrel is removed, the wall is therefore subjected to well known boundary conditions.

The selection of this operation should be helped by engineering judgment, bearing in mind the role of the experiment, the understanding of the spandrel influence and its quality on the global behaviour of the tested specimen. For the in-plane test described in this work, it was decided to remove the spandrel due to its constitution and to obtain well known boundary conditions.

Concerning the load application, the connection between the actuators and the walls could be made by various approaches; the adopted one consisted of a steel ring around the specimen, placed and tied with connecting rods along the steel pieces, as partially shown in Figure 2.4 c), in order to distribute the shear force along the wall. Finally, displacement transducers must be placed to monitor the wall deformation during the experiment and attached to external reference points.

(a)   **(b)**   **(c)**
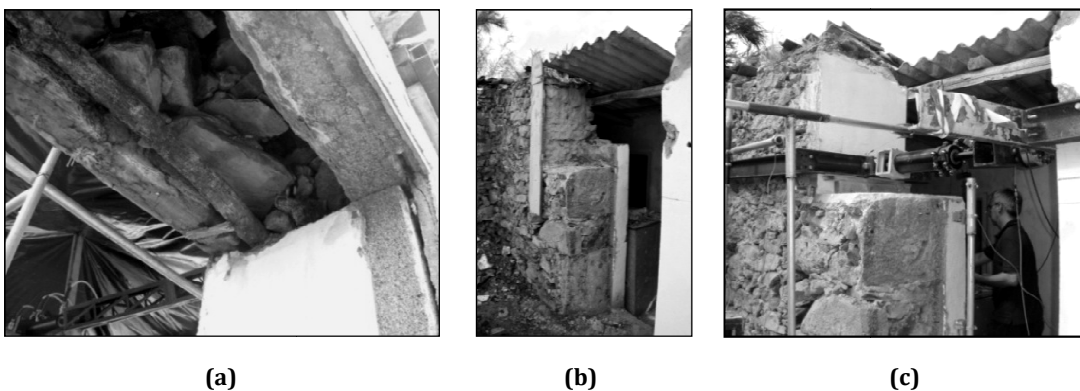
Figure 2.4. In-plane test preparation: a) spandrel constitution in the tested construction; b) spandrel removal; c) insertion of connecting rods and actuators

As mentioned before, contrarily to laboratory tests wherein strong and stiff reaction structures are available to perform tests up to *a priori* known maximum loads, the outcome of the adopted self-equilibrated testing scheme is very dependent on the available strength of the element

chosen to serve as reaction structure. This means that, although the testing system is displacement controlled, the reaction element has to provide larger strength and stiffness than the specimen envisaged to be tested. Thus, for a setup with two panels assumed to have similar response types, the reaction panel demand ($F_{p,R}$) must fulfil the condition $F_{p,R} > F_{p,T}$, where $F_{p,T}$ is the peak strength of the tested panel. Once the later value is reached, the reaction panel demand does not increase further and the experiment can proceed up to the tested element's collapse.

In this line, it is reasonable to expect that the reaction demand for walls with similar constitution is not significantly different, which means that a parallel association (Figure 2.5 a)) of two similar panels adequately connected may provide the required reaction to allow testing the desired panel (Tested panel) without reaching nonlinear response of the "reaction walls" assemblage. In this case, the total stiffness of the reaction structure, $K_{t,R}$, is given by $K_{T,R} = K_{1,R} + K_{2,R}$, where $K_{1,R}$ and $K_{2,R}$ are, respectively, the stiffness of reaction panels 1 and 2.

Additionally, based on the schematic response diagrams depicted in Figure 2.5 for the illustrated panels (wherein the isolated one is the tested panel), the experiment can be performed without major damage on the reaction panels provided the relation $F_{e,R} > F_{max,T}$ is fulfilled, where $F_{e,R}$ is the elastic strength of the assemblage of panels 1 and 2, and $F_{max,T}$ is the tested panel peak strength. This condition shall not be difficult to ensure, by providing an effectively strong and stiff spandrel link between each reaction panel.

(a)   **(b)**
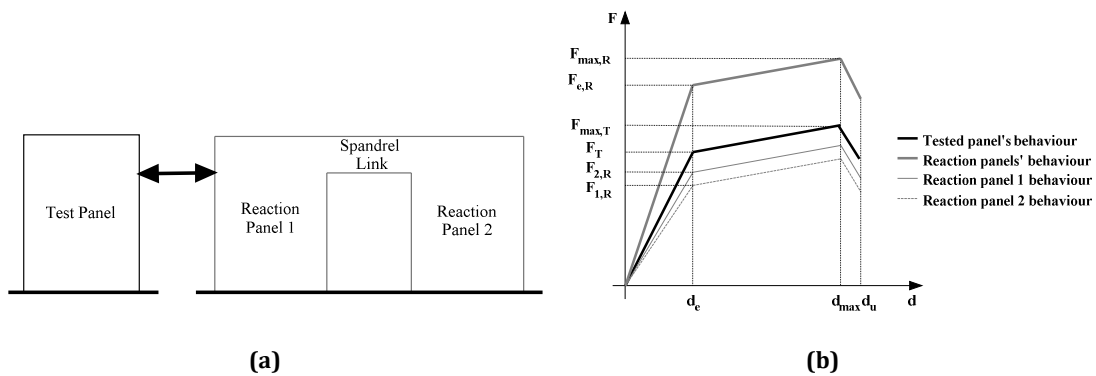
Figure 2.5. Test panel vs. reaction panels' behaviour: schematic layout, a), and response, b).

Finally, as for the out-of-plane tests, displacements should be measured externally to the actuation system, allowing the test control to be made based on absolute displacements rather relative ones.

The problems referred in section 2.3.2.1 concerning the use of flexible reaction structures are valid also for this type of tests and may be inclusively more severe due to the larger in-plane stiffness and smaller displacement capacity when subjected to in-plane loads. For the case

herein presented, some more detail is shown in section 2.3.3 regarding the reaction structure for the test.

2.3.3. Buildings and elements tested

Traditional constructions of Faial Island have common characteristics which are present in the cases herein addressed. Most of these structures in rural areas are 1-2 storey height with double leaf with poor infill (*sacco*) stone masonry walls performing as bearing structures where basalt blocks are used for the wall leaves. The outer face (external leaf) is generally more regular than the inner one (internal leaf) and quite often with a surface mortar cover. The arrangement of blocks around the openings, especially at door alignments, includes larger and more regular stone blocks than the other wall zones.

A typical representation of these walls constitution is presented in Figure 2.6, where the mentioned characteristics can be observed both for an existing wall (Figure 2.6 a)) and for new wall under construction (Figure 2.6 b)).

The cyclic response of masonry panels was experimental analysed during test campaigns on two different buildings, named "Casa do Salão" (S) and "Casa Nova" (CN), for assessing their in-plane and out-of-plane behaviour. These constructions were damaged during the 1998 Azores earthquake with partial collapses (roofs and local failures) which did not affect the tested structural elements; the houses were left abandoned since 1998, after the earthquake, which allowed performing these tests thanks to the kind authorization of the owners.

(a)   (b)
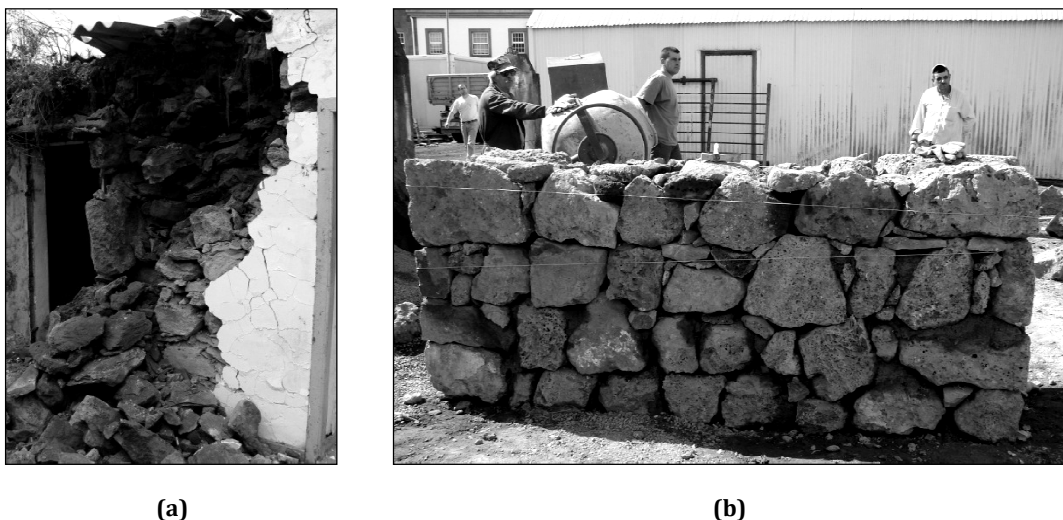
Figure 2.6. Typical double leaf stone masonry walls from Azores: a) internal constitution (existing wall); b) wall under construction

The S and CN construction structures were similar concerning both in plan wall distribution, height (one storey) and construction typology, including similar materials. Pictures, schematic layouts and monitoring schemes are included in Figure 2.7 (house S) and Figure 2.8 (house CN) with reference to the tested elements and to actuators' positions. Figure 2.8 shows that the CN test involved only one displacement transducer at the façade (another transducer was used at the rear wall). The reason to such reduced monitoring scheme is a consequence of *in-situ* test where it is not possible to control all the conditions. In that case, the rain did not permit to use an extensive measurement of displacements but, even so, it was possible to obtain the global response through the hysteresis loop.

(a)

(b)

(c)
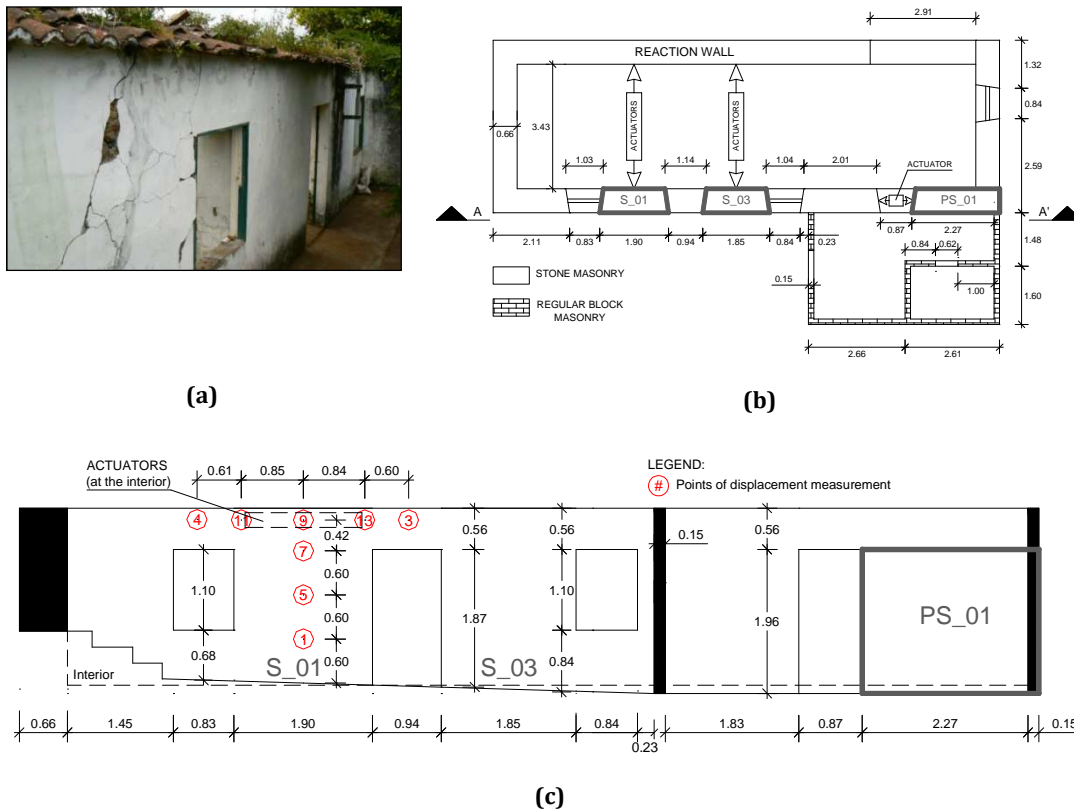
Figure 2.7. Building S: a) main façade picture; b) plan view; c) main façade (A-A') with displacement monitored points (numbered circles) for S_01 panel test (similar scheme was used for S_03 panel)

(a)

(b)

(c)
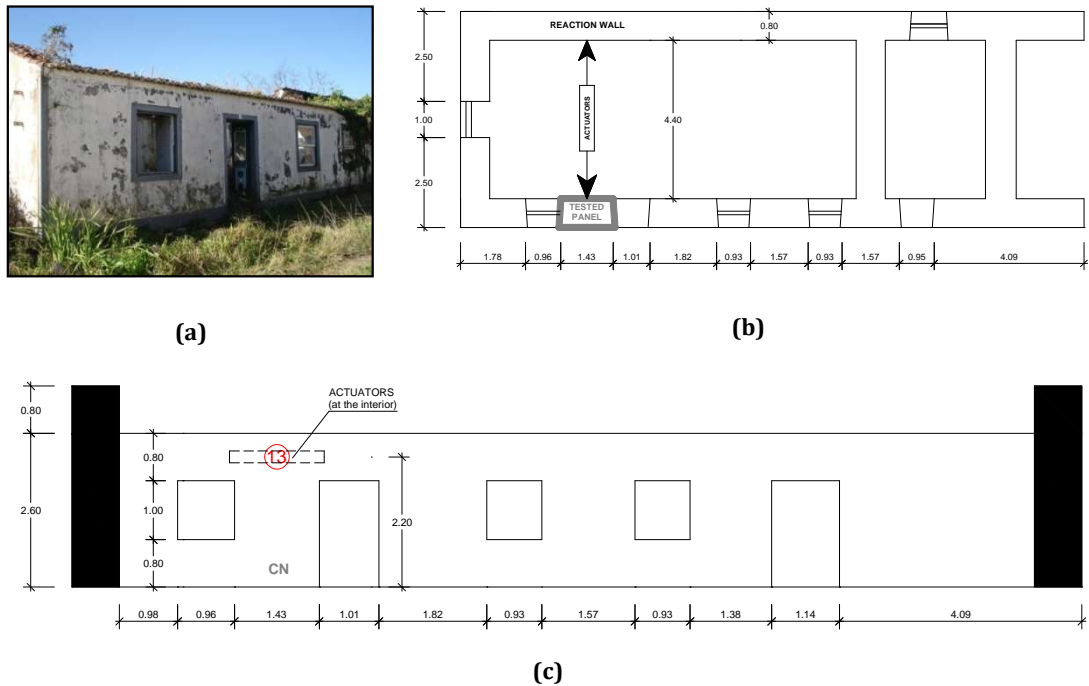
Figure 2.8. Building CN: a) main façade picture; b) plan view; c) main façade

For both cases (building S and CN), the rear walls were used as the reaction structures due to their larger stiffness and strength characteristics provided by the continuity (no openings). In addition, the reduced effective height of the rear wall in house S clearly contributes for increased strength and stiffness, which was of particular convenience for that house since it allowed making the out-of-plane tests even on the strengthened specimens.

A detailed observation of Figure 2.7 b) shows a returning wall near the S_03 right spandrel beam which (as shown latter on) influences the response of the tested specimen for outward movements.

In addition to the out-of-plane tests on S_01, S_03 and CN specimens, an in-plane test was performed on the PS_01 wall of house S, mainly aiming at the assessment of its in-plane behaviour under horizontal cyclic loads and of the corner effects influence on its response. In this line, it is worth stressing that the orthogonal regular block masonry wall of the annex zone was not efficiently connected to the tested wall due to different construction phases of each building part, thus without any interlocking between elements of both walls. Therefore, any corner effects that may show-up are essentially due to the other part of the transverse wall made of traditional masonry.

The reaction required to perform this in-plane test was provided by a series of strengthened wall panels in the direction of the tested wall, including the panels S_01 and S_03 with dimensions not very different from the PS_01 specimen.

2.4. STRENGTHENING SOLUTIONS

The improvement of seismic resistance of old masonry structures is mandatory for vulnerable construction built in moderate – high seismicity regions in order to reduce the damage extent. This requirement is recognized and also foreseen in modern codes such as Eurocode 8 – Part 3 (CEN 2005b).

As a result of the damage observed after the 1998 Azores earthquake (as reported by Oliveira and Malheiro (1999) and Oliveira *et al.* (2008)), several strengthening/retrofit interventions were performed on the existing building stock, including several monuments and governmental buildings. A number of different techniques were applied with different purposes, such as bearing walls' strengthening, improvement of connections between structural elements and/or floors' stiffness increase, in order to increase the seismic performance of the existing buildings. Some major guidelines were addressed by Carvalho *et al.* (1998) and Costa and Arêde (2006) for the after earthquake interventions, similar to the proposals suggested by other researchers (Dolce *et al.* 2001) and some included in current Eurocode 8 – Part 3 – Annex C.5 (CEN 2005b).

The more or less intrusive character of some of the suggested and used techniques, it is not the major goal of this work, although it is recognized to be a topic of significant importance that deserves being discussed elsewhere due to the impact it may have on non-structural related issues such as higrothermic performance of the constructions subject to those strengthening proposals. Therefore, attention is focused here essentially on the structural performance perspective, complemented with some comments on intervention costs.

The first technique applied was a sort of reinforced concrete jacketing as recommended in Eurocode 8 – Part 3 – Annex C.5.1.7 (CEN 2005b) and explained briefly in Costa (2002) for Azorean constructions. As a personal opinion, for the scheme proposed herein, this terminology ("reinforced concrete jacketing") is too strong since it is often understood as an overall and complete envelope of a given structural element (typically beam or column) which is very difficult to implement in the case of walls in real masonry constructions due to the presence of spandrels and windows; moreover, it usually amounts to a considerable thickness of new reinforced concrete layers which is not the case herein proposed. Therefore, the designation of *reinforced connected plaster* was adopted, because: *i)* it is actually made of plaster (binder and small aggregate, typically thin-medium grain size sand); *ii)* it is reinforced with an appropriate steel mesh and, *iii)*, it consists of two leafs, one in each wall face (internal and external) which are connected by appropriate rods duly anchored within the leaf thickness.

This strengthening was adopted in both the S_01 and S_03 wall specimens (shown in Figure 2.7) with the detailing illustrated in Figure 2.9.

VERTICAL CROSS SECTION

STONE MASONRY

1st LAYER OF PLASTER AND JOINTS FILL

METALLIC MESH

CONNECTORS WITH MAX. SPACING OF 1.50 m

SURFACE MORTAR

(a)   (b)

Figure 2.9. Reinforced connected plaster operation: a) schematic representation; b) application.

It is worth mentioning also that the strengthening proposal used for these experiments was lighter than the one presented in Costa (2002), since a wider stainless steel mesh was used together with smaller and simpler connectors made of normal construction rebars, bent and anchored to the mesh inside the plaster layer. This strategy allowed reducing the leaf thickness and the execution time and cost, while ensuring the same global behaviour. The overlap of the steel mesh was defined as 0.10 meter in the longitudinal direction and 0.15 meter in the vertical direction, while the mesh was oriented with the larger steel percentage in the transverse horizontal cross section (see Figure 2.9 b)) in order to optimize the strength for both in-plane and out-of-plane behaviour. Finally it should be referred that this technique itself does not guarantee the anchorage of the reinforcement at foundations level, but this issue is taken into account with another strengthening scheme.

VERTICAL CROSS SECTION

METALLIC SHAPE CONNECTING THE BEAM

WOOD BEAM

GALVANIZED NAIL 60 mm Ø6mm

CONNECTOR WITH STEEL PLATE 100 X 100 mm2

M16 BOLT

METALLIC SHAPE WITH 3 mm

1.40 m

1.60 m

FRONT VIEW

(a)   (b)   (c)
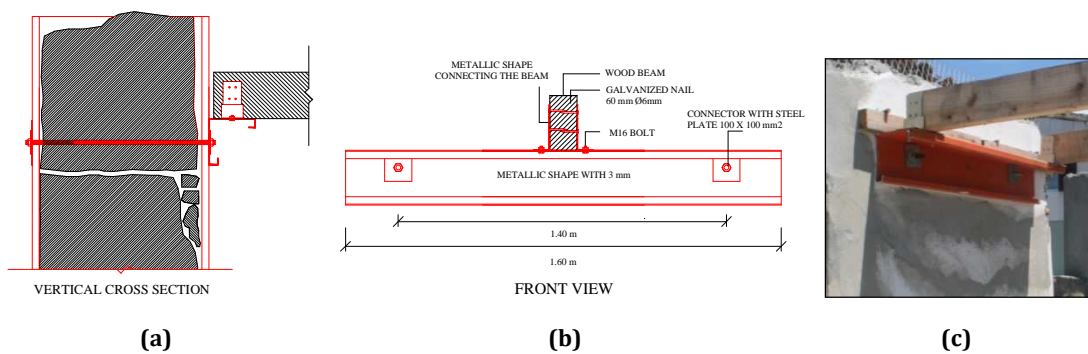
Figure 2.10. Strengthening of the connection between walls and floor/roof beams: a) cross section view; b) front view; c) application.

The second strengthening technique tested consisted of a restraining connection between parallel walls and the floor/roof, using steel plates and wood beams as connecting elements (Figure 2.10). The main objective of this strengthening type is to restrain effectively out-of-plane movements of façades, connecting the building as a box with the steel shapes acting as a

ring beam, as presented in Costa and Arête (2006) and commonly adopted in strengthening interventions. However, for the test purposes, the steel shape was just applied locally as shown in Figure 2.10 c) and for the panel S_01.

The third strengthening scheme tested during the experimental campaign was based on the introduction of reinforced concrete beams at the foundation level in order to anchor the steel mesh, as represented in Figure 2.11. These beams are adopted together with at least the first technique (reinforced connected plaster) aiming at increasing the maximum strength of the panel by making use of the tensile contribution of the steel mesh duly anchored in the foundation.

(a)   (b)
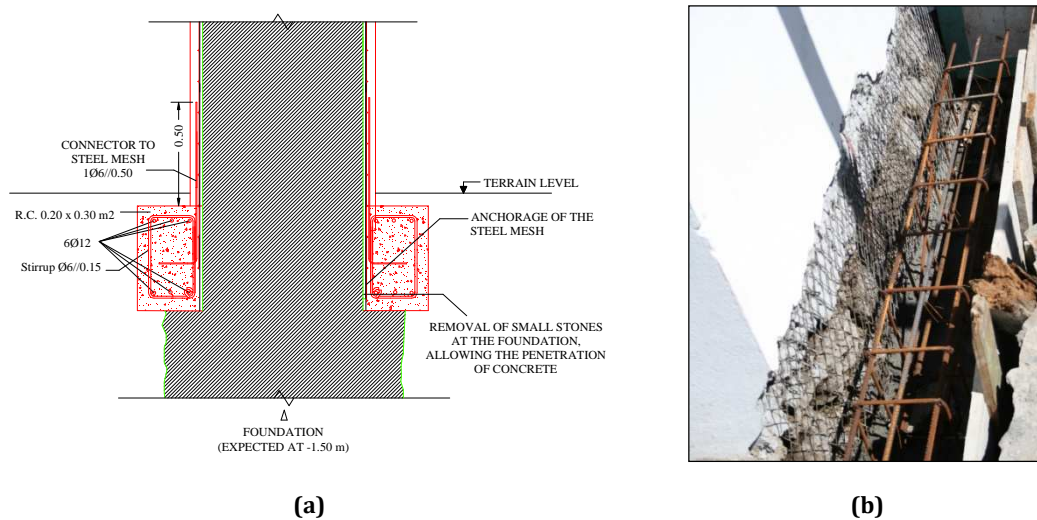
Figure 2.11. Strengthening at the foundation level: a) schematic representation; b) application to S_01R2

This strategy was applied in the S_01 panel after having been tested with the first plus the second strengthening schemes (S_01R specimen), thus leading to the S_01R2 specimen. The connection to the foundation was achieved by removing the mortar cover near the foundation and by overlapping the steel mesh from the foundation with that from the wall as shown in Figure 2.11 b). Some "ad-hoc" connectors (made of common steel rebars) were also inserted in the wall voids and left embedded in the foundation beams.

Table 2.1 presents a summary of the strengthening solutions applied during the experimental test programme and the costs associated with each operation, while Figure 2.12 shows the zones where the different strengthening techniques were applied at the wall.

Table 2.1. Strengthening techniques applied for each panel

	S_03R	S_01R	S_01R2	Cost* (€/m)
Reinforced connected plaster	x	x	x	147
Connection between walls and floor/roof		x	x	162
Reinforced concrete beams at foundation			x	775
Cost (€)	786	821	2292	

(*) Average costs computed for a floor height of 2.5 meter, distance between façades of 3.5 meter and continuous foundation beams
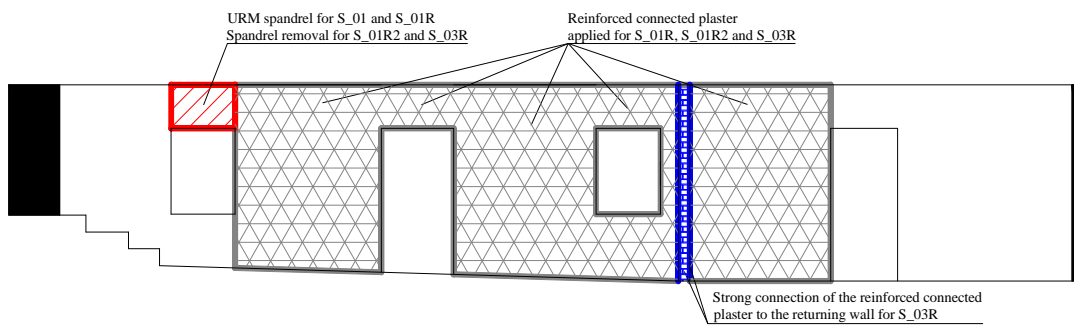
Figure 2.12. Representation of the strengthening techniques applied on the complete wall

2.5. Discussion of Obtained Results

2.5.1. Out-of-plane tests

2.5.1.1. General comments

The following paragraphs report on the test results obtained during the experimental campaigns concerning the out-of-plane tests, highlighting the improvement of the seismic resistance by the use of strengthening techniques.

The tests were carried out according to the following sequence: the S_01 original panel was first tested as well as the CN panel; then the S_03R and the S_01R specimens were prepared and tested in that same order; finally the S_01R2 specimen was completed (after prior testing of S_01R) and tested. In total, four out-of-plane tests were performed with the two panels S_01 and S_03.

A qualitative and quantitative succinct comparison among the different used schemes is presented which is thought to be helpful on the selection of the adequate solution to adopt for each individual construction in future strengthening/rehabilitation interventions.

Displacements are shown both in terms of absolute values and also in relation to the wall thickness (Δ = absolute displacement; t = wall thickness). The positive sense of displacements corresponds to the pushing sense of the actuators (outward movement of the walls).

2.5.1.2. Test results and comparisons

Figure 2.13 presents the force *vs.* displacement curves obtained for the walls (S_01 and CN) tested in the original conditions, i.e. without strengthening schemes. Each plot also includes the maximum expected envelope resulting from rigid body overturning of the mobilized part of the wall (the central pier and the two adjacent spandrel beams).

(a)   **(b)**
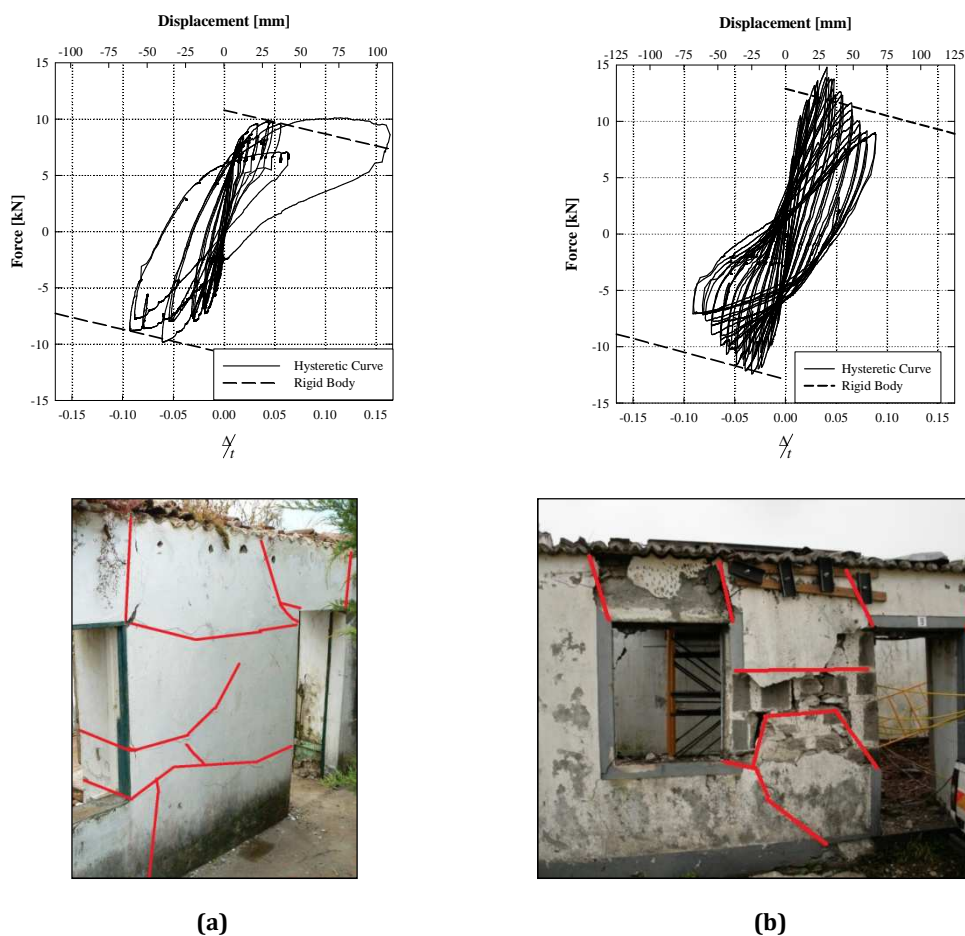
Figure 2.13. Force *vs.* displacement curves (superimposed with rigid body motion maximum envelopes) and exterior main cracking pattern for the URM walls: a) S_01; b) CN

As a first comment, it should be referred that the S_01 test was the first experiment using this testing scheme which led to unpredicted response of the actuation system. Actually, the control system was not able to produce accurate displacement controlled cyclic loops which yielded to a significant pushing of the wall in one sense. This pulse affected the global results because it was not possible to study the strength degradation due to cyclic behaviour which was expected

to yield a lower strength value for larger displacements and higher energy dissipation during the whole test duration. This was the main reason to perform a new test in another URM wall (CN specimen) that led to completely defined cycles with good discretization of the post peak behaviour in terms of strength degradation and energy dissipation.

Concerning the walls' behaviour, the out-of-plane response was characterized by a significant displacement capacity, with horizontal and diagonal cracks both along the wall and at the connections to spandrel beams, particularly for the S_01 test. However, significant strength degradation was observed after the achievement of maximum strength, especially in the case of CN test, where several cycles highlight this behaviour. The collapse mechanism obtained is similar to that one observed in the façade wall of Figure 2.2 b) after the 1998 Azores earthquake.

From the analyses of the hysteresis loops, a value of $\Delta/t \approx 4$ % seems to be consistent for the computation of maximum strength, while $\Delta/t \approx 9$ % may be observed as ultimate displacement capacity. From the analysis of CN results, and considering a strength degradation of 20% in the framework of displacement based assessment of the out-of-plane behaviour, a $\Delta_u/t = 6$ % ratio may be suggested for ultimate displacement ratio. If these considerations are applied for S_01, it is possible to observe that the second cycle in the positive sense after the strong pulse leads to a value close to that ratio.

It should be referred that these figures are significantly lower that the value proposed by the Italian Code (OPCM no. 3274 2005) for the non linear static safety check for seismic assessment through rigid-body analysis, where $d_u*/t = 40\%$. If locally incompatible conditions were considered as suggested in that code (e.g. unseating of floor joists), the ultimate displacement value would be closer to the experimental values obtained, but this would have no direct relation with the real behaviour during the tests, because the limits above presented were obtained due to wall behaviour and not due to local incompatible conditions.

The linear envelope of the response obtained through a rigid body overturning formulation based on the system equilibrium yields to a good estimation of the maximum strength response and seems to be conservative in the case of strong pulses as actually occurred. For this formulation, the elements dimensions were used considering a unit weight of 19.0 kN/m^3 as recommended by Costa (2002) for this type of material, and consistent with the Italian Code (OPCM no. 3274 2005) for materials with these characteristics.

In order to correctly infer the efficiency of the strengthening techniques previously presented in section 2.4, a direct comparison between the URM and the retrofit/strengthened specimens are introduced in terms of force *vs*. displacement response curves and respective envelopes shown in Figure 2.14.

(a) **(b)**
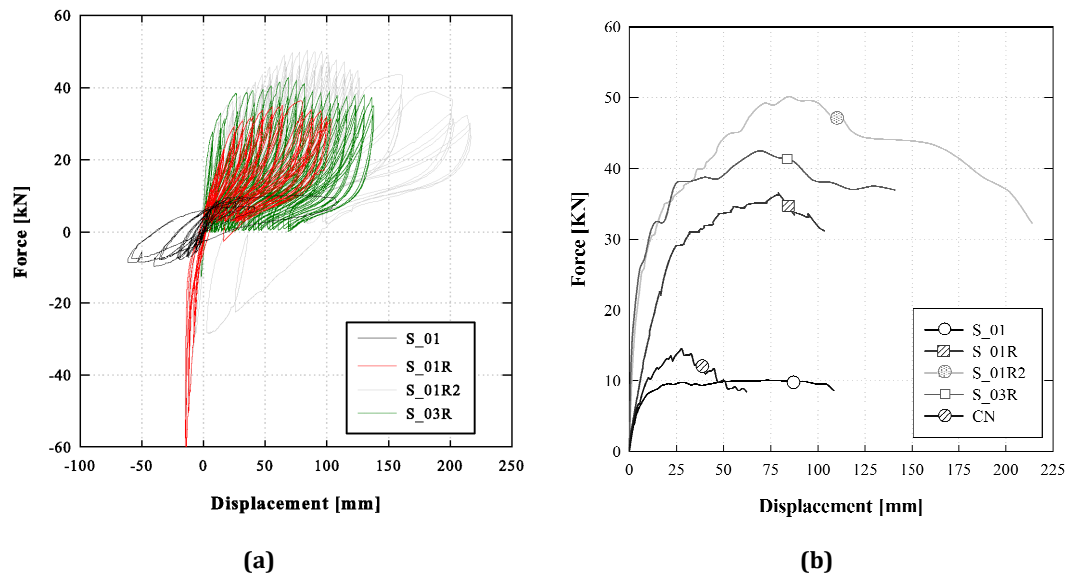
Figure 2.14. Strengthening influence in global behaviour: a) hysteresis loops; b) response envelopes

Figure 2.14 shows that the cycles performed on the strengthened specimens are quite asymmetric, mainly developing in one sense (push or outward). The reason for this evidence is twofold. On the one hand, for inward wall movements, and after a relatively small displacement is reached, the axial load is transmitted by compression forces in the wood beams, eventually leading to local buckling; as expected, the presence of wood beams well connected to the walls modifies the seismic behaviour of the wall by mechanically restraining inward movements. On the other hand, the associated out-of-plane collapses of these walls generally occur in the outward sense as observed in post earthquake surveys of damage buildings (Figure 2.2). For these reasons, only the first cycles were tested in both senses to infer the connection quality of the entire strengthening scheme, whilst the remaining part of the tests was performed only under load-unload cycles in the outward sense.

The hysteretic response of the different strengthening schemes was similar due to the use of reinforced connected plaster, characterized by small energy dissipation between cycles and some pinching effect. Moreover the strength decrease around 75 mm (100 mm for S_01R2) was a result of damage at the connection to wood beams (responsible for some energy dissipation and shown in Figure 2.15 a), which highlights the importance of a good connection among the several elements. It should be referred that the S_01R2 test demonstrated also the importance of detailing on strengthening interventions. A short lap splice of the steel mesh led to concentrated damage in a given section of the wall (Figure 2.15 b)), also recognized after the 1997 Umbria-Marche earthquake and mentioned in Penazzi *et al.* (2001), which means that detailing and correct execution are mandatory to ensure the desired behaviour of strengthened specimens.

| (a) | (b) | (c) |
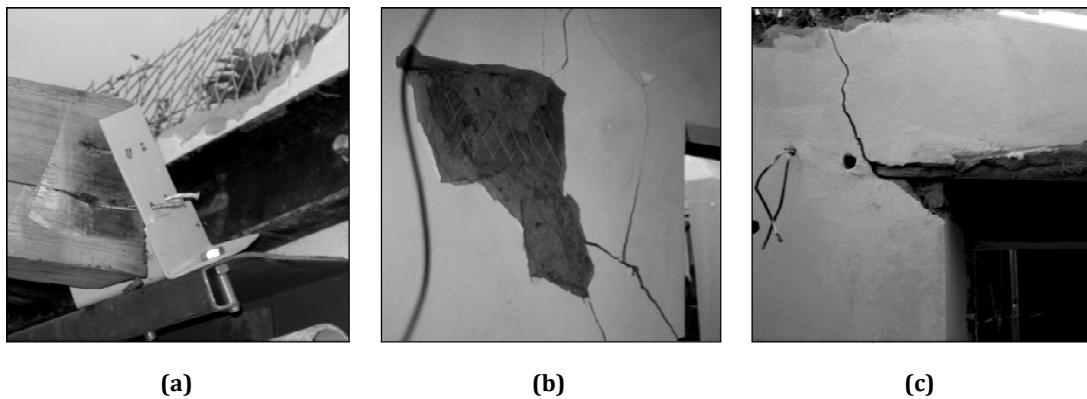
Figure 2.15. Particularities observed during the experiments: a) yielding and destruction of the connection to the wood beam; b) incorrect lap splice with damage concentration; c) damage at the connection between spandrel and pier

Last but not the least, as expected for the strengthened specimens, the damage concentration was mainly observed at the connection between spandrels and the pier (Figure 2.15 c)) but with ductile behaviour due to the steel mesh, contrarily to the URM tests where no ductility was observed in this zones. It should be also referred that the strengthening applied on S_01R2 enforced rocking of the wall plus the reinforced concrete foundation leading to a higher strength observed than S_01R; in case these foundation beams were linked to other transversal ones (foundation lintels) then it could be expected even larger strength due to the contribution of the steel mesh in tension.

The differences among the tests, namely in terms of initial stiffness, maximum strength and displacement, clearly observable in Figure 2.14 b), are reported in Table 2.2.

Table 2.2. Tests results concerning the out-of-plane experiments

	K_{ini} (kN/m)	F_{max} (kN)	d_{max} (mm)
S_01	1709	10.1	108.3 (68.1)*
CN	1844	14.5	66.6
S_01R	2193	36.3	103.4
S_03R	9244	42.5	140.8
S_01R2	6955	50.1	213.9

(*) Displacement due to undesired outward motion; in brackets the displacement reached in the other sense

Concerning the initial stiffness values, the differences between the URM and strengthened specimens is remarkable particularly where continuity among the distinct elements (pier and spandrels) was ensured (S_03R). However, the larger initial stiffness of S_03R is also related to the presence of the well connected returning wall adjacent to one of the spandrel beams, as

mentioned previously in section 2.3.3 and observable in Figure 2.7 c), while for the case of S_01R2 this observation is due to the presence of the reinforced concrete foundation, as mentioned earlier.

The out-of-plane behaviour of masonry walls is not the main resisting mechanism developed by the structure to sustain earthquake motions which is mainly resisted by the in-plane response of the walls. However the larger stiffness and strength values observed in the strengthened specimens ensures the capacity to sustain stronger ground motion levels without significant deformation, thus avoiding partial collapses of floors/roofs or formation of local mechanisms, due to their remarkable displacement capacity with no significant damage.

The strengthening scheme based on reinforced connected plaster transforms the typical heterogeneity of a stone masonry wall into more monolithic elements (spandrels and piers) with ductile connections between them. This modification is explicitly represented in Figure 2.16 a) where the vertical displacement profile of the strengthened specimens is compared with the URM result (S_01). In this figure, the vertical profile for the maximum displacement level of S_01 (close to 100 mm) is presented together with the profile for the same displacement level obtained during the other tests. In addition to that, the vertical displacement profile corresponding to the maximum displacement obtained for the S_03R and S_01R2 tests are also included.
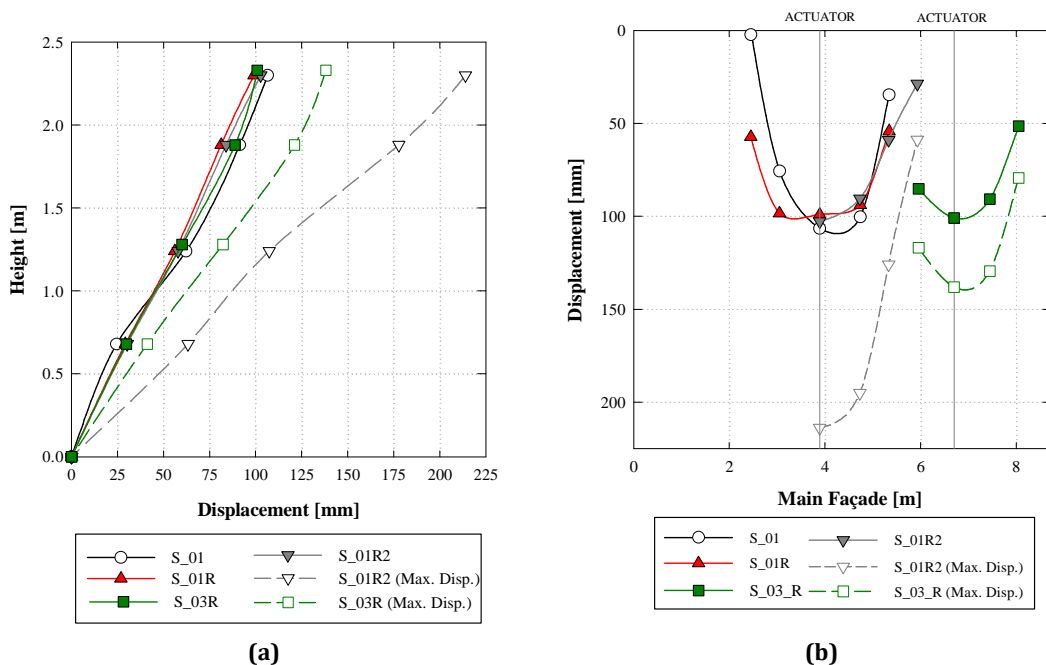
Figure 2.16. Displacement profiles: a) vertical; b) longitudinal

These results are also shown for the horizontal displacement profile exhibited in Figure 2.16 b), where the longitudinal axis extremes (main façade at 0 and 8.3 meter) correspond to returning walls (presented clearly in Figure 2.7 b).

The vertical profile of the URM (S_01) is characterized by a double inflection curve originated by horizontal cylindrical hinges which can be observed in the inferior part of Figure 2.13 a) by horizontal cracking lines originating separated rotating bodies. For the strengthened specimens, it is clear that a rigid body rotation occurred as evidenced by the corresponding vertical displacement profiles of these walls due to the monolithic characteristics of the element.

For larger displacement levels (as the case of S_03R and S_01R2), the formation of horizontal cylindrical hinges modified the response of the wall leading to a partitioned behaviour of two elements with connection between them.

Concerning the horizontal displacement profile of the tested walls, the main difference between the URM and the strengthened specimens remains on the mobilization of the spandrel beams and adjacent elements. Actually, from Figure 2.16 b), it is clear that while for the S_01 case the displacement at the end of the spandrels is almost null, for the strengthened specimens the wall was globally involved through bending along its length (this applies even for the S_01R where the strengthening was applied just in one spandrel and the S_01R2 where there was the absence of one spandrel). Therefore it is possible to conclude that the applied technique for improving the out-of-plane behaviour of stone masonry walls is effective and actually contributes for the local and global behaviour enhancement of the façade ensuring homogeneity and continuity.

The influence of strengthening schemes, in terms of energy dissipation capacity and integrity of the masonry walls, can be inferred from Figure 2.17 and Figure 2.18. The later, in particular, refers to the efficiency of each scheme conveyed by the ratios between values obtained for strengthened solutions and those from the original situation. Figure 2.17 clear shows that the URM case (S_01) is not able to exhibit adequate seismic behaviour due to the lack of energy dissipation and displacement capacity (underestimated because no cycles were performed). By contrast, however, the CN wall exhibited some energy dissipation (due to the cyclic behaviour) though with reduced displacement capacity and extensive damage when compared with the strengthened specimens. It should be referred the linear branch exhibited by the S_01R2 and S_03R after reaching Δ/t = 0.10 (100mm and 75mm, respectively), highlighting a proportional relation between displacement and energy dissipation capacity originated by the rigid body rotation. The S_01R2 strengthening scheme is definitely the most effective when compared among the others as evidenced in Figure 2.18, regarding displacement, strength and energy dissipation capacity.
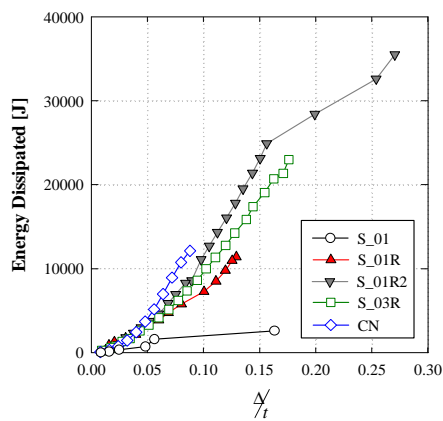
Figure 2.17. Displacement vs. Dissipated energy.
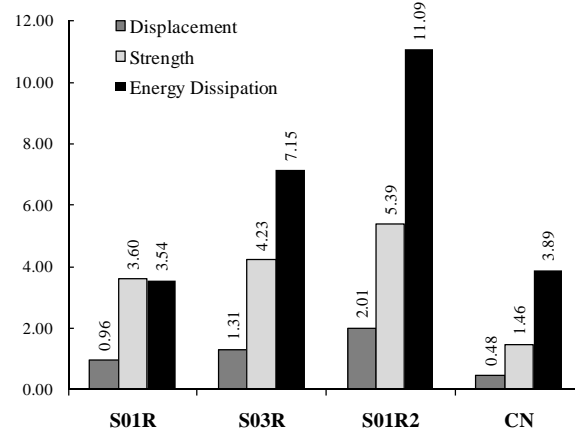
Figure 2.18. Comparison of strengthening schemes efficiency against S_01 result.

2.5.1.3.   Remarks on efficiency and adequacy of adopted strategies

The above included results allow concluding that the proposed strengthening/rehabilitation/retrofitting interventions, most of them actually executed after the 1998 Azores earthquake, are effective and can be recommended for future interventions on existing buildings.

Despite the fact that experimental evidence supported the efficiency of the different strengthening techniques presented in section 2.4, a final decision on which technique should be used must involve an analysis of efficiency *vs.* cost aiming at maximizing the performance with lower costs.

Such an exercise was made by considering a ranking interval of 1 to 5 defined for the following four evaluated parameters: maximum strength; displacement capacity; energy dissipated and strengthening intervention cost (the later taken from Table 2.1). The analysis is comparative between each strengthening technique and the original wall (S_01) and develops as follows.

The best performance among the three strengthening techniques for each parameter is assigned a value of 5, while the worst performance (given by the unreinforced specimen) takes the grade value of 1; for the other remaining wall the grades are linearly interpolated. The overall ranking R_k of each strengthening solution is defined by Eq. (2.1), where d_k, F_k, E_k and C_k are, respectively, the ranking obtained for maximum displacement, strength, energy dissipated and intervention cost. The factor P represents the influence of cost in the final decision. The partial and final average ranking values are listed in Table 2.3, while the impact of intervention cost in the overall ranking R_k (which might support the final decision) is represented in Figure 2.19.

$$R_k = (1-P) \cdot \frac{d_k + F_k + E_k}{3} + P \cdot C_k \qquad (2.1)$$

Table 2.3. Strengthening efficiency evaluation

Wall	Disp. (d_k)	Strength (F_k)	Energy (E_k)	Average ranking	Cost (C_k)
S_01R	1.00	2.96	1.26	1.74	4.91
S_03R	1.51	3.68	3.05	2.75	5.00
S_01R2	5.00	5.00	5.00	5.00	1.00

Table 2.3 and Figure 2.19 show that, despite the best performance of wall S01R2 given by the overall ranking, the high cost of this strengthening operation does not lead to the most effective solution for a cost influence higher than 35%; in that case, the S_03R solution, consisting of reinforced connected plaster with effective connection to returning walls, is the preferable one.
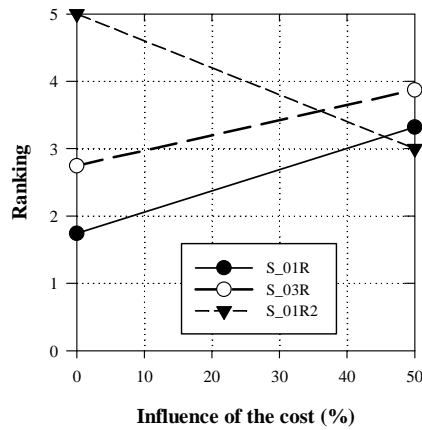
Figure 2.19. Impact of intervention cost in the final strengthening ranking

However, it is worth noting that the adoption of these techniques might not be an immediate and/or straightforward decision because, on the one hand, they should be applied respecting the historical and culture existence of each individual construction (which may not be compatible with the intrusive nature of subjacent to these types of interventions) and, on the other hand, if the structure cannot fulfil the minimum requirements to sustain earthquake actions with an accepted damage level or ensuring life safety, the notable improvement of seismic resistance obtained by these techniques should be considered for reducing economic and life losses.

Finally, regarding the adequacy and efficiency of the adopted experimental test setup, it is possible to infer that despite the difficulties inherent to the first test, the other experiments were able to provide a comprehensive assessment of the out-of-plane behaviour of stone masonry walls with strengthening techniques (giving estimates of the maximum and ultimate strength,

the ultimate displacement with complete discretization of the post peak behaviour and the energy dissipation), fulfilling completely the main goal of this work.

2.5.2. In-plane test

In this subsection the in-plane test experimental results are described, on the one hand to high-light the capability of this *in-situ* test setup to assess the in-plane behaviour of masonry piers subjected to their natural conditions and, on the other hand, to comment on the observed be-haviour and to infer some conclusions regarding the in-plane behaviour of this type of ma-sonry.

Figure 2.20 depicts both the observed behaviour of the masonry pier during the experimental test in terms of force *vs*. displacement curve and final cracking pattern, where positive dis-placements stand for wall pushing. It is possible to observe that the global wall behaviour was characterized by diagonal cracking and shear sliding, wherein the major cracks developed since the test beginning and enlarging until the last phase. The asymmetry obtained on the response is correlated to the different cross section mobilized for positive or negative displacements.

The main results obtained from the experimental test are presented in Table 2.4, where $d(F_{cr})$ is the drift corresponding to the first crack, F_{max} is the maximum strength, $d(F_{max})$ is the drift level corresponding to F_{max}, μ_Δ is the displacement ductility, F_e is the yielding force from the bilinear approximation curve, d_e is the yielding drift of the bilinear and d_u is the ultimate displacement defined for a drop of 20% in terms of strength.

A bilinear idealization of the response was performed using the Italian Code proposal and pre-sented by Frumento *et al.* (2009) for $F_e = 0.7 F_{Max}$ and considering $d_u = d(F = 0.8 F_{max})$, where F_e represents the intersection point between the two curves (the experimental envelope curve and the bilinear one, as explained in Frumento *et al.* (2009)).

According to this procedure, the displacement ductility $\mu_\Delta = 5.5$ is obtained, a value considera-bly high for old stone masonry (often suggested as $2.0 \leq \mu_\Delta \leq 3.0$). However observing the curve in the negative sense, a value within this range would be appropriate. Unfortunately it was not reasonable to compute the bilinear idealization of the response for the negative sense because a strong nonlinearity (Figure 2.21) with significant residual displacement was observed ($d(F_{cr})$ = 0.008% drift) since the very beginning of the test which affects the results for the bilinear curve leading to unrealistic values (e.g. after the first positive cycle, for $d = 0$ mm, $F = -10$ kN).

(a)   (b)
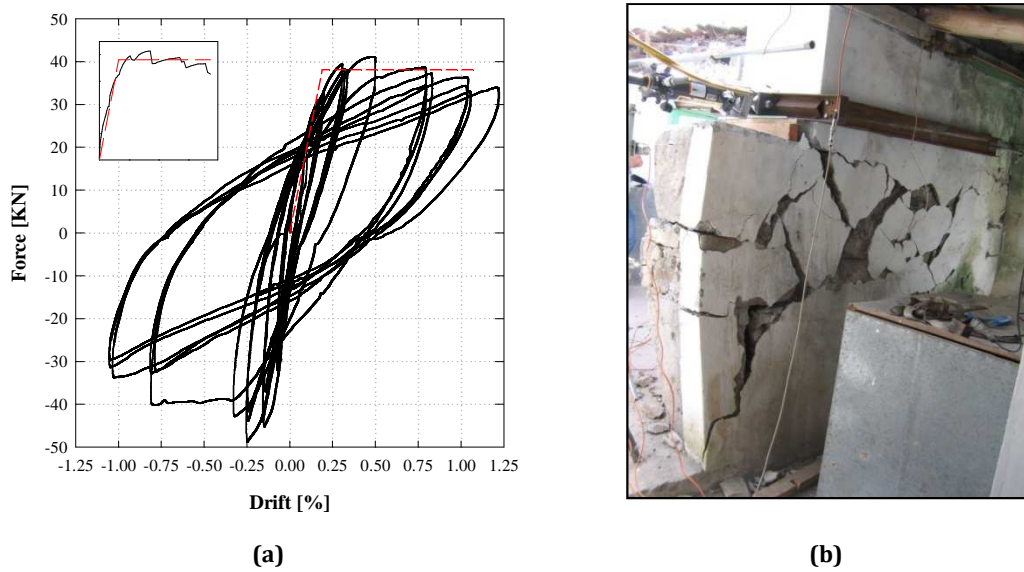
Figure 2.20. In-plane test result: a) hysteresis loop with bilinear idealization; b) final cracking pattern.

Table 2.4. Summary of the experimental evidence for in-plane test

	$d(F_{cr})$	F_{max}	$d(F_{max})$	μ_Δ	F_e	d_e	d_u
Positive	0.008 %	41.4 kN	0.5 %	5.5	38 kN	0.19 %	1.1 %
Negative	-	47.8 kN	0.23 %	-	-	-	0.82 %

Another interesting and useful result for assessment purposes is the definition of the elastic properties and effective stiffness. From the experimental evidence, it was possible to define the initial stiffness (computed through the experimental data) and to compare it against an ideal elastic stiffness computed for a cantilever taking into account the flexural and shear stiffness. The initial elastic modulus value was adopted as 0.2 GPa (as found by Costa (2002)), using a shear modulus ratio of $G = 0.3\ E$, which leads to the final values presented in Table 2.5 that adequately match the proposed initial values.

Table 2.5. Material properties and stiffness evaluation

E (MPa)	G (MPa)	K_{ini} (MN/m)	K_{ini}/K_{el}	K_{eff}/K_{el}
0.23	0.07	40.8	101.3 %	28.6 %

The effective stiffness ratio was computed using the effective stiffness obtained with the bilinear approximation of the response and the elastic stiffness. It is interesting to note that the value obtained was around 30%, thus considerably different from the usual assumed ratio of 50% used for current practice, which leads to considerable differences from the observed behaviour as shown in Figure 2.21.

In order to observe the evolution of hysteretic behaviour during the test, Figure 2.22 presents the evolution of the equivalent hysteretic damping computed by Eq. (2.2) and presented initially by Shibata and Sozen (1976). In this expression, A_h refers to the area inside one loop, while F_m and d_m are, respectively, the maximum force and maximum displacement achieved in the same loop.

$$\xi\left(\%\right) = 100 \cdot \frac{A_h}{2\pi F_\mathrm{m} d_\mathrm{m}} \tag{2.2}$$
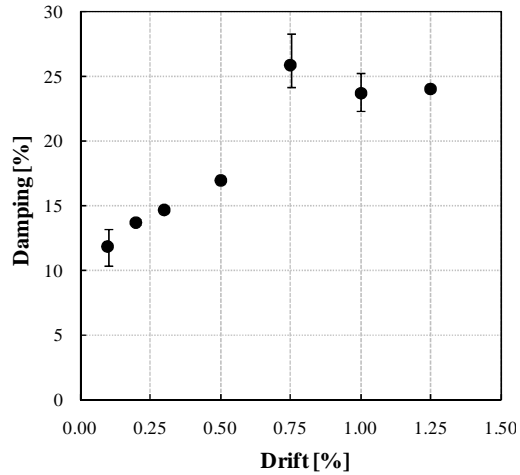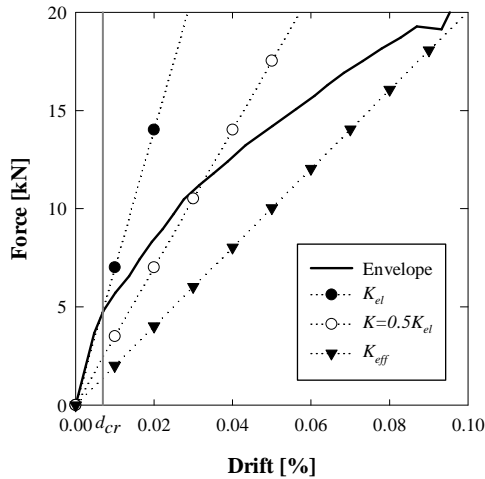
(*) For a drift = 1.25% a symmetric behaviour was assumed due to the absence of response in the negative sense.

Figure 2.21. Evaluation of elastic and effective stiffness against experimental evidence.

Figure 2.22. Drift vs. equivalent hysteretic damping.

The evolution of hysteretic damping through the test is very interesting. Even for small drift values as 0.1%, the hysteresis is significant leading to an equivalent hysteretic damping value of 12% mainly explained by permanent deformations developed at the joints already for small displacement levels. It is a considerably high value which is not usually associated to this type of material (double leaf stone masonry with poor infill). The evolution of hysteretic damping is almost linear with the evolution of drift up to the formation of a complete diagonal crack to the foundation which occurred for the drift cycle of 0.75%. Therefore it led to significant residual deformations along the wall and an equivalent hysteretic damping level of 26%. The final part

of the test (drift of 1.0% and 1.25%) shows a constant hysteretic damping level close to 25% as a result of the severe damage observed and permanent deformations of the wall.

2.6. CONCLUSIONS

The work presented in this chapter described a complete *in-situ* test campaign which aimed at characterizing the out-of-plane behaviour of stone masonry walls and strengthening solutions already applied and recommended in current codes, starting from the presentation of the test setup up to detailed analyses and comparisons of the obtained results. For these purposes, an experimental test setup was developed and described as a useful and feasible procedure to help on understanding the in-plane and out-of-plane behaviour of existing constructions on their original conditions. The developed test setup allows performing cyclic tests on a displacement controlled way by using as reference positions the measurements of displacement transducers completely independent of the actuation system.

Despite some drawbacks of *in-situ* experiments, mainly related with logistics and less controlled environment, the adopted test setup based on a self-equilibrated action-reaction scheme provides a means of characterizing adequately masonry elements (or even other type of elements) in their original *in-situ* conditions, thus contributing to the reduction of uncertainties associated with laboratory experimental tests. However the developed test setup has also some drawbacks concerning the actuation and control system (mainly related to the flexibility of the reaction structure) for which a few pertinent comments are included concerning the conditions for using this setup.

The practical applicability and efficiency of the test setup was evidenced by a large set of experiments already performed with the proposed system, though not all referred herein. Quite consistent results were obtained confirming the feasibility and features of this type of experiment, with particular emphasis on the possibility of performing displacement controlled cycles and achieving complete post peak behaviour with strength degradation up to the imminent collapse of the specimen.

Five out-of-plane tests were addressed here, both on original and strengthened specimen walls. For these tests, besides force-displacement comparison, another interesting comparison of strengthening schemes in the form of cost *vs.* benefit analysis is presented taking advantage of the experimental data obtained during the tests which yielded a detailed characterization of the out-of-plane behaviour of *sacco* stone masonry walls.

This setup was also applied to one in-plane test in order to demonstrate the applicability of this setup to other purposes, for which the obtained result analysis is included and compared to present recommendations from literature.

Finally, it is worth mentioning that, beyond preliminary preparations of the tested houses and posterior wall strengthening works, the tests were carried out with a reduced staff (five persons). Each test included all the specimen's preparation, installation of actuation system and instrumentation; just out of curiosity, the total time allocated for each test was between one or two days, including all the inherent activities.

Chapter 3.

OUT-OF-PLANE BEHAVIOUR OF EXISTING STONE MASONRY BUILDINGS: EXPERIMENTAL EVALUATION

SUMMARY

Masonry structures can be considered as the simplest type of structures concerning its assemblage but, at the same time, it is one of the most complex construction materials in terms of mechanical properties and correct behaviour assessment. In this context, the work herein presented aims at describing an experimental testing campaign recently carried out in order to characterize the out-of-plane behaviour of traditional masonry constructions.

Taking advantage of the existence of a traditional two-storey masonry building abandoned after the 1998 Azores earthquake, several *in-situ* tests were defined and performed with the application of quasi-static cyclic loads at the building top level in the out-of-plane direction. In addition, the efficiency of retrofitting and/or strengthening techniques applied during the 1998 Azores reconstruction process was also experimentally evaluated.

Finally, an overall discussion of these techniques is presented, resorting also to previous tests' results carried out in Chapter 2, aiming at inferring and suggesting quantifications of strengthening techniques' contributions for future interventions on existing buildings. For this purpose, simple analytical mechanical approaches were adopted in order to provide numerical estimates of strength that were found in good agreement with the experimental results.

3.1. INTRODUCTION AND MOTIVATION

Experimental studies are widely recognized as fundamental contributions for a correct characterization of structural components taking into account its constitution, behaviour, mechanical characteristics and so forth. This is true for all types of buildings, although for current materials and constructive techniques (essentially based on reinforced concrete and steel) the experimental information can be considered at a much developed and stable level. However, although it accounts for a quite significant part of the built stock, the masonry construction (and the traditional stone masonry in particular) still remains with important lack of experimental characterization because it is strongly dependent on its constitution, materials, constructive process and actual connection conditions between different structural elements.

This lack of reliable experimental parameters for traditional masonry characterization, combined with its significant vulnerability evidenced during seismic occurrences in several locations around the world in general (and in the Azores islands in particular, as focused in this work) has led to a progressive discredit of the potential of traditional stone masonry construction. However, despite these serious shortcomings, still that technique presents other quite relevant advantages concerning physical aspects of construction (e.g. hygrothermic and acoustic behaviour), as well as environmental, energetic and socio-cultural.

Thus, considering also the economic importance of achieving standards of sustainable construction, namely by reducing the massive construction with reinforced concrete and steel that involve high energy costs in areas of small buildings, it is easy to accept the great relevance of obtaining credible and realistic experimental results on the actual behaviour of traditional masonry structures, particularly in important seismic zones.

Bearing this in mind, the work presented herein focuses on an experimental campaign performed on an existing full scale two storey building damaged during the 1998 Azores earthquake, where the out-of-plane behaviour of masonry panels was assessed through experimental tests.

3.2. EXPERIMENTAL TESTING: FRAMEWORK AND DESCRIPTION

3.2.1. Out-of-plane action and response in masonry panels

Seismic excitation introduced at structural supports spreads in height through the vertical elements, which, in the case of traditional construction essentially consists on masonry walls. This action is responsible for the mass excitation of the various components of the construction (structural or non structural), developing inertia forces that must be opposed by ex-

isting bearing elements. If this is not possible due to strength characteristics of these elements, then global structural collapse is likely to occur, enforcing the energy input imparted to the system to be balanced by kinetic, potential and dissipation energy associated with the collapse motions. This energy balance at global level also holds at the local level of each structural element and sub-structures likely to transform into mechanisms during the seismic action. This is typically the case of masonry panels' failure, due to the excitation of local modes in specific parts of a structure that may even lead to its partial or total collapse.

The first aspect is normally associated with large panels, typically façades or panels at floor levels or in between floors, among others as reported in existing studies (D'Ayala and Speranza (2000); Neves *et al.* (2007); (Neves *et al.* 2012)). The second issue is related with the local collapse of walls, that can also lead (or not) to the partial or total collapse of the structure, which mainly depends on the structural typology and its redistribution capacity.

However, the out-of-plane collapse of masonry panels most often occurs due to instability of elements rather than by exceeding the bending strength limit (which is bounded by the compressive strength of the panel compressed zones); in that sense, the capacity of displacement accommodation becomes the dominant parameter of the seismic behaviour analysis.

One of the objectives of out-of-plane testing in masonry panels is to properly understand and simulate the effect of the seismic action. However, because the mass of these walls is horizontally and vertically distributed in the panel, the testing systems used inside laboratory environments have resorted to shaking tables (mainly on reduced scale specimens, e.g. Bothara *et al.* (2010), and rarely on full scale ones, (e.g. Magenes *et al.* (2010a)) or, alternatively, to the use of airbags (e.g. Griffith *et al.* (2007) for lab experiments and Derakhshan (2011) for field tests) or water bags (e.g. Mosallam (2007)) aiming at reproducing the distributed inertia forces resulting from seismic excitation.

Nevertheless, the application of forces concentrated on the panels is also a commonly used technique in order to overcome the complexity inherent to the above described techniques. Thus, the action is simulated by the application of specific loads in order to impose out-of-plane deformation in the panel, where the number of loading points depends on the type of test to be carried out. Usually a linear load is applied in the case of vertical bending, one or two linear loads in the case of horizontal bending and four loads in the case of bi-axial bending, as used respectively by Willis *et al.* (2004), Dusi *et al.* (2007) and Penna *et al.* (2007).

Despite the limitations of out-of-plane experiments on masonry panels with concentrated load at the top, it is the simplest technique to be implemented *in-situ* because it involves a relatively simple and compact apparatus and reduced total weight of the testing system, as reported in Chapter 2.

3.2.2. Test setup used for in-situ experiments

The methodology used to perform the desired *in-situ* tests falls in the same research line of previous research works presented in Chapter 2, using the self-equilibrated testing scheme reported in Chapter 2, wherein the actuator is placed inside a given building perpendicularly to the wall specimen to be tested, in order to impose monotonic or cyclic out-of-plane loads under controlled displacement conditions. The reaction to the actuator is provided by the so-called "back wall", thus configuring a self-equilibrated system which does not required any external reaction structure.

External reference frames to the actuation system should be used to attach the monitoring devices in order to obtain absolute displacements of the complete structure, which are used as input to the actuator's control algorithm (PID in the present case).

Figure 3.1 represents the application of this testing scheme to the structure reported in this work where it is possible to observe its simplicity. The experimental tests were monitored with draw-wire displacement transducers mounted on an auxiliary structure (yellow scaffold in Figure 3.1 a)), allowing measuring the out-of-plane movements of the façade.

For the various tests the displacements were monitored on a number of points arranged according to a T-configuration in each wall (façade and back wall), where at least three points were placed horizontally, plus a minimum of two others on the vertical axis of the masonry wall under testing. A load cell was placed at the extremity of one actuator in order to measure and control the total load applied to the walls. The monitoring scheme will be presented in more detail in the following section.

Displacements were imposed with multiples of 6 mm (1/100 of the wall thickness) until one of the following requirements were fulfilled: i) strength degradation of 20% relative to the maximum measured strength exhibited; ii) instability or safety conditions no longer ensured.

(a)   (b)

Figure 3.1. In-situ actuation system for the tested building: a) CS_01 test; b) preparation of the CS_02R test

3.2.3.   Structure and tested panels

The structure tested and reported herein is a two-storey house which had a partial collapse of the roof during the 9th July 1998 earthquake in *Faial* island, *Azores*. The house tested during the experimental campaign reported in this work is the same house used for the field experimental tests presented by Costa (2002) back in 2001.

The building (presented in Figure 3.2) is located in a place called *Canada do Sousa* (*Canada* means a small road surrounded by canes) near the east entrance of *Cedros* village. It consists of a typical construction of the area, made of well trimmed stone blocks materializing double leaf with poor infill stone masonry walls (*sacco* masonry) with adequately interlocked corners and regular horizontal stone courses where large sized stones alternate along the wall length with other stones (connectors) to link the two leafs of the wall. This two storey house has a total height of 5.0 m, with a wide ground-floor normally used for agricultural purposes and the upper floor for housing with outside stairs. The bottom part has two doors and a large opening that breaks the façade symmetry at that level (observable in Figure 3.2 d)); three windows in symmetrical positioning are located at the upper façade level. Laterally, the house has almost "blind" triangular gables providing partial support to the former existing roof that was made by two planes inclined towards the main and backwards façade. The house is partially buried since the natural soil level in the back wall is well above the wall foundation (as shown in Figure 3.2 b)), contributing as a very important factor for greater resistance of this wall when compared with the main façade.

The house is made of regional volcanic trachyte, consisting on stone masonry walls with dry joints, thus without any type of mortar; the wall stability is essentially ensured by gravity and does not present any kind of coating, outside or inside. Based on the traditional

constructive practice of that rural region, the flooring structure would probably have consisted of wooden rafters with floor boards. The roof (although no longer present) should have been made of wooden rafters supported on the main and back walls supporting ceramic tiles. It was only possible to see evidence of tile mortar in their connection to the walls.

(a)

(b)

(c)

(d)

(e)
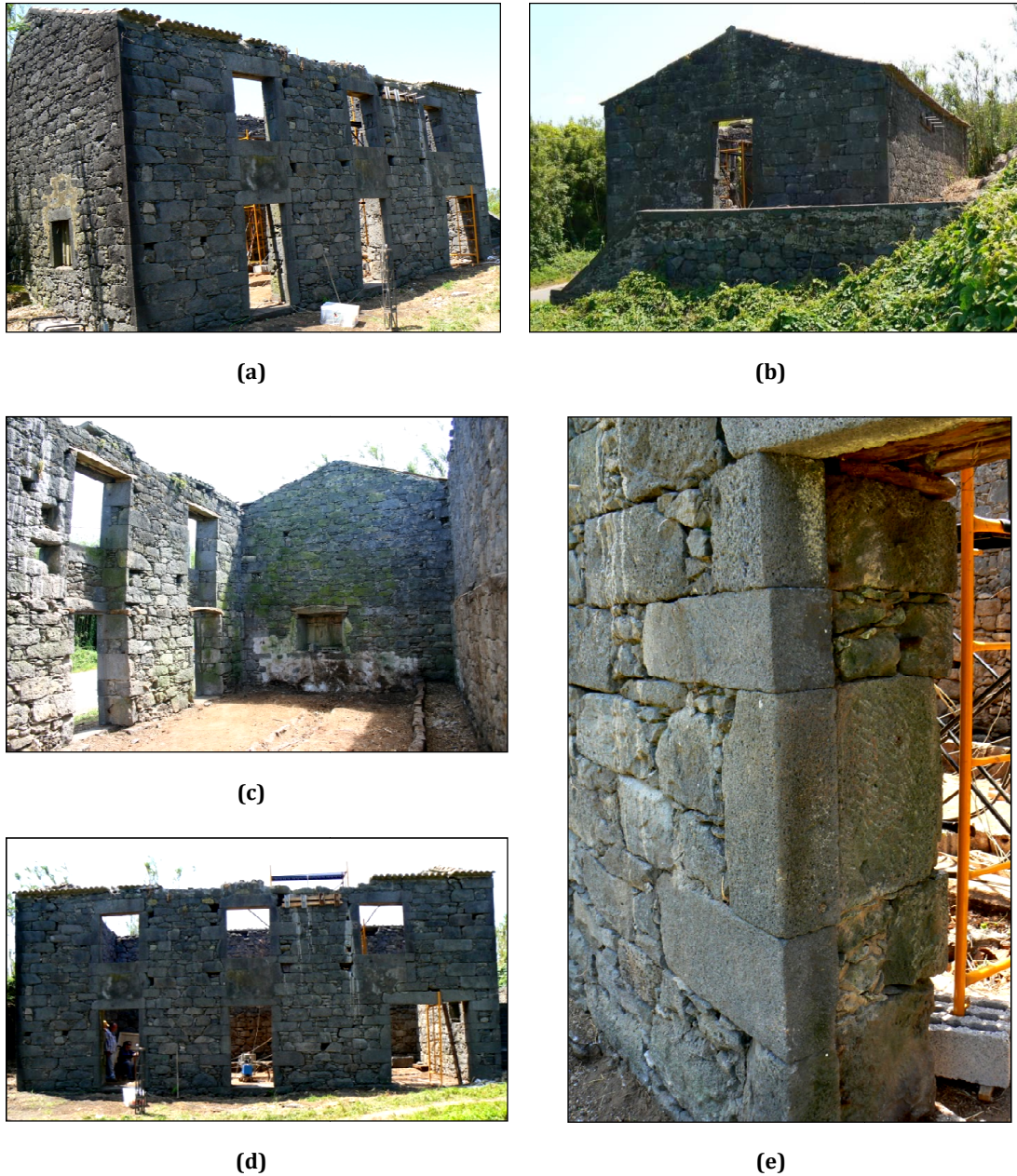
Figure 3.2. *Canada do Sousa* building (CS): a) Southeast view; b) Northwest view; c) interior view; d) main façade; e) detail of wall's typology and assemblage

Figure 3.3 shows all the dimensions of *Canada do Sousa* (CS) building as well as the position of the actuators. It should be referred that two panels with similar characteristics were tested, namely CS_01 and CS_02, presented also in Figure 3.3 a) and b). As it will be presented in section 2.4, these panels were strengthened leading to a total number of 4 tests denoted as

CS_01, CS_01R, CS_02S and CS_02R, where "R" stands for retrofit and "S" means strengthened specimen.

As mentioned in the previous section 3.2.2, out-of-plane movements were monitored with displacement transducers attached to an external reference frame. Figure 3.3 presents the monitored points for test CS_01 and CS_01R, similar to the monitoring apparatus used for CS_02R with the transducers shift towards CS_02 panel. The points monitored during the CS_02R included also points on the returning wall, attempting to evaluate the influence of the connection to these wall in the final results, but negligible displacements were measured.
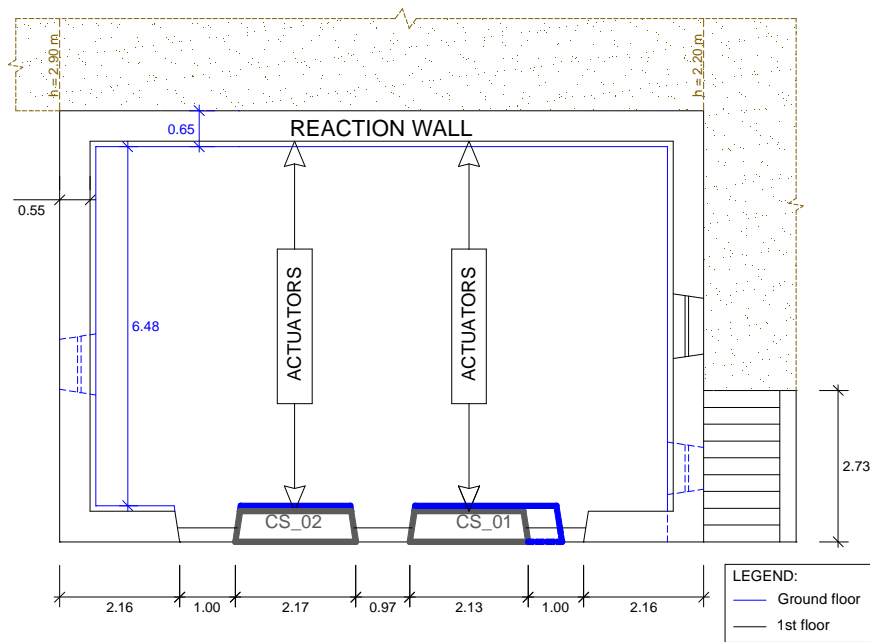
(a)
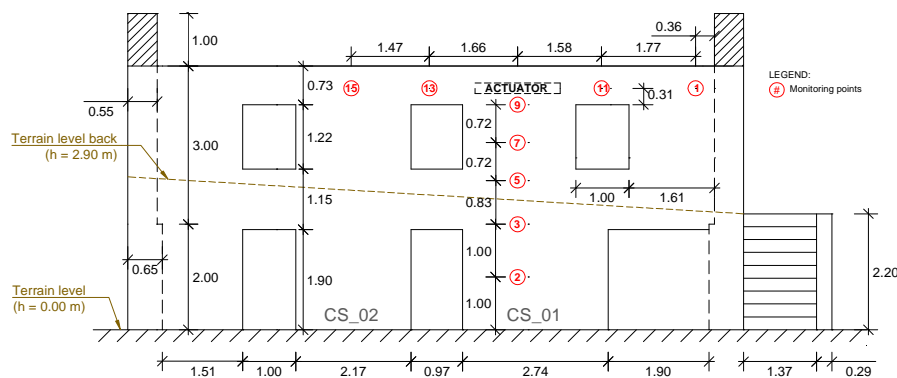
(b)

Figure 3.3. *Canada do Sousa* **(CS) building: a) plan view with the position of the actuators for tested panels CS_01 and CS_02; b) main façade with position of the monitoring points for CS_01 and CS_01R tests**

3.2.4. *Strengthening techniques*

The experimental campaign aimed at characterizing the out-of-plane behaviour improvement of masonry walls resulting from the use of strengthening techniques. The tested techniques were based on recommendations issued after the 1998 Azores earthquake (Carvalho *et al.* 1998) and also suggested in Costa and Arêde (2006). The main objective of the different strengthening schemes is based on the achievement of the efficiency of connections between horizontal and vertical elements.

As mentioned before and referring to Figure 3.3, a total number of 4 tests were performed: 1 test in the original wall (CS_01 test); 1 test in the CS_01 retrofitted panel (CS_01R test) and 2 tests in the CS_02 panel (CS_02S and CS_02R).

The first strengthening scheme consisted on the strengthening of the connection between the wall and the roof through a mechanical system, similar to that illustrated in Figure 3.4 b) and schematically shown in Figure 3.6. The connection makes use of mild steel folded plates (that should materialize a ring beam) fixed by tie rods to connect both walls' leaves and screwed connections between these folded plates and other vertical steel plates which are nailed to the wood beams supported by the horizontal ring beam.

The second one (depicted in Figure 3.4) relied on the adoption of an effective connection between the wall and the top wooden beams as well as a connection at the first floor level with the inclusion of the wooden floor pavement. The connection to the wall was similar to the connection between the wall and the roof, possible to observe in Figure 3.4 b).

| (a) | (b) |
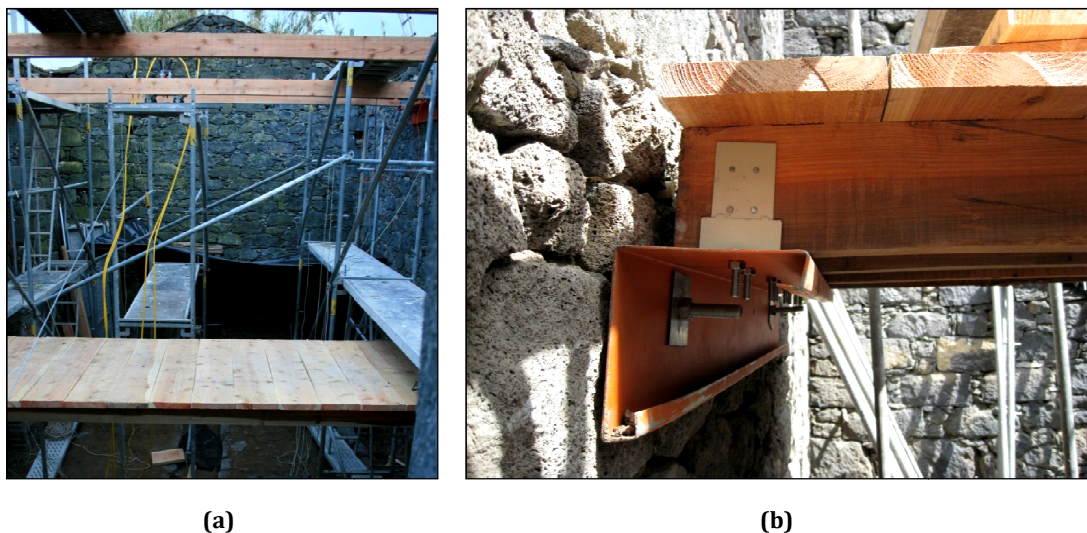
Figure 3.4. Strengthening applied on CS_01R test: a) general view; b) detail of the connection at 1st floor level

The third and last technique tested in the Canada do Sousa house (Figure 3.5) aimed at assessing the efficiency of a corner strengthening on the walls' out-of-plane behaviour. For this reason, a scheme commonly applied nowadays mainly in the centre/south of Portugal, more particularly in Lisbon, was applied consisting on the application of a reinforced plaster at the interior wall's face with connectors to the outer leaf. Although this connection to the outer leaf is commonly made using connectors grouted within the interior of the wall, for the purpose of the experiment herein described a different (and simpler) mechanical connection was applied resorting to small L-shape steel bars embedded at joints' level to provide external anchorage for the transverse connector rods, as evidenced in Figure 3.5 b).

(a)   (b)
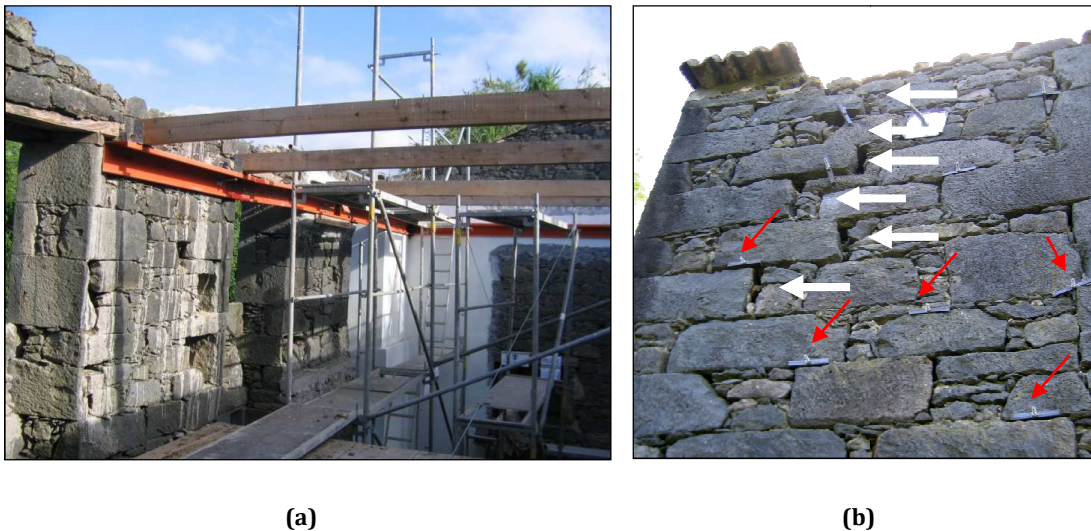
Figure 3.5. CS_02R test: a) internal view; b) southeast corner: Leaf connector's detail (red arrows) and observable damage after CS_02S test with joint torsion along the corner (white arrows)

Since the objective was to study the corner effect on the wall behaviour, this strengthening scheme was just adopted on the corner, returning and back walls, leaving the tested specimen in the same conditions as for the CS_02S test, as presented in Figure 3.6. In this way, it was possible to quantify the wall behaviour improvement due to the corner reinforcement. It should be referred that, for the CS_02R test, the continuity of the folded steel shape at the roof level was ensured in order to behave as a ring beam connecting all the vertical elements and the horizontal ones. However the stiffness of this steel shape is small due to small web's thickness, which just corresponds to a very small increase on the total building weight.
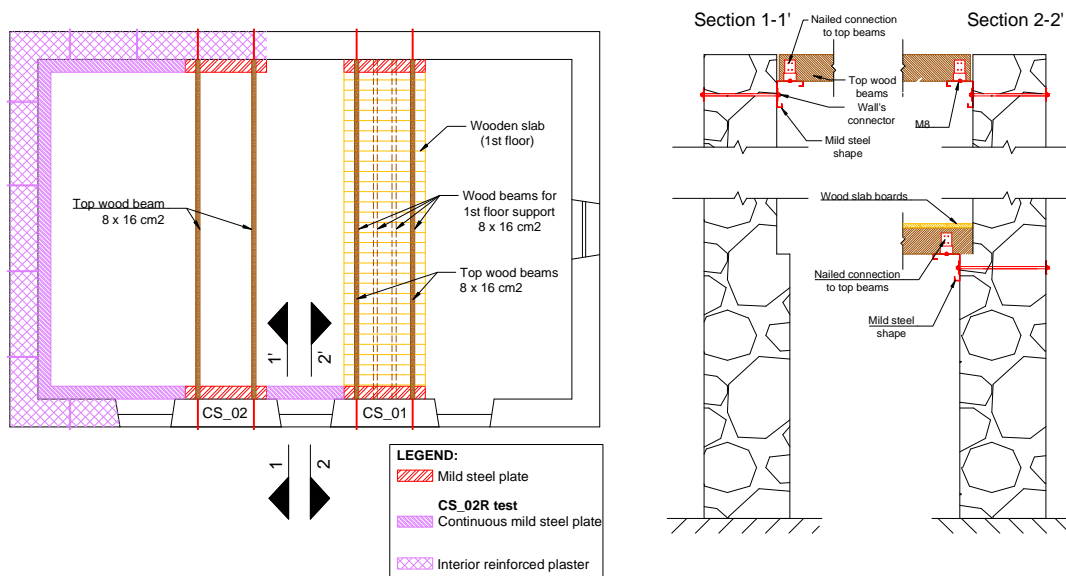
Figure 3.6. Representation of the location of the applied strengthening/retrofit techniques: left, plan view; right, section view: 1-1': CS_02S test; 2-2': CS_01R test

Table 3.1 summarizes the strengthening schemes tested during the experimental campaign, in order to clarify all the techniques used on each test. Moreover, taking into consideration that CS_01 and CS_02S panels were not repaired after the tests, CS_01R and CS_02R can be considered retrofitted specimens while CS_02S is a strengthening scheme directly applied on the original undamaged panel.

Finally, it should be referred that the chronological sequence of experiments was: CS_01; CS_01R; CS_02S; CS_02R.

Table 3.1. Summary of the applied techniques

Technique	CS_01R	CS_02S	CS_02R
Connection between walls and roof	x	x	x
Connection at 1st floor level	x		
Corner strengthening with interior reinforced connected plaster and continuous steel shape			x
	retrofit	strengthening	retrofit

3.3. RESULTS AND DATA INTERPRETATION

The large in-plane and height dimensions of the tested building enforced several concerns regarding equipment and technicians. Therefore, the experiments performed in *Canada do Sousa* were not accomplished until a desired strength decrease of 20%, as commonly

adopted for lab experimental tests. For the case of the performed experiments, safety conditions of material and technicians prevented continuing the experiments until the desired strength decrease. This was relevant especially for the CS_01R test because the test was stopped in the early stages due to damage concentration at the spandrel beams.

For the CS_02S and CS_02R tests, the maximum displacement level achieved was the same as for the unreinforced specimen (CS_01), thus permitting direct behaviour's comparison between unreinforced and strengthened/retrofit specimens. However, no further displacement levels were imposed in order to ensure safety conditions for dismounting the test setup.

It should be referred that the results for inward movements (negative displacements) of the strengthened specimens were affected by the influence of the top wooden beams prone to buckling; therefore, the results cannot be totally and directly compared amongst the different tests.

Figure 3.7 a) presents the force vs. top displacement curves for the performed experiments, while Figure 3.7 b) includes the envelope curves of the experiments for outward movements.

The first observation perfectly visible in the obtained results is the significant strength increase exhibited by the strengthened specimens (more than twice). In particular, concerning the comparison of results for panels CS_02S and CS_02R, the later clearly exhibits a larger strength although it refers to a retrofitted panel based on the former after having been tested. This fact is mainly due to the efficiency of the horizontal folded steel plate which connects the panel to the returning wall. This can be confirmed by observing in more detail the descending branches of these two test plots, wherein some release of accumulated elastic energy can be found for the CS_02R case as demonstrated by the descending branch which it is not a vertical drop as in the CS_02S panel. Such elastic response component is likely to be due to the horizontal mild steel plate behaviour, which is also supported by the progressive strength increase of CS_02R when compared to CS_02S.

(a)   (b)
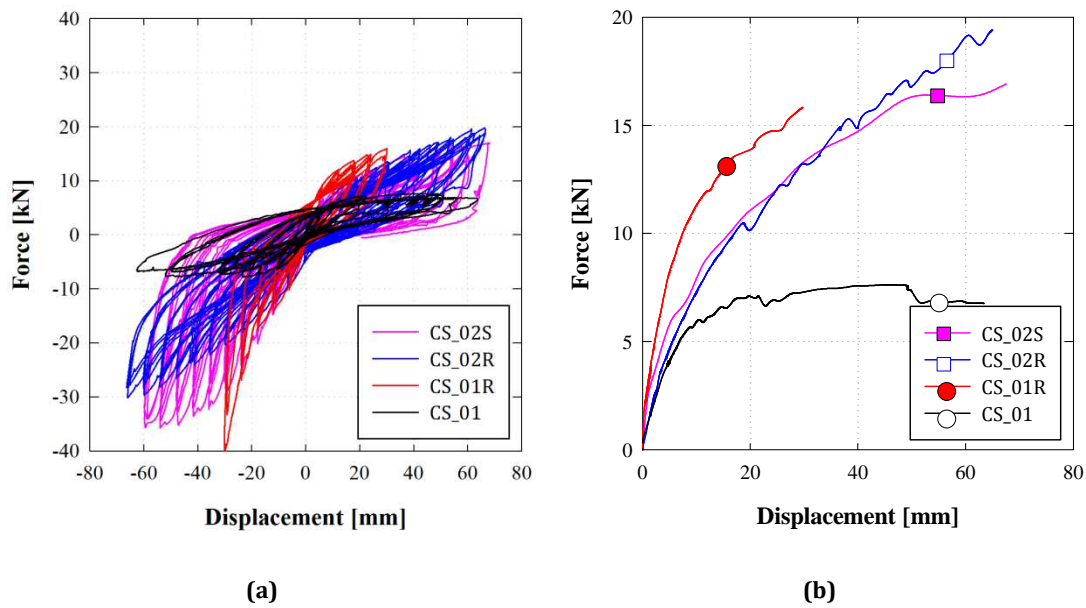
Figure 3.7. Force vs. displacement curves: a) full cycles; b) envelope for outward movements.

The initial stiffness exhibited by the CS_01R was significantly higher than that of the remaining specimens mainly due to the connection at the first floor level, as presented in Table 3.2 (values were computed from the obtained experimental curves) where it is also possible to observe similar initial stiffness between the original specimen CS_01 and the retrofitted one CS_02R, which is mainly related with the existing damage on the masonry spandrels (due to previous experiments) and the low stiffness of the used steel shape.

Table 3.2. Summary of the experimental results

	K_{ini} [kN/m]	F_{max} [kN]	d_{max} [mm]
CS_01	1013	7.6	63.7
CS_01R	3929	15.8	29.7 [*]
CS_02S	1747	16.9	67.6
CS_02R	1171	19.4	66.6

[*] Test stopped earlier due to safety reasons

The height wise vertical displacement' profiles during the tests are presented in Figure 3.8 and Figure 3.9, where it is clearly observable the influence of strengthening techniques on the distribution and concentration of damage along the wall height.
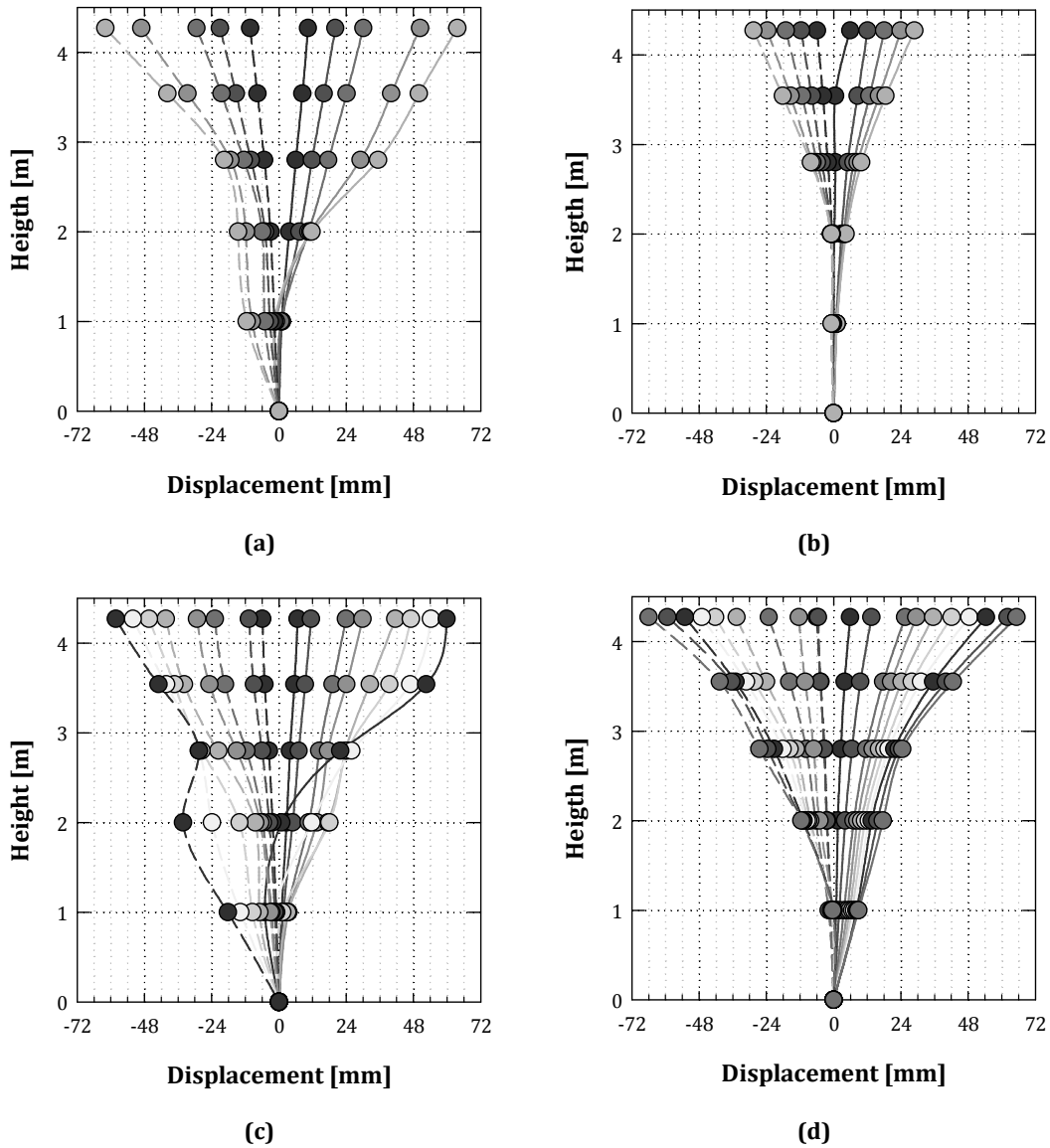
Figure 3.8. Height wise profiles of vertical displacements (positive outwards) for all tests: a) CS_01; b) CS_01R; c) CS_02S; d) CS_02R

In general terms, it is possible to conclude that, contrarily to what could be expected, the imposition of a concentrated load did not lead to damage concentration at the top of the wall where the force was applied. In fact, the walls were found to be globally mobilized, mainly behaving in flexure/rocking mode for the initial displacement range ($\Delta < \pm 24$ mm), while for increasing displacements the damage concentration at the 1st floor level (2.0 meters high) is notable for both CS_01 and CS_02S cases due to the variation of wall thickness. It should be also referred that CS_02S test led to significant crack opening along the edge between the main façade and the returning wall, as depicted previously in Figure 3.5 b).

As expected, CS_01R test showed that the presence of a connection at the 1st floor level avoided the aforementioned concentration of damage, because the wall rotation concentrated

above this level as observed in Figure 3.8 b). Indeed, this is even clearly identified in Figure 3.9, which includes a direct comparison between maximum displacements and average chord rotations (or drifts) among the different tests.

Finally, the continuity between vertical elements introduced in CS_02R case (with the inclusion of the mild steel plate) led to a more homogeneous distribution of displacement and damage along the wall height, as evidenced in Figure 3.8 d).

This effect is even clearer on Figure 3.9 b), where the height wise rotation increase is smooth. It should be also highlighted the rotation concentration at the bottom on CS_02S panel due to permanent deformations of the wall along the 1st floor.

(a)   (b)
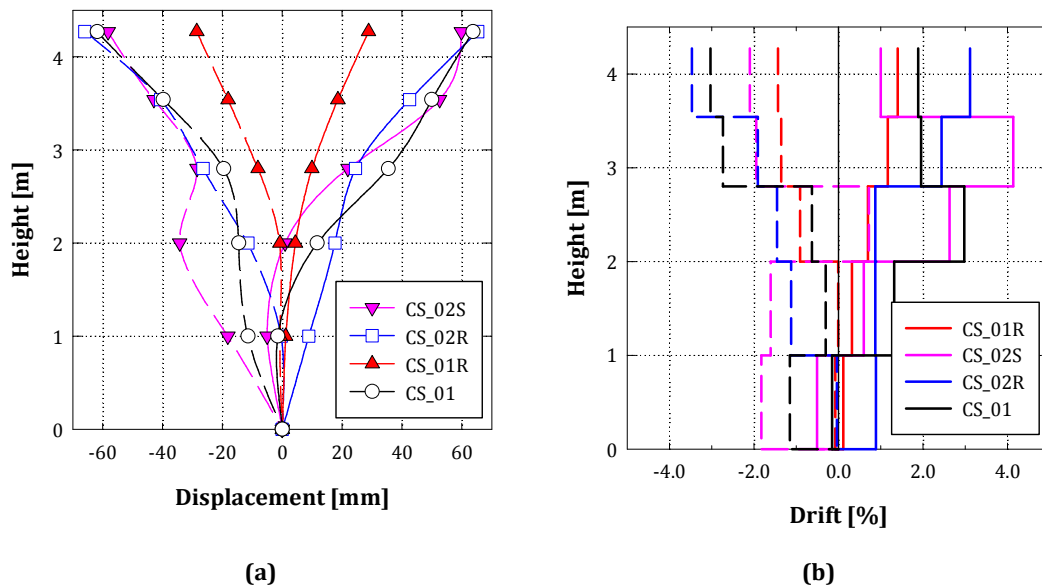
Figure 3.9. Vertical profiles for maximum wall deformations: a) displacements; b) drift.

From the observation of Figure 3.8 and Figure 3.9 it is possible to infer that CS_02R exhibited the most desirable behaviour with a more homogeneous distribution of rotations along the wall's height. Moreover, if horizontal displacements profiles are analyzed along the wall façade length (Figure 3.10, where the horizontal axis corresponds to the length of the main façade), the connection between tested panels and spandrels is found to influence the global behaviour of the wall. Once again, the effective connection along the wall top perimeter with the mild steel shape turned out possible a more adequate distribution of loads and therefore the measured displacements were smoother.

Finally, it is worth highlighting the damage observed on the top spandrel beam between panel CS_01 and CS_02, also identified on the measured displacements along its length (6.0 m).

(a)   **(b)**
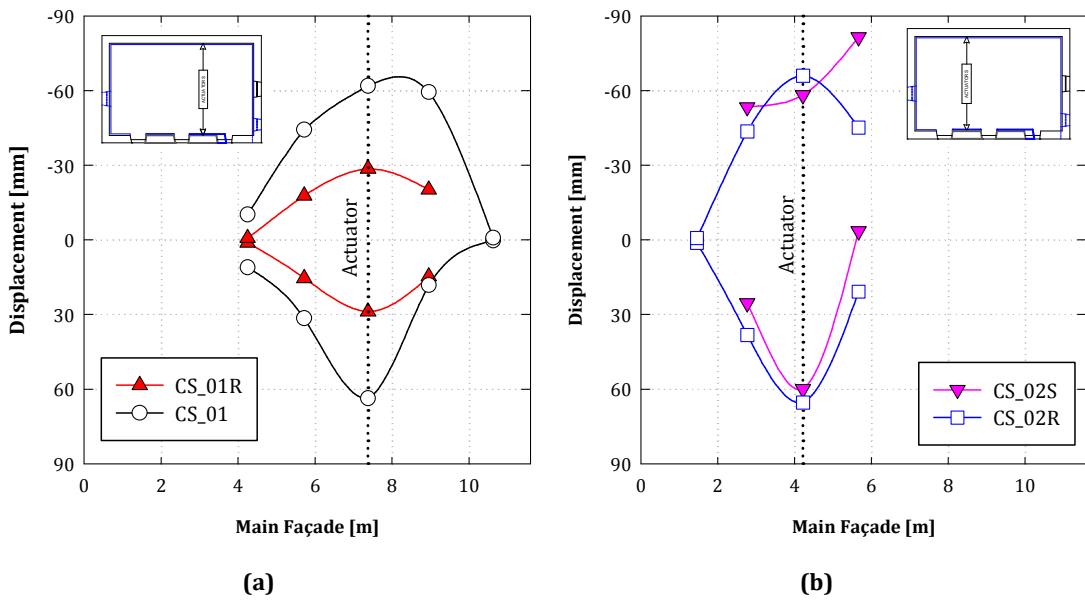
Figure 3.10. Horizontal displacements profile for maximum displacements (positive outwards)

Figure 3.11 a) presents curves of displacement Δ/t ratio vs. energy dissipation reached during the tests (where Δ is the measured displacement and t is the thickness of the wall), while Figure 3.11 b) shows a direct ratio between results from the strengthened specimens and the original wall (CS_01) in terms of energy dissipation, strength and displacement capacity. Since CS_01 and CS_02 are very similar panels, it is possible to compare directly the results of the corresponding tests.

(a)   **(b)**
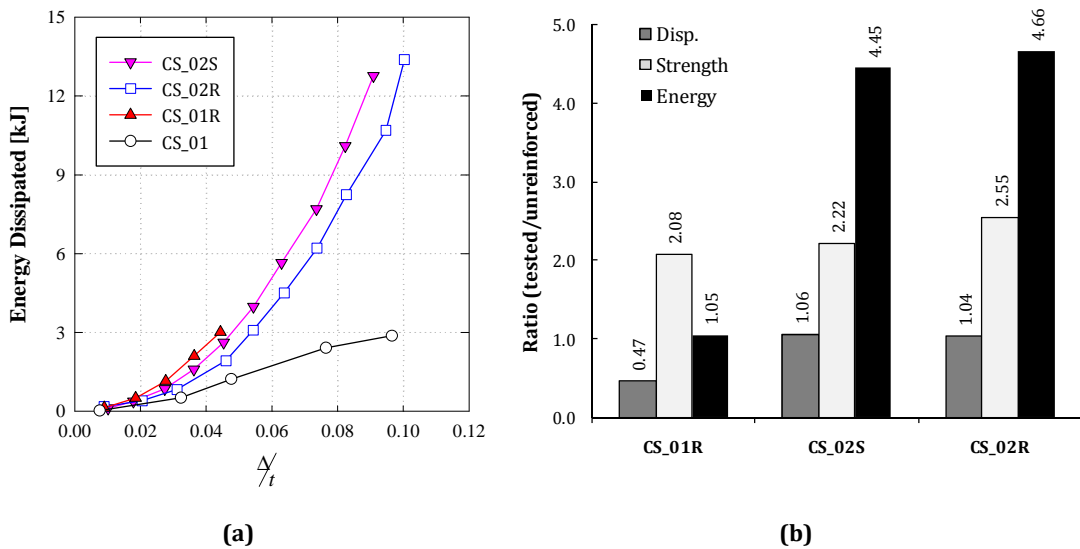
Figure 3.11. Comparison between experimental results: a) displacement vs. energy dissipation; b) global comparison against unreinforced specimen

The first conclusion that it is possible to infer from Figure 3.11 relates to the applied strengthening techniques' efficiency in terms of energy dissipation and strength. Moreover, it is

worth pointing out that, despite the smaller maximum displacement imposed during the CS_01R test (which, as mentioned before, was early stopped due to safety conditions) and contrarily to the other strengthened panels, the CS_01R specimen exhibited the largest energy dissipation for the same displacement level due to the presence of an efficient connection at the 1st floor level.

As a general conclusion, the strengthening techniques led to a minimum increase of 2x on panels' strength and 4x on energy dissipation capacity; note that, although without results for the same displacement level, the observed behaviour of panel CS_01R allowed concluding that the corresponding final values of both strength and dissipated energy were expected to be higher than the results obtained for CS_02S and CS_02R.

3.4. BEHAVIOUR ASSESSMENT AND EFFICIENCY EVALUATION

3.4.1. Overall comparison of strengthening schemes' efficiency

Since the experimental campaign herein reported is part of an extensive work developed, it is of great interest to compare different strengthening schemes used after the 1998 Azores earthquake and commonly used nowadays in pre/post earthquake intervention.

Bearing this in mind, the results previously obtained for a one-storey house and presented in Chapter 2 will be used together with the results included in the present chapter, aiming at inferring conclusions on the out-of-plane global behaviour of strengthened stone masonry panels.

The experimental results of those experiments made on the so-called *Salão* house are referenced with "*S*", where S01 stands for an unreinforced stone masonry panel, while S01R, S01R2 and S03R refer to panels retrofitted with different techniques. The main difference relative to the panels tested in the *Canada do Sousa* house is the application of reinforced connected plaster in all the strengthened panels.

Figure 3.12 and Figure 3.13 show the overall comparison between original and strengthened specimens in terms of energy dissipation, strength and displacement capacity. It should be referred that the hysteresis loops for the second set of results (herein included from Chapter 2) were obtained for the maximum displacement of the unreinforced specimen (S01, d_{max} = 108 mm) rather than the ultimate displacement.

(a)   (b)
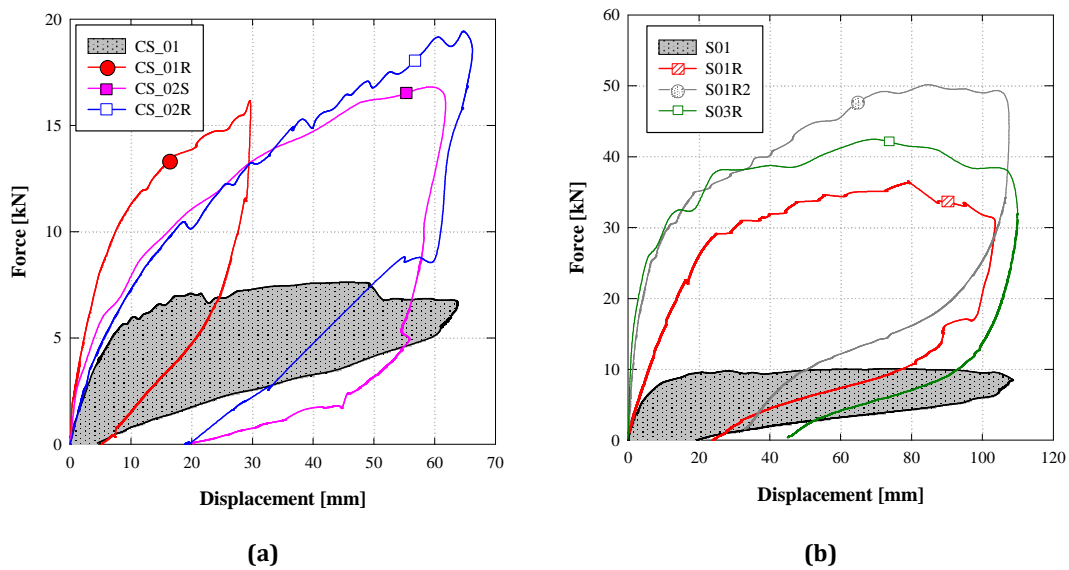
Figure 3.12. Envelope of the hysteresis loops until achievement of the maximum displacement of the unreinforced specimen: a) *Canada do Sousa* (CS) building; b) *Salão* building (S), from Chapter 2

Despite the differences on the dimensions and masonry type of the tested panels in the *Canada do Sousa* (CS) and *Salão* (S) houses, some general conclusions can be pointed out.

First, the presence of reinforced connected plaster led to higher strength and energy dissipation on the tests performed in *Salão* (S) when compared to those in *Canada do Sousa* (CS) although similar top roof connections were used in both buildings. However, it is worth recognizing that reinforced connected plaster is not the only technique providing better out-of-plane behaviour, and its use in some situations can be arguable (and possibly not usable), particularly in cases where the historical and cultural built heritage is to be respected.

Figure 3.13 summarizes the efficiency of the strengthening techniques adopted during the experimental campaign herein reported, including the results obtained from Chapter 2. However, the energy values shown in Figure 3.13 differ from those presented in Chapter 2 because the former are related to the energy dissipated up to a displacement level similar to the unreinforced specimen and considering the envelope of the hysteresis loop, while the later corresponded to the full hysteretic behaviour and ultimate displacement. Otherwise it would not have been possible to directly compare the results obtained in both experimental campaigns.
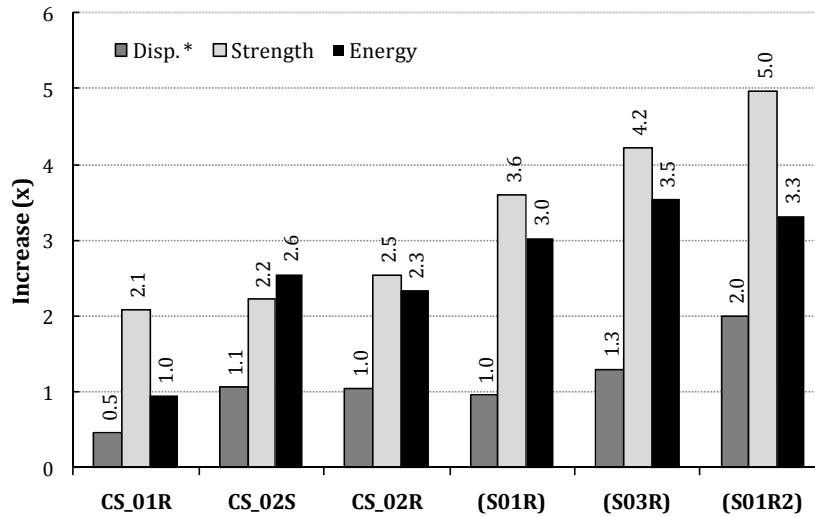
(*) Maximum displacement observed during the full test and not the displacement level used to compute the energy dissipation.

Figure 3.13. Global results obtained with the strengthened specimens compared to original ones (unreinforced), including the results from the other experimental campaign reported in Chapter 2

The energy dissipation provided by the strengthening schemes adopted in the experimental campaign is significant and leads to a satisfactory improvement (larger than twice as much that of the unreinforced panel). Moreover, for the experiments where reinforced connected plaster is used, the energy dissipation capacity of panels is further increased more than three times.

3.4.2. Comparison with analytical predictions

The analytical predictions herein performed are based on static equilibrium considering flexural/rocking behaviour, taking into account the contribution of the strengthening techniques, namely timber connections and reinforced connected plaster. The masonry shear strength (for both unreinforced and reinforced cases) was neglected for piers and spandrels, contributing to simpler analytical predictions. The influence of the adjacent spandrels is not considered for the unreinforced specimens, in accordance to a conservative assumption. However, for the retrofitted/strengthened specimens, the formation of the plastic hinge in the spandrel beams (represented by M_{sp}) due to the presence of reinforced connected plaster was considered as observed during the experiments.

Table 3.3 presents the simplified models used to compute the maximum strength exhibited by the tested specimens in both test campaigns (*Canada do Sousa* and *Salão*), where the blue dot represents the considered rotation point.

Table 3.3. Simplified analytical models used for maximum strength prediction

Test	Section view	Plan view
CS_01		
CS_01R		
S01		
S01R		
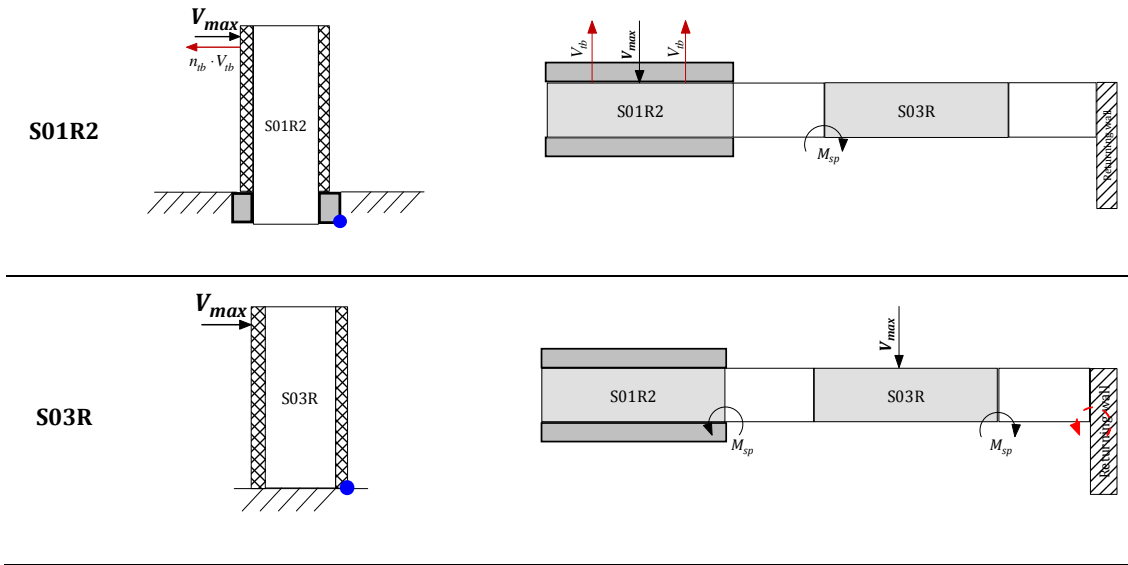
For the S03R case, the plastic hinge in the spandrel beams was not formed at the expected location (represented by the dashed arc line), appearing at the connection between the pier and the spandrel, as shown in Table 3.3.

The contribution of the timber beams was computed using Eurocode 5 (CEN 2004) formulation for steel-to-timber connections for the observed failure mode (thin steel plate) given by equation 8.9 of EC5, represented here by Eq. (3.1) for each nail per shear plane,

$$F_{v,Rk} = \min\left(0.4 \cdot f_{h,k} \cdot t_1 \cdot d ; 1.15 \cdot \sqrt{2 \cdot M_{y,Rk} \cdot f_{h,k} \cdot d} + \frac{F_{ax,Rk}}{4} \right) \qquad (3.1)$$

where $f_{h,k}$ is the characteristic embedment strength in the timber member, t_1 is smaller of the timber side member thickness or the penetration depth (for the present case is the penetration depth, t_1 = 75 mm), d is the fastener diameter (square nail of 3 mm), $M_{y,Rk}$ is the characteristic fastener yield moment and $F_{ax,Rk}$ is the characteristic withdrawal capacity of the fastener.

The $f_{h,k}$ value (15.53 MPa, in the present case) is given by equation 8.15 of EC5, while $M_{y,Rk}$ (equal to 4698 Nmm) is obtained through equation 8.14 of EC5, represented here respectively by Eq. (3.2) and (3.3), for square nails without predrilled holes.

$$f_{h,k} = 0.082 \cdot \rho_k \cdot d^{-0.3} \qquad (3.2)$$

$$M_{y,Rk} = 0.45 \cdot f_u \cdot d^{2.6} \qquad (3.3)$$

In the previous equations, ρ_k is the characteristic timber density (*cryptomeria japonica*, 260 kg/m^3, according to Carvalho (1996)) and f_u is the tensile strength of the wire (considered equal to the minimum value of 600 N/mm^2 provided in EC5). Concerning the value of $F_{ax,Rk}$, a null value was considered in accordance to EC5 proposal and to a conservative assumption.

The total shear force resisted by the connection applied to "tie" the walls (V_{tb}) is given by Eq. (3.4), using the total number of nails used (8 per connection).

$$V_{tb} = n_{nails} \cdot F_{v,Rk} = 8 \cdot F_{v,Rk} = 6.1 \text{ kN} \tag{3.4}$$

As mentioned before, the contribution of the spandrels on the unreinforced panels (CS panels and S01) was neglected. However, for the experiments with reinforced connected plaster at the spandrel beams level, the contribution was included taking into account pure flexure behaviour of the spandrels and taking into account only the influence of the steel mesh (contribution of the mortar in compression was neglected). The maximum moment resisted by the strengthened section ($M_{Rk,sp}$) is given by Eq. (3.5),

$$M_{Rk,sp} = M_{sp} = h_{sp} \cdot \left(0.9 \cdot t_{sp} \cdot f_{syk} \cdot A_{s,x}\right) \tag{3.5}$$

where h_{sp} is the spandrel height (0.56 m in *Salão* house), t_{sp} is the thickness of the spandrel (0.75 m, to take into account the new cement mortar cover), f_{syk} is the characteristic yield strength of the steel mesh (stainless steel 355 MPa) and $A_{s,x}$ is the steel mesh area in the main direction (2.5 cm²/m). The contribution of the reinforced connected plaster to the total out-of-plane strength of the panel (V_{rc}) is given by Eq. (3.6), where l_{force} is the distance between the application of the force and the location of the plastic hinge in the spandrel, according to the layout presented in Table 3.3.

$$V_{rc} = \frac{M_{Rk,sp}}{l_{force}} \tag{3.6}$$

Depending on the retrofit/strengthening techniques applied, the maximum strength of a panel is given by

$$V_{max} = V_u + V_{rc} + n_{tb} \cdot V_{tb} \tag{3.7}$$

where V_u is the maximum force of an unreinforced panel (obtained from the static equilibrium and not considering the spandrel beams) and n_{tb} is the number of timber connections for the considered mechanism.

A global comparison between predicted vs. experimental results is presented in Table 3.4 and Figure 3.14, where the applicability of simple analytical models provided quite good estimates of the panels' maximum strength in a conservative approach. No predictions are presented for the CS_02R case because there was no available information regarding the mechanical characteristics of the steel shape used.

Table 3.4. Predicted vs. experimental results

	Prediction [kN]	Experimental [kN]	Error [kN]	Error [%]
CS_01	7.4/8.9	7.6	-0.2	-2.4
CS_01R	19.6	16.3*	3.3*	20.4*
CS_02S	19.6/37.6	16.8*	2.8*	16.8*
CS_02R	-	19.4*	-	-
S01	8.1	10.1	-2.0	-20.2
S01R	32.7	36.3	-3.6	-9.8
S03R	39.0	42.5	-3.5	-8.3
S01R2	40.5	50.1	-9.6	-19.1

(*) The maximum strength was not achieved during the experimental test
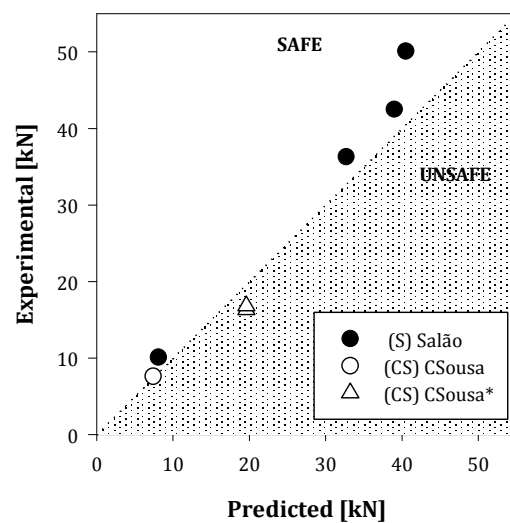
Figure 3.14. Predicted vs. experimental results

However, it should be referred that the results above described have subjacent the condition of neglecting the following contributions: *i)* the masonry compressive strength; *ii)* the mortar under compression in the computation of maximum flexural strength of a reinforced spandrel; *iii)* the masonry shear strength. Thus, the variability of mechanical properties of masonry panels' (unreinforced or reinforced) is not included in these analytical predictions, since only the wall weight is taken into account. In addition, this study is based on the application of EC5 formulation for quantifying the out-of-plane of masonry walls' strengthening with nailed timber beams as well as common approaches for computation of maximum flexural strength of a member with symmetric reinforcement (reinforced connected plaster).

Therefore, it was found that simple analytical formulations led to consistent results for predicting the maximum strength of retrofit/strengthened panels under out-of-plane loads.

Finally, it is worth stressing that the analytical and experimental results for CS_01R and CS_02S panels were also included in this comparative study although the experimental tests did not achieve the panels' maximum strength due to safety reasons. However, taking into account the consistency obtained for the *Salão* test campaign, the expected maximum strength for the above mentioned panels should have been similar or higher than the predicted one as listed in Table 3.4.

3.5. CONCLUSIONS

This chapter reported an experimental campaign carried out in an existing two storey house from Faial Island, Azores, Portugal, which avoided usual difficulties on correctly simulating masonry properties and assemblage details normally inherent to laboratory tests. Two wall panels of this building were out-of-plane loaded, providing relevant information (displacements, strength and energy dissipation) that was analyzed and discussed. In addition, the influence of strengthening techniques used after the 1998 Azores earthquake was also tested making use of the existing walls which were strengthened and retrofitted. It was found that the strengthening techniques were effective, increasing the strength and energy dissipation capacity when compared to the original specimen.

These results were analyzed together with similar ones obtained from another experimental campaign on a one storey house and general conclusions were drawn such as the contribution of reinforced connected plaster for the increase of strength and energy dissipation of out-of-plane loaded masonry walls. However, other strengthening techniques were tested which have shown adequate performance, thus providing suitable interventions complementary (or even alternative) to the application of reinforced connected plaster.

Finally, some simple analytical mechanical models were used to predict the maximum strength of the specimens from which good estimates were obtained, therefore supporting the applicability of simple calculations for this type of tests. However more comparisons with other type of walls and load applications (distributed) should be performed to increase the consistency of the obtained results in these experiments, attempting to validate the adopted simple analytical models.

Chapter 4.

OUT-OF-PLANE BEHAVIOUR OF A FULL SCALE STONE

MASONRY FAÇADE

SUMMARY

The out-of-plane response of walls in existing stone masonry buildings is one of the major causes of vulnerability commonly observed in post-earthquake damage surveys. In this context, a shaking table test campaign was carried out on a full scale masonry façade mainly focusing on the characterization of its the out-of-plane overturning behaviour. The structure tested on the shaking table is a partial reproduction of an existing building from Azores, damaged during the 9 July 1998 Faial earthquake. The definition of the tested specimen as well as the selection of the input ground motion is reported in this chapter. A specific emphasis is given to the definition of the time-history to be applied during the tests since it was felt as an essential and crucial part of the work in order to obtain the desired overturning behaviour. The accelerogram to be imposed was selected from a large set of accelerograms (74) by means of a step-by-step procedure based on several numerical analyses resorting to the rocking response of rigid blocks. Regarding the experiments, the out-of-plane behaviour of the *sacco* masonry façade is presented in terms of displacements, velocities and accelerations recorded during the shaking table tests. A one-sided rocking response of the façade was observed prior to collapse. The impacts were clearly identified in the acceleration records. The façade overturning occurred with the expected failure mode, as predicted in the design of the test.

Finally, some conclusions are drawn regarding the observed behaviour and particular features of this type of stone masonry constructions which may influence the global behaviour of the façade.

4.1. INTRODUCTION

Stone masonry buildings are probably the structures most vulnerable to earthquakes (apart from Adobe) despite their antiquity and heritage value. In fact, also recent earthquakes (e.g. L'Aquila, Italy 2009; Lorca, Spain 2011) showed that the out-of-plane behaviour of masonry buildings, without effective strengthening techniques, leads to partial or global overturning of walls, also called as local failure mechanisms. These mechanisms formed during earthquakes hitting masonry buildings, whose dynamic behaviour is commonly accepted to be characterized by rigid body overturning, are one of the major causes of life and economical losses during seismic events.

Despite the importance of out-of-plane behaviour of walls in life safety, this problem has not been tackled with the deserved importance, particularly supported by experimental evidence where few experimental researches have been carried out so far on stone masonry buildings with the main goal of characterizing their out-of-plane behaviour.

Some attempts were made to characterize experimentally the behaviour of masonry structures resorting to shaking table tests, generally on brick or stone masonry buildings but recurrently on reduced scaled specimens, even in recent studies (e.g. Costley and Abrams (1995); Tomazevic *et al.* (1996b); Benedetti *et al.* (1998); Griffith *et al.* (2004); Dolce *et al.* (2008); Bothara *et al.* (2010); Tomaževič and Weiss (2010)). One of the first and largest experimental campaigns performed to characterize the out-of-plane behaviour was made by ABK (1981), on full scale brick and block masonry walls. However, very few shaking table tests were found concerning full stone masonry buildings using real scale models such as Juhásová *et al.* (2007) or more recently Magenes *et al.* (2010a).

However, only the shaking table tests on brick masonry reduced scale specimens performed by D'Ayala and Shi (2011) under sinusoidal signals have addressed more specifically the out-of-plane problem, as well as a more complete experimental characterization through shaking table tests of a simple full scale double leaf stone masonry façade performed by Al Shawa *et al.* (2011). Indeed, this last work focuses mainly on one-sided rocking of a stone masonry façade with two returning walls, considering a preliminary defined overturning mechanism of the façade.

Apart from the above mentioned, no further information is available in the literature specifically regarding the dynamic out-of-plane behaviour of *sacco* (sack) masonry walls (double-leaf with poor infill material) resorting to shaking table tests on full scale buildings.

Thus, the experimental characterization of the out-of-plane behaviour of stone masonry façades is a topic of significant research interest, taking into account a realistic reproduction of

existing constructions as well as specific seismic motions, which are able to induce the desired rocking response and collapse of the façade through global overturning.

For this reason, the problem of the out-of-plane behaviour of stone masonry walls is studied herein resorting to a full scale shaking table test campaign carried out on a partial reproduction of an existing building made of *sacco* masonry, as commonly found in Portugal and in other Mediterranean areas.

The first part of the work focuses on the selection of the specimen based on a realistic physical full scale model of a building constituted by a *sacco* stone masonry façade with a window opening and a gable wall, differently from the simplified specimens found in previous shaking table experiments. Moreover, the procedure adopted for the selection of a proper ground motion (suitable to trigger the overturning mechanism) is described resorting to simple numerical models.

Afterwards, the description of the experimental campaign performed on the triaxial shaking table of LNEC (Laboratório Nacional de Engenharia Civil, Lisbon, Portugal) is made. A detailed analysis and data interpretation of the obtained results is presented as well as some particularities of the behaviour of *sacco* masonry walls, where assemblage geometry and leafs heterogeneity determine the global behaviour of the façade.

4.2. DESCRIPTION OF THE TEST SETUP

The shaking table tests were performed at LNEC (Laboratório Nacional de Engenharia Civil, Lisbon) at NESDE department (Earthquake Engineering and Structural Dynamics Division). This facility has a tri-axial shaking table with restrained rotational degrees of freedom by a passive system based on a set of high torsion stiffness tubes. The tests were performed unidirectionally along the shaking table transversal axis because, for this specific study, the out-of-plane response of a masonry façade was desired and, therefore, the table longer dimension was fully profited to build the longest possible façade. Thus, the masonry façade was excited only in the out-of-plane direction without interferences in/from the perpendicular direction.

4.2.1. Characteristics of the shaking table

The transversal axis of the LNEC shaking table (ST) includes two actuators placed in the same transversal direction but in the opposite sides of the shaking table. When the shaking table tests were carried out, the digital control was done both in terms of displacement and acceleration, with more predominance of displacements on the low frequency range (< 3 Hz) and accelerations more important for higher frequencies. All the pressure provided by the oil pumps

and accumulators was driven to the transversal axis, providing the experimental test with the maximum shaking table speed in order to ensure a proper response for velocity peaks at maximum velocity with 2 seconds long. It should be referred that both the physical facilities as well as the control of the shaking table were recently upgraded, thus improving its capacity and the dynamic response features. Table 4.1 shows the characteristics of the shaking table taking into account the properties of the used experimental model presented later in section 4.2.2.

The LNEC shaking table presents characteristics suitable for the envisaged seismic tests due to its significant dimension (4.6 x 5.6 m^2, respectively, in the longitudinal and transversal directions) and total payload (40 ton). Concerning the performed test, the total specimen plus foundation mass reached approximately 35 ton, close to the maximum capacity of the shaking table (40 ton), leading to a mass ratio (specimen/shaking table) around 1. For the total model mass (35 ton) the table–model interaction should be predictable and possible to cope with the target motions.

Table 4.1. Characteristics of the transversal axis of the shaking table with the tested model

Shaking table dimensions [m^2]	4.6 x 5.6
Frequency range	0 – 40 Hz
Stroke (0 to peak) [mm]	±200
Maximum peak velocity [cm/s]	80
Maximum acceleration [g]	0.8 (for a payload of 40 ton)
Mass of the table [ton]	40
Maximum specimen dead mass [ton]	40
Maximum specimen/ST mass ratio	1

With the tested specimen, the shaking table has good response parameters for a strong pulse, characteristic of a near-fault ground motion, reaching 0.8 g for maximum horizontal acceleration, 80 cm/s for maximum velocity and ± 200 mm maximum displacement capacity.

A top view of the shaking table is presented in Figure 4.1 where it is possible to observe the main direction of excitation of the model (red arrow). The actuators are also visible in the figure, showing the two transversal ones mounted in opposite senses while the longitudinal one is placed between two strong struts connected to torsion tube (to restrain yaw rotations of the table).

Figure 4.1. Top view of the LNEC triaxial shaking table with a specimen after collapse (H1 specimen), with representation of the transversal direction

4.2.2. Characteristics of the model

A large number of models could be selected to be tested under out-of-plane excitations, making use of different lengths, heights, real or scaled specimens. However, the selection for a real scale specimen was made because the correct simulation of typical stone masonry constructions resorting to scaled specimens is very difficult due to material heterogeneity, complexity of interlocking forces, etc.

At this point, the selection for a two-storey house was raised as a solution to study the out-of-plane behaviour of a real construction. However, the size of such specimens would be limited by the dimensions of the shaking table and by the required safety conditions to perform the tests. In addition, since the maximum possible length of the façade was limited to 4.3 m long, the reproduction of a real two-storey building with such a main façade would not be representative of a real construction and, therefore, should be avoided.

For this reason, a one-storey house, representative of a typical construction type of Azores and the Mediterranean area, was selected for the general typology of the tested specimens. However, still the limitation of shaking table dimension did not allow selecting the main façade and, therefore, a lateral façade was chosen to be tested, including also one opening and a gable wall as commonly found in post-earthquake surveys with severe out-of-plane damages (Figure 4.2).

Figure 4.2. Damage and collapse of the gable and transversal wall, Azores 1998 earthquake

Two similar specimens were tested on the shaking table, conveying real scale replicas of a part of an existing masonry house from Faial Island, Azores, which suffered severe damage during the 1998 Azores earthquake (Figure 4.3 a)). Indeed, similar masonry walls were previously tested under out-of-plane cyclic loads (Chapter 2 and Chapter 3) and more information regarding the out-of-plane dynamic behaviour should be provided to increase the knowledge level of this type of constructions.

In order to simulate the boundary conditions induced by the walls perpendicular to the lateral façade, buttress walls were included in the test specimens (Figure 4.3 b)).

The specimens were built by masons who work on this type of constructions and respecting traditional techniques; the walls were 0.65 m thick and made of stone sack ("sacco") masonry (double leaf with infill), leading to global specimen dimensions of 4.3 x 2.15 x 2.7 m^3 (3.35 m high at the gable) as shown in Figure 4.4.

(a)   (b)

Figure 4.3. Masonry house façade reproduced on the shaking table tests: a) real existing building in Azores; b) specimen at LNEC shaking table

The walls were constituted by granite blocks of different dimensions assembled in two leaves, the inner leaf with 20 cm thickness and outer one with 25 cm; in between, the infill was placed consisting of different dimension smaller stones as well as mortar leading to the total 65 cm. The mortar used to build the specimens relied on traditional lime mortar with fluvial sand (1:3) without any pozzolanic properties, contrarily to the real existing building where volcanic ashes (with pozzolanic properties) are commonly used in this type of construction. Since pozzolanas' effect was not considered a major factor in the overall behaviour of the façade, the traditional lime mortar was deemed appropriate. No masses were placed at the top of the façade because, beyond their lightness, traditional roof typologies from Azores are supported in the main walls (front and rear) as shown in Figure 4.2 b).

(a)   **(b)**
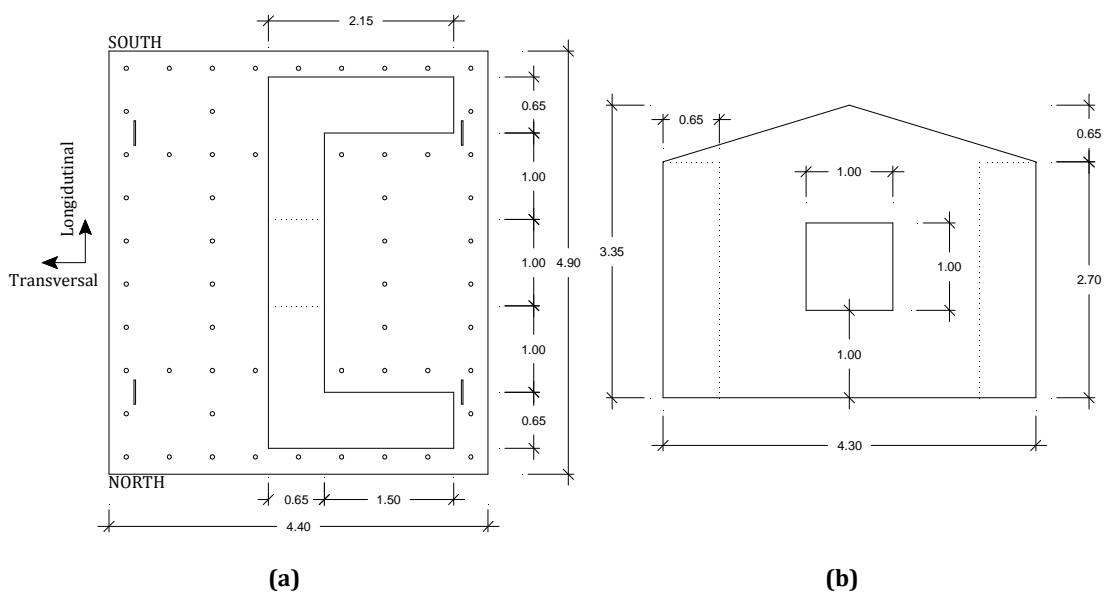
Figure 4.4. Dimensions of the specimens: a) plan view with reinforced concrete foundation; b) main façade

In Figure 4.5 a) it is possible to observe a detail of the masonry wall including the infill materials, while Figure 4.5 b) presents the global view of the façade without mortar cover. Joints were filled in with the same type of lime mortar, also used to make the finishing plaster cover 2 cm thick, over which lime paint was applied (also known as whitewash), as shown in Figure 4.3 b).

(a)   **(b)**
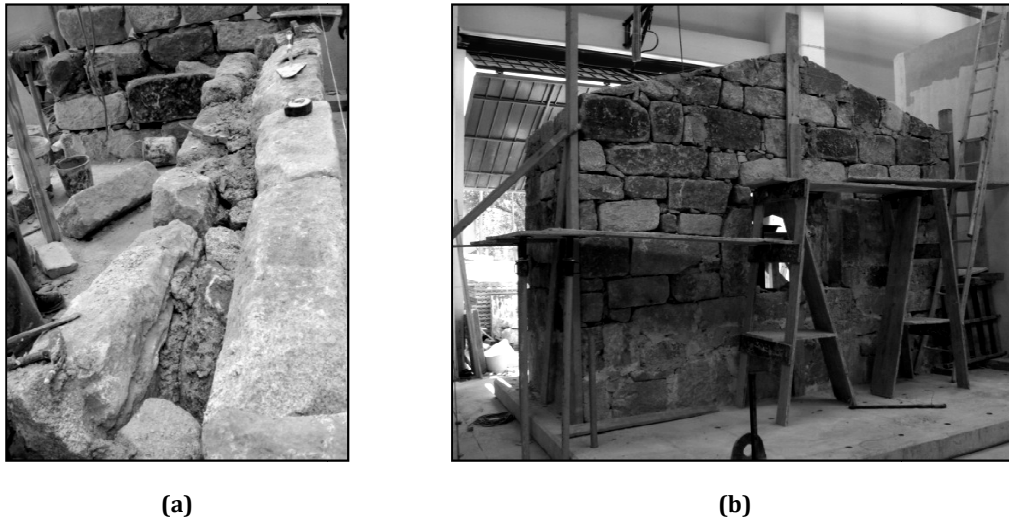
Figure 4.5. Specimen under construction: a) detail of *sacco* masonry of the main façade; b) main façade without mortar cover

In what concerns stone interlocking, 6 through stones (connecting stones) were placed between the inner and outer leaves of the masonry façade (Figure 4.6 a) and b)) in order to enforce both leaves working together, as well as to provide interlocking at the outer leaf corners. However, since the major objective of the tests was the analysis of the façade overturning, a strong interlocking between the façade and the returning walls was not desirable (details in Figure 4.6 c) and d)). By contrast, the returning walls' leaves were well interlocked by headers along the length and height, as illustrated in Figure 4.6 c) and d).

The lime mortar was tested according to EN 1015-11 standard, leading to 1.28 MPa and 0.53 MPa, respectively for compressive and flexural strength.

As mentioned at the beginning of this section, two similar specimens were constructed and tested on the shaking table, according to time schedule described in Table 4.2.

As a final reference, both specimens were constructed above a heavily reinforced concrete slab (ϕ16//0.125) with overall dimensions 4.4 x 4.9 x 0.20 m^2.

(a)

(b)

(c)

(d)
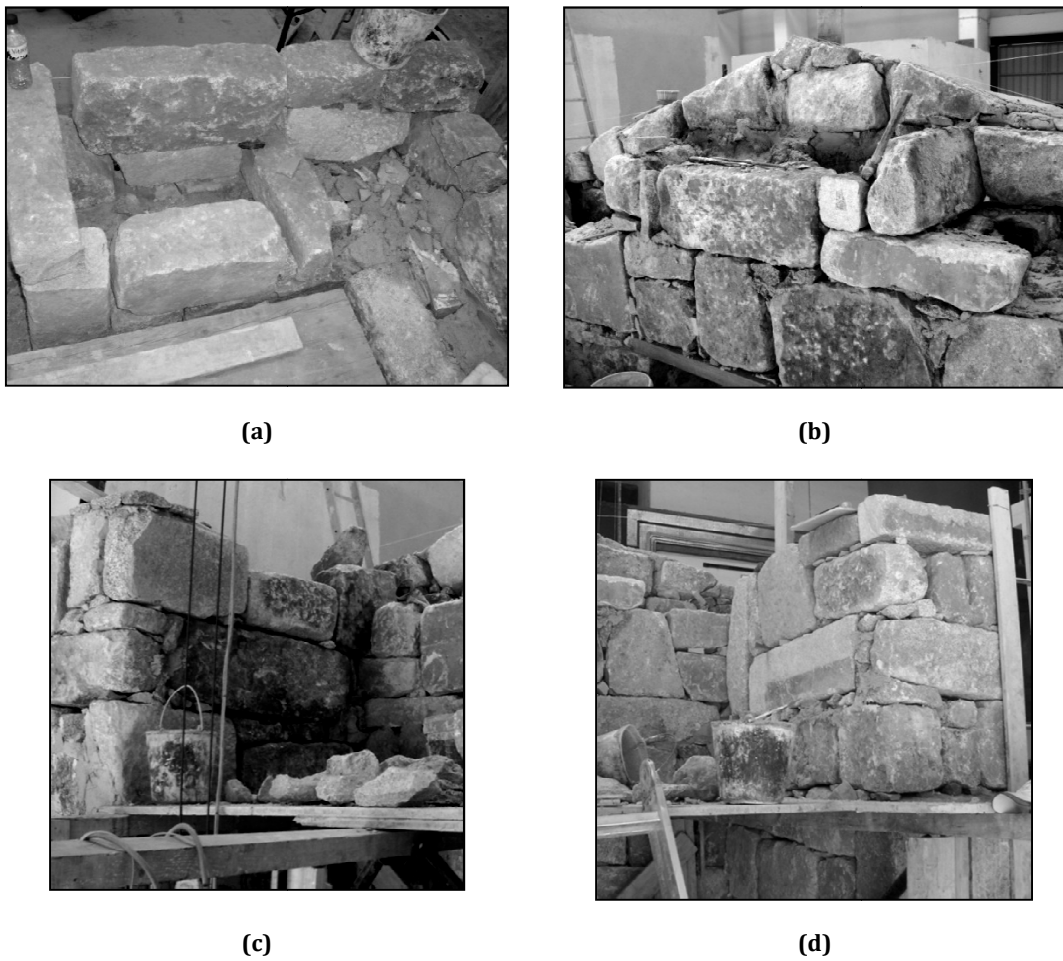
Figure 4.6. Details of the construction phase: a) through stones at the façade; b) through stones placed at gable; interlocking between façade and: c) south wall; d) north wall

Table 4.2. Timetable for construction and test of the masonry houses

Specimen	Construction		Shaking table test	Maturation time
	Start	End		
H1 (House 1)	27 December 2010	02 January 2011	15 March 2011	2 ½ months
H2 (House 2)	16 August 2010	25 August 2010	4 November 2010	2 ½ months

4.2.3. Monitoring set up

The instrumentation adopted to monitor the experimental tests was composed of 19 accelerometers (referred in the following sections as Acc), 12 draw wire displacement transducers (referred as T) and 2 LVDTs according to the instrumental setup presented in Figure 4.7.

Accelerometers were directly connected to the masonry house on steel capsules specially built for the experiment (steel cylinders), in order to protect the accelerometers from damage during the possible specimen collapse. These accelerometers were also used to describe the dynamic characteristics of the system. The draw wire displacement transducers were attached to a reference frame placed inside the masonry house (Figure 4.8), thus allowing directly obtaining displacements of the house relative to the shaking table.
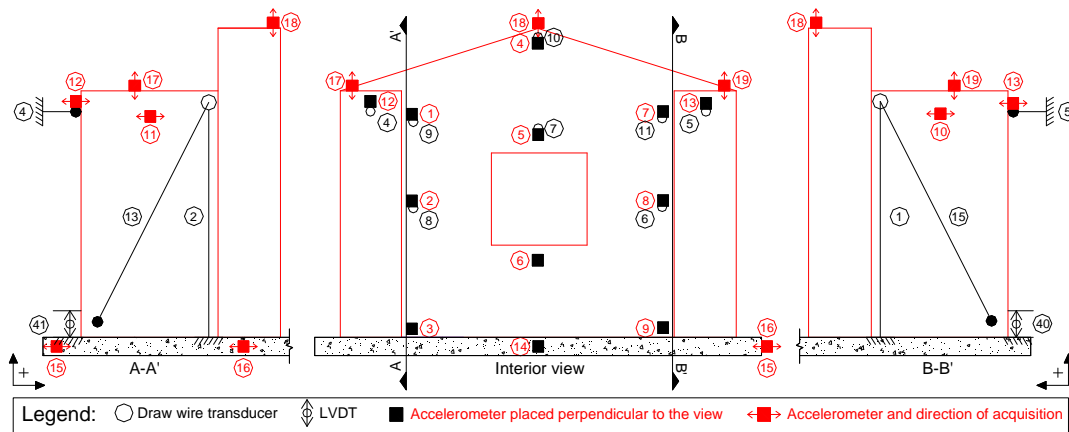
Figure 4.7. Test setup used for the shaking table tests resorting to accelerometers and displacement transducers (internal views)

Redundancy in the acquisition was ensured with the use of accelerometers and wire transducers. Moreover, since the wall was expected to overturn with complete collapse, wire transducers allowed describing the overturning mechanism up to the collapse. The acquisition during the shaking table tests was performed at the sampling frequency of 500 Hz using the LNEC data acquisition system. A general view of the test setup is presented in Figure 4.8 where it is possible to observe the reference frame, draw wire transducers as well as accelerometers placed inside the steel cages.
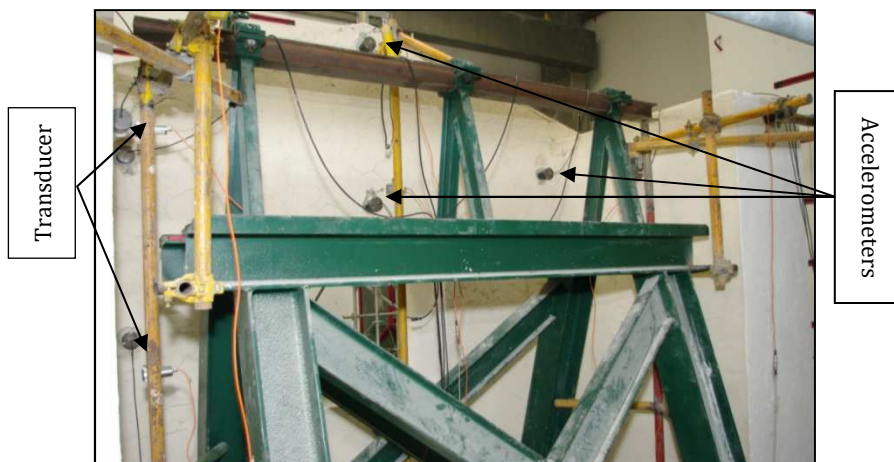
Figure 4.8. Test setup (interior view): reference frame, draw wire transducers and accelerometers inside steel cages

4.3. SELECTION OF THE GROUND MOTION

4.3.1. Main objectives to be achieved with the selected accelerogram

The selection of accelerograms to be used as ground motion on the experimental tests was an important and specific part of the work. Since the main objective of the shaking table tests was to evaluate the overturning behaviour of a masonry façade, an accelerogram to be selected had to potentiate that type of response, without severally damaging the specimen or disaggregating the walls nor fully exhausting the capacities of the shaking table in acceleration, velocity or displacement.

Therefore care had to be taken because the peak ground acceleration, usually the main parameter used to describe ground motions, is not sufficient to predict the overturning of a façade. Out-of-plane collapses are commonly correlated to near-fault ground motions due to marked directivity effects on the ground motion, where acceleration and velocity peaks provide forward, backward or forward/backward pulses. Instead of accelerations (which can be considered force related), velocities (directly related with energy quantification) may provide further information and be correlated to the collapse of a rigid body rocking around the base derived from the energy conservation principle.

4.3.2. Parameters influencing the selection of the ground motion

Through several numerical simulations, Decanini *et al.* (2006) found that velocity measures, such as Peak Ground Velocity (PGV) and the Housner intensity have good correlation with the overturning of rigid bodies. Similar type of studies carried out by Liberatore and Santansiero (2009) evidenced that, for blocks with high slenderness ratios, the overturning is governed by the semi-length of the block and the maximum spectral displacement, S_{max}, and, therefore, the displacement-response spectrum gives an idea of the possible damage of rocking bodies for that level of slenderness. On the other hand, PGA is the main parameter which governs the overturning of squat walls because higher accelerations are needed to activate rocking and overturning.

For a slender block which may undergo rocking around a given rotation centre O, the necessary conditions for such behaviour depends on the friction coefficient, μ_s, and the ground acceleration, $\ddot{u}$. Assuming that the necessary condition of no sliding is fulfilled (Aslam *et al.* 1980), i.e. $\mu_s > 2y_{cg}/t$ (see Figure 4.9) and that oscillation angles are small (Housner 1963), the threshold PGA which triggers the rocking motion ($\ddot{u} = PGA_{min}$) is given by the geometrical parameter α obtained from Eq. (4.1), which expresses the equality of the overturning and the stabilizing moments.
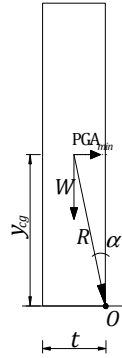
Figure 4.9. Rigid block under rocking: schematic representation of the involved parameters

$$\frac{\text{PGA}_{min}}{g} \geq \tan(\alpha) \qquad (4.1)$$

According to Figure 4.9, W is the weight of the block with mass m, y_{cg} stands for the position of the gravity centre, t is the block thickness, O is the rotation point, g is the gravity acceleration, while R and α are geometrical parameters of the block.

The achievement of PGA$_{min}$ does not mean that the block will collapse; in fact it just states that the rocking motion will be triggered. For this reason, slender blocks have small values of PGA$_{min}$ to initiate rocking and the opposite holds for squat walls. However, for slender blocks, the amount of accumulated energy (mainly kinetic) is more important and it is correlated to the block velocity rather than acceleration.

Also, the work of Makris and Roussos (2000) evidenced that the toppling of smaller blocks is more sensitive to the peak ground acceleration, whereas the toppling of larger blocks depends on the incremental ground velocity, which is the net increment of the ground velocity along a monotonic segment of its time histories, also mentioned by Housner (1963). The analysis made on the first cited work took into account the p value ($p^2 = WR/I_0$, related to the block dynamic characteristics, where I_0 is the polar moment of inertia around the rotation point O) and different type of pulses (simulated as trigonometric functions), obtaining the relation of the minimum velocity for overturning with the period of a trigonometric function and block geometrical characteristics (R).

Summing up, the main parameter which governs the overturning of a rigid block rocking around the base seems to be the velocity, associated with the PGA threshold value for the activation of rocking motion. Moreover, if the energy conservation principle is considered for a block moving with a given velocity v at the base and the movement of the foundation suddenly stops, the minimum value which overturns the block may be given by the equilibrium of the total energy before stop ($E_{T,0}$, with kinetic and potential energy contribution) and after stop

($E_{T,collapse}$, with contribution of potential energy at instability of the block), as expressed by Eq. (4.2).

$$\Rightarrow E_{T,0} = E_{T,collapse} \Leftrightarrow \frac{1}{2}mv^2 + mgy_{cg} = 0 + mgR \Leftrightarrow$$

$$\Leftrightarrow \frac{1}{2}v^2 = g\left(R - y_{cg}\right) \Leftrightarrow$$

$$v_{\min} = \sqrt{2gR\left[1 - \cos(\alpha)\right]} \tag{4.2}$$

However, since the ground motions do not follow simple trigonometric functions or start/stop cycles (as mentioned by Housner (1963), where a similar approach is made taking into account the duration of the ground acceleration), the selection of the accelerogram to be imposed by the shaking table should be done bearing in mind both Eq. (4.1) and (4.2), as well as the frequency content and response spectra, where the former equation is mandatory while the latter may be seen as a target value. One reason for such approach relies on the type of specimen that will be tested, which is flexible rather than rigid and may be damaged before reaching such velocity level.

4.3.2.1. Procedure outline for the ground motion selection

A large set of accelerograms (70) was available from the Reluis project (more information available in Decanini *et al.* (2006)) which were selected in previous works (Sorrentino *et al.* 2006) where the dynamic analysis of masonry façades, simulated as rigid bodies, was performed considering slenderness ratios ranging from 5 up to 10 (two heights were selected: 3.0 m and 8.0 m). In the cited work, good correlation was found between overturning frequency and Housner intensity as well as PGV, which ranged from 24.6 cm/s to 126.4 cm/s in the selected set of accelerograms. All the signals available were natural records from different seismic zones (mainly European and North American records) in order to cover a large range of PGVs. In addition to these signals, ground motions recorded during the 9 July 1998 Azores earthquake and the 6 April 2009 L'Aquila earthquake were added to the set of the accelerograms. The first added ground motion refers to the main motivation of the performed work because, as seen in Figure 4.2, this earthquake caused severe damages on the type of construction to be tested on the shaking table. The L'Aquila earthquake originated also similar damages on Italian constructions comparable to the test specimens and was a recent event recorded by several earthquake stations with good signals, contrarily to the Azores earthquake where only one average record (with soil filtering and amplification effects) with the three components (NS, WE and vertical) was available (the one used in the analysis). The main characteristics of these two ground motion records are reported in Table 4.3.

Table 4.3. Main characteristics of the ground motions added to the initial set of accelerograms

Earthquake	Record	Location	PGA (g)	PGV (cm/s)	Components
9 July 1998 Azores	Observatório Príncipe Alberto do Mónaco - HOR	Horta, Faial	0.40	29.4	NS and WE
6 April 2009 L'Aquila	FA030 - AQG	L'Aquila Valle Aterno – Colle Grilli	0.49	35.7	NS and WE

However, as mentioned by Liberatore and Santansiero (2009), European records exhibit peaks at high frequency content while North American records usually have peaks at lower frequencies and higher PGVs. On the one hand, the first option should be preferred but, on the other hand, it was necessary a seismic excitation which potentiate the overturning of the masonry façade.

Therefore, the ground motion selection was made according to the three different following stages:

1) selection of 5 accelerograms, from the large set of ground motions, through numerical analysis;

2) evaluation of the frequency content through response spectra for the selected ground motions;

3) imposing these signals to the bare shaking table and take a final decision based on the observation of its movement (engineering judgment) and frequency content.

4.3.2.2.   Preliminary numerical results and selection of ground motion

For the above mentioned reasons, numerical analysis were performed based on three possible mechanisms of façade overturning taking into account the façade's geometry (as proposed by Lagomarsino (1998) and D'Ayala and Speranza (2003) shown in Figure 4.10), in order to find an accelerogram which triggers the rocking behaviour of the wall. Selection should be made of a ground motion which triggers the rocking motion of all mechanisms of a multibody system, within the shaking table capacities. The numerical analyses were made with MD Adams™ (Multibody Dynamics Simulation, Automatic Dynamic Analysis of Mechanical Systems) software (MSC 2012a) with concentrated nonlinearity at the contact interface (in terms of sliding friction without cohesion as well as restitution coefficient (Housner 1963) for impacts). Since the aim of this numerical work was the prediction of the behaviour prior to the tests, no information of the specimens regarding these values was available. Therefore, preliminary values were based on information from literature (when available) as reported in Table 4.4.

(a)   **(b)**   **(c)**
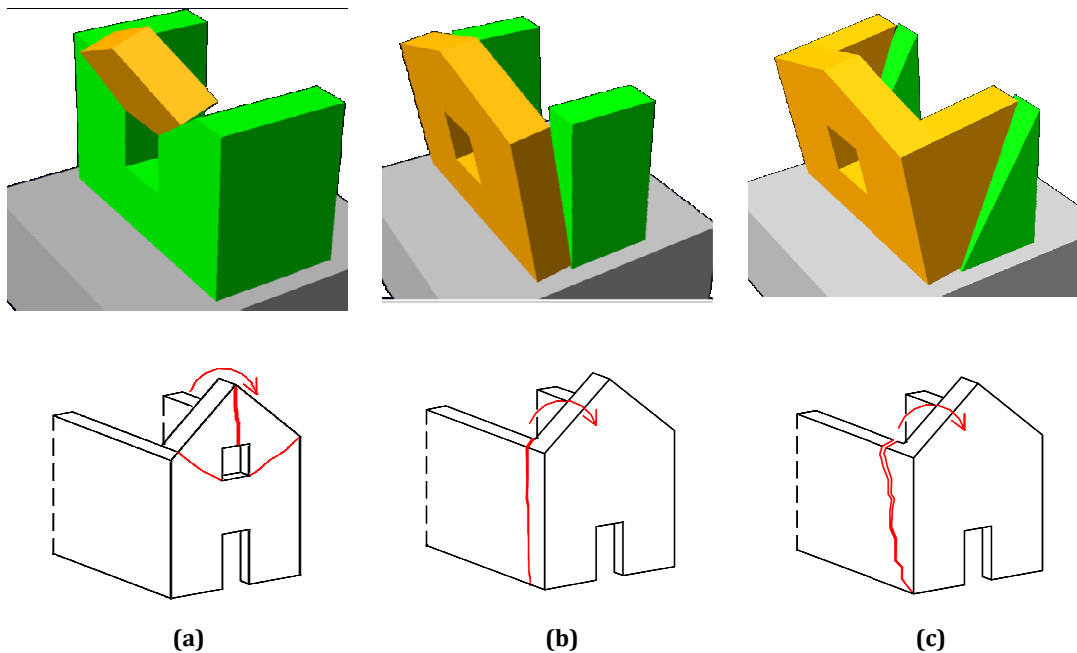
Figure 4.10. Mechanisms considered for the selection of the ground motion (top) and correspondence with existing proposals (Lagomarsino 1998) (bottom); green parts are fixed to the ground, yellow parts are free to rock: a) gable mechanism (MEC0); b) façade mechanism (MEC1); façade plus returning walls mechanism (MEC2)

Table 4.4. Parameters used in the preliminary numerical analysis

Specific weight (ρ) (kN/m³)	Static and dynamic friction coefficient (μ)	Coefficient of restitution (r)
19.0 (Costa 2002; NTC 2008)	0.7 (Vasconcelos and Lourenço 2009)	0.1

The most likely mechanism to form seems to be MEC0 which could be easily triggered due to the presence of the opening. Since the main objective of the test was to excite the complete façade, the analyses obtained with the other 2 mechanisms were necessary for the selection of the input motion of the shaking table.

Therefore several numerical analyses were performed considering the three mechanisms (MEC0, MEC1 and MEC2) and the 74 ground motions. The accelerograms were scaled to 0.6 g (75% of the maximum acceleration of the shaking table) in order to have some reserve on the capacities of the table to excite more severely the specimen (if necessary).

The global numerical results were analyzed by plotting the ratio (δ/Δ_u) *versus* time (where δ is the maximum displacement and Δ_u is the instability displacement for the considered mechanism) as shown in Figure 4.11 which only represents the numerical data obtained for the se-

lected ground motions and most excited mechanisms, MEC1 and MEC2, after stage 1 (more information is presented in Appendix A). Since a unitary ratio means theoretical instability, it was found that the mechanisms were triggered mainly under North American records (low frequency pulses) and not by European records.
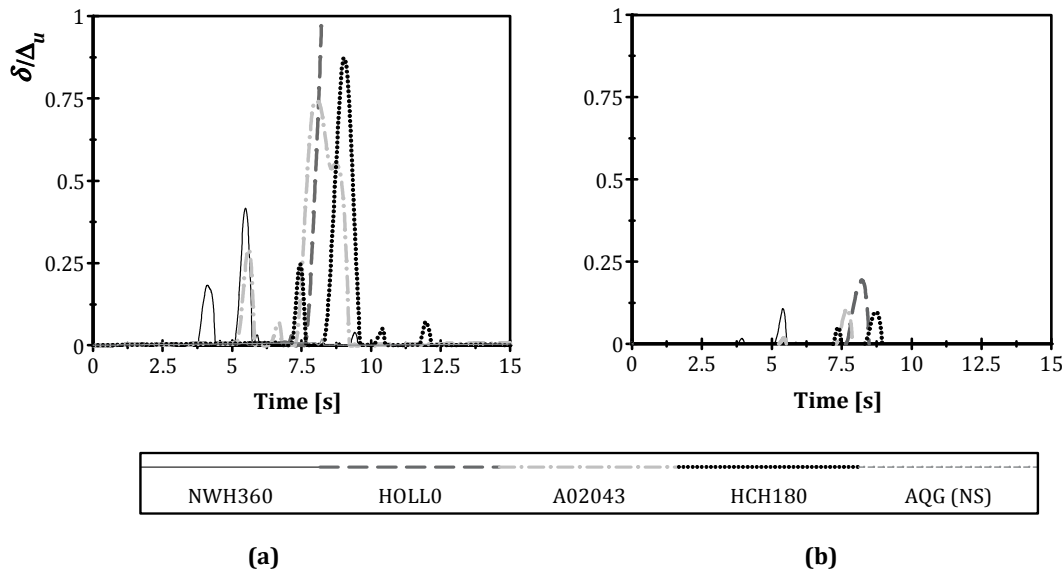
Figure 4.11. Numerical results in terms of normalized top displacement demand obtained using the selected ground motions for the two considered mechanisms: MEC1, (a), and MEC2 (b).

Bearing in mind the above findings, the numerical results and the shaking table capacities, the accelerograms presented in Table 4.5 were selected from the initial set of 74 ground motions, including also the L'Aquila record due to its importance in the recent history despite no significant rocking occurred. In addition, beyond the earthquake magnitude M_w and the epicentre distance D_f, the above mentioned ratio (δ/Δ_u) is also included for evidencing the expected damaging potential of each record.

Table 4.5. Ground motions selected

Earthquake	Record	M_w	D_f [km]	PGA (g)	PGV (cm/s)	Displacement ratio (δ/Δ_u) (*)		
						MEC0	MEC1	MEC2
Northridge	NWH360	6.7	4.0	0.59	96.9	0.07	0.42	0.11
Loma Prieta	HOLL0	6.9	33.0	0.37	63.0	0.10	Collapse	0.19
Loma Prieta	A02043	6.9	47.4	0.27	53.6	0.09	0.74	0.11
Loma Prieta	HCH180	6.9	27.8	0.21	45.0	0.02	0.87	0.10
L'Aquila	AQG (NS)	5.8	4.3	0.49	35.7	0.00	0.02	0.00

(*) Numerical data computed with records scaled to PGA = 0.60 g

From the results of Table 4.5, NWH360 and AQG(NS) records present the lower epicentre distances (D_f), from which marked directivity effects can be expected. However the L'Aquila ground motion is not able to excite significantly any overturning mechanism for the considered specimen due to the frequency content of the signal. An interesting point of these two records relies on the proximity to the epicentre, similar to the epicentre distance ($\simeq$5 km) of the most damaged zones of Faial Island struck by the 1998 earthquake.

The next stage consisted on the observation of the record response spectra in order to avoid valleys or peaks off the desirable period range (0.25 s < T < 0.75 s). Figure 4.12 presents the pseudo-acceleration and pseudo-velocity response spectra (5% damping) for the selected ground motions (Appendix A provides response spectra for all ground motions analysed).
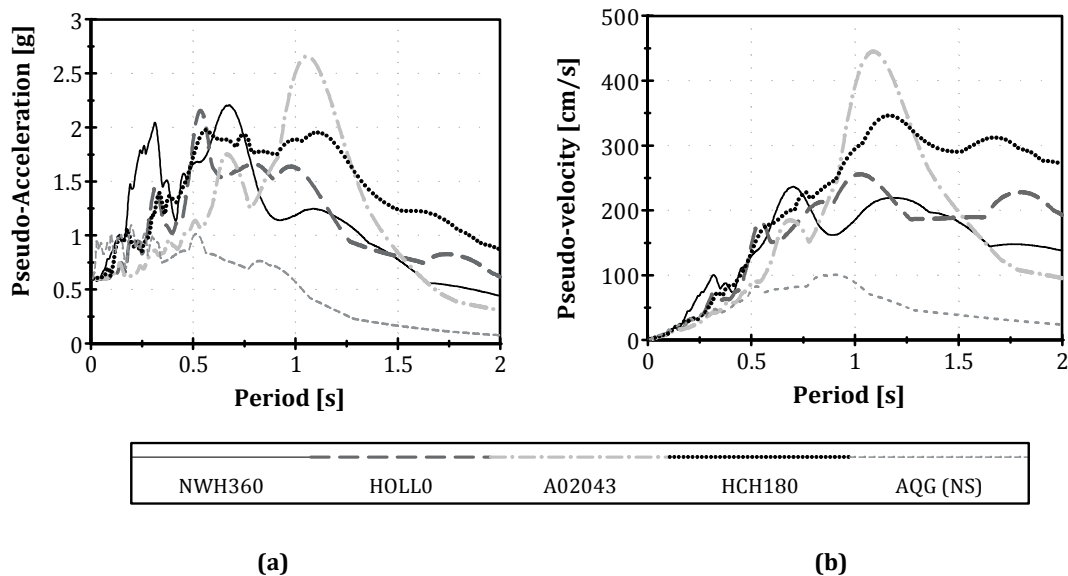
Figure 4.12. Response spectra (ξ = 5%) within the region of interest (0 < T ≤ 2 s) of the selected ground motions scaled to 0.6 g: a) pseudo-acceleration; b) pseudo-velocity

It is possible to observe that the Loma Prieta records (HOLL0, A02043 and HCH180) contain high velocity peaks around T = 1 s, while the acceleration spectra show less excitation for periods lower than 0.5 sec (frequency $f \geq$ 2Hz). On the other hand, the Northridge record (NWH360), although not as severe as the Loma Prieta records (Table 4.5), shows higher frequency contents (0.25 s < T < 0.75 s, 1.33 Hz < f < 5 Hz) than all other records. Moreover, the scaling of the other records to 0.6 g may lead to unrealistic ground motions (too severe motions may be obtained) while NWH360 accelerogram was recorded with PGA = 0.59 g. A comparison between the L'Aquila record and the other considered records shows that the former has a frequency content dominated by higher frequencies as well as lower velocities.

The final decision concerning the accelerogram choice was based on the observation of the bare shaking table motion with the previous signals, from which the NWH360 record was selected

as the input for the shaking table tests. The signal was filtered at long vibration periods (high pass Fourier filter, f_{cut} = 0.2 Hz), in order to fully explore the limits of the table without affecting the final results, leading to the final characteristics presented in Table 4.6 and Figure 4.13.

Table 4.6. Characteristics of the input motion for the shaking table tests

Displacement range [mm]	PGV [cm/s]	PGA [g]
358.0	86.7	0.59
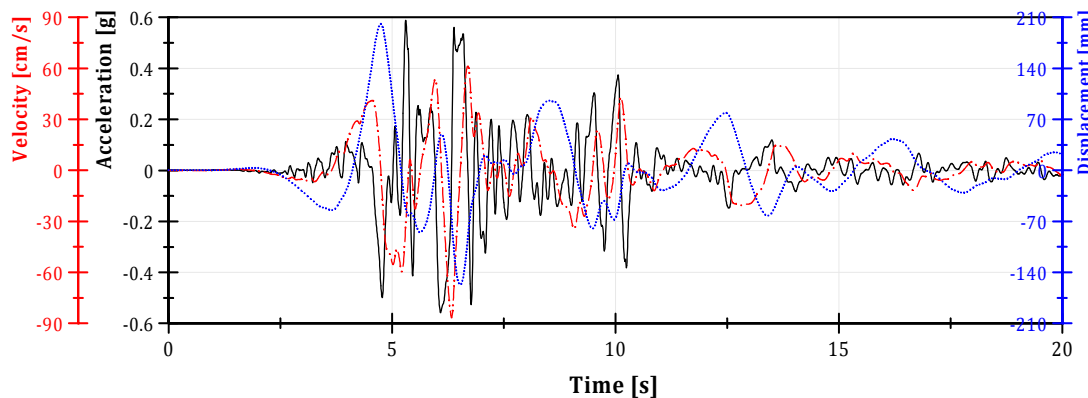
Figure 4.13. Input ground motion for the shaking table tests: 17 January 1994 Northridge earthquake recorded at Newhall Fire station (NWH360) filtered at low frequencies, (zoom at time interval 0 ≤ t ≤ 20 s).

It should be referred that the nature of the ground motion used on the shaking table tests was not a major scope of this work. In fact, the main goal consisted on obtaining a ground motion which would trigger the desired overturning mechanism without damaging severally the wall before collapse. This requirement enforced a thorough selection strategy because a wrong choice of the input record could lead to undesired effects and mechanisms. For instance, the use of high frequency content ground motions (as European records), which may not trigger the overturning mechanisms, could trigger local in-plane mechanisms and cause disaggregation of the walls, which were not the aim of the experimental work.

4.4. TEST EVOLUTION AND EVALUATION OF THE SHAKING TABLE RESPONSE

Two specimens were tested on the shaking table on different time intervals, as a result of the collapse of the first specimen at an unexpectedly early stage. Indeed, the first experimental test had a specimen-table interaction problem due to an inappropriate tuning of the table which led to a severe seismic excitation that collapsed the model. On the other hand, the second specimen was tested with an adequate tuning of the shaking table, which allowed performing five test stages (for increasing intensity levels) with the expected collapse occurring at the fifth stage.

However, in order to have an increasing level of excitation along this description, H1 is defined as the specimen which sustained five acceleration stages, while H2 is the one subjected to a sole extreme excitation. A summary of the test campaign performed is presented in Table 4.7 for the two specimens including intermediate stages for modal identification, where the PGA_{ST} levels are relative to the maximum acceleration acquired on the reinforced concrete foundation (acc14, according to Figure 4.7).

Table 4.7. Summary of the test campaign

Model	Stage	Scale factor	PGA [g]	PGA_{ST} [g]
H1	Identification (CAT00)	Pink Noise	-	-
	L1	10%	0.059	0.076
	Identification (CAT01)	Pink Noise	-	-
	L2	20%	0.118	0.146
	Identification (CAT02)	Pink Noise	-	-
	L3	40%	0.235	0.302
	Identification (CAT03)	Pink Noise	-	-
	L4	60%	0.352	0.419
	Identification (CAT05)	Pink Noise	-	-
	L5	80%	0.470	0.535
H2	Identification (CAT00)	Pink Noise	-	-
	L1	50%	0.294	1.976[(*)(**)]

(*) Problems on the input motion due to inappropriate tuning of the shaking table

(**) Data acquired from the shaking table accelerometers due to the collapse of the specimen

The modal identification was made by means of a pink noise (with low energy at high frequencies) introduced into the shaking table with frequencies ranging from 0.1 to 30 Hz, while the data post processing and analysis was made by the LNEC-SPA (Signal Processing and Analysis Tools for Civil Engineers) software (LNEC 2009) resorting to common signal processing techniques. For the present case, modal frequencies were identified using the frequency response functions (FRF) through the Welch method (Bendat and Piersol 2000; Candeias 2008), from the observation of peaks, amplitudes and coherences of the Bode diagrams (Candeias 2008).

Regarding the response of the shaking table during specimen H1 tests and despite slight mismatching between input and acquired data regarding the PGA levels observable in Table 4.7

(related to high frequency components), the response spectra presented in Figure 4.14 shows good agreement.

The data is shown for the base accelerometer (acc14) and the shaking table accelerometer (the accelerometer used for the above described adaptive tuning), the latter with better correlation to the input signal. The measured signal was then processed with low-pass Fourier filter (cut-off frequency of 25Hz) and offset removal. For stage L5 (80%), the presented data is relative to the accelerometer on the shaking table for both cases, because the accelerometer acc14 record was affected by the façade's collapse.

(a)   (b)
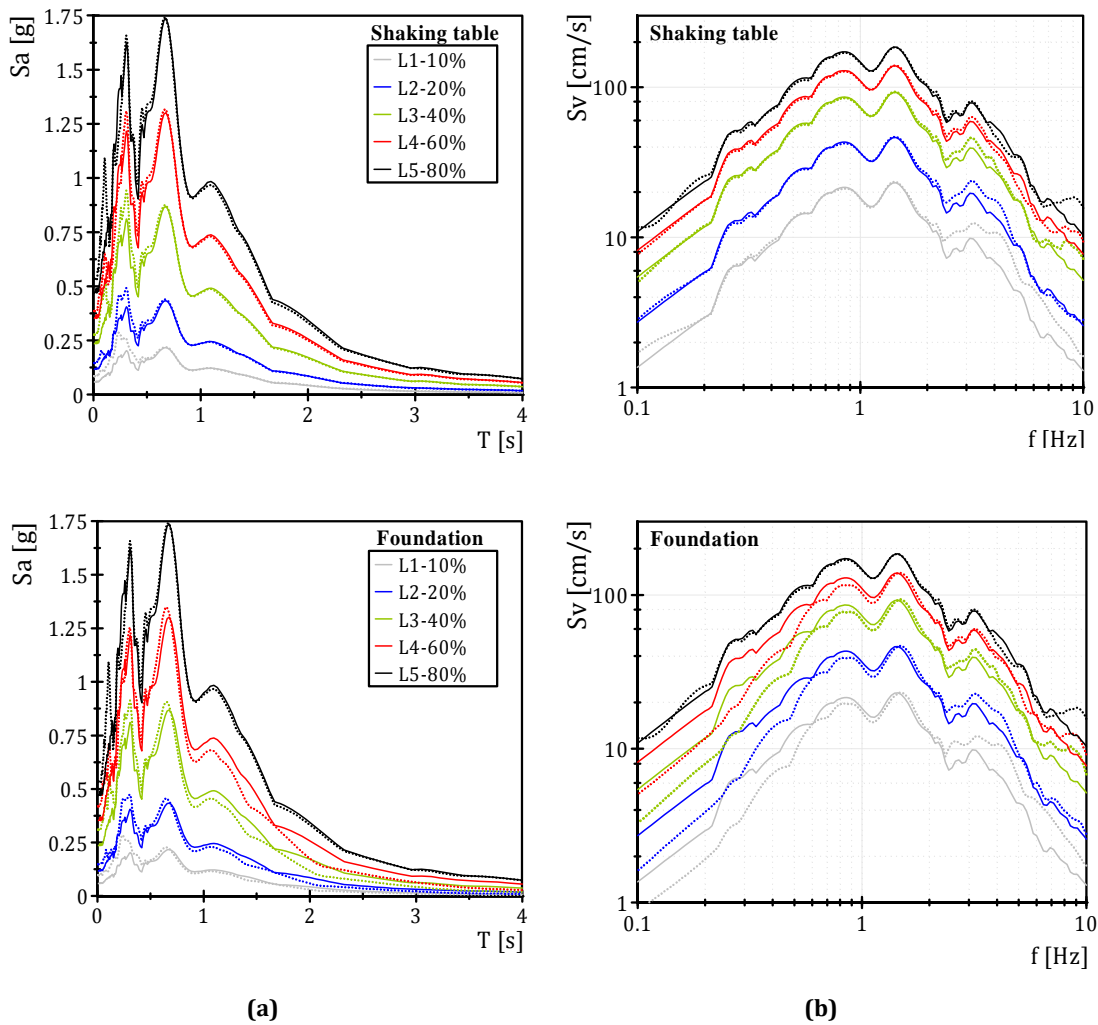
Figure 4.14. H1 - Comparison of response spectra between input reference (solid lines) and measured feedback data (dot lines), at the shaking table (top) and r.c. foundation (bottom) in terms of acceleration, a), and pseudo-velocity, b)

As it is possible to observe, the shaking table accelerometer exhibits a perfect match between the input and the acquired signals. It can be also referred that, for increasing amplitude levels,

the shaking table ability to reproduce the seismic motion increased substantially due to signal/noise ratio amplification.

Concerning the r.c. foundation accelerometer (acc14), an excellent agreement for accelerations and good reproduction of velocities was obtained during the shaking table tests for all excitation levels (for the frequency range of interest, 0.5 Hz < f < 5 Hz, the desired velocities were quite well achieved).

Regarding the behaviour of the H2 specimen, no comparisons will be presented because no relevance was found on the obtained data concerning the shaking table response. The data acquired with the instrumentation during the test H2-L1 will be presented in following section 4.5, just out of curiosity when an extreme ground motion excites a construction of this type.

4.5. ANALYSIS OF EXPERIMENTAL DATA

In the initial part of this section, the observed behaviour of the specimens is briefly discussed, while in following subsections a more detailed analysis is made with the presentation of experimental data. It should be referred that all the data was post processed by LNEC-SPA and National Instruments DIAdem™ software (NI 2010a).

4.5.1. General overview

For what concerns specimen H1, the most interesting results are presented in this subsection mainly relative to test stages L3, L4 and L5 (40%, 60% and 80%) because these are the ground motion levels which excited the specimen. For the other two test stages, no relevance was found in the obtained results. Nevertheless, the complete set of used ground motions is presented in Figure 4.15.
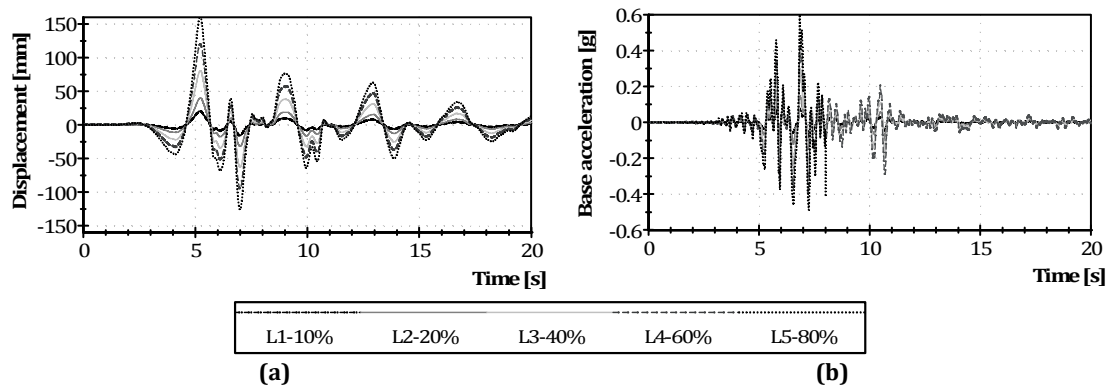
Figure 4.15. Input ground motions used during the shaking table tests in specimen H1: a) displacements (shaking table data); b) accelerations (recorded at base accelerometer, acc14)

The behaviour exhibited by H1 specimen during the experiments can be divided in two different phases: *i)* for level stages L1, L2 and L3 (10%, 20% and 40% scaling factor), the specimen behaved monolithically; *ii)* for stages L4 and L5, the wall exhibited a response mainly characterized by rotation of the whole façade at the window level, including small horizontal and vertical bending (flexural component) of the façade between the returning walls.

Figure 4.16 shows the specimen cracking pattern in the stage prior to collapse, where the formation of the main overturning mechanism is evidenced. Indeed, the outer leaf exhibited vertical flexural cracks as well as cracks in the window jambs (Figure 4.17 (a) and (b)), while the inner leaf showed the formation of the gable overturning mechanism, as obtained at the final collapse pattern (Figure 4.17 (c)). The horizontal crack at the window bottom level (which can be considered as a cylindrical hinge for the overturning mechanism) was formed only at the final L5 test stage (80%).
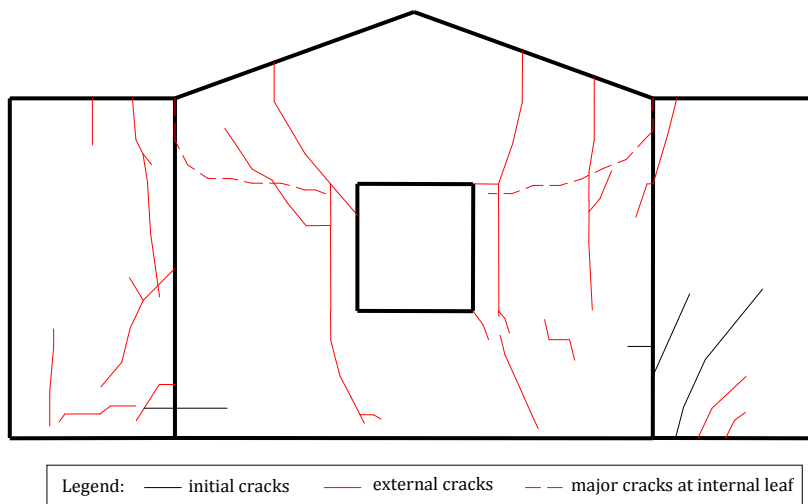
Figure 4.16. Simplified cracking pattern for H1 specimen: external view prior to L5 test (80%)

The mechanism mobilized the whole wall and gable, involving the outer leaf at the window level as a result of the compression strut. This is shown in Figure 4.17 a) and b), where it is possible to observe that, above the window, the total wall thickness was mobilized out-of-plane, while at the window level only the outer leaf is mobilized, particularly at the façade right side as evidenced in Figure 4.17 c). It is worth referring that the façade did not mobilize any portion of the returning walls during the out-of-plane collapse.
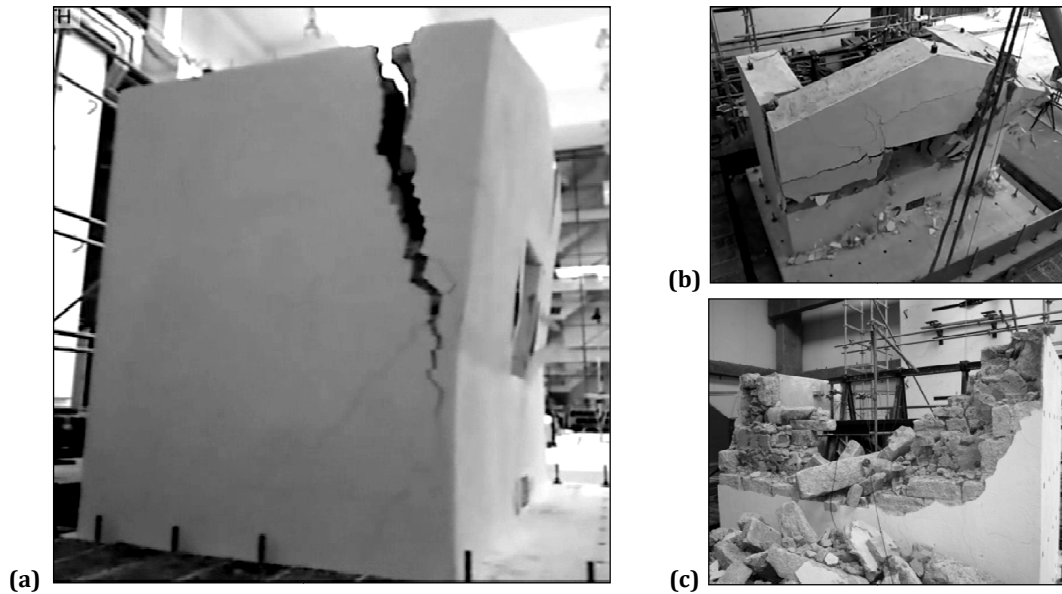
Figure 4.17. H1 specimen: mechanism for the L5 (80% signal) ground motion: a) south view at forward motion peak (*t* = 6.85 s); b) top east view, after backward motion (*t* = 7.52 s); c) collapsed façade

Figure 4.18 presents a detailed evolution of the collapse mechanism at the forward-backward pulse of the ground motion. As evidenced in Figure 4.18 a), significant cracking occurred at the peak forward displacement due to the masonry façade rocking (red arrows) and flexural component due to a fragile zone (blue arrow, with the vertical crack caused by quasi-continuous head joints). For the backward motion, the wall inertia led to the collapse of the north part of the façade (only the outer leaf) and a formation of a horizontal hinge (visible horizontal crack) at the window top level (red arrow).
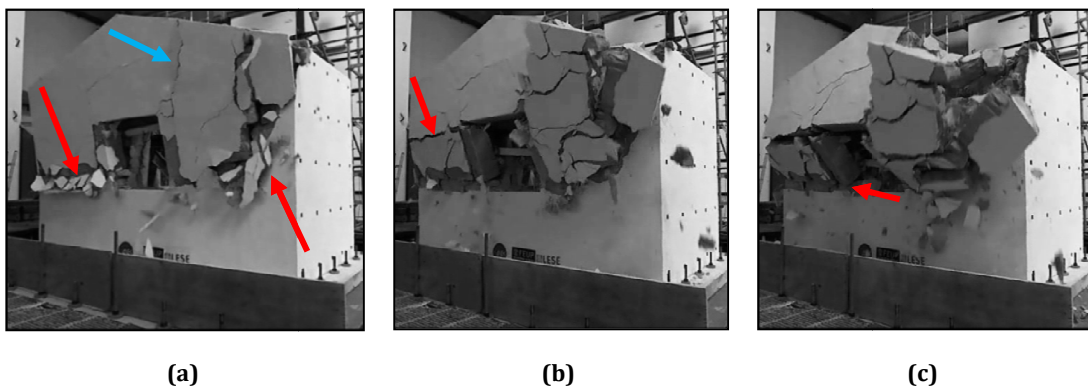
Figure 4.18. Photographic sequence of the collapse mechanism of H1 specimen: *t* = 7.1 s, (a), *t* = 7.52 s, (b), and *t* = 7.68 s , (c) (collapse of right corner and horizontal hinge at top window level)

This out-of-plane vulnerability was increased by the presence of the window and by the existence of a single vertical stone at the window jambs (also identifiable in the cracking pattern shown in Figure 4.16). Indeed, since the window jamb stones are more vulnerable to instability

due to their vertical position, the overturning potential of these elements is higher than the others, thus further contributing to the masonry façade collapse, as shown in Figure 4.18 c) where the rotation of the vertical jamb stone is evidenced by the red arrow.

These above described results are consistent with the values observed for the main mode frequency (included in Table 4.8), which remained almost the same for test levels L1 and L2, starting to decrease after stage L3 in agreement with the damage observed in the specimen (also described in Table 4.8).

Table 4.8. Tests evolution and observed damage

Stage	Scale factor	f (Hz)	Behaviour of the façade	Damage and observed behaviour
H1-CAT00	Pink Noise	9.8	-	Small vertical cracks at façade due to transportation
H1-L1	10%	-	Monolithic	No visible damage
H1-CAT01	Pink Noise	9.8	-	-
H1-L2	20%	-	Monolithic	No visible damage
H1-CAT02	Pink Noise	9.3	-	-
H1-L3	40%	-	Slight flexural response	Small vertical cracks at the façade and diagonal cracks at returning walls
H1-CAT03	Pink Noise	7.8	-	-
H1-L4	60%	-	Rigid body motion at window level (one-sided rocking)	Façade detachment at the window level (1.0 meter) and cracks at the gable
H1-CAT05	Pink Noise	4.6	-	-
H1-L5	80%	-	Rigid motion body at window level with small torsion	Façade collapse caused by instability of the outer leaf at window level
H2-CAT00	Pink Noise	7.6	-	Vertical cracks due to transportation (quasi-continuous head joints from window frame to the gable)
H2-L1	50%(*)		Strong flexural and rigid body behaviour when overturned	Complete collapse of the façade with returning walls ("explosion")

(*) Unexpected behaviour of the shaking table leading to the model collapse

Concerning the specimen H2, its shaking table test was unsatisfactory (as previously mentioned) due to problems on the actuation system of the shaking table. Both the ground motion introduced in the shaking table and the target motion are illustrated in Figure 4.19, where it is

possible to observe a complete disagreement between the target and the acquired signal in the high frequency content.

(a) (b)
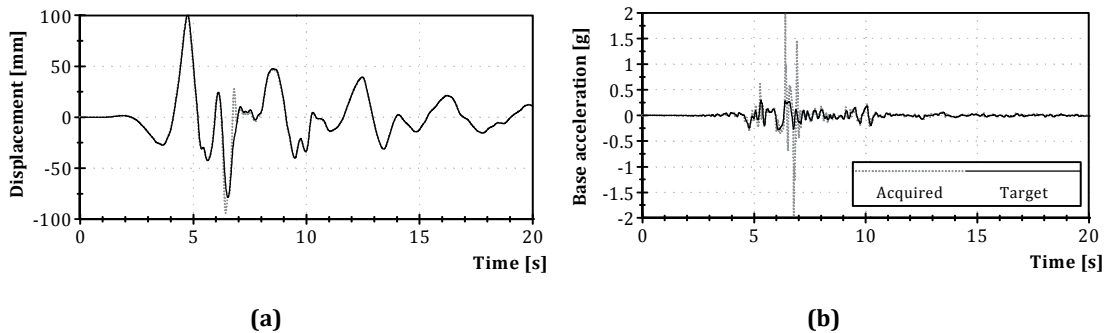
Figure 4.19. Specimen H2. Input ground motion acquired on the shaking table: a) displacements; b) accelerations.

Despite that, the response can be described as: *i)* overall flexural behaviour of the main façade (mainly of the gable wall) between the returning walls and, *ii)* full overturning of the façade including a portion of the returning walls. The overturning caused by that extreme seismic action (PGA≃2.0 g), also highlighted the particularities of a *sacco* masonry façade response under out-of-plane loads. Indeed, the instability was caused not only by a global overturning but also due to collapse of small stones of the outer leaf (Figure 4.20), as in the case of H1 specimen. It seems that the instability was achieved for a top displacement $\Delta = t_{leaf}$ rather than $\Delta = t_{wall}$ as could be theoretically expected for a rigid body rotation of the complete wall about a given pivot section.
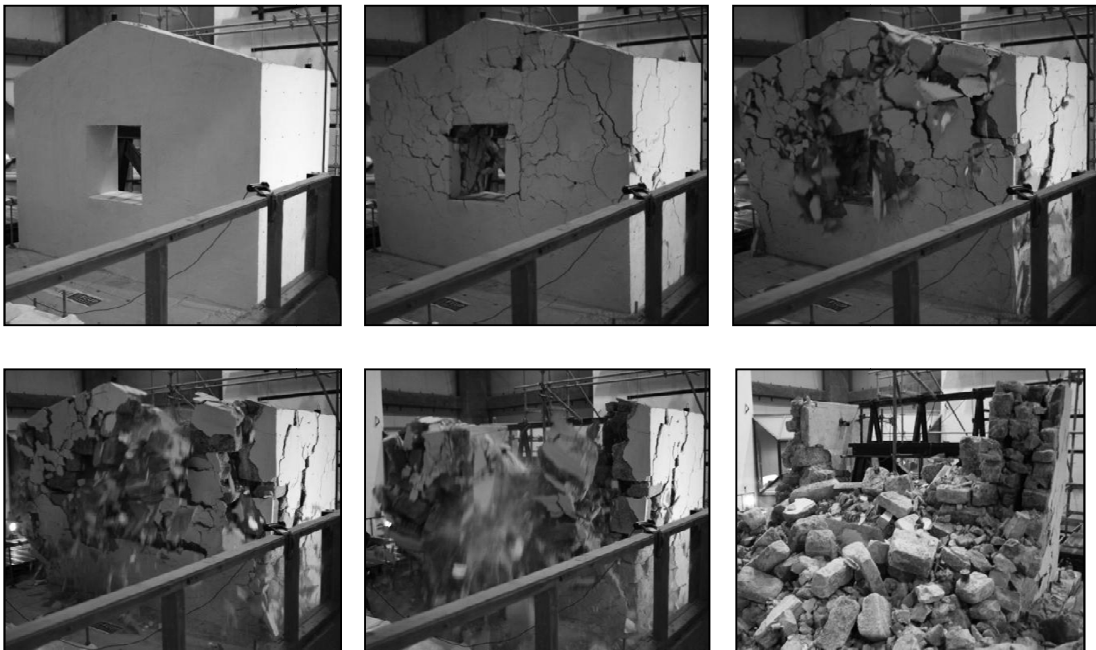
Figure 4.20. Damage evolution and collapse of the H2 specimen.

Finally, as expected, the window opening increased the vulnerability of the façade due to the collapse mechanisms which were triggered involving only the gable motion. However, another interesting observation is worth highlighting: as for the H1 case, the window frame stones were the most vulnerable elements of all the façade because of the orientation of the window jamb stones. In the third image of Figure 4.20 it is possible to observe that the first parts entering into collapse are the window jamb and lintel. Since no cohesion or tensile resistance is available in the remaining façade to compensate for the lack of support at window level, the whole collapse of the façade occurs.

4.5.2.   Shaking table test results

Figure 4.21 presents the displacement time history of the top wire transducer (T10, according to Figure 4.7) for the abovementioned stage levels (L3, L4 and L5) and for the time range where relevant displacements occurred ($2.5 < t < 12.5$ s). Due to the large difference of magnitude order for the displacement time history of L5 test (80% intensity) relative to the other test levels (40% and 60% intensities), the former is described by two different curves: the black dash-dot line refers to the left axis, which corresponds to the common scale shared by the three test stage levels, while the black dot line is plotted according to the right axis (full scale axis for the stage L5 only) where the collapse of the façade is clearly evidenced at about t = 7.7 s.
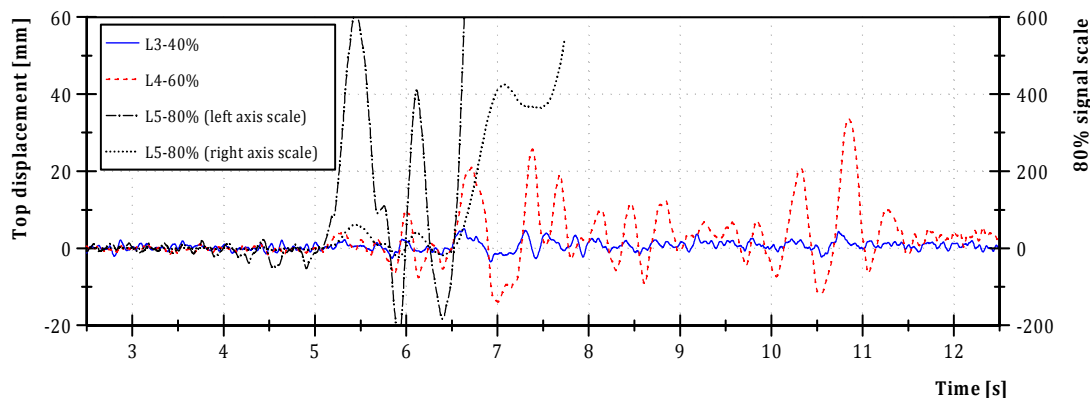
Figure 4.21. H1: Top displacement time histories for stages L3, L4 and L5

The rocking mechanism of the façade was activated at stage L4 (60%), which is visible after t = 6 s when increasing larger amplitude displacements (when compared to L3-40%) were recorded up to the peak value $\Delta_{max,L4}$ = 33.6 mm. After mechanism activation, the façade behaved mainly in one sense (displacements were found more pronounced in the positive sense) with different vibration periods and amplitudes, as expected in rocking behaviour (depending on the initial velocity or initial rotation and regardless of stiffness). However, no rebounding after impacts was observed in the top transducer data because both positive and negative displacements were recorded, but probably influenced by the flexural behaviour of the façade.

When subjected to the 80% scaled NWH360 ground motion, the façade exhibited a pure rocking performance leading to collapse due to instability of the outer leaf. In fact, initial rotations were recorded until the major pulse of the seismic motion, which led to a significant displacement demand of the wall (Δ≥400 mm). Although the trend of the wall was to recover from that large rotation (as evidenced by inflection of the displacement curve at about t = 7.2 s), it did not become possible due to the collapse of the outer leaf at the window level (as observed in Figure 4.18), thus leading to the complete disaggregation of the façade for t > 7.5s.

Identification of impacts

The identification of the façade impacts on the returning walls and the corresponding mechanism activation, observed at L4-60% level, is not easy to define because the whole façade mobilization did not occur at a precise time. However, analysing the acceleration records, it was possible to identify the impacts.

The original acceleration records were filtered with a high-pass Fourier filter (f_{cut} = 50Hz) to obtain the signal high frequency content corresponding to the impacts of the façade. This procedure was carried out for L3-40% and L4-60%, in order to validate the results with the L3-40% level (where no impacts were expected to be detected in the acceleration records) and to identify the impacts at L4-60% level (with the high frequency peaks detection).

The acceleration results obtained with the described procedure are presented in Figure 4.22, as along with the accelerometers positions in order to facilitate the interpretation of the results.

From Figure 4.22, it is possible to observe that during the L3-40% stage (black lines) no impacts occurred because no peaks can be observed, with the exception of Acc1 record. The peak observed at t = 7.5 s is related to the first cracks of the façade, as mentioned in Table 4.8.

On the other hand, the acceleration records for L4-60% stage show a significant increase of acceleration peaks related to the high frequency content of the impacts of the façade. When observing the North (Acc1, Acc2 and Acc3) and South (Acc7, Acc8 and Acc9, the latter with data acquisition problems) aligned records, it is possible to observe a non symmetrical behaviour. As expected for a heterogeneous façade, the North part was more vulnerable than the South one, as observed in the collapse (Figure 4.18) with the outer leaf detachment at the North part of the wall. The peaks observed until t = 6 s are related to the first detachment of the outer leaf, also observed in the video records.
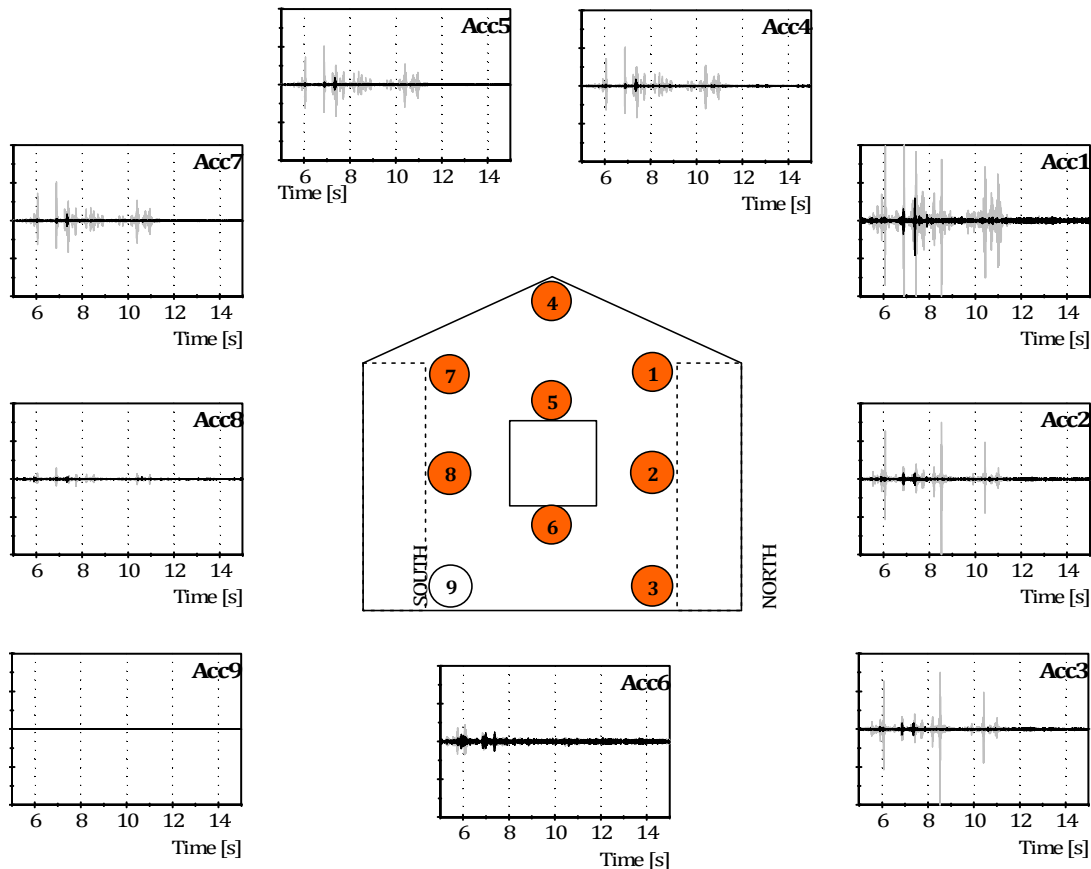
Figure 4.22. Identification of impacts from acceleration high frequency content for L3-40% (black lines) and L4-60% (grey lines) stages in the same vertical scale (+/-0.4g), including the representation of the position of the accelerometers (exterior view)

At t = 6.85 s, it is clearly identifiable the first impact of the façade in the returning walls in all the records, more pronounced in Acc1, Acc4, Acc5 and Acc7, the records of the accelerometers placed at the top and involved in the rocking motion. From this point on, the number of peaks in all the acceleration records exhibited the façade rocking behaviour , which was not identifiable in the previous test level (L3-40%) and was not observable for t > 11 s.

In conclusion, the mechanism activation occurred at t = 6.85 s with a subsequent rocking behaviour of the masonry façade during the remaining part of the tests.

Other interesting results are depicted in Figure 4.23 for test levels L3, L4 and L5, referring to displacement time histories of points along vertical alignments (referred to as T8 & T9, T7 & T10 and T6 & T11) and along sub-horizontal alignments (T8 & T7 & T6 and T9 & T10 & T11) of the façade. The former are likely to evidence the wall out-of-plane behaviour and the formed mechanisms, while the latter provide information about the torsion that the façade may have exhibited (which is mainly influenced by the interlocking to the returning walls).

As evidenced in Figure 4.23, displacements were more pronounced at the centre of the façade due to the presence of the opening and gable. However, comparing the displacements T9 and

T11, respectively to T8 and T6, it can be observed that the façade global overturning above the window level was mobilized for L4 and L5 stages; indeed, at the upper level below the gable (T9 and T11), significant displacements occurred while in the lower façade part (T8 and T6) no significant displacements were recorded.
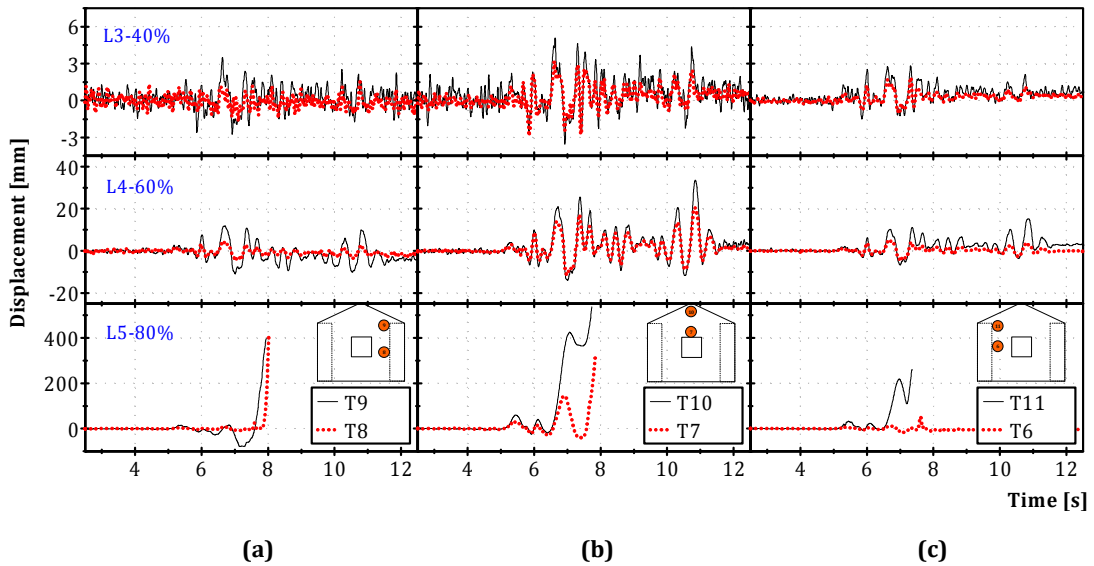
Figure 4.23. Displacement time histories for different test levels along: (a) vertical North alignment; (b) vertical Central alignment and (c) vertical South alignment

By observing closer T9 and T11 data for L4, it is very interesting to notice that, while T9 contains also negative displacements (possibly due to partial rotation of the façade around the North returning wall), T11 response is mainly characterized by one-sense displacements (positive) conveying a pure one-sided rocking. This statement takes further relevance by the closer observation of L5 stage where only positive displacements were acquired for T11 and T6. Finally, a slight torsional response of the façade occurred because larger displacements were obtained for T11 (south side) when compared to T9 (north side), as clearly observable in stage L5.

It should be referred that the ultimate displacement obtained for T8 in stage L5 is in the opposite sense to what was observed at the end of the experimental test (at the transducer location, the inner leaf did not collapse at the window level). The behaviour of T8 should have been similar to T6 (one-sided rocking) and the acquired data may be explained by the falling of some parts of the façade to the interior which interfered with the monitored displacements of T8.

Out of curiosity, the position of the rotation axis of the façade may be determined assuming a pure rocking behaviour of the façade. Since the vertical distance between these two monitoring points is known, the position of the rotation axis from T10 (h_r) can be estimated by Eq. (4.3),

where h_{10} and h_7 refer to the height of the monitored points, while Δ_{T10} and Δ_{T7} are the acquired displacements on the referred positions.

$$h_r = \frac{(h_{10} - h_7) \cdot |\Delta_{T10}|}{\Delta_{T10} - \Delta_{T7}}$$

(4.3)

The results of h_r obtained using this approach were filtered with a low pass 3rd order Butterworth filter ($f_{cut\text{-}off}$ = 8 Hz) to remove undesired peaks and plotted for stages L4 and L5 in Figure 4.24, where the global trend of the wall behaviour can be analyzed for the time intervals with larger recorded displacements; positive values of h_r are obtained for outward rotations while negative values stand for rotations to the interior. It should be referred that the results must be carefully considered because of the precision of the wire transducers, mainly in the L4 stage.

(a)

(b)
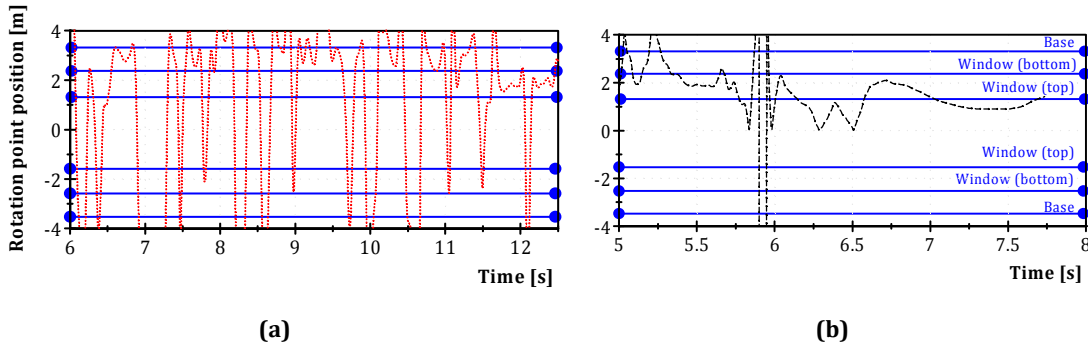
Figure 4.24. Position of rotation axis (h_r) of the façade for: a) L4-60% stage; b) L5-80% stage

From the joint observation of Figure 4.23 and Figure 4.24, it is possible to note that the initial rotations of the wall (stage L4) occurred around the wall base (6.5 < t < 8.0 s), followed by rocking around the bottom of the window in subsequent peak displacements (10.0 < t < 11.0 s). This shift of the rotation point from the wall base to the window bottom is also evident in the first two oscillations of the façade during the L5 stage (5.0 < t < 6.0 s). Finally, the rotation point moves between the bottom (t = 6.75 s) and the top of the window (t = 7.5 s) at the collapse of the façade, in accordance with the observed behaviour presented, respectively, in Figure 4.17 a) and Figure 4.18 b).

The acceleration amplification factors, computed as the ratio between the maximum acceleration acquired on a given accelerometer and the maximum acceleration of the reinforced concrete foundation slab, are presented in Table 4.9 for different points of the main façade (accelerometers identified according to Figure 4.7). It should be referred that the acceleration records were filtered (using a Fourier filter) by removing of high frequency components (f > 25 Hz) in order to avoid the effect of façade impacts at the returning walls which would affect the computed amplification factors. This analysis was also performed for t < 7.1 s, prior to the collapse of the specimen in order to achieve meaningful values.

Table 4.9. Acceleration amplification factors of the main façade for different stage levels

Stage	Max. base acceleration [g]	North top (acc 1)		Centre bellow window (acc 6)		Centre above window (acc 5)		Centre top of gable (acc 4)		South top (acc 7)	
		+	-	+	-	+	-	+	-	+	-
L1-10%	0.08; -0.10	1.14	1.18	1.13	1.14	1.43	1.37	1.87	1.56	1.47	1.36
L2-20%	0.15; -0.15	1.45	1.27	1.17	1.10	1.51	1.30	1.77	1.47	1.51	1.33
L3-40%	0.30; -0.31	1.66	1.24	1.13	1.02	1.75	1.31	2.25	1.59	1.48	1.27
L4-60%	0.42; -0.39	1.84	1.60	1.27	1.16	2.08	1.36	2.85	1.59	1.92	1.28
L5-80%	0.54; -0.49	1.81	1.37	1.59	1.74	0.80	1.48	1.33	1.06	1.13	2.18

NOTE: positive accelerations in the W-E sense (to the exterior of the façade) and negative for E-W sense (to the interior of the façade)

The amplification factors in the positive sense show a linear increase trend with the increasing of ground motion levels, more pronounced at the centre of the façade due to the its flexibility. Moreover, the amplification level is quite similar in both edges (North and South) despite the difference for stage L5. However, in the negative sense, a constant amplification is achieved with the increment of ground motion acceleration despite the value of 2.18 obtained for the south side of the façade, probably caused by impacts of the façade in the south returning wall. This fact (constant amplification factor) may evidence a pure rigid body motion of the front façade because, for negative accelerations, no restraining exists for the inertial forces (i.e. re-turning walls), in contrast with what happens for the positive accelerations.

It is also interesting to analyse the overall differences observed between L4 and L5. In L4 test, the amplification factor raised up to 2.85/1.59 at the top of the gable, while for L5 it decreased significantly both at the top of the gable and above the opening. This is due to the overturning mechanism triggered at stage L4, after having reached a threshold acceleration level, which results from the self-weight of the formed mechanisms, as well as from friction and tensile forces due to interlocking and presence of mortar at the interfaces. Since these extra sources of restraining (friction and tensile stresses) are eliminated once the formed mechanism is acti-vated, subsequent levels of acceleration lower than to the previous ones are required to initiate rocking (only conditioned by the self-weight and geometry of the formed mechanism).

This evidence is also presented in Figure 4.25, where the top displacement (T10) is plotted *versus* the top acceleration (acc4), filtered by a Butterworth 3rd order low pass filter with a cut-off frequency above the frequencies obtained through modal analysis (Table 4.8) for each test level (e.g. for stage L5 the frequency obtained before the test (CAT05) was 4.6 Hz, for which the cut-off frequency was taken as 5.0 Hz). Therefore, the façade motions for the main vibration

mode are identified, where lower frequencies are also present due to important rocking behaviour of the masonry façade. A similar procedure was used in previous shaking table tests found on the literature (e.g. Peng and Iwan (1992); Benedetti *et al.* (1998); Bothara *et al.* (2010)) to identify the response of the first mode of vibration, taking into account a narrow filter around the identified frequencies of this mode.
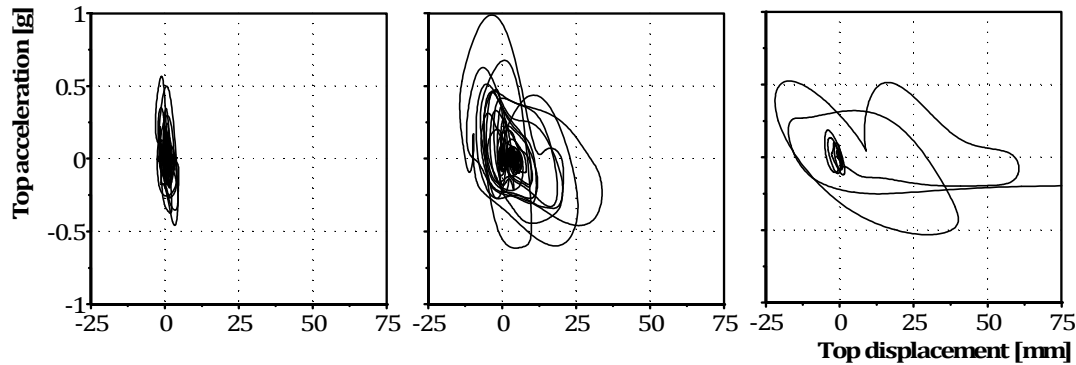
Figure 4.25. Top absolute acceleration vs. top displacement plot, filtered for the main vibration mode. From left to right: L3-40%, L4-60% and L5-80%.

The behaviour of the façade until stage L3 was mainly within the linear range, as the exhibited in the figure. However, in the subsequent stages L4 and L5, the behaviour was strongly non-linear due to damage and formation of the overturning mechanism.

As expected, the maximum acceleration is higher in the positive sense due to the presence of the returning walls, reflected also in the achieved displacement (smaller in the negative sense when compared to positive ones). The shape of the curves presents a maximum negative acceleration value of -0.62 g (achieved at L4 stage) which can be the threshold acceleration to form the overturning mechanism. The stiffness and strength degradation is also observable but it is influenced, in the positive displacement sense, by the rocking behaviour of the façade and not the flexural one which may lead to misinterpreted stiffness evaluation.

Another interesting observation relies on the L5 curve (Figure 4.25), when compared to the displacement time history previously presented (Figure 4.21). It is possible to observe that the first peak displacement is achieved for 60 mm with an acceleration of -0.25 g, while the following peak displacement of 40 mm reflects an increase of the acceleration level (-0.5 g). However, at the major ground motion pulse, which prompted the façade collapse, the acceleration level reaches again 0.25 g. Therefore it is possible to observe that the rocking behaviour leads to similar values of acceleration levels being somehow independent of previously experienced displacements. In fact, a smaller displacement, occurring after a higher displacement had been previously achieved, should not occur with a higher acceleration for a response based only on the system flexibility (because the stiffness and strength degradation should decrease with the

number of repetitions). This observation is in accordance with the nature of rocking behaviour and it was interesting to verify its occurrence in the experimental test.

As a matter of curiosity, and taking into account a simplified activated overturning mechanism (full overturning of the façade at the window level, as depicted in Figure 4.17) and the corresponding geometry, the following geometrical parameters were obtained, as well as the corresponding values of acceleration and velocity as the output of equations (4.1) and (4.2).

Table 4.10. Geometrical and triggering parameters of the simplified overturning mechanism

y_{cg}[m]	x_{cg}[m]	α [rad]	R [m]	PGA_{min}[g]	v_{min} [cm/s]
1.295	0.295	0.224	1.328	0.23	80.8

As reported in Table 4.10, the minimum acceleration (PGA_{min}) which triggers the rocking motion was achieved for small values of the seismic motion, as also presented in Table 4.8. However, the minimum velocity necessary to overturn the block was only achieved for the last test stage (L5-80%), as evidenced in Figure 4.26 through the velocity time histories. It is worth referring that v_{min} value is relative to the centre of gravity, closely located to the position of the accelerometer (acc5) placed above the window.
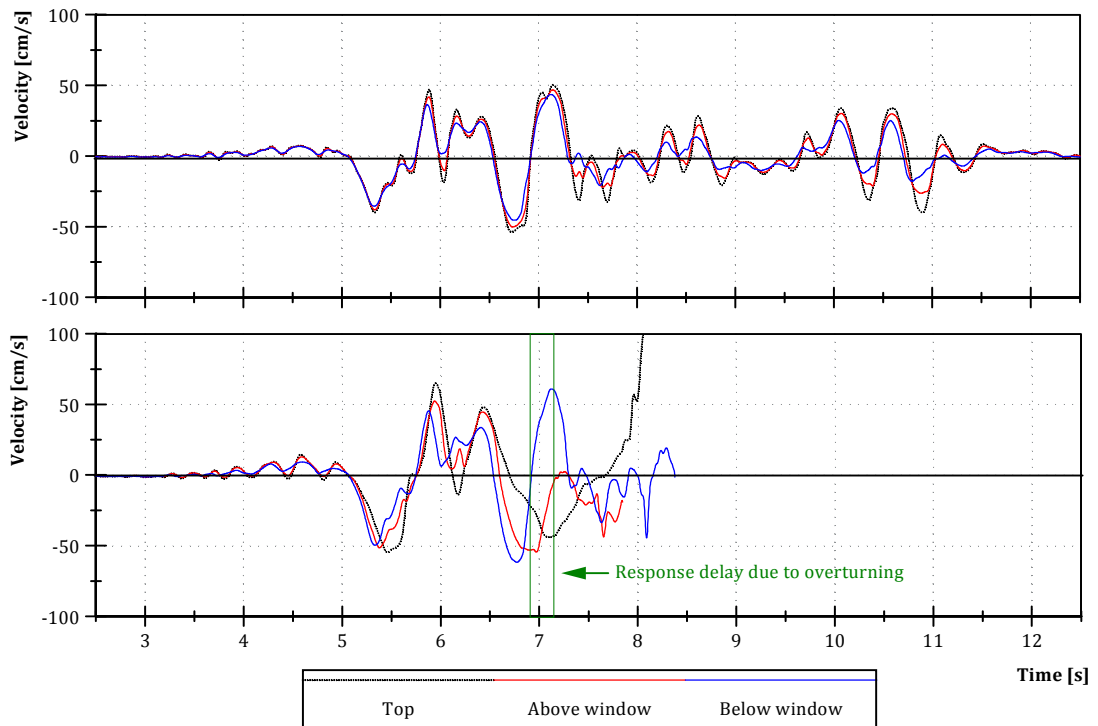
Figure 4.26. Velocity time histories, respectively, for L4 (upper plot) and L5 (lower plot) tests.

The velocity time histories are consistent with the rocking behaviour of the masonry façade. When observing L4, it is clear that the responses of the analysed façade points are in the same motion phase, reaching a maximum velocity of 50 cm/s. However, for the L5 test, the rocking motion of the façade above the window level yielded an out-of-phase response, observable in the lower plot of Figure 4.26. The maximum velocity achieved above the window level was 55 cm/s (62 cm/s below window; 65 cm/s at the top and prior the collapse), significantly far from v_{min} but leading to a ratio $v/v_{min} \simeq 0.70$.

In conclusion, although not having achieved directly the required theoretical v_{min} value to overturn the façade, and considering that the interaction between the rocking façade and the remaining specimen was important to trigger the specimen failure, 0.70 v_{min} and the outer leaf instability may be seen as possible indicative measures to predict the collapse of a *sacco* masonry façade after triggering of the overturning mechanism.

4.6. CONCLUSIONS

The work herein presented reports full scale shaking table tests performed at LNEC (Lisbon, Portugal) focused on the characterization of the out-of-plane dynamic behaviour of a stone masonry façade.

The structure to be tested was selected based on the goals of the research project, which aimed at studying the out-of-plane overturning behaviour of a full-scale realistic reproduction of an existing stone masonry façade. A detailed description of this structure is included.

In addition, the selection of an input ground motion capable of triggering the overturning mechanism, compatible with the shaking table capacities, was an important part of the work. For this purpose, and using 74 different accelerograms, several numerical analyses were carried out based on the rocking behaviour of rigid bodies taking into account three predefined overturning mechanisms likely to occur, wherein the dynamic characteristics of the seismic motions played a major role in the final selection. At the end, a ground motion was selected with characteristics typical of near-fault events (usually correlated to the collapse of masonry façades due to velocity pulses).

The selected seismic motion proved to be adequate taking into account the main goal of the shaking table test (i.e., no significant damage should be imparted to the masonry walls prior to activation of the overturning mechanism) because no significant damage was induced in the masonry (neither disaggregation nor local damages occurred) until the achievement of a threshold acceleration leading to an overturning mechanism. However, from the observation of the tests it was concluded that another test run with the same or other accelerogram, scaled so

as to enforce the response between the mechanism triggering and before the structure collapse, would have been very fruitful in better characterizing the out-of-plane behaviour. Furthermore, it should be referred that the preliminary numerical simulations to select the ground motions did not provide a precise reproduction of the expected behaviour, but still they were very helpful on defining a suitable accelerogram from the large available set.

Concerning the experiments, five test stages were made in one specimen and only one test level was performed in the other one. All the tests were interspersed with modal identification for assessing the damage of the structure by analysing the modifications of the main vibration frequency.

Regarding the behaviour of the tested specimens (mainly H1, the one tested with the expected shaking table response), a global rocking behaviour of the masonry façade was observed with cylindrical hinges formed at the window level. A successful identification of the façade impacts at the returning walls was made resorting to the high frequency content of the acceleration records of the façade.

Energy dissipation occurred due to these impacts on the return walls, thus reducing the one-sided rocking of the façade after the impact, without rebounding effects. It was also observed that the masonry assemblage strongly influenced the behaviour and final collapse mechanism of the façade due to a quasi-continuous vertical joint from the window frame up to the top of the gable. Indeed, the vertical orientation of the window jambs led to the façade collapse, mainly due to the instability of these elements. The collapse was also found correlated with the instability of the outer leaf rather than the global wall instability. Thus, for multi-leaf masonry façades, a maximum displacement capacity lower or similar to the thickness of the outer leaf may provide an indicator of the maximum displacement capacity.

Slight torsion of the façade was observed due to the better interlocking to the North returning wall rather than to the South one. It was also possible to estimate the position of the rotation axis of the façade based on the assumption of rigid body overturning, which was found to be positioned mainly between bottom and top of the window level. The threshold acceleration value for façade overturning was also observed in the experimental data, either in terms of acceleration amplification factors or acceleration *vs.* displacement records at the top of the gable (a sort of pseudo-capacity curve). Moreover, a ratio of 0.70 v_{min}, where v_{min} is obtained by energy conservation assumptions, may be seen as a condition for the collapse of a *sacco* masonry façade.

As a final remark, the shaking table tests allowed concluding that, although the out-of-plane behaviour of a masonry façade may be assumed as a rigid body rotation around a certain pivot axis, for multi-leaf masonry structures the instability is governed by the outer leaf as well as the masonry assemblage.

Chapter 5.

EXPERIMENTAL AND ANALYTICAL EVALUATION OF THE FREE ROCKING BEHAVIOUR OF A STONE MASONRY WALL THROUGH EQUIVALENT BLOCK APPROACH

SUMMARY

The evaluation of the dynamic behaviour of rocking elements is directly correlated to the energy dissipated due to the impacts at the base interface, which can be represented by means of a coefficient of restitution. This schematization is commonly accepted as representative of the out-of-plane response of stone masonry walls. An experimental campaign (in a lab environment) aiming at assessing the value of this coefficient for a *sacco* granite masonry wall is presented in this work. The rocking motion at a predefined bed joint level was induced in the tested specimens in order to validate a novel test setup designed to assess the coefficient of restitution value by means of a realistic reproduction of the rocking behaviour of a single element, under the hypothesis of an infinitely stiff system above the bed joint level.

As the main objective of the work was to assess the rocking behaviour of a masonry wall which looses energy at the impacts at a certain joint level, the flexural behaviour was not desirable and had to be avoided. For this purpose, a test setup based on the equivalent block approach (EBA) was developed. In the final section of this work, comparisons between experimental and numerical results are presented together with some preliminary conclusion on the appropriate modelling strategy and the values of the coefficient of restitution to be used for the seismic assessment of the out-of-plane rocking behaviour of multi-leaf masonry walls.

5.1. INTRODUCTION

The out-of-plane vulnerability of traditional unreinforced masonry walls is the major cause of large extent of destruction of existing masonry buildings during several earthquakes, as observed, for example, in L'Aquila (Italy, 2009, Figure 5.1 a) and more recently in Lorca (Spain, 2011, Figure 5.1 b) and c)). In both such events near-fault effects with strong directivity could be noticed based on the post-earthquake observation of the distribution of damages to the historical structures. Apart from the case of buildings with good connections between perpendicular walls and between walls and floors, the observed damage was essentially due the out-of-plane response of walls, leading in some cases to the complete collapse.

The dynamic behaviour of these elements may be simulated by a rigid body model rocking at the base level, where the energy is dissipated through impacts. Two main observations may be addressed for these models: elements under two-sided rocking, as in the case of Figure 5.1 a) and b); elements under one-sided rocking, as the case of Figure 5.1 c) and most of the masonry façades of existing buildings.

(a)   **(b)**   **(c)**
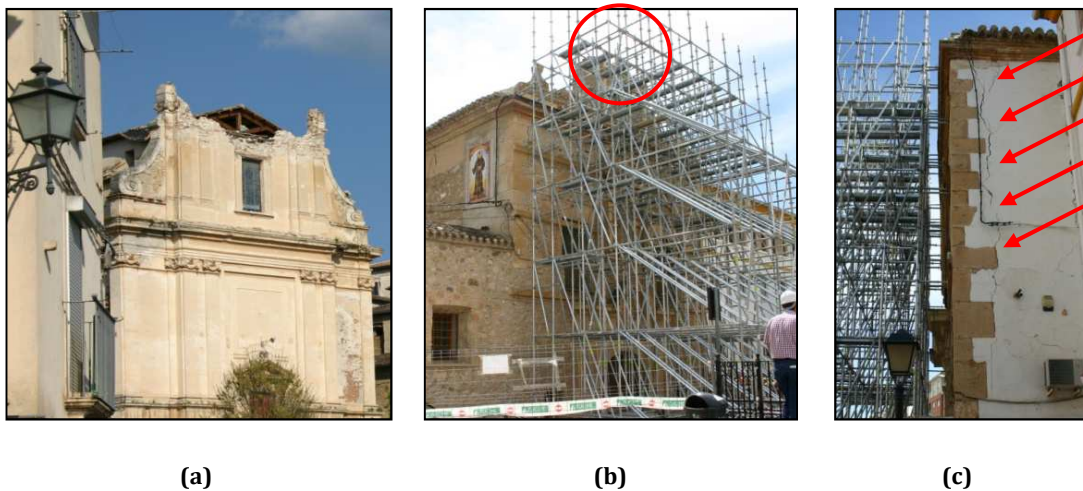
Figure 5.1. Out-of-plane damages caused by recent earthquakes: a) San Demetrio nè Vestini, L'Aquila earthquake; b) and c) Lorca earthquake: bell tower collapse and overturning mechanism formed with temporary structure to prevent out-of-plane collapse

The majority of the works (experimental or numerical) found in the literature concerning the rocking behaviour of rigid bodies are related to two-sided rocking (Housner 1963; Aslam *et al.* 1978; Priestley *et al.* 1978; Yim *et al.* 1980; Wong and Tso 1989; Lipscombe and Pellegrino 1993; Makris and Roussos 2000; Liberatore and Spera 2001; Peña *et al.* 2007), including several experimental tests on different type of materials (e.g. concrete blocks Aslam *et al.* (1978), concrete masonry with rigid elements at the base and different foundation elements (Priestley *et al.* 1978), marble blocks (Liberatore and Spera 2001), granite stones (Peña *et al.* 2007)). However, concerning masonry walls, only the recent work by Sorrentino *et al.* (2011) aimed at determining experimentally the main parameter which governs the rocking behaviour of an

element, i.e. the coefficient of restitution, *r*. Other works can be found in the literature where this coefficient is used, as the work by Sharif *et al.* (2007) regarding clay brick masonry walls, but the experiments were not specifically performed to determine this parameter.

The rocking behaviour of a infinitely rigid body subjected to a rotation value θ can be represented by the equation of motion of Eq. (5.1), based on Figure 5.2 and initially presented by Housner (1963), in the framework of the so-called classic rocking theory.

$$I_O \ddot{\theta}(t) = -W \; R_0 \; \sin\left[\alpha_0 - \theta(t)\right] \tag{5.1}$$
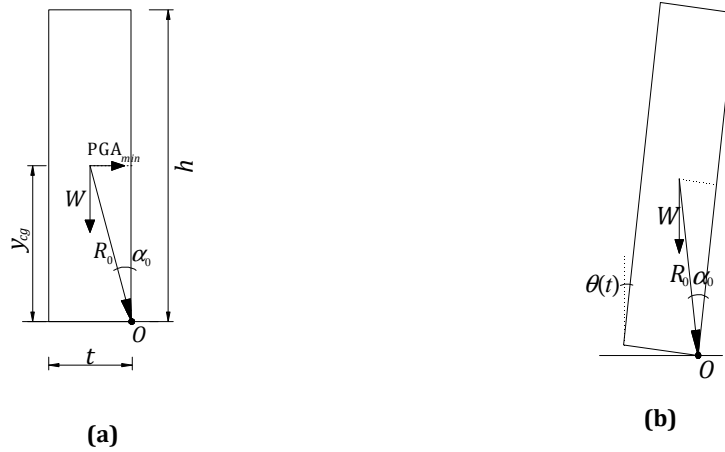
Figure 5.2. Geometrical parameters involved on a rocking motion: a) $\theta(t) = 0$; b) $\theta(t) > 0$

In Eq. (5.1), I_O is the rotational moment of inertia relative to the wall corner *O*, *W* is the block weight, θ(*t*) is the block rotation at a given instant *t*, $\ddot{\theta}(t)$ is the corresponding angular acceleration, while R_0, α_0 and y_{cg} are geometrical parameters (where the latter stands for the height of the block gravity centre). Setting $WR_0 / I_O = p_0^2$, where p_0 is a measure of the dynamic characteristics of the block (Makris and Roussos 2000), the equation of motion becomes:

$$\ddot{\theta}(t) = -p_0^2 \left[\sin\left(\alpha_0 - \theta(t)\right)\right] \tag{5.2}$$

The angular velocity of a block under free rocking around the base can be correlated before and after the impacts. As firstly introduced by Housner (1963), the kinetic energy ratio (r_E) correlates the angular velocity before and after the impact and is expressed by Eq. (5.3), where $\dot{\theta}_n$ is the peak angular velocity at the instant t_n immediately before the impact *n*, while $\dot{\theta}_{n+1}$ is the angular velocity immediately after the impact at the base, derived from the assumption of kinetic energy conservation.

$$r_E = \left(\frac{\dot{\theta}_{n+1}}{\dot{\theta}_n}\right)^2 \tag{5.3}$$

However, other authors have defined this kinetic energy ratio as the coefficient of restitution (e.g. Makris and Roussos (2000)) and, in fact, it was found somehow non-consensual the definition of the coefficient of restitution mentioned in several works. The first definition of that coefficient was presented by Aslam *et al.* (1978), as a direct ratio between angular velocities (r_v) as presented in Eq. (5.4).

$$r_v = \frac{\dot{\theta}_{n+1}}{\dot{\theta}_n}$$ (5.4)

Comparing Eq. (5.3) with Eq. (5.4), it is clear to identify that:

$$r_E = r_v^2$$ (5.5)

The main difference between both definitions relies on the parameter used to relate the angular velocity before and after the impact. In the case of Housner formulation (defined as classic rocking theory, CRT, in the following sections) the coefficient is presented for the kinetic energy of the block, while the definition by Aslam *et al.* is given directly for the angular velocities ratio. This last definition is the most used in the works found relevant in this framework (Yim *et al.* 1980; Giannini 1984; Winkler *et al.* 1995; Andreaus and Casini 1999; Liberatore and Spera 2001; Makris and Konstantinidis 2003; Konstantinidis and Makris 2005; Sorrentino *et al.* 2008a; Sorrentino *et al.* 2011) and it will be the one used in the following section (defined as $r = r_v$), despite the definition presented by the classic theory (Priestley *et al.* 1978; Makris and Roussos 2000; Zhang and Makris 2001).

Bearing this in mind, the maximum value of the coefficient of restitution (r_{max}) for an inelastic impact at the base, for a homogeneous wall can be shown to be given by Eq. (5.6) (Housner 1963).

$$r_{max} = 1 - \frac{3}{2}\sin^2\alpha_0$$ (5.6)

However, several discrepancies are usually found between experimental and theoretical results. Some modifications to include the effect of bouncing in the rocking motion are reported in the literature, as introduced by Lipscombe and Pellegrino (1993), which were found to be more relevant for slenderness ratios ($\lambda = h/(2\,y_{cg})$) smaller than 4. For the specimens tested in the present experimental work, the slenderness ratios take the values of 4.6 and 4.7, thus higher than 4 and, therefore, no bouncing is considered.

In the same line, no sliding is likely to occur because, as presented by Shenton (1996), the necessary condition of a block to enter a rocking motion without sliding is $\mu_s > 1/\lambda$, where μ_s is the static friction coefficient. The largest value of $1/\lambda$ of the experiments is 0.22, thus considerably lower than the expected μ_s values of this type of masonry and mortar (in the range of 0.6-0.8 (Vasconcelos and Lourenço 2009)).

From the literature survey it was found that no experimental tests were carried out so far in order to determine the coefficient of restitution (r) on *sacco* masonry walls, addressing the problems and particularities of the heterogeneity presented in this type of masonry assemblage. Therefore, in order to contribute for gathering further knowledge about this issue, the present work aims at describing a detailed analysis of free rocking tests performed on this type of masonry using a novel test setup based on the equivalent block approach. Moreover, a comparison between test results' interpretation is presented as well as numerical model procedures to simulate the dynamic behaviour of the tested specimens.

5.2. LABORATORY FREE ROCKING TESTS

5.2.1. Equivalent block approach (EBA)

The behaviour of a rigid body rocking around the corners at the base is represented by Eq. (5.1) and governed by two main parameters inherent to the block: p_0 and α_0. The former is expressed in terms of the block mass and inertia properties but its value (p_0) is theoretically independent of the particular values of W, R_0 and I_0, in the sense that the same p_0 value can be obtained from different combinations of W, R_0 and I_0. By contrast, the latter (α_0) is strictly related to the block geometry, as depicted in Figure 5.2 for an infinitely rigid body.

Hence, a theoretical block may be represented by an "equivalent block" if the p_0 and α_0 values are similar to the theoretical ones. This is the core idea of the test setup presented in the next section which, in the experimental campaign reported herein, aimed at representing the full overturning of a façade above the first bed joint level of a *sacco* masonry wall, 3.0 meter high and 0.65 meter thick, of a real construction.

This approach can be also applied to reduced scale specimens for the experimental study of the rocking behaviour, with the specific aim of determining the restitution coefficient, while in such cases it does not provide directly information on the ultimate conditions, which are related to the loss of equilibrium of the block and hence to its actual dimensions as well as scale effects (Housner 1963).

In reality, interface contact is not infinitely rigid due to the mortar joint material, as shown in Figure 5.3. Thus, the introduction of a flexible interface in the model is likely to reproduce better the rocking behaviour of such type of masonry wall. Consequently, the dynamic equation of motion must include a new contribution which accounts for the moment due to the mortar joint reaction, thus shifting the rocking point to the interior of the block (Figure 5.3), being the reaction force W placed at a distance a_f from the edge, which leads to Eq. (5.7).
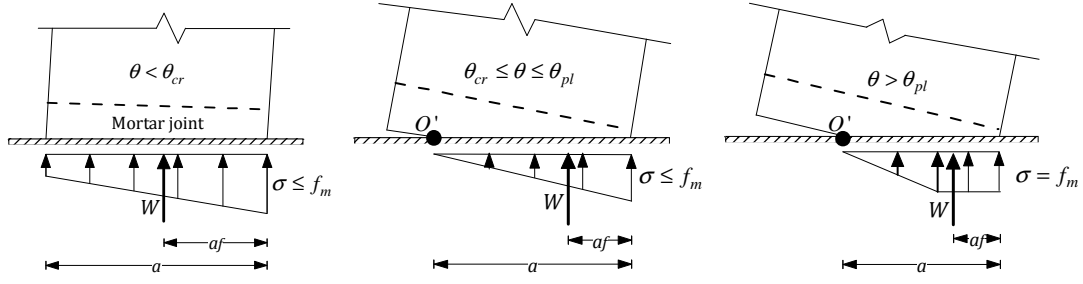
Figure 5.3. Contribution of interface flexibility for different loading cases

Moreover, the rotational moment of inertia ($I_0[\theta(t)]$) should be computed relative to a new rotation point O' (not coincident with the edge O), which may vary if a flexible interface at the base is considered.

$$I_{0'}\left[\theta(t)\right]\cdot\ddot{\theta}(t) = -W\cdot\left[R_0\sin\left[\alpha_0 - \theta(t)\right] - a_f\left[\theta(t)\right]\right] \tag{5.7}$$

If the mortar joint is assumed to be flexible and the upper and lower elements are taken as infinitely rigid, it is possible to compute directly the position of the reaction force, $a_f(\theta)$, through the block's rotation θ, correlated to the curvature χ, by $\chi = \theta/e$, where e is the thickness of the mortar joint.

As shown in Figure 5.3, the position of the reaction point should be computed for three different cases: *i*) full contact; *ii*) cracked section; *iii*) cracked section with partialization.

For a flexible interface with normal stiffness k_n ($k_n = E/e$, where E is the mortar Young's modulus) and compressive strength f_m, it is possible to compute the exact location of the reaction force. In particular, the relation between extensions (ε) and rotation (θ) at imminent cracking ($\theta = \theta_{cr}$; null stress at one of the edges) is given by:

$$\begin{cases} \chi_{cr} = \dfrac{\theta_{cr}}{e} \\ \varepsilon_{cr} = \chi_{cr}\, t \end{cases} \Leftrightarrow \varepsilon_{cr} = \dfrac{\theta_{cr}}{e}\, t$$

Since the reaction force (W) is given by $W = \sigma\, t\, l\, /2$, the imminent cracking rotation, θ_{cr}, is given by Eq. (5.8).

$$\theta_{cr} = \frac{2\,W}{l\,k_n\,t^2} \tag{5.8}$$

The section's partialization is achieved for the threshold rotation presented in Eq. (5.9), by assuming a bilinear elastic representation of the joint's compression behaviour (although beyond the present work scope, more complex masonry constitutive laws could be used but time-efficient solutions may not be obtained).

$$\theta_{pl} = \frac{f_m^2 \, l}{2 \, W \, k_n} \tag{5.9}$$

Therefore, the position of the reaction force at the joints' interface can be obtained with the following expressions:

i)   for $\theta(t) \le \theta_{cr}$:

$$a_f \left[\theta(t) \right] = \frac{t}{2} - \frac{t \, l}{12 \, W} t^2 \, k_n \, \theta(t) \tag{5.10}$$

ii) for $\theta_{cr} \le \theta(t) \le \theta_{pl}$:

$$a_f \left[\theta(t) \right] = \frac{1}{3} \sqrt{\frac{2 \, W}{l \, k_n \, \theta(t)}} \tag{5.11}$$

iii) for $\theta(t) \ge \theta_{pl}$:

$$a_f \left[\theta(t) \right] = \frac{1}{2} \left[\frac{W}{f_m \, l} + \frac{1}{12} \frac{f_m^3 \, l}{W \, k_n^2 \, \left(\theta(t) \right)^2} \right] \tag{5.12}$$

It is possible to observe that the values of f_m (joint compressive strength) and k_n (joint normal stiffness) influence the reaction force position but in different ways. Moreover, the second contribution for the right hand side of Eq. (5.12) may be neglected if the rotation of the block is significant, yielding the approximate solution presented by Eq. (5.13).

$$a_f \left(\theta \right) = \frac{W}{2 f_m \, l} \tag{5.13}$$

In order to analyze the influence of mechanical parameters in the reaction force position, Figure 5.4 shows plots of $a_f[\theta(t)]$ against the rotation θ, for different values of k_n and of f_m, computed for a block with similar characteristics to the specimens presented in this work (dimensions of 1.3x0.65x3.0 m³ and specific weight of 19.0 kN/m³). It should be referred that mechanical characterization tests were made in lime mortar specimens according to EN 1015-11 standard (CEN 1999), leading to 0.53 MPa and 1.28 MPa, respectively for flexural and compressive strength. In addition, Figure 5.4 also includes a comparison between the exact and approximate solution for $\theta(t) > \theta_{pl}$ given, respectively, by Eq. (5.12) and (5.13), where the dotted lines refer to the approximate solution.

Figure 5.4 shows that the (a_f - θ) curve is defined by three different branches, representative of each state of the cross section. It is possible to observe that, for the range of mechanical parameter values typical of this type of walls, the linear elastic range is valid only for very small rotation levels ($\theta < 10^{-4}$ rad, even with k_n = 0.6 MPa/mm). Therefore the linear elastic behaviour of the section may be neglected for the computation of the element behaviour.
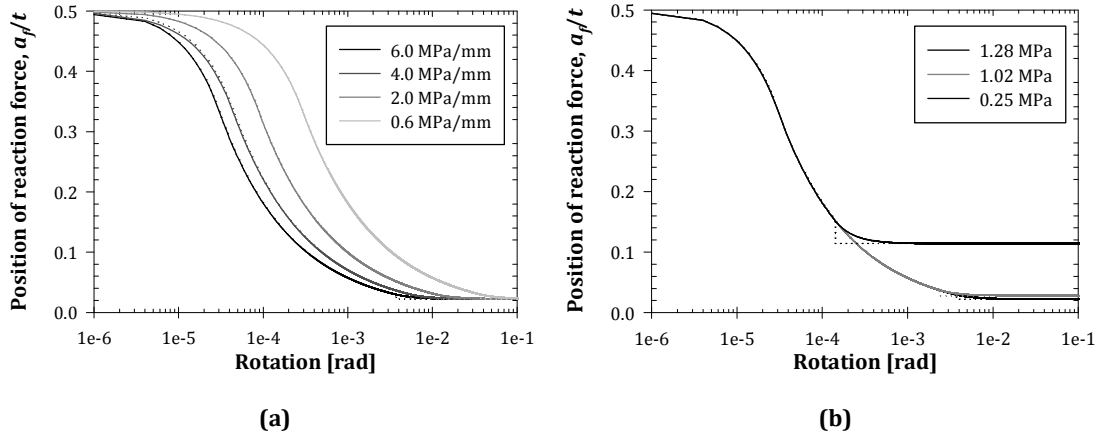
Figure 5.4. Comparison between exact (solid line) and approximate solution (dotted line). Influence of: a) joint normal stiffness, k_n, for f_m = 1.28 MPa; b) compressive strength, f_m, considering k_n = 6.0 MPa/mm

Concerning the cracked section without section partialization, it may be important for very low values of k_n (0.6 MPa/mm), while for usual ones the complete section partialization may be assumed. Finally, for cross section partialization, the approximate solution is well matching the exact one and therefore it can be used; differences are observable only for minimal rotations values (θ < 0.001rad).

Taking into account the range of mechanical properties' values estimated for this type of walls, the position of the reaction force can be assumed as the one given considering the complete partialization of the section, as observable in Figure 5.4. For this reason, the simplification in the computation of the rotational moment of inertia to be used in Eq. (5.7) can be made because the rotation points are placed at a fixed distance from each edge of $a = 2\,a_f$. Therefore, the rotational moment of inertia can be adequately approximated by a constant value, independent from the block's rotation θ.

For other type of elements, where the computation of the rotational inertia cannot be assumed as constant (as explained in the previous paragraph), the equation of motion which takes into account the shift of the rotation point (bearing in mind Eq. (5.7)), is given by Eq. (5.14), where R_0 is the geometrical distance R for the initial position (θ = 0).

$$\ddot{\theta}(t) = -p^2 \left[\sin\left[\alpha_0 - \theta(t) \right] - \frac{a_f\left[\theta(t) \right]}{R_0} \right] \tag{5.14}$$

If $p^2 = WR_0/I_0[\theta(t)]$, and the section is theoretically rectangular, the influence of the rotational inertia $I_0[\theta(t)]$ only affects the value of p, given by:

$$p = p\left[\theta(t) \right] = \sqrt{\frac{g\,R_0}{\frac{1}{12}\left(t^2 + h_{eq}^{\,2} \right) + R\left[\theta(t) \right]^2}} \tag{5.15}$$

where h_{eq} is the height of the equivalent block (given by Eq. (5.16) which leads to the same rotational moment of inertia of the original structure) and $R[\theta(t)]$ is the distance from the gravity centre to the rotation point. This value, dependent of the rotation value, is obtained by Eq. (5.17), where a is the distance of the rotation point to the edge, as defined above.

$$h_{eq} = \sqrt{\frac{3\,g\,I_O}{W} - t^2} \qquad (5.16)$$

$$R\left[\theta(t)\right] = \sqrt{y_{cg}^2 + \left[\frac{t}{2} - a\left[\theta(t)\right]\right]^2} \qquad (5.17)$$

The following Figure 5.5 illustrates the influence of the rotational inertia in the dynamic property of the block (p, from Eq.(5.15)), for different slenderness ratios (λ) and for a range of positions of the rotation point (given by the ratio a/t).
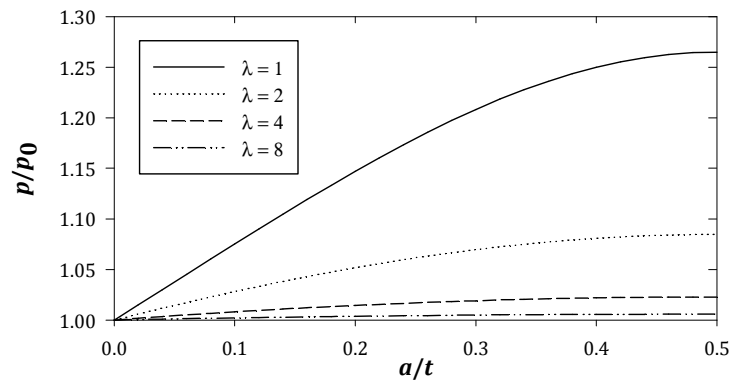
Figure 5.5. Influence of neutral axis depth (a/t) in the dynamic properties (p) of systems with flexible interface, considering different slenderness levels (λ).

For slenderness values higher than $\lambda > 4$ (as the tested elements reported in the following sections) a reasonable approximation is obtained considering $p = p_0$, where p_0 is the value obtained for infinitely rigid behaviour. Visible differences may result only for small rotation levels (high a/t values), where the rotation point is located towards the interior of the element.

Concerning the effect of the mechanical parameters, it can be seen that the influence of k_n is reduced within the range of usual values ($2.0 < k_n < 6.0$ MPa/mm for the used mortar, with characteristics similar to those obtained in previous studies (Almeida 2000)), being relevant only for unrealistic values of joint normal stiffness (0.6 MPa/mm). However, the influence of compressive strength is found to be very significant for the position of the reaction force, as observable in Eqs. (5.9) and (5.12) and in Figure 5.4.

For this reason, the compressive strength of the joint mortar seems to be important in the correct computation of the reaction force position, differently from the normal stiffness influence. Bearing this in mind, it is possible to directly introduce the flexibility of the interface in the

rocking motion of the block, which modifies the global behaviour of the element by shifting inwards the position of the rocking point (as illustrated Figure 5.6 a)) Moreover, Eqs. (5.10), (5.11) and (5.12) allow computing the variable angle $\alpha(\theta)$ (evidenced in Figure 5.6 b) and helpful for the experimental data interpretation addressed in latter sections), directly from the block rotation θ according to Eq. (5.18).

$$\alpha(\theta) = \tan^{-1}\left(\frac{t/2 - a(\theta)}{y_{cg}}\right) \tag{5.18}$$

Finally, the full dynamic equation of motion can be described by Eq. (5.19) where "sgn" stands for the signum function and p may be computed either for the undeformed configuration or taking into account its full computation. It should be referred that considering a flexible interface at the base contact leads to a different equation from that of infinitely rigid contact (Eq.(5.2)).

$$\ddot{\theta}(t) = -p^2\left\{\sin\left(\alpha_0 \cdot \operatorname{sgn}\left[\theta(t)\right] - \theta(t)\right) - \frac{1}{R_0} \cdot a_f(\theta) \cdot \operatorname{sgn}\left[\theta(t)\right]\right\} \tag{5.19}$$

The previous equation takes into account only geometrical parameters with the exception of k_n and f_m which are correlated to the material properties of the interface, and should be the same for the original and equivalent structure. Therefore if p, α_0, R and W are similar to the original block, the use of an EBA test setup is expected to simulate the rocking behaviour of the original element.

(a)   **(b)**   **(c)**
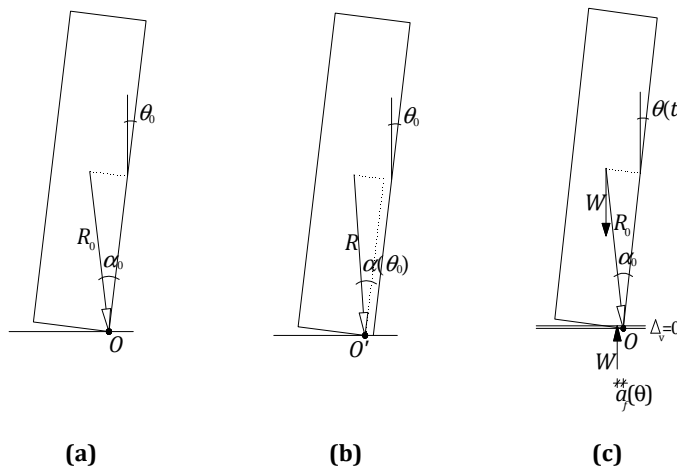
Figure 5.6. Models for the simulation of the dynamic rocking behaviour of the tests, parameters and governing equations: a) fully rigid; b) semi-rigid; c) flexible

$\boldsymbol{p} =$	$p_0 = WR_0/I_0$	$p_0 = WR_0/I_0$	$p = WR_0/I_{0'}[\theta(t)]$
$\boldsymbol{\alpha} =$	α_0	$\alpha(\theta_0)$	α_0

Governing equations:

a) $\ddot{\theta}(t) = -p_0^2 \left\{ \sin\left[\alpha_0 \cdot \text{sgn}\left[\theta(t) \right] - \theta(t) \right] \right\}$

b) $\ddot{\theta}(t) = -p_0^2 \left\{ \sin\left[\alpha\left[\theta_0\right] \cdot \text{sgn}\left[\theta(t) \right] - \theta(t) \right] \right\}$

c) $\ddot{\theta}(t) = -p^2 \left\{ \sin\left[\alpha_0 \cdot \text{sgn}\left[\theta(t) \right] - \theta(t) \right] - \dfrac{1}{R_0} \cdot a_f\left(\theta \right) \cdot \text{sgn}\left[\theta(t) \right] \right\}$

In summary, three different models (Figure 5.6) can be considered when analyzing and simulating the experimental results of masonry walls rocking at the base: *i*) <u>fully rigid</u>: rigid block and rigid interface (with fixed rotation point at the edge); *ii*) <u>semi-rigid</u>: rigid block and flexible interface (with fixed rotation point inside the section at $O'(\theta_0)$, dependent on the interface properties); *iii*) <u>flexible</u>: rigid block and flexible interface (variable rotation point O'; moments taken at O and moment of inertia given by $I_{O'} = I_O[\theta(t)]$; $a_f = a_f[\theta(t)]$).

In the following sections, α_0 stands for the geometrical parameter taking into account the undeformed position (case *i*)) while α (or $\alpha(\theta_0)$) refers to case *ii*).

5.2.2. Description of the specimens and test setup

The test setup developed specifically for this type of experiment consisted on a rigid element connected to a small masonry wallette, with geometrical parameters, mass and a rotational inertia, so as to represent an equivalent block to simulate the original structure. The small wallette consisted of two layers of masonry assembled with a poor mortar representative of a realistic *sacco* masonry wall (double leaf with poor infill). The bottom masonry layer was rigidly connected to a reinforced concrete foundation (fixed to the lab strong reaction floor) using reinforced cement mortar (mechanically connected to the foundation through steel rebars, Figure 5.7 a)), and mechanical connectors, Figure 5.7 b), screwed at the bottom of the masonry blocks that were placed over the fresh mortar (Figure 5.7 c)).

The presence of the connectors at the stone levels prevents any uplifting of the stones, but the infill was not fully restrained at the foundation. Between the two masonry layers, the bed joint is made of traditional lime mortar and respecting the traditional constructions techniques.

The second (and top) masonry layer is similar to the bottom layer, but the steel connectors were placed on the top of the stones in order to connect them to the upper element (a small reinforced concrete slab), as shown in Figure 5.7 d). This small reinforced concrete slab was placed at the top to provide appropriate connection (using threaded rods) to the masses located above the wallette, thus ensuring a proper link and distribution of the load.

(a)   (b)

(c)   (d)
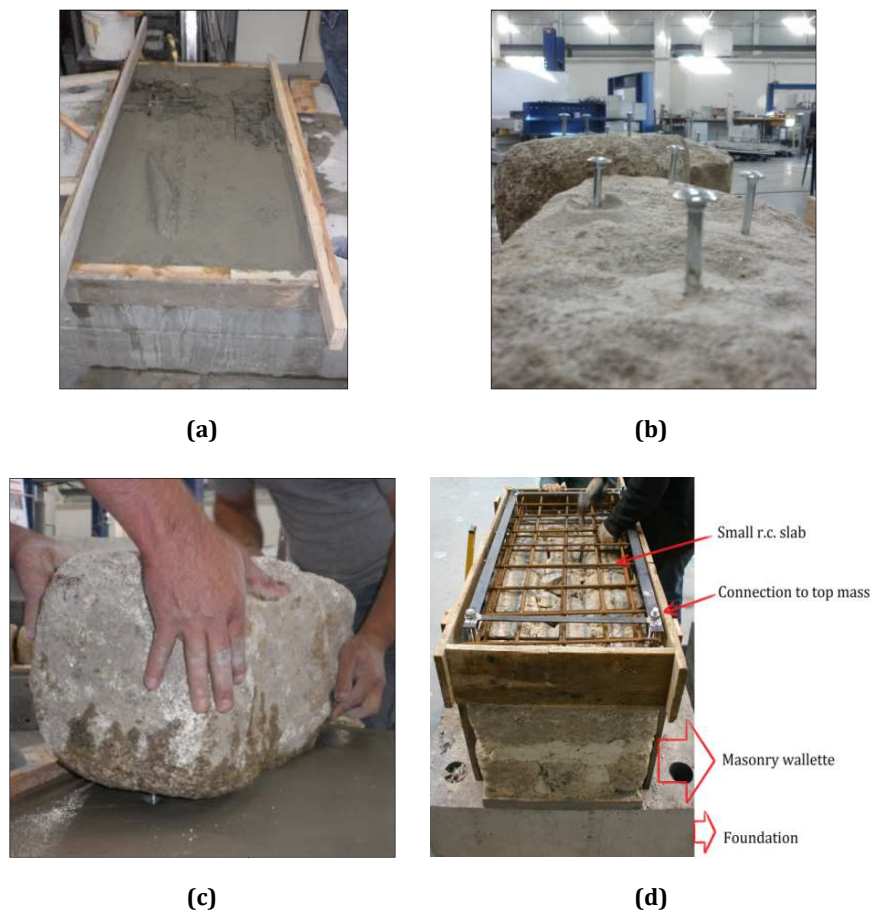
Figure 5.7. Test setup details: a) bottom layer; b) stone connectors; c) first stone with fresh mortar; d) detail of the connection at the top of the wallette

A general overview of the complete test apparatus is shown in Figure 5.8, where it is also possible to observe a cable connecting the wall to an actuator which allowed imposing initial rotation to the wall by a predefined value θ_0, after which it was left to rotate under free rocking motion by cutting the cable. Since the test campaign aimed at taking into account the joint degradation and repeatability, the test procedure involved four different initial rotation values, each test being repeated sequentially between three to five times, as shown in Table 5.1. Initial rotation values (θ_0) are considered taking into account the ratio $\theta_0/\alpha(\theta)$, noting that $\theta_0 = \alpha = \alpha(\theta)$ leads to the theoretical instability of the system.

At the end of the tests, a repetition was made for each rotation level, from the largest to the smallest value. For the test procedure validation and evaluation of the joints degradation, two specimens, FR1 and FR2, were tested, as reported in Table 5.1. For a given specimen, each test identification is composed by the specimen name, the test name and the test number. As an example, FR1-L3-R refers to the test of specimen FR1 subjected to the initial rotation level L3 (θ_0/α = 0.35), and the final repetition performed at the end of the tests.

Table 5.1 highlights the number of tests and repetitions performed for each test as well as the adopted sequences.

(a)   **(b)**   **(c)**
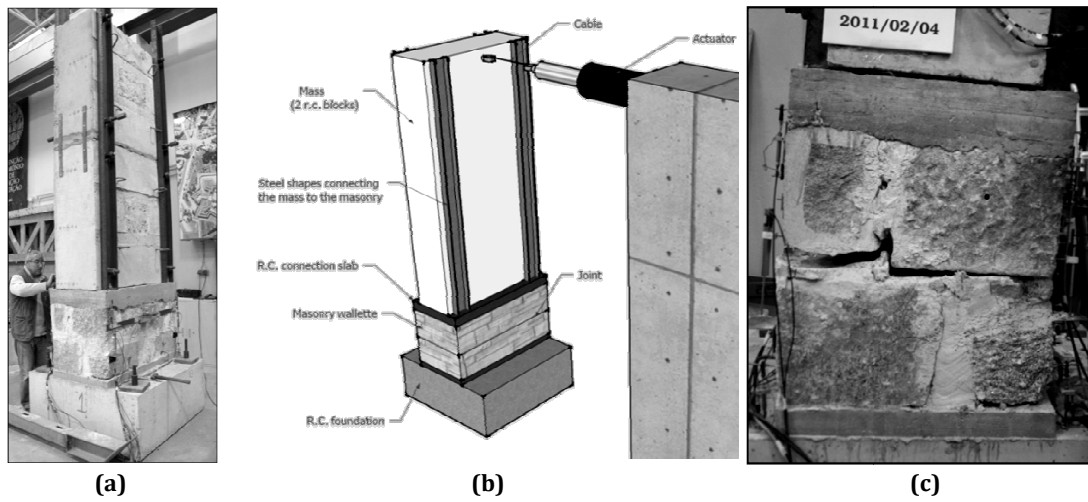
Figure 5.8. View of the test apparatus: a) preparation; b) schematic representation; c) joint opening at initial rotation (FR1-L4-1 test)

Table 5.1. Test sequences and details

Specimen	θ_0/α	Test name	Tests number	Tests	Total number of tests
FR1	0.05	L0 (a)	-	5	18 + 3 repetitions at the end
	0.15	L1	1*, 2*, 3, 4*, 5*	5	
	0.25	L2	1, 2, 3*, 4*, 5	5	
	0.35	L3	1, 2, 3, 4, 5	5	
	0.40	L4	1, 2, 3	3	
	0.35	L3	R	1	
	0.25	L2	R	1	
	0.15	L1	R	1	
FR2	0.35	L3	1, 2, 3	3	9 + 3 repetitions + 3
	0.25	L2	1, 2, 3	3	
	0.15	L1	1, 2, 3	3	
	0.35	L3	R	1	
	0.25	L2	R	1	
	0.15	L1	R	1	
	0.40	L4	1, 2, 3	3	

(a)   Initial test with small displacement to check the efficiency of the setup and data acquisition
▪   (*)   Data not acquired due to acquisition problems

Indeed, because one of the objectives was to assess the test repetition, the sequence followed in FR2 was the inverse of that for FR1, with the exception of L4 which was performed at the end of all the other test levels (including final repetitions) due to limitations of displacement range at the beginning of the test.

As described later in section 5.3, the influence of repetitions in the final results will be quite interesting, somehow questioning some conclusions obtained by other authors in tests with other materials. The FR2 specimen was subjected only to three tests for the same rotation level because in FR1 it was noticed that the influence of repetitions was important, causing mortar damage and influencing the subsequent experiments with different initial rotation levels. Hence three valid tests were considered sufficient to capture the behaviour and joint degradation effect for a given rotation level L# (where # stands for the numbering adopted in Table 5.2).

As mentioned at the beginning of this section, the top mass was selected to have properties similar to those of a 3.0 m high masonry façade. This was achieved by means of 2 reinforced concrete masses connected to the masonry wallette, as illustrated in Figure 5.8. Since two specimens were used, the height of the wallettes was different, leading to different values of the equivalent structure, as presented in Table 5.2, where it is also possible to observe that the dynamic characteristics (p) of the equivalent structure and the geometrical parameters (R, α_0 and y_{cg}) are in accordance to the original masonry wall, as well as the total weight (W). The value of α_0, as explained previously, is obtained considering the infinitely rigid behaviour at the joint level.

Table 5.2. Comparison between original and equivalent structure

System	Weight [kN]	Height [m]	Rotational inertia [kg m²]	R_0 [m]	p [rad/s]	α_0 [rad]	y_{cg} [m]
Original	48.2	3.0	15426	1.535	2.19	0.213	1.50
FR1	51.3	2.9	16107	1.525 (-0.7%)	2.20 (+0.5%)	0.215 (+0.9%)	1.487
FR2	52.8	2.9	17652	1.574 (+2.5%)	2.17 (-0.9%)	0.208 (-2.3%)	1.538

5.2.3. Monitoring system

The adopted monitoring system (Figure 5.9) consisted of draw wire displacement transducers (with good dynamic features), accelerometers, tiltmeters and LVDTs (Linear Voltage Displacement Transducers) in order to assess the value of the coefficient of restitution.

Small LVDTs were used to check the efficiency of connections between the masonry wallette and the adjacent RC elements. They were placed at each corner of the wallette for measuring joint normal opening between each material layer. At the masonry bed joint layer, spring LVDTs were placed in order to take into account larger joint opening values.

(a) **(b)**
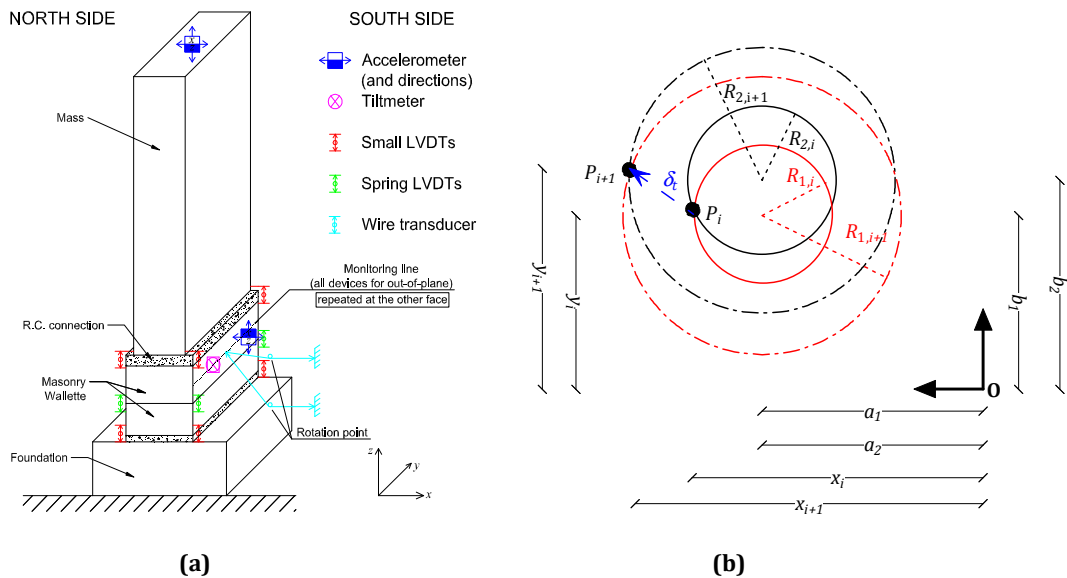
Figure 5.9. Monitoring system: a) perspective view; b) computation of displacements with two wire transducers in the same vertical plane and two rotation points

A monitoring horizontal line was defined at mid-height of the top stone masonry layer, where draw wire position transducers were placed, together with two accelerometers (in the x and z directions, in order to check the initial velocity) and a tiltmeter. This monitoring line was adopted at the opposite faces of the wallette, in accordance with Figure 5.9 a), and it was found essential to compute the angular velocity and consequently the coefficient of restitution. Although the rotation angle should be obtained directly from the tiltmeters, they exhibited poor dynamic behaviour leading to erroneous results. At the end, these devices were only used to monitor the initial rotation θ_0. The accelerometers were used to have redundancy in the test setup as well as to obtain the periods of vibration through Fourier spectra during the experimental tests, thus contributing to assess the behaviour of the specimens.

The rotation angle was computed with the draw wire transducers' measurements based on the geometry of the monitoring system and test apparatus due to the unsatisfactory dynamic characteristic of the tiltmeters. Displacements in two orthogonal directions (*dx* and *dy*) as well as displacement magnitude δ_i are computed by the geometrical intersection of two circles in the same plane. These circles are measured with the draw wire position transducers because displacements are monitored in relation to a fixed rotation point (observable in Figure 5.9 a)). A similar procedure was found in the literature (Mouzakis *et al.* 2002) where the 3D rotation of blocks were monitored resorting to 9 wire transducers.

The presence of two transducers placed in the same vertical plane turns out possible to determine the exact position of the measured point at time i by intersecting the two circles with radius R_1 and R_2 as depicted in Figure 5.9 b), where p_i and p_{i+1} are the positions of the point p at time step i and $i+1$ and (a_1, b_1) and (a_2, b_2) are, respectively, the coordinates of the rotation points of transducers 1 and 2. The complete procedure is presented in Appendix B.

5.3. EXPERIMENTAL RESULTS AND DATA INTERPRETATION

The present section focuses on the validation of the experimental test setup, by comparing the obtained experimental results with theoretical ones, and on the estimation of the restitution coefficient for *sacco* stone masonry walls from the acquired experimental data.

5.3.1. *Validation of experiments and tests results*

In the following paragraphs, several result comparisons are made for validating the experimental setup and the equivalent block approach (EBA) and, on the other hand, for comparing the specimen behaviour against pure rocking response for different restitution coefficient (r) values. The tests provided a large amount of data, from which the rotation and angular velocity time histories are the most important information for this study. However, due to chapter length limitations, only a few selected results are described as representative of the global observed behaviour (all experimental data is presented in Appendix B). Data post-processing was made resorting to a computer program specifically developed on the LabVIEW™ (NI 2010b) platform, in order to analyse individually each test data, from a total number of 36 free rocking tests as listed in Table 5.1. Figure 5.10 shows the results obtained for FR1 and FR2 specimens under the rotation level L2 ($\theta_0/\alpha = 0.25$), where a clearly different behaviour can be observed for the two specimens.
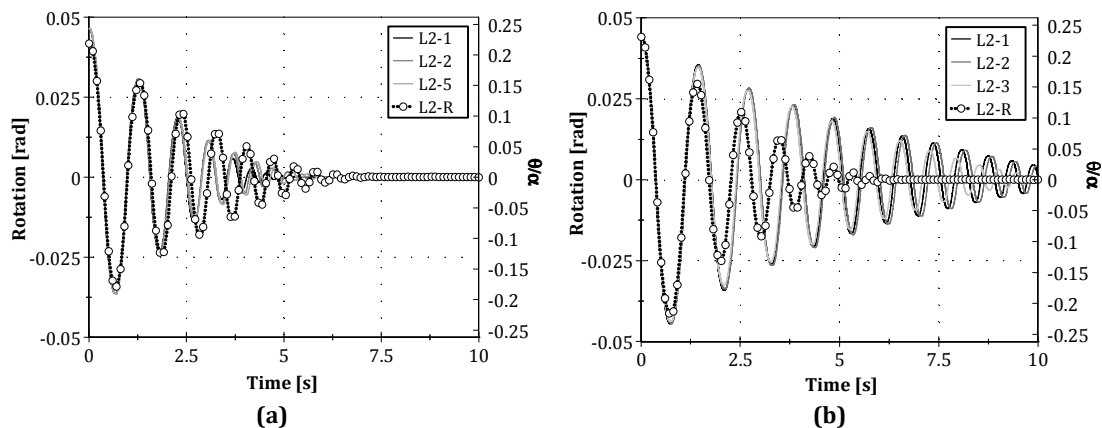
Figure 5.10. Rotation and angular velocity time history acquired for L2 tests: a) FR1; b) FR2

The agreement between each test is excellent with the exception of the final repetition (L2-R) which presents the effect of the deterioration of the coefficient of restitution due to the repeated tests. The FR2 specimen for L2-3 shows also a faster decrease of rotations velocities after t = 7.5 s, which is possibly due to the effects of repetitions.

Regarding the quality of the obtained results, a small variability was obtained in some cases for the same initial rotation level. This result may be caused by the heterogeneity of the mortar interface and granite blocks' assemblage and by some influence of the scheme used to release the wall (affecting the initial velocity of the wall), as the case of FR1-L3. However, in general, it did not influence the final results and conclusions obtained from the whole experimental campaign.

In general terms, the adopted test setup and data acquisition scheme proved to be consistent and provided results with good quality for analysing the rocking behaviour of *sacco* masonry walls resorting to the EBA. The angular velocity plots also present useful information for assessing the coefficient of restitution directly from experimental evidence.

The validation of the test setup was made by comparing the experimental results obtained from each test (with each initial rotation value) against theoretical estimates of important response parameters proposed by the classic rocking theory (Housner 1963) for rocking blocks subjected to free vibration with initial rotation (θ_0, or $\varphi_0 = \theta_0/\alpha$) and no initial angular velocity or acceleration.

Three different comparisons are presented in terms of:

i) period of vibration, Eq. (5.20), taking into account the *n*-th impact for a given *r* value:

$$T_n = \frac{4}{p}\tanh^{-1}\sqrt{r^{2n}\left[1-\left(1-\varphi_0\right)^2\right]}$$ (5.20)

ii) rotation angle, Eq. (5.21), under free vibration and energy dissipation for the same *r* value:

$$\varphi_n = 1-\sqrt{1-r^{2n}\left[1-\left(1-\varphi_0\right)^2\right]}$$ (5.21)

iii) rocking period versus initial rotation, as given by Eq. (5.22):

$$T = \frac{4}{p}\cosh^{-1}\left(\frac{1}{1-\varphi_0}\right)$$ (5.22)

Periods of vibration (*T*) were calculated based on the peaks of the recorded angular velocities because they are not influenced by permanent rotations that the block may experience (which would yield to erroneous values of rocking periods). Therefore, the vibration periods *T* were computed taking into account the sequence of vibration, represented by Eq. (5.23) where *n*

refers to the *n*-th impact of the block, from a total of *N* impacts, and $t_n\left(\dot{\theta}_n^{\max}\right)$ is the time corresponding the *n*-th peak of angular velocity.

$$T_n\left(s\right) = \begin{cases} 4 \cdot t_1\left(\dot{\theta}_1^{\max}\right), \text{ if } n = 1 \\ 2 \cdot \left[t_{n+1}\left(\dot{\theta}_{n+1}^{\max}\right) - t_n\left(\dot{\theta}_n^{\max}\right)\right], \text{ for } 2 \leq n \leq N \end{cases} \tag{5.23}$$

The agreement between theoretical and experimental results is achieved by computing the theoretical curves using the parameter $\alpha = \alpha(\theta_0)$. This parameter, which affects the calculation of φ_0 and φ_n, reflects the influence of the interface flexibility in the response and seems to be very important for correctly evaluating the tested specimens' behaviour; by contrast, its influence on the final value of p was found to be insignificant.

The values of $\alpha(\theta_0)$ were computed by considering k_n = 6.0 MPa/mm, a typical value for this type of mortar interface and f_m = 1.28 MPa, in accordance with the mechanical characterization tests performed on mortar samples. It is known that for a mortar layer in between stone (or brick) units, the mortar compression strength tends to be increased due to the confining effect provided by the contact between mortar and unit, which results from the mortar lateral expansion (due to Poisson effect) that is opposed by the shear forces developed in the interface. In this work it was not possible to evaluate this effect, but still a good agreement was achieved between experimental and theoretical results by using the f_m value obtained from standard mortar tests.

Consistently with the previously mentioned results, Figure 5.11 shows the comparison between theoretical and experimental data for L2 tests on both specimens throughout the whole impact sequences, wherein the theoretical results are calculated using Eq. (5.20) and Eq. (5.21), while the global results given by Eq. (5.22) are presented and compared later in Figure 5.12. The overall set of results is presented in Appendix B.

The agreement obtained between experimental and theoretical data is good for the adopted range of restitution coefficient r values (used to compute the theoretical curves), which are based on the results presented in the next section 5.3.2.

The comparison between theoretical curves and experimental data in terms of rotation vs. impacts (as in previous works to determine the restitution coefficient, e.g. Sorrentino *et al.* (2011)), shows an excellent agreement in both specimens. However, looking at the plots of vibration period vs. impacts, the agreement is not so good, particularly for the FR2 specimen, which requires use of higher r values than for rotation vs. impacts plots (see Figure 5.11 b). In fact, observing in detail the top graph of Figure 5.11 b), it is possible to infer that L2-R is acceptably reproduced with $r = r_{max}$, while for the other tests (L2-1, L2-2 and L2-3) the theoretical curves with r = 0.95 underestimate the response (i.e., a higher value of r would be required). By

contrast, the bottom plot of Figure 5.11 b), shows an opposite trend because tests L2-1, L2-2 and L2-3 are correctly simulated with $r = 0.95$ while L2-R is overestimated with $r = r_{max}$. A more detailed presentation of r and r_{max} values is made in the following section.

(a)   (b)
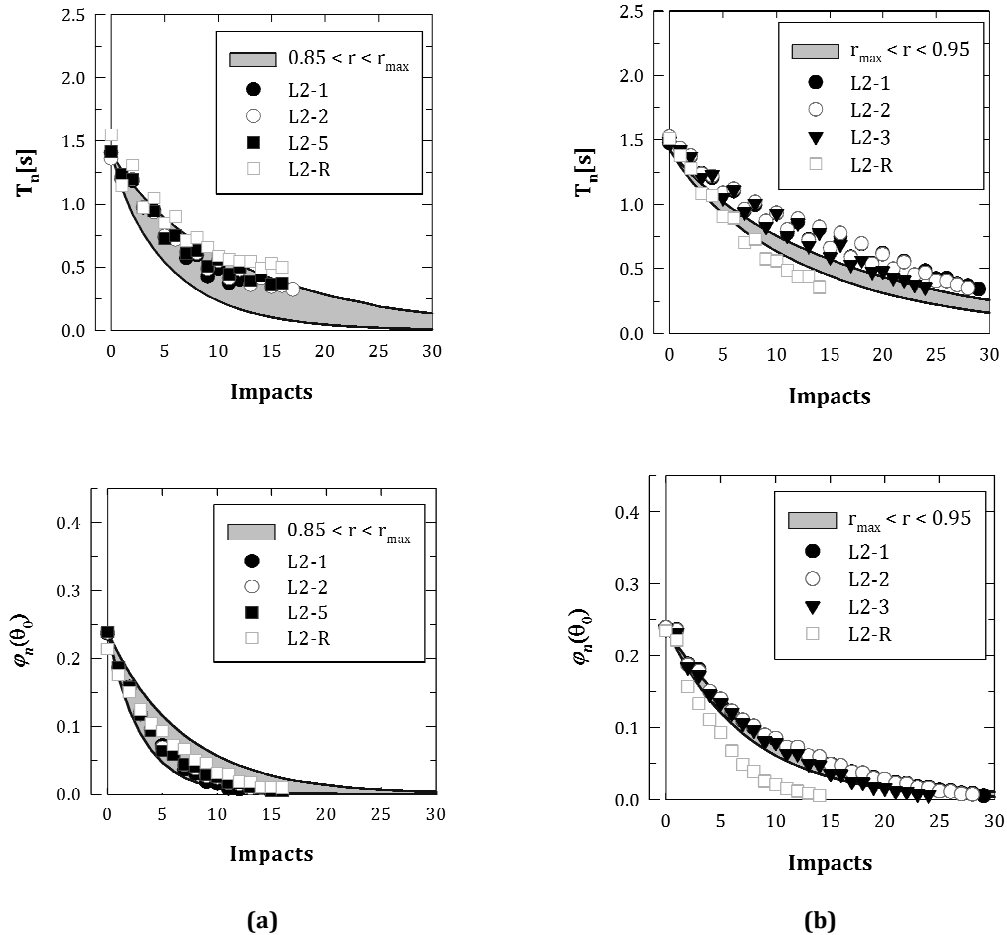
Figure 5.11. Comparison between theoretical and experimental results in terms of periods of vibration and rotation angles (top, Eq. (5.20); bottom, Eq. (5.21)): a) FR1-L2; b) FR2-L2

As mentioned above, the experimental data from both specimens were also subject to a global validation using Eq. (5.22) to plot the theoretical relation of the rocking period vs. corresponding (initial) rotation and to make the comparison with all the pair of values (T, θ_0/α), considering all the impacts at the base. The agreement between the experimental data and theoretical curves can be noticed in Figure 5.12 for all test levels (including all recorded impacts) and both specimens (FR1 and FR2).

Furthermore, as mentioned above, the definition of the angle α (which is necessary to compute the theoretical curve in terms of $\varphi = \theta/\alpha$) can be made by considering an infinitely rigid interface or a flexible one; thus, it is evaluated according to these two possibilities and the corresponding (T, θ/α_0) and (T, $\theta/\alpha(\theta_0)$) graphs are also included and compared in Figure 5.12.
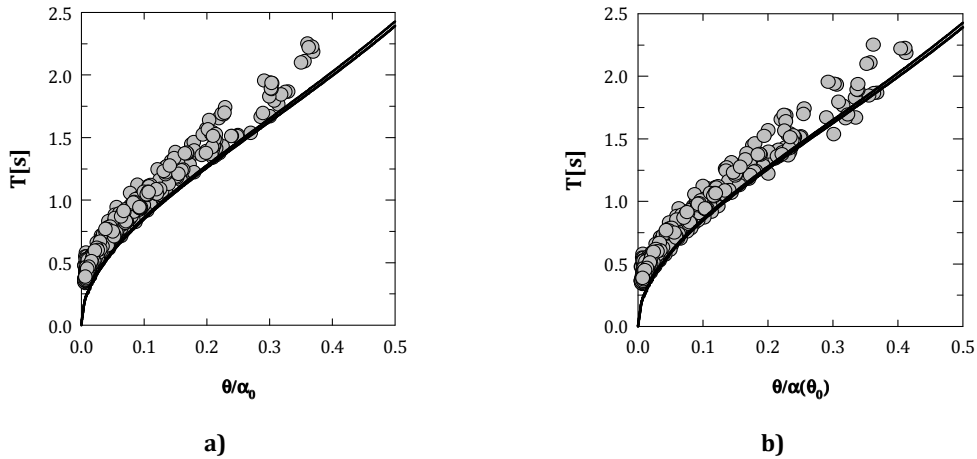
Figure 5.12. Global comparison between theoretical (Eq. (5.22)) and experimental data for FR1 and FR2, considering both specimens: a) fully rigid body; b) semi-rigid model, $\alpha(\theta_0)$

As it is possible to observe in Figure 5.12 b), $\alpha = \alpha(\theta_0)$ yields to better results when compared to $\alpha = \alpha_0$ (Figure 5.12 a)). It is worth mentioning that this same conclusion was also observed in the plots corresponding to Eqs. (5.20) and (5.21) but it is not reported herein.

In conclusion, according to Figure 5.12 b), the experimental-theoretical agreement is good and the general trend of the interaction curve is the expected one, which supports the validation of the test setup (including the equivalent block approach) and the data obtained with the experiments.

5.3.2. Determination of the coefficient of restitution

The main goal of the performed experimental tests consisted on the evaluation of the restitution coefficient (r) for masonry façades with rocking behaviour. Bearing in mind the relation between r and $\dot{\theta}$, the restitution coefficient values were evaluated following two approaches, namely: *1*) using exclusively the experimental results in terms of angular velocities, briefly denoted as EAV; *2*) adopting the classic rocking theory (CRT), resorting to the relation between the number of impacts n and the maximum expected rotation (written in a convenient form) and using the measured rotations.

5.3.2.1. Experimental evidence using measured angular velocities (EAV)

Concerning the first mentioned case (resorting exclusively to experimental evidence), the r value was computed with the data acquired for: *i*) consecutive peaks; *ii*) peaks in the same sense. For case *i*), the definition of the restitution coefficient (r) is given by Eq. (5.24), where n is the nth-impact of the block:

$$r = \frac{\dot{\theta}_{n+1}}{\dot{\theta}_n} \tag{5.24}$$

It was observed that using Eq. (5.24) leads to inconsistent values of r because the block is not perfectly symmetric and small modifications of α and R were found to have strong influence on the computed values. Thus, case *ii*) was also adopted, aiming at avoiding this inconsistency by assuming that the coefficient of restitution is equal for two consecutive peaks and, therefore, the evaluation is performed for peaks in the same sense of motion; this leads to Eq. (5.25) which can be considered an average value, as depicted in Figure 5.13.

$$r = \sqrt{\frac{\dot{\theta}_{n+2}}{\dot{\theta}_n}} \tag{5.25}$$

However, using this procedure, the value of the first impact at the base cannot be computed because two or three consecutive peaks are necessary (two if Eq. (5.24) is used or three when adopting Eq. (5.25)) and it is influenced by asymmetries of the specimens.
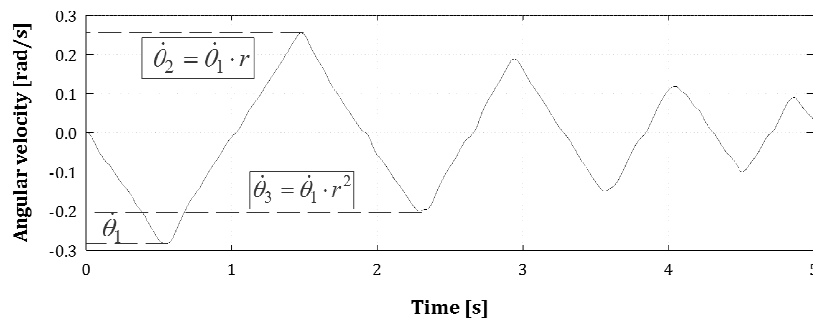
Figure 5.13. Computation of the coefficient of restitution taking into account peaks in the same motion sense (experimental data from FR1-L4-1 test)

Moreover, although this approach has the advantage of finding the restitution coefficient directly from the experimental evidence (thus avoiding assuming a theoretical relation between consecutive peaks), it must be recognized that the quality and confidence on restitution coefficient values for low velocity and small rotation angles may be strongly influenced by the sensitivity of the monitoring system.

It is worth mentioning that a similar procedure was found in the literature by Liberatore and Spera (2001), where the angular velocity was computed through the peak rotation but affected by the geometrical value α. However, since the interface is not fully rigid, the geometrical parameter α influences the results obtained with the cited procedure and should not be applied in the present work.

5.3.2.2.   Classic rocking theory using measured rotations (CRT)

In previous experimental works performed by other authors, such as Peña *et al.* (2007) and more recently Sorrentino *et al.* (2011), the coefficient of restitution is calculated assuming a pure rocking behaviour of the specimen, wherein that coefficient is directly obtained from the maximum rotation after the n-th impact (θ_n). In order to compare also the present experimental results against this procedure, the restitution coefficient is computed based on the classic theory presented by Housner (1963), by assuming that r can be estimated according to the following equation:

$$r = \sqrt[2n]{\frac{1-\left(1-\left|\varphi_n\right|\right)^2}{1-\left(1-\left|\varphi_0\right|\right)^2}} \tag{5.26}$$

where $\varphi_0 = \dfrac{\theta_0}{\alpha(\theta_0)}$ and $\varphi_n = \dfrac{\theta_n}{\alpha(\theta_0)}$ refer, respectively, to the initial rotation and to the maximum rotation after the n-th impact. The latter is taken from the experimental readings.

5.3.2.3.   Results obtained and data interpretation

The results of restitution coefficients for the tested specimens FR1 and FR2 are shown, respectively, in Figure 5.14 a) and Figure 5.14 b), which correspond to the plots of restitution coefficients computed for the rotation level L2 (as an example) using the results shown in Figure 5.10. For reference purposes, the maximum theoretical restitution coefficients are indicated in Figure 5.14 by the horizontal lines included in the graphs, which correspond to $r_{max,FR1}$ = 0.931 and $r_{max,FR2}$ = 0.935, respectively, for FR1 and FR2, computed by using Eq. (5.6) and considering the α_0 value of each specimen.

Restitution coefficients (r) plotted in Figure 5.14 were computed by the two above described methods, namely the <u>EAV</u> approach (detailed in sub-section 3.2.1 and resorting to Eq. (5.25)) and the <u>CRT</u> approach (detailed in sub-section 3.2.2 and resorting to Eq. (5.26)).

Figure 5.14 shows an important effect of impact repetitions in the restitution coefficient, which, however, influences both specimens in opposite ways. Moreover, the higher restitution coefficient corresponds also to larger number of impacts of FR2 when compared to FR1. The influence of $\alpha(\theta_0)$ for computing the restitution coefficient through CRT was also evaluated, leading to an insignificant deviation of about 1%.

(a)   (b)
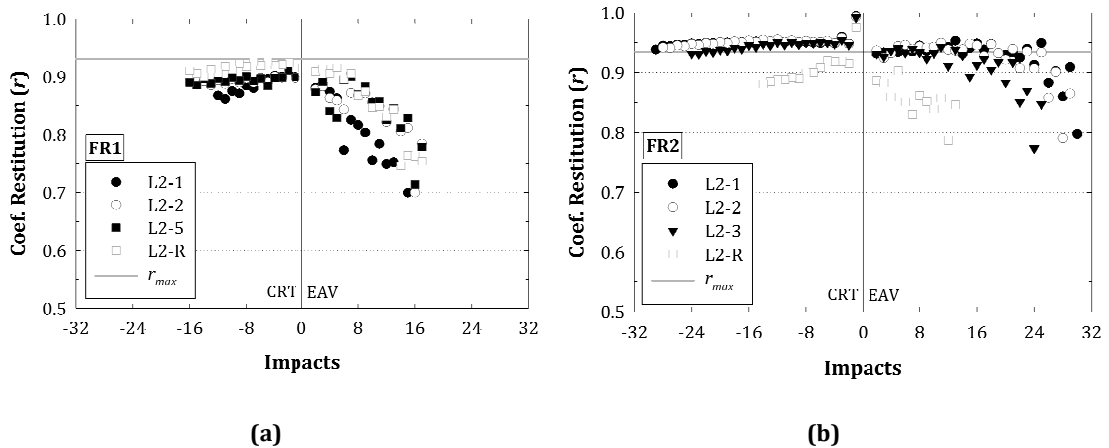
Figure 5.14. Coefficient of restitution obtained through classic theory (CRT) and experimental evidence (EAV) for L2 rotation level: a) FR1; b) FR2

Considering again the computation of restitution coefficient values with the two adopted approaches, the global results obtained for both specimens are illustrated in Figure 5.15. As reported in the figure legend, for each number of impacts, all r values are plotted for both FR1 and FR2 specimens, as well as their average values (with +/- one standard deviation interval), the 95% percentile values and the maximum theoretical values (r_{max} = 0.931 and 0.935, respectively for FR1 and FR2).
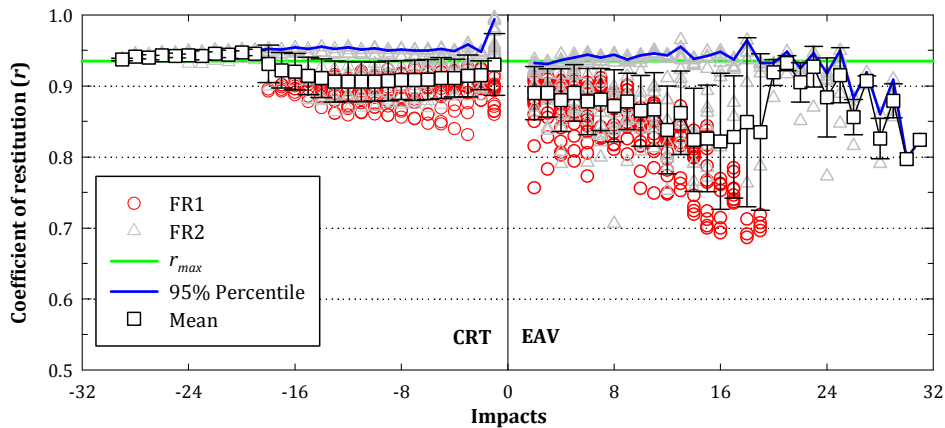
Figure 5.15. Coefficient of restitution obtained through classic theory (CRT) and exclusive experimental evidence (EAV) considering all obtained results.

From the overall analysis of the obtained results (including some others not presented herein), five main observations were clearly identifiable: *i)* the *r* values obtained through CRT are higher when compared to those obtained from EAV (+3.7% for the first impacts and +6.5% for the mean global values); *ii)* the dispersion of results obtained through EAV is significantly larger than that obtained with the CRT (the latter appearing very consistent); *iii)* the effects of repetitions influences significantly the coefficient of restitution; *iv)* the *r* value is not affected by

the amplitude of the rocking motion; *v)* the dispersion of results increases with the increasing number of tests.

Concerning the latter finding, the scatter of values obtained using the EAV approach increases with the number of impacts (e.g. Figure 5.14 b) and Figure 5.15), which might be related with the influence of monitoring devices' resolution for small rotation levels. Moreover, the values obtained with the CRT approach provide more reliability when compared to the EAV ones, which is also observed in the simulation of the experiments through analytical models (presented in section 5.4).

Table 5.3 presents a summary of the main results obtained with the experimental tests performed for each level (L1, L2, L3 and L4) as well as a global analysis. The results are shown in the same sequence as the experimental tests, highlighting the effects of repetitions in the restitution coefficient value. Moreover, it is worth referring that the presented global mean values are calculated taking into account all the impacts and the number of tests performed for all displacement levels, i.e. it is not the direct average of the mean values of L1, L2, L3 and L4.

The analysis of maximum values obtained through EAV shows that the restitution coefficient decreases its maximum as the number of tests increases (and it does not seem to be correlated to the initial rotation level), which is more clear for the specimen FR2.

The restitution coefficient values obtained through CRT led to a better match with the theoretical behaviour when compared to those obtained from EAV, due to the mentioned problems of the latter related with the direct determination from the experiments, despite the good agreement observed for the initial impacts. Therefore the calculation of *r* values through the classic theory with measured rotations is the recommended procedure and these values will be used in the following paragraphs as the adopted experimental results.

As a personal opinion, the tests which preceded FR1-L1 and the 5 tests for the same rotation level might be responsible for this significant difference, because the repetition effect seems to be important for multi-leaf masonry walls. This conclusion gains importance if the FR2-L4 results are taken into account, i.e., *r* = 0.894 after 12 tests (according to Table 5.1 and numerous impacts at the interface, because it tends to a value similar to FR1 (*r* = 0.895).

Table 5.3. Summary of the global averaged coefficient of restitution (r) results
(values in brackets refer to r/r_{max} for each specimen)

		Average		Std. Dev.		Maximum		95% Percentile	
		CRT	EAV	CRT	EAV	CRT	EAV	CRT	EAV
FR1	L1	0.909	0.701	0.013	0.091	0.941	0.833	0.927	0.825
		(0.98)	(0.75)			(1.01)	(0.89)	(1.00)	(0.89)
	L2	0.899	0.835	0.014	0.055	0.926	0.916	0.923	0.906
		(0.97)	(0.90)			(0.99)	(0.98)	(0.99)	(0.97)
	L3	0.884	0.827	0.022	0.053	0.923	0.912	0.919	0.905
		(0.95)	(0.89)			(0.99)	(0.98)	(0.99)	(0.97)
	L4	0.904	0.841	0.011	0.068	0.916	0.909	0.914	0.905
		(0.97)	(0.90)			(0.98)	(0.98)	(0.98)	(0.97)
	Global[a]	0.895	0.819	0.019	0.074	0.941	0.916	0.922	0.905
		(**0.96**)	(**0.88**)			(**1.01**)	(**0.98**)	(**0.99**)	(**0.97**)
FR2	L3	0.939	0.915	0.014	0.036	0.996	0.965	0.948	0.945
		(1.00)	(0.98)			(1.07)	(1.03)	(1.01)	(1.01)
	L2	0.943	0.912	0.021	0.041	0.994	0.953	0.958	0.948
		(1.01)	(0.98)			(1.06)	(1.02)	(1.02)	(1.01)
	L1	0.921	0.872	0.022	0.050	0.949	0.937	0.947	0.930
		(0.99)	(0.93)			(1.01)	(1.00)	(1.01)	(0.99)
	L4	0.894	0.839	0.022	0.037	0.958	0.903	0.949	0.892
		(0.96)	(0.90)			(1.02)	(0.97)	(1.01)	(0.95)
	Global[a]	0.931	0.895	0.026	0.049	0.996	0.965	0.954	0.945
		(**1.00**)	(**0.96**)			(**1.07**)	(**1.03**)	(**1.02**)	(**1.01**)
Global		0.913	0.857	0.023	0.062	0.996	0.965	0.938	0.925

[a] Global values obtained accounting for the total number of impacts from all the tests rather than a direct average between each test level.

Figure 5.16 shows the effects of repetitions in the restitution coefficient determined resorting to the CRT approach. The black columns represent the average values for the tests without the final repetition (R) in the test sequence order, while the dashed columns represent the restitution coefficient obtained only with the final repetition test.

(a)   **(b)**
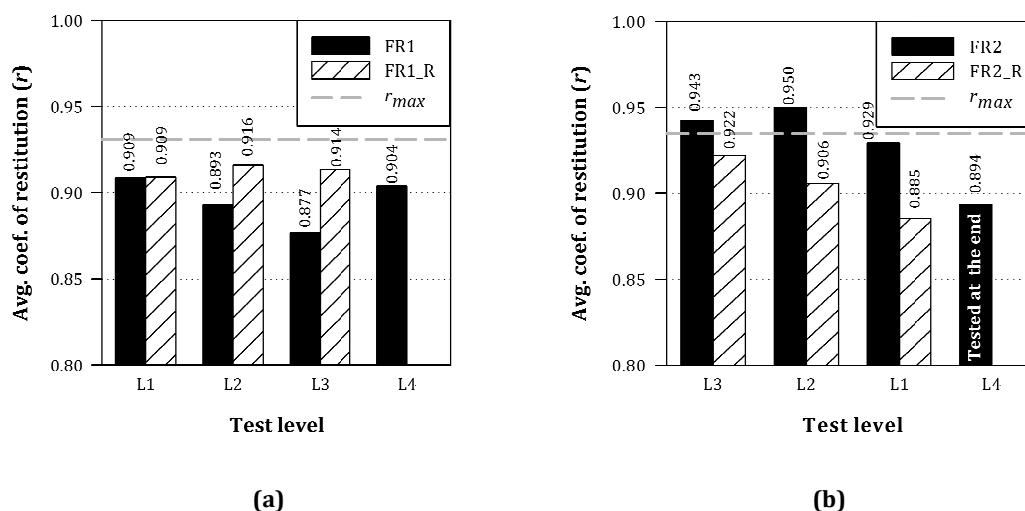
Figure 5.16. Effects of repetitions in the coefficient of restitution using the classic theory: a) FR1; b) FR2

The effects of repetition in the restitution coefficient are quite apparent, since the number of tests influences the r value for this type of masonry walls; however, no consistent trend was found: while for FR2 it tends to decrease (as expected due to deterioration at the joint level), FR1 tends to stabilize or even to increase. It follows that more experiments should be performed and particular care should be taken when analyzing experimentally this type of walls due to repetition effects.

Moreover, the ratio $r/r_{max} = 0.95$ recently proposed by Sorrentino *et al.* (2011) (denoted as $e_{exp}/e_{an,2s}$ in the cited work) should be carefully used, because, as shown in Figure 5.16 b), it may not be the upper bound and r values higher than r_{max} can be obtained, leading to non conservative assumptions. In fact, for initial impacts, the r values were close or even higher than r_{max} in both tested specimens, as illustrated in Figure 5.15.

Taking into account the 95% percentile of the experimental data and the average value plus one standard deviation (depicted in Figure 5.15), a value of $r = r_{max}$ may be proposed to be used in the analysis of the rocking behaviour of stone masonry walls similar to the tested type. The effects of repetition may lead to the ratio $r/r_{max}=0.95$ as proposed by Sorrentino *et al.* (2011).

5.4. NUMERICAL MODEL SIMULATIONS AND COMMENTS

Another main objective of the presented work was also to develop a procedure which could be able to correctly simulate the rocking behaviour of the tested walls (*sacco* stone masonry). For this purpose, the three different approaches presented previously in section 5.2.1 were used, namely: *i*) the fully rigid model (classic theory), which is the most common to simulate the rigid body rocking behaviour; *ii*) the semi-rigid model ($\alpha = \alpha(\theta_0)$); *iii*) flexible model ($\alpha = a[\theta(t)]$).

Particularly concerning the last model, it should be referred that the influence of dilatancy in the computation of the geometrical parameters was not taken into account and the joint stiffness and strength degradations were also neglected.

A parametric analysis was performed in order to assess the efficiency of the different proposals to simulate the behaviour of the tested masonry wall. For the models *ii*) and *iii*), the parameter which could be also evaluated (apart from the restitution coefficient r) were the new $\alpha(\theta_0)$ and the joint compressive strength (f_m) in the case of the flexible model. The option to derive the required values directly from the experiments, as adopted in previous works which resorted to the minimization of error functions (e.g. Wong and Tso (1989)and more recently Peña *et al.* (2007)), was not considered in this case. This study was aiming at attempting to simulate the observed behaviour with some realistic assumptions (thus avoiding any sort of numerical-experimental fitting) and at understanding how the referred parameters influence the rocking response of a *sacco* stone masonry wall.

The range of adopted values in the parametric analysis was: $0.850 \leq r \leq 1.000$ (intervals of 0.005); $0.15 \leq \alpha \leq \alpha_0$ rad (intervals of 0.005 rad) and $0.20 \leq f_m \leq 1.30$ MPa (intervals of 0.10 MPa). The analyses were performed in MATLAB® (MathWorks 2009) environment which directly computed the solution for two cases: *1*) fully rigid and semi-rigid body behaviour, for the cases of Figure 5.6 a) and b), where the difference relies only in the α value; *2*) flexible model, with inclusion of flexible interface in the equation of motion, for Figure 5.6 c).

The solution for case *1*) is a closed-form one and it is reported on previous works by Hogan (1990) (for positive and negative rotations) and afterwards by Makris and Roussos (2000) for the general solution of a rigid block subjected to a cyclic pulse. The equations which allow computing the time histories of rotation and angular velocity are presented herein by Eqs. (5.27) and (5.28), respectively, as a result of Eq. (5.1) already included in section 5.1.

$$\theta(t) = \begin{cases} \dfrac{\dot{\theta}_0}{p}\sinh(pt) + (\theta_0 + \alpha)\cosh(pt) - \alpha, \text{ for } \theta < 0 \\ \dfrac{\dot{\theta}_0}{p}\sinh(pt) + (\theta_0 - \alpha)\cosh(pt) + \alpha, \text{ for } \theta > 0 \end{cases} \tag{5.27}$$

$$\dot{\theta}(t) = \begin{cases} p\dot{\theta}_0\cosh(pt) + p(\theta_0 + \alpha)\sinh(pt), \text{ for } \theta < 0 \\ p\dot{\theta}_0\cosh(pt) + p(\theta_0 - \alpha)\sinh(pt), \text{ for } \theta > 0 \end{cases} \tag{5.28}$$

The MATLAB routine computes the solution for the initial rotation θ_0 until reaching $\theta = 0$. The next half period time history is computed taking into consideration $\theta_0 = \theta_n$ and the restitution coefficient which correlates the angular velocity at time step before (*i*-1) and after (*i*) the impact *n* in the form: $\dot{\theta}_0 = \dot{\theta}_n = \dot{\theta}_i = r\,\dot{\theta}_{i-1}$. The solution for case *2*), the flexible model, was computed via a state-space formulation using a standard ordinary differential equations (ODE)

solver available in MATLAB, namely the explicit 4th-5th order Runge-Kutta the Dormand-Prince pair (Dormand and Prince 1980), which was found to be the most accurate when compared to the others ODE solvers available in MATLAB and commonly used in the other cited works.

The simulation of the experimental results with the numerical models was computed and analyzed through the squared correlation coefficient (also known as R^2), selecting parametric values which led to the best correlation of each run and test level. Only the first 5 seconds ($t \leq 5\ s$) of the data (experimental and numerical) were considered in the comparisons in order to avoid errors induced by low amplitude rotations.

Some representative results are included in Figure 5.17 relative to the FR1-L4 test with two different models. For the semi-rigid model, the best values were evaluated for the restitution coefficient (r) and the $\alpha(\theta_0)$ value, while, for the flexible model, the best estimates were obtained also for the r coefficient and for the joint compressive strength (f_m). The gradient is relative to the R^2 value with the scale vertical bar presented at the right hand side of the figure. The numerical results of the fully rigid model are not included because no good correlation was found.

(a)   **(b)**
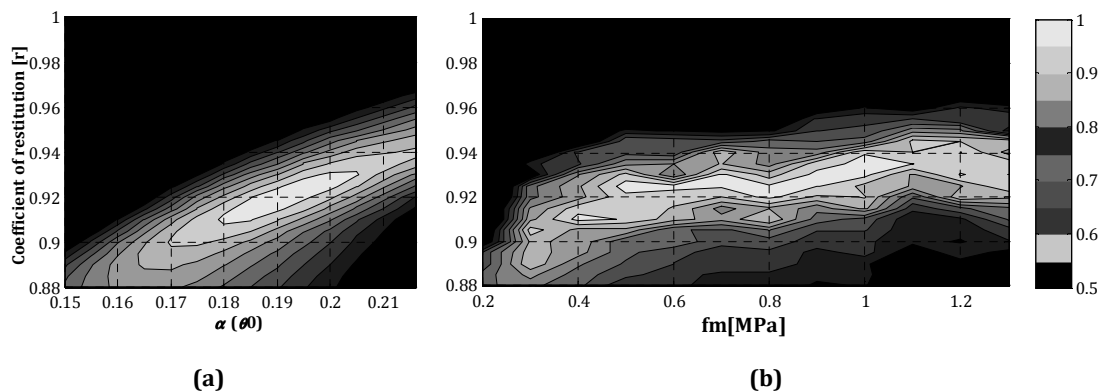
Figure 5.17. Results obtained from the parametrical analysis of FR1-L4 test: a) semi-rigid model; b) flexible model.

From the observation of Figure 5.17 a), the influence of $\alpha(\theta_0)$ in the final result is found important to obtain a satisfactory simulation of the experiments. Indeed, the range of values achieving $R^2 = 0.9$ is wide and interesting for future computations.

Since the mortar compressive strength (necessary to compute $\alpha(\theta_0)$) can be sufficiently estimated, the range of $\alpha(\theta_0)$ values (for $0.50 < f_m < 1.28$ MPa, $0.165 < \alpha < 0.195$ rad) will correspond to a good R^2 coefficient (Figure 5.17 b)), substantially better than the R^2 value (0.885) obtained for α_0 (0.216 rad) (Table 5.4).

The results obtained with better correlation (average values considering all the tests performed for a given specimen and an initial rotation level L#) between numerical and experi-

mental data are presented in Table 5.4. The values of f_m^* are calculated using Eq. (5.29), computed by imposing α as an input.

$$f_m^* = \frac{W}{l \cdot \left[t - 2 \cdot y_{cg} \cdot \tan\left(\alpha\left(\theta_0\right)\right)\right]}$$

(5.29)

In general, the fully rigid model could not be used for this type of walls because it did not lead to results with good correlation with experimental data (especially for the case of FR2). Regarding the other two considered models, both of them provide results with fair correlation ($R^2 \geq 0.89$).

The restitution coefficient values reached with the semi-rigid and flexible models are close each other and closer to the experimental ones. With two exceptions (FR1-L3 semi-rigid model; FR2-L2 flexible model), the experimental values of r are consistently lower than the values obtained with the numerical models and the average ratio of $r/r_{max} = 1.02$ was achieved for both specimens and both models.

Table 5.4. Summary of the analysis performed (average values), final repetitions not included

| | | MODEL | | | | | | | | Experimental |
| | | Rigid, α_0 | | Rigid, $\alpha(\theta_0)$ | | | | Flexible | | | |
	Test sequence	R^2	r	R^2	r	α_0	$f_m{}^*$ [MPa]	R^2	r	f_m [MPa]	r
FR1	L1[a]	0.781	0.95	0.976	0.925	0.18	0.36	0.941	0.92	0.4	0.909
	Error		4.51%		1.76%				1.21%		
	L2	0.823	0.93	0.985	0.91	0.185	0.42	0.983	0.915	0.5	0.899
	Error		3.45%		1.22%				1.78%		
	L3	0.869	0.9	0.971	0.88	0.19	0.51	0.947	0.885	0.6	0.884
	Error		1.81%		-0.45%				0.11%		
	L4	0.885	0.94	0.978	0.92	0.19	0.51	0.978	0.925	0.5	0.904
	Error		3.98%		1.77%				2.32%		
	Average	0.84	0.93	0.978	0.909	0.186	0.45	0.962	0.911	0.5	0.895
	Error		3.91%		1.56%				1.79%		
FR2	L3	0.87	0.97	0.992	0.94	0.175	0.38	0.989	0.935	0.4	0.939
	Error		3.30%		0.11%				0.43%		
	L2	0.747	0.985	0.99	0.955	0.17	0.33	0.974	0.95	0.3	0.943
	Error		4.45%		1.27%				0.74%		

FR2	L1	0.414	0.995	0.908	0.945	0.15	0.22	0.893	0.945	0.2	0.921
	Error		8.03%		2.61%				2.61%		
	L4	0.758	0.955	0.96	0.915	0.165	0.30	0.957	0.92	0.4	0.894
	Error		6.82%		2.35%				2.91%		
	Average	0.532	0.969	0.928	0.943	0.169	0.31	0.958	0.938	0.3	0.931
	Error		4.08%		1.29%				0.75%		

[a] Only one test with experimental data acquired

Since the error obtained when experimental tests are simulated using a numerical model including the flexible interface (semi-rigid or flexible model) is very small, it follows that the maximum theoretical values r_{max} may be used for the analyses of this type of masonry walls within a conservative perspective. However, the use of values even higher than the maximum theoretical one should not be disregarded, as evidenced in Table 5.4, where values larger than r_{max} can be found (e.g. FR2-L3).

From the obtained results, the inclusion of the flexible interface seems to be an important contribution for the adequate characterization of the rocking behaviour of *sacco* stone masonry walls, also mentioned by Giuffrè (1993) and Lagomarsino and Resemini (2009) in the quantification of seismic multipliers for mechanisms activation.

Figure 5.18 presents a direct comparison between the experimental data for FR1-L4 test level (considering all the runs) as well as numerical results obtained with each model using the parameters presented in Table 5.4.

As shown in Figure 5.18 a), the experimental and numerical data is in very good agreement using the semi-rigid model as well as the flexible one. Moreover, if one compares directly the mentioned models, no visible differences can be observed. Conversely, the fully rigid model leads to worse results.

(a)　　　　　　　　　　**(b)**
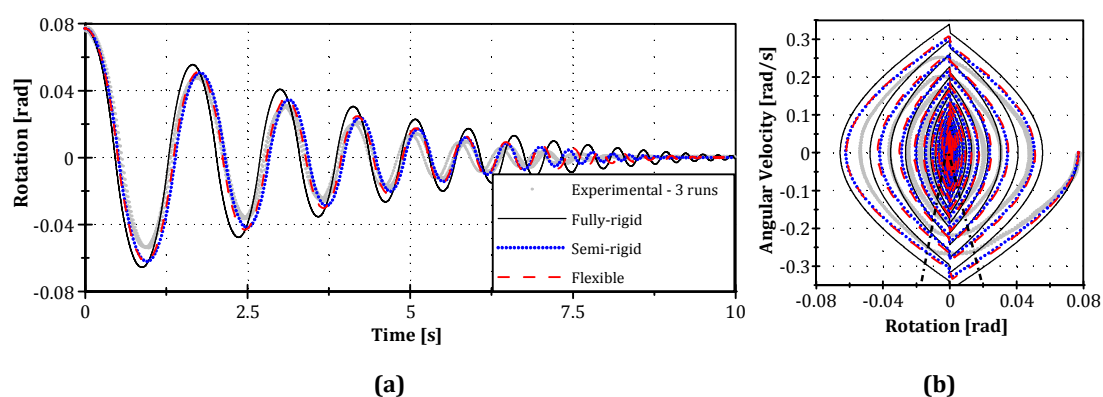
Figure 5.18. Comparison between experimental (FR1-L4) and numerical results obtained with the three models: a) rotation time histories; b) phase plane representation.

Figure 5.18 b) presents the experimental and numerical data in phase plane form, where rotation vs. angular velocity curves can be compared and analyzed. By inspecting the experimental data of Figure 5.18 b), it is possible to observe a constant velocity range close to θ = 0 (represented inside a pair of dotted lines in Figure 5.18 b)), which may be explained by hysteretic energy dissipation at the mortar joint level. In fact, since the models only take into account the energy dissipated at the impacts (through the restitution coefficient), the dissipated energy due to the inelastic behaviour of the joint is not represented, even in the flexible model which only accounts for the elastic energy contribution rather than the inelastic one.

From the obtained results and comparison, it is possible to conclude that the use of the flexible model does not yield any extra information when compared to the semi-rigid one because the flexibility is only important for very small rotation values. Therefore, based on the described results, the semi-rigid model seems to be appropriate for simulating the rocking behaviour of masonry façades considered in this work, with the further advantage of being faster than the flexible one due to the closed-form solution of the ordinary differential equation.

5.5. CONCLUSIONS

The evaluation of energy dissipation through impacts at the base of a rigid block rocking around its base corners was experimentally assessed with a new proposed experimental/numerical method named as equivalent block approach (EBA), where the real properties of masonry façades are simulated with an equivalent structure having geometric and dynamic properties similar to the reference one. The test setup developed for these experiments, as well as the acquired data, proved to be reliable and the influence of joint flexibility was detected as an important parameter to take into account on walls similar to the tested specimens (double-leaf or *sacco* stone masonry walls). Moreover, the effect of repetitions influenced the so-called restitution coefficient by reducing its value as the number of tests is increased.

A global relation trend was found between the theoretical maximum value of the restitution coefficient and the experimental data, being the average experimental value smaller than the theoretical one. Considering the average values, the specimen with smaller number of tests (FR2) provided a restitution coefficient (r = 0.931) very close to the maximum theoretical one (r_{max} = 0.935), while for the other specimen (FR1, with more tests than FR2), a ratio of r/r_{max} = 0.96 was found, similar to what proposed in Sorrentino *et al.* (2011). When the 95% percentile values are taken into account, as in the case of the assessment of existing buildings for which the assumption of conservative values should be suggested, the experiments showed that the maximum theoretical value (r_{max}) may be considered but higher values should not be disregarded. A maximum ratio of r/r_{max} = 1.02 was obtained considering the 95% percentile. Finally, no dependence was found between the motion amplitude and the coefficient of restitution. However, since the number of tested specimens is rather reduced (2), it is clear that more experiments on this type of masonry should be performed in order to support these preliminary statements.

Regarding the analytical simulation of the experimental behaviour, a good combination of simple and efficient model was found, if a flexible interface at the joint level is considered with the semi-rigid model. When compared to a model with full flexible interface consideration, the overall agreement of the semi-rigid model with the experimental data showed to be similar (or

even better) than the flexible model. For simplicity and time-efficiency in analyses of overturning of masonry façades, the semi-rigid model seems an appropriate choice to be used with consistent values of the compressive strength (f_m) and normal stiffness (k_n) of the joint interface for adequate evaluation of the geometrical parameter α.

Chapter 6.

SIMULATION OF THE OUT-OF-PLANE BEHAVIOUR OF EXISTING MASONRY BUILDINGS THROUGH MULTIBODY DYNAMICS

SUMMARY

The assessment of the out-of-plane behaviour of masonry façades is currently made resorting to the definition of the so-called local mechanisms, with static force-based approaches and, more recently, with some displacement-based proposals. Local mechanisms consist of kinematic chains of masonry portions, often regarded as rigid bodies, with nonlinearity concentrated in predefined contact regions.

In this work, the dynamic behaviour of local mechanisms is simulated through multibody dynamics, permitting to obtain the nonlinear response with efficient time history analyses which directly take into account the characteristics of the ground motion and the amplification/filtering effect of the structure. The proposal is validated with experimental results of two full scale shaking table tests on stone masonry buildings: a *sacco* masonry façade tested at LNEC shaking table (Chapter 4) and a two storey double leaf masonry building tested at EUCENTRE. Promising results were obtained where filtering and amplification effects of the structure were seen to be important for the correct simulation of the tests. Comparisons with simplified models are also presented. Finally, a proposal for the seismic assessment of masonry buildings is presented taking into account the in-plane and out-of-plane behaviour of the structure, making use of multibody dynamics for simulation of the out-of-plane response.

6.1. INTRODUCTION AND BRIEF STATE-OF-ART

The out-of-plane behaviour of existing masonry buildings is a particular response of a complete structure commonly included within the so-called local mechanisms,, which may not affect directly the overall behaviour of the building, although in some cases the development of a global response of the building may be inhibited by the early formation of local mechanisms. Moreover, among the several possible mechanisms as reported by Giuffrè (1993), Lagomarsino (1998) or D'Ayala and Speranza (2003), the collapse of one of such mechanisms may lead to partial or full collapse of the complete structure due to the absence of load bearing capacity of the remaining elements. Several computer programs based on these local mechanisms were already developed, such as FaMIVE (D'Ayala and Speranza 2002), c-Sisma (Modena *et al.* 2009) or CINE (Milano *et al.* 2009); however, all of them are based on the evaluation of the static multiplier of the seismic action (or collapse load factor) (e.g. (Giuffrè 1993; Restrepo-Vélez and Magenes 2009)), thus related to force-based approaches.

The mechanisms, mainly based on several post-earthquake surveys, are predominantly defined from the existing geometry (and corresponding boundary conditions and connections between horizontal and vertical elements), wherein the most probable mechanism to form is given by limit equilibrium analysis (Heyman 1966) carried out for each mechanism (e.g. D'Ayala and Speranza (2003)). Despite the need of *a priori* definition of the mechanisms, non dependent on the dynamic behaviour of the structure, these methods provide force-based results which are consistent with the evidence gathered from post-earthquake surveys, as also recently observed (e.g. 2009 L'Aquila earthquake (Quintela 2009)).

However, the mechanism activation, which may be obtained by such force-based procedures, does not imply the overturning/collapse of a masonry wall, as also observed by Quintela (2009). Since the overturning occurs by wall instability rather than the achievement of masonry compressive strength, the displacement capacity of the wall is not taken into account in force-based procedures. In fact, many experimental and analytical studies carried out in different places (Lam *et al.* 1995; de Felice and Giannini 2001; Doherty *et al.* 2002) have shown that dynamically loaded walls can sustain acceleration well in excess of the limit implied by their static capabilities, as also mentioned by Morandi (2006).

Indeed, as reported in Magenes and Penna (2011), displacement-based procedures based on the kinematics of masonry portions (Lagomarsino 2006) were developed (e.g. (Giuffrè 1993; Giuffrè and Carocci 1996)), further refined (e.g. (de Felice and Giannini 2001; Doherty *et al.* 2002; Griffith *et al.* 2003; Sorrentino *et al.* 2008a; Lagomarsino and Resemini 2009)) and are already suggested in the commentary to the Italian code (NTC 2008; M.I.T. 2009) supported by some experimental data (e.g. (Griffith *et al.* 2004; Restrepo-Vélez and Magenes 2009; Vaculik *et al.* 2010; Al Shawa *et al.* 2011)).

However, simple bilinear or trilinear force-displacement curves (e.g. (Doherty *et al.* 2002)) may be used for seismic assessment (e.g. Figure 6.1, from Magenes and Penna (2011)), where, according to the Italian code displacement-based procedure, only the ultimate displacement capacity needs to be defined as the minimum of: *i*) 40% of the instability displacement of the mechanism); *ii*) maximum displacement compatible with the stability conditions of secondary elements (e.g. slab support).
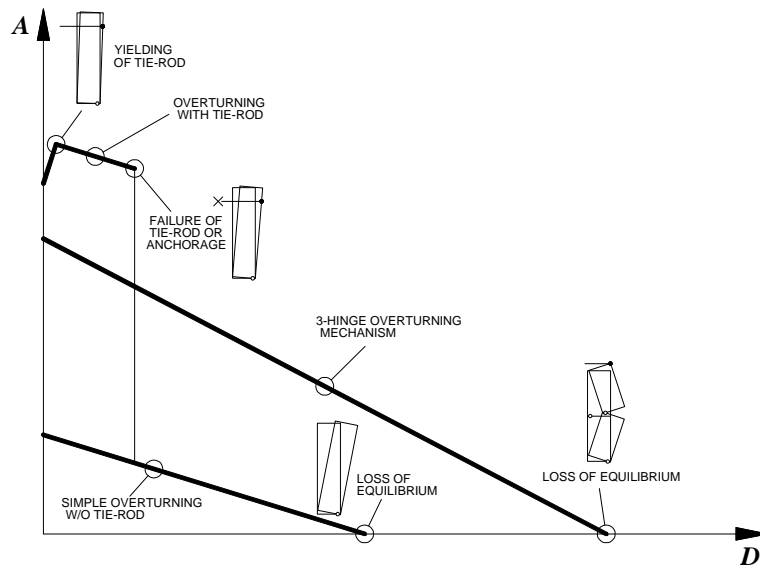
Figure 6.1. Example of static nonlinear capacity curves for out-of-plane mechanisms of a façade with and without tie-rods (Magenes and Penna 2011)

Although some important improvements have been made, an adequate tool for the simulation of the out-of-plane dynamic response of masonry walls is still needed. The energy content of the excitation (with velocity pulses possibly due to directivity effects strongly influencing the out-of-plane response) and of the element (kinetic energy potentially inducing overturning) should be adequately accounted for in such a tool, in order to correctly assess the seismic capacity for relevant displacement limit states. Indeed, this is quite a complex problem where different conclusions were obtained by different authors when correlating the characteristic of the seismic action and the expected wall's behaviour.

As an example, de Felice and Giannini (2001) found that the peak ground velocity (PGV) provides a good characterization of the seismic action and, therefore, proposed a correlation between PGV and mechanism activation according to two failure modes of a masonry façade with returning walls. In the work of Sorrentino and Masiani (2007), some correlation degree was found between the seismic action and the dynamic response of a rigid block rocking around the base using PGV and Housner intensity. On the contrary, Resemini *et al.* (2008) could not find a direct relation between the characteristics of the seismic action and the response of a rigid block, while weak correlation was found with PGV and spectral displacement.

From the above mentioned reasons, an effective tool is needed to account for the complex mechanisms (involving more than just one element) and the characteristics of the seismic action, in order to correctly simulate the out-of-plane dynamic behaviour of complex masonry local sub-systems. Obviously, this tool should be adequately tested and validated with proper dynamic experimental data in order to be proposed for seismic assessment of existing structures.

6.2. PROPOSED NUMERICAL APPROACH

The numerical approach proposed to simulate the out-of-plane dynamic behaviour of masonry buildings is based on the definition of masonry portions which are representative of the formed local mechanisms. These local mechanisms, activated by out-of-plane seismic loads, can be modelled as kinematic chains of masonry portions (normally assumed as infinitely rigid bodies) whose nonlinear behaviour is concentrated at the contact regions. The nonlinear behaviour is represented by a sliding friction law (of Coulomb type without cohesion, in the present work), as well as unilateral contacts (where impacts between bodies lead to energy dissipation which can be computed by means of an energy ratio coefficient); in addition, the contact regions are assumed to have infinite compressive and null tensile strengths.

The definition of a model with masonry portions and contact elements at the interface may have some similarities to the modelling technique used by Oliveira *et al.* (2002) to interpret the damage observed in a lighthouse after an earthquake, where resort was made to a simple 3D approximation of the geometry by macro masonry blocks for calculus simplification. Yi *et al.* (2006) also used a procedure somewhat similar to the one proposed herein to perform 3D nonlinear pushover analyses, where masonry panels were modelled by 3D FEM continuum bodies and contact elements were adopted, placed at predefined macrocracking interfaces, using a Coulomb friction model at contact surfaces.

In the present case, the out-of-plane dynamic behaviour of masonry buildings is simulated through multibody dynamics (considering contact elements and rigid bodies, although flexible ones can be also used (Shabana 2005)). Analogous results may also be obtained by modelling the linear behaviour of elastic bodies by means of the finite element method (e.g. Yi *et al.* (2006) followed this approach for their in-plane nonlinear static analyses).

A schematic example of the proposed methodology based on multibody systems is presented in Figure 6.2. As mentioned by Shabana (2005), in general, a multibody system is defined to be a collection of subsystems called bodies, components or substructures. The motion of the subsystem is kinematically constrained because of different types of joints, and each subsystem or component may undergo large translations and rotational displacements. If the bodies consti-

tuting the multibody system are rigid, the body deformation under consideration is small (theoretically null) and has no effect on the gross body motion. Therefore, the rigid body motion in space can be completely described by using six generalized coordinates, namely three translational and three defining the orientation of the body.
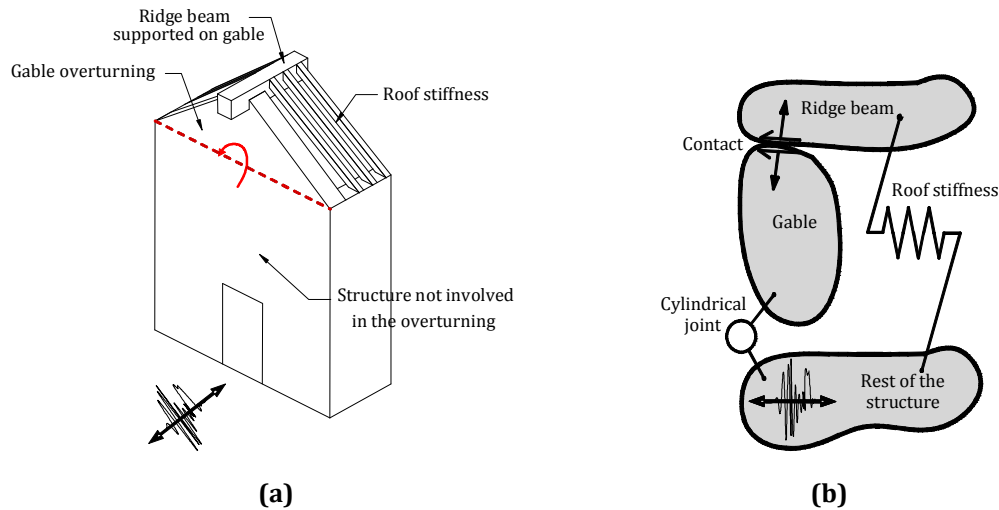
Figure 6.2. Proposed methodology: a) schematic representation of a local mechanism; b) equivalent multibody system

The motion of the bodies can be constrained by system mechanical joints such as revolute or spherical, among other possible constraints. For a system with n_b rigid bodies and n_c active constraint equations in a three-dimensional space, the number of system degrees of freedom (DOF), also often called as Mobility (*M*), is given by the Grübler criterion (Grübler 1883), Eq. (6.1), adopted below in the numerical algorithm presented in section 6.3.

$$DOF = 6 \times (n_b - 1) - n_c \tag{6.1}$$

It is possible to observe that, with a reduced number of DOF, several rigid bodies representing masonry portions may simulate the dynamic behaviour of a multibody system, i.e. of a given local mechanism formed during an earthquake. If other sources of constraints are present in the multibody system, the computation of the mechanism mobility M may be modified using other criteria, as reported by Grigore (2005).

The drawback of the proposed approach for the out-of-plane seismic assessment of masonry façades relies on the need of correctly defining the rigid bodies associated to the collapse mechanism, which may involve several masonry portions to simulate the global overturning of the building. However, the use of simplified collapse mechanisms defined in previous works (see section 6.1) may help in the definition of the most vulnerable ones.

On the other hand, the use of time-history analysis, considering either synchronous or non-synchronous excitation, allows for a direct incorporation into the analysis of the dynamic characteristics of the seismic action, generally expressed in terms of displacement (or acceleration) time series. Hence, although the structural model is still somewhat simplified, the analysis procedure is able to account for strong motion characteristics such as velocity pulses and duration, which can be crucial in the assessment of the out-of-plane stability.

Indeed, large displacements due to low frequency motions, induced by velocity pulses that trigger rocking of masonry elements, are simulated with rigid multibody systems, while small displacements arising from high frequency structure motions (due to distributed flexibility) are not simulated by this model.

Since the out-of-plane collapse of masonry walls is induced by the element instability rather than strength requirements, the collapse of masonry façades may be adequately simulated making use of the numerical approach proposed herein, for which the main parameters involved in the dynamic behaviour of each rigid body are the mass and the corresponding rotational inertia.

6.3. NUMERICAL MODEL DEFINITION

For the application of the proposed procedure, an adequate computer code should be selected where the previously mentioned requirements are fulfilled. Since multibody dynamics is widely applied in mechanical, automotive and aerospace engineering (among others), robust computer codes are available for this type of analysis; in the present work, it was selected the MSC Adams 2012™ software (Multibody Dynamics Simulation - Automatic Dynamic Analysis of Mechanical Systems (MSC 2012a), formerly known as MD Adams in prior releases).

For the analyses presented in this work, the stiff integrator GSTIFF (Gear 1971) was used, with the SI2 formulation technique implemented in the Adams/Solver (C++) (MSC 2012c). Concerning the nonlinearity at contact regions, a "Poisson" model for impacts was used resorting to the restitution coefficient (to account for energy dissipation) and penalty regularization for the normal force calculation. It is worth mentioning that, for pure rocking, the restitution coefficient can be correlated to the energy ratio before and after impacts (r), as firstly presented by Housner (1963) and discussed in Chapter 5; as for the penalty regularization, increasing penalty values lead to better normal force accuracy. More details are available in Appendix C and in MSC (2012b).

A validation of the contact algorithm was made for one-sided and two-sided rocking, comparing the obtained results with the exact theoretical solution (presented in Appendix C). An excellent

simulation was obtained for the one-sided rocking response, while for two-sided rocking no energy dissipation was achieved. The disagreement for two-sided rocking is explained by the impact detection criterion implemented in Adams/Solver, wherein impacts are considered to occur when separation of colliding bodies is detected. In fact, if the relative velocity between two colliding bodies remains close to zero after impact, this situation is algorithmically accepted as a permanent contact rather than an impact. This is precisely what happens for two-sided rocking of rigid bodies and, therefore, is not adequately simulated by MSC Adams.

However, for the purposes of the numerical analyses presented in this work, one-sided rocking governed the response of the simulated local mechanisms and therefore the MSC Adams code could be used.

The friction model adopts a simple velocity-based friction model for contact interfaces (MSC 2012a) with four parameters: μ_s - static friction coefficient; μ_d - dynamic friction coefficient; v_s - static friction transition velocity; v_d - dynamic friction transition velocity. Figure 6.3 reports a schematic representation of the referred friction model.
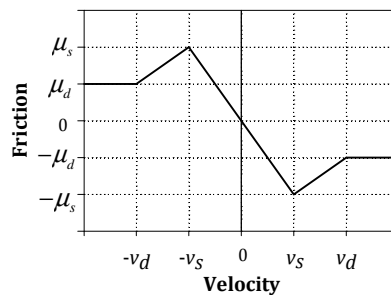
Figure 6.3. Friction model used in ADAMS solver

6.4. NUMERICAL SIMULATIONS

6.4.1. LNEC shaking table tests simulation

6.4.1.1. Presentation of the shaking table tests

The shaking table tests simulated in the present work refer to full scale seismic experiments performed at the LNEC (Laboratório Nacional de Engenharia Civil), Lisbon, and reported in Chapter 4. As stated in the mentioned chapter, the shaking table tests aimed at characterizing the out-of-plane behaviour of a full scale masonry façade (3.35 meter height) with two returning walls at the edges (plan dimensions of the specimen: 4.3 x 2.15 m²) built on *sacco* stone masonry (double leaf walls with poor infill; total thickness of 65 cm). An unidirectional ground motion (17th January 1994 Northridge earthquake, recorded at Newhall Fire Station NWH360)

was specifically selected expecting to activate an overturning mechanism. Five different test levels (L) were performed, corresponding to the following scaling factors and PGA levels: 10% (0.06 g), 20% (0.12 g), 40% (0.24 g), 60% (0.35 g) and 80% (0.47g). At the last stage (L5-80%), the complete overturning of the façade occurred.

In order to validate the numerical model, the last two stages (L4-60% and L5-80%) will be used: *i*) the first represents the mechanism activation and subsequent rocking motion of the façade; *ii*) the last stage traduces the complete overturning behaviour of the masonry façade.

6.4.1.2.   Definition of the model properties and considered mechanisms

The numerical simulations of the shaking table tests started with the definition of the overturning mechanism of the façade. Based on the experimental evidence, a simplified geometry was considered in order to validate the proposal for evaluating the out-of-plane behaviour of masonry façades. The mechanism defined in the numerical model, which involved an overturning of the façade from the window level up to the top (Figure 6.4 a)), led to the simulation of three geometries. Moreover, since the separation occurred between the façade and the returning walls, these two parts were modelled as different rigid bodies with a contact interface between them where vertical impacts could occur. During the tests, a stair step failure of the façade was observed at the cross section level (Figure 6.4 b)) and, therefore, this evidence was also taken into account in the numerical simulation models.

(a)   (b)

Figure 6.4. Collapse mechanism formed: a) global overturning; b) collapse picture at the end of the shaking table test L5-80% with leafs' step failure

The adopted models were based on the observed collapse mechanism but a simplification of the failure mode, without representation of the multiple leaves, was made in two cases. The main objective of such a simplification was to evaluate also the effectiveness of simplified models, commonly used for the seismic assessment of masonry façades.

Three numerical models were developed to simulate the experiments and to evaluate the modelling influence in the final results:

i.   The simplified model 1 (**M1**, Figure 6.5 a)) - the model is divided into four different bodies: two of them at the bottom part of the mechanism (at the window level, bodies 1 and 2) rotating along a cylindrical hinge positioned at the bottom of the window level, while impacts can occur in the inclined interface with the fixed part of the model (body *Fx*); one element at the top part (body 3) which is likely to slide and induce vertical impacts along a horizontal contact interface (two-sided rocking) with the bottom parts (bodies 1 and 2), and to produce horizontal impacts in the vertical portions (one-sided rocking) of returning walls (body *Fx*);

ii.   The simplified model 2 (**M2**, Figure 6.5 b) – the dynamic part is only constituted by one continuous element (body 1), wherein the main façade rotates along a cylindrical hinge positioned at the bottom of the window level; impacts can occur with the rest of the structure (body *Fx*), both in the inclined and vertical interfaces (one-sided rocking);

iii.   The "As is" model (**MAi**, Figure 6.5 c), which reproduces the collapse mechanism formed during the shaking table test, taking into account the presence of the three leafs and corresponding stair step failure. The masonry part involved in the dynamic response of the mechanism is obtained assembling three different rigid bodies, similarly to model M1. However, the differences relative to model M1 consist in the presence of horizontal (impact and friction, two-sided rocking) and vertical (impact, one-sided rocking) contact interfaces at the bottom part (bodies 1 and 2, observable in Figure 6.5) simulating the stair step failure, as well as a non-symmetric failure mechanism reproducing the collapse observed during the test.
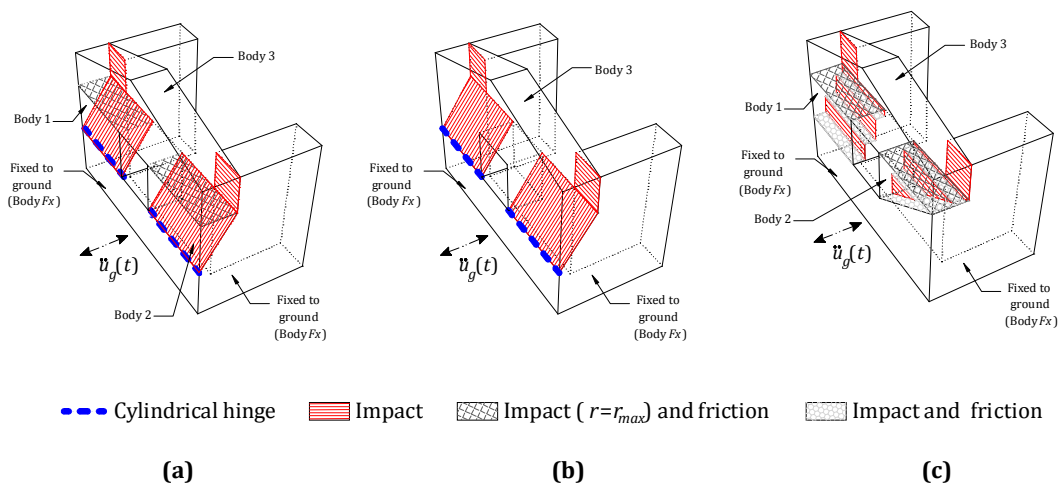
Figure 6.5. Mechanisms considered and subsequent numerical models: a) simplified M1; b) simplified M2; c) MAi model

Concerning the parameters used in the numerical model, no mechanical characterization of masonry samples was made. However, values for the specific weight were available from geo-metrical characterization of small masonry wallettes tested for other purposes (Chapter 5), with a value of 1950 kg/m³, also in accordance with literature values (e.g. (Costa 2002; NTC 2008)). The adopted parameters are listed in Table 6.1, where a wide range of values is consid-ered regarding the friction and vertical restitution coefficients due to absence of characteriza-tion data.

Table 6.1. Parameters used in the numerical model

Volumic mass [kg/m³]	Friction coefficient		Friction transition velocities [m/s]		Coefficient of res-titution		Penalty factor
	Static (μ_s)	Dynamic (μ_d)	Static (v_s)	Dynamic (v_d)	r_{1s}	$r_{2s} = r_{max}$	
1950	from 0.2 to 1.0		0.001	0.01	from 0 to 1.0	0.533	1x10⁸

Based on the geometry of the top element (body 3, Figure 6.5), it is possible to define the maximum value of the restitution coefficient for two-sided rocking (r_{2s}), despite not being cor-rectly simulated with MSC Adams, as mentioned in section 6.3. As shown in the two-sided free rocking tests performed in Chapter 5, the proposal of Housner (1963) for the maximum value of this coefficient, expressed by Eq. (5.6) from Chapter 5, may be used resorting also to Eq. (6.2) to compute the α_0 angle value, which is the instability rotation angle of a rigid block, consider-ing an infinite compressive strength of the interface.

$$r_{max} = 1 - \frac{3}{2}\sin^2 \alpha_0 \tag{5.6}$$

$$\alpha_0 = \tan^{-1}\left(\frac{x_{cg}}{y_{cg}}\right) \tag{6.2}$$

Taking into account the geometry of "Body 3" (x_{cg} = 0.325 m; y_{cg} = 0.483 m), the following re-sults are obtained: α_0 = 0.592 *rad*; $r_{2s} = r_{max}$ = 0.533. Concerning the restitution coefficient for one-sided rocking (r_{1s}), the restraining conditions associated with the rigid body allow rocking, bouncing and free flight. An energy ratio in the form of coefficient of restitution taking rota-tional and translation effects into account should be adequate, while an angular velocity ratio as suggested by Sorrentino *et al.* (2011) for one-sided rocking is not satisfactory for the present case. The same comments can be made for the "As is" model. It should be referred that the same restitution coefficient was used for all the vertical impacts, thus reducing the variability of the numerical parameters in the performed analyses.

The friction and restitution coefficient values (for one-sided rocking) were subjected to a simple parametric study to infer their importance on the final results, as presented in the following subsection. Similar values were used for static and dynamic friction coefficients and small friction transition velocities were adopted to minimize their influence on the dynamic response.

Finally, the penalty factor was defined based on a sensitivity analysis, which allowed selecting the value that leads to reasonable results with reduced time cost, notwithstanding the fact that more accurate results can be obtained for higher penalty values.

6.4.1.3. Numerical analysis results

In this subsection, the evaluation of the proposed methodology for assessment of the out-of-plane performance of masonry façades was made by comparing the obtained numerical results with the experimental data obtained from LNEC shaking table test.

Since the numerical model simulates the behaviour of the masonry façade within the rigid body assumption considering large masonry portions, the main objective to cope with dynamic analyses was to adequately reproduce the displacement time history peaks expected for a masonry façade, representative of an overturning mechanism. Moreover, maximum expected accelerations experienced by the façade should be also taken into account and compared to the experimental data, confirming the validity of the rigid body overturning of the masonry façade.

Because the overturning mechanism was triggered only at stage L4 (60%), no significance on the numerical data should be found for comparisons with lower values of the seismic input.

Regarding the input motion of the numerical model ($\ddot{u}_g(t)$), applied to "Part *Fx*" (Figure 6.5), the acceleration recorded during the shaking table tests at the bottom window level, below the formed overturning mechanism, was used (acc 6, from Chapter 4). Thus, the filtering and amplification effects of the masonry structure are included in this record.

A first analysis is made and presented for the stage L4 (60%), comparing numerical and experimental data in the form of displacements and accelerations. It allows identifying the mechanism activation by observing the displacement time histories. Moreover, the influence of the input motion on the final response is evaluated, showing that the structure's filtering and amplification effects become evident in the numerical results. Concerning the second benchmark (L5-80%), the collapse of the façade is simulated with two different geometrical models and compared with experimental displacement time histories.

It has to be referred that the first numerical results presented in the following subsections are related to the MAi model (presented in Figure 6.5) in order to compare the experimental results with the numerical model with the better reproduction of the collapse mechanism. At the

end, comparisons of MAi model with the other simplified ones (M1 and M2) are also included in order to evaluate the adequacy of simplified models to reproduce complex collapse mechanisms.

L4-60% stage

The L4-60% stage can be seen as the benchmark because the mechanism activation was achieved for this motion level and therefore the rocking motion of the façade may be correctly compared to the numerical model.

Several parametric analyses were made regarding the definition of the friction coefficient (μ) as well as the restitution coefficient (r) to assess the influence of numerical parameters on the final results. It was found that the friction coefficient did not influence significantly the final results, which allowed reducing the scatter found in the range of literature values ($0.6 \leq \mu \leq 0.7$, for granite blocks with lime mortar (Vasconcelos and Lourenço 2009)); in fact, visible differences in the parametric numerical responses were obtained only for $\mu = 0.2$, which is a rather low value for stone masonry. However, sliding can occur during one-sided rocking of the upper part (Part 3). As the position of the impact's normal force at the returning walls may not be aligned with the centre of mass, the eccentricity created may cause rotation and sliding of the rigid body. This effect can also occur by some penetration permitted with the used penalty value.

Also, although the influence of the restitution coefficient (r) on the final results was found very important, it was observed only for non-realistic values of r ($r \geq 0.4$) for the considered one-sided rocking. Therefore it is possible to conclude that, should adequate values of μ and r be provided, their influence in the final results is not expected to be significant. Conceptually, the displacements magnitude is not affected by the restitution coefficient but by the dynamic properties of the rigid bodies. The restitution coefficient affects the rocking behaviour after impacts, and for such small values ($r \leq 0.3$), its importance may not be relevant and may not interfere in the posterior dynamic response.

An example of parametric analyses, within the range of realistic values for friction and restitution coefficient, is presented in Figure 6.6, where it is also possible to observe the good agreement between experimental and numerical results after the mechanism trigger, mainly in terms of displacement peaks.
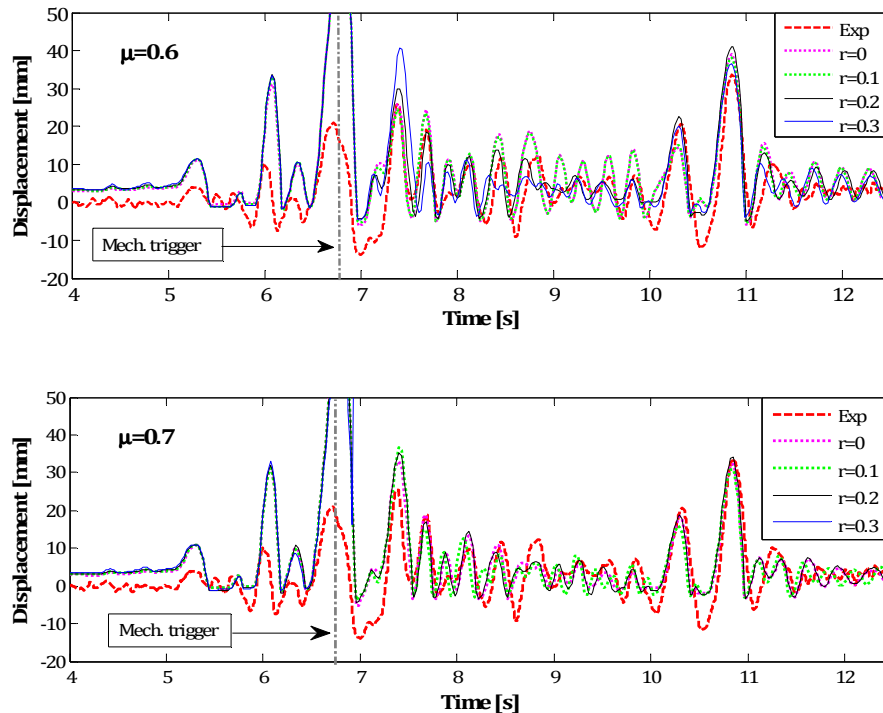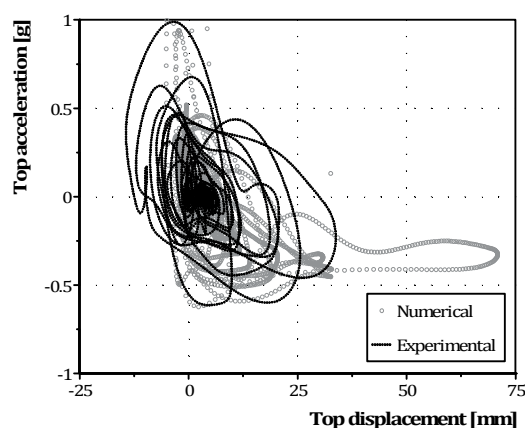
Figure 6.6. Experimental and numerical top relative displacement time histories: top (μ = 0.6 and 0 ≤ r ≤ 0.3); bottom (μ = 0.7 and 0 ≤ r ≤ 0.3).

Figure 6.6 shows the influence of the friction and restitution coefficients on the final results. For one-sided rocking as the present case, within the analysed range of the restitution coefficient, this friction coefficient does not influence significantly the final results and the trend of all the numerical plots is similar. Indeed, the friction coefficient modification from μ = 0.6 to μ = 0.7 leads to a more stable response of the masonry façade, showing results almost coincident for different coefficients of restitution. Moreover, the activation of the mechanism is important when analysing the experimental and numerical curves; indeed, once the mechanism is triggered, the numerical model simulates adequately the dynamic behaviour of the masonry façade but no realistic data is obtained before such activation.

From the previous figures, the best model parameters were found to be μ = 0.7 and r = 0.1 for one-sided rocking (r_{1s}), and, therefore, these values were used for the subsequent analysis presented hereafter.

The numerical top displacement vs. acceleration curve is presented in Figure 6.7, where the numerical results were filtered with a 3rd order Butterworth low-pass filter (f_{cut} = 8 Hz); this is consistent with the filtering process of the experimental curve that was used in order to remove also the high frequency contents of the data arising from impact forces (Chapter 4). It should be referred that, if no filter is applied, the interpretation of the numerical results is not meaningful due to high frequency acceleration peaks.

Figure 6.7. Displacement vs. acceleration curves: comparison between experimental and numerical results

From Figure 6.7, it is possible to observe a rather fair agreement between the experimental and numerical results of acceleration for outward movements (positive displacements), including the post peak strength. Moreover, the numerical response envelope for positive displacements is also in agreement with the experimental data. The discrepancy in terms of maximum positive displacements is due to the absence, in the experimental data, of any mechanism prior to the strong pulse which activated it (as already stated in the interpretation of Figure 6.6), while in the numerical simulation this mechanism is assumed from the very beginning of the analysis.

For the response in the negative sense (negative displacements and positive accelerations), the returning walls' effect is clearly evident in the numerical curve. Indeed, horizontal impacts associated to one-sided rocking led to numerical accelerations significantly higher than the experimentally measured.

Regarding the hysteretic behaviour, as expected, the specimen dissipated more energy than the numerical model, probably due to the shear deformation and flexibility of the masonry façade which cannot be captured by the numerical model. Since the main objective of the numerical model was to simulate the dynamic behaviour of the masonry façade in terms of maximum expected displacement and acceleration, it can be concluded that the model was able to capture well the overturning response for this ground motion level (L4-60%).

Finally, the influence of the selected input motion in the final response of the masonry façade was evaluated. Four different input motions were used and analyzed, namely: *i*) the original NWH360 record, scaled to 60% ("NWH360"); *ii*) the shaking table acceleration record ("ST"); *iii*) the records of the reinforced concrete foundation accelerometer ("Foundation"); *iv*) the accelerometer data at window level (acc6, below the formed mechanism, "Window"). The study of this influence was made taking into account the same numerical parameters used for Figure 6.7 ($\mu = 0.7$, $r_{1s} = 0.1$), leading to the final results shown in Figure 6.8.
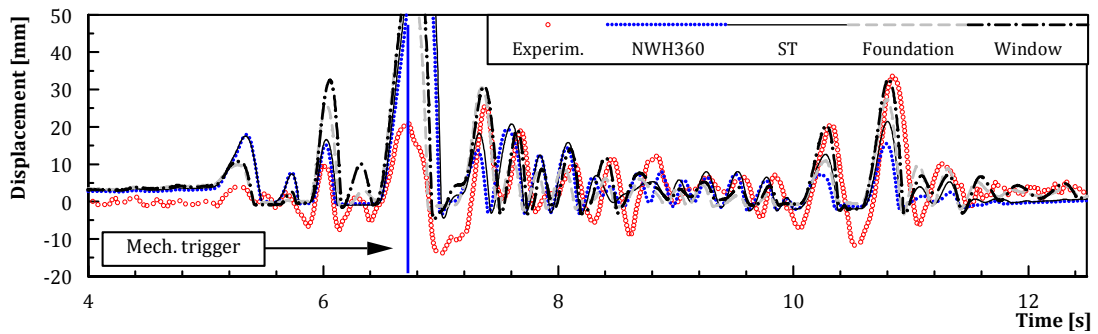
Figure 6.8. Influence of the input motion in the reproduction of the façade's dynamic behaviour

Figure 6.8 shows clearly that the original input motion ("NWH360") led to results significantly different from the experimental data and from those obtained with the most accurate input motion ("Window"). This conclusion is also valid for the shaking table input ("ST") as well as the foundation one ("Foundation"), the latter with numerical results closer to the experimental ones. However, differences in the displacement magnitude are observable between foundation input and the window one, which results from the input motion filtering due to the masonry structure.

The window input seems to be remarkably accurate for peak displacement prediction after triggering the overturning mechanism. Therefore, it is possible to conclude that the closest data to the formed mechanism should be used as input for assessing the out-of-plane behaviour of masonry façades. The effect of structure's filtering and amplification of the seismic input can be seen somewhat similar to recent studies for motion definition to be used in the assessment of out-of-plane behaviour of unreinforced masonry buildings (e.g. (Menon and Magenes 2008; Menon and Magenes 2011a; 2011b)), as also addressed by Lagomarsino and Resemini (2009) and Magenes and Penna (2011).

The numerical analysis results allowed concluding that a correct input which traduces the dynamic properties of the structure should be provided to the numerical model in order to simulate the real conditions that the formed out-of-plane mechanism is subjected to. This means that both current force-based approaches and dynamic analyses should consider the filtering and amplification effect of the structure, and future developments should be made to overcome this problem.

L5-80% stage

Concerning the simulation of the masonry façade collapse (for L5-80% stage, PGA = 0.47g), two different models were adopted: *i*) the original model used to simulate the rigid overturning of the façade (i.e., the previous L4-60% simulation); *ii*) a model modified by including rigid bodies to simulate the three leaves at the window level in order to take account for the observations made during the shaking table test (namely, the collapse induced by the outer leaf instability).

Indeed, the influence of multiple leaves in the out-of-plane response of masonry walls is very important, decreasing the strength and displacement capacity, as studied and reported by de Felice (2011). Despite the macro representation of different leaves by the present model, its influence on the response is important as presented in the following together with the final results.

The numerical parameters used in these analyses are those calibrated from the L4-60% stage simulation ($\mu = 0.7$, $r_{1s} = 0.1$, $r_{2s} = r_{max}$). The simulation of the different leaves' response (using the so-called "numerical multiple leaves" model), is illustrated in Figure 6.9 and it was made considering no tensile nor shear contact between them, with nonlinearity only due to impacts between leaves. The connection with the remaining structure is similar to the original model (friction and impacts at horizontal contacts; only impacts at vertical ones). Figure 6.9 allows observing the correct simulation of the façade collapse taking into account the outer leaf instability: the overturning of the façade at the window level is quite evident, as well as the contribution of the outer leaf to the façade instability.

Observed	Simulated	Observed	Simulated
(a)		(b)	
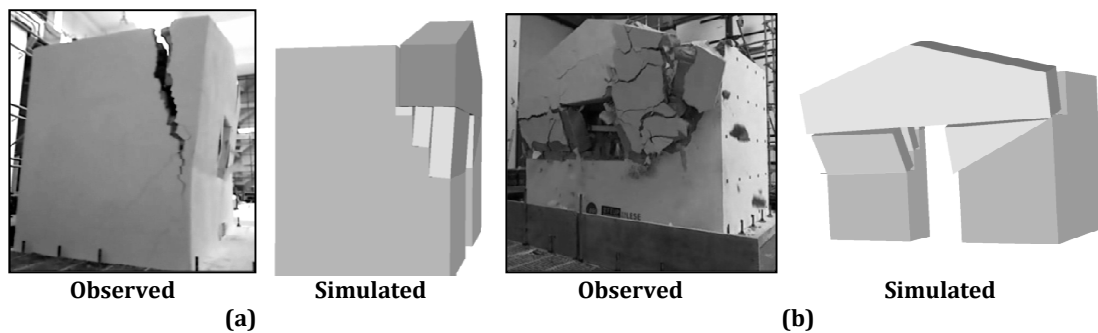
**Figure 6.9. Comparison between numerical and experimental deformed shape:
a) at peak displacement before collapse ($T = 6.85$ s); b) at imminent collapse ($T = 7.52$ s)**

The numerical model did not include the different leaves in the upper part (Body 3) because, as shown in Figure 6.9 a), it was not involved in the main overturning mechanism. Therefore, the deformed shape of the numerical model cannot represent exactly the experimental one, which involved the outer leaf instability at collapse (Figure 6.9 b)). Nevertheless, the experimental collapse mechanism is satisfactorily reproduced by the numerical model.

The displacement time histories obtained with both models ("Original" and "Multiple leaves") are presented in Figure 6.10, where the comparison with the experimental data can be observed.

Figure 6.10 highlights the importance of considering different leaves when predicting the masonry façade collapse by overturning. In fact, the original model, used to simulate the L4-60% test (Figure 6.7), is not able to reproduce the collapse mechanism of the *sacco* masonry wall because it does not consider the heterogeneity of the masonry at the cross-section level. As observed in the experimental campaign, the façade collapse occurred by the outer leaf instabil-

ity rather than global instability of the wall. For this reason, a model taking into account the different leaves is more adequate to simulate the collapse of a *sacco* masonry façade, as evident in Figure 6.10 and in accordance with the numerical results presented by de Felice (2011). Actually, although a less good agreement between the numerical and experimental results during the initial motion part (from 5.3 to 6.7 s), due to larger deformability of the numerical model façade that includes three unconnected leaves (comparatively to the real specimen), still the numerical model allowed capturing the façade collapse induced by the outer leaf instability.
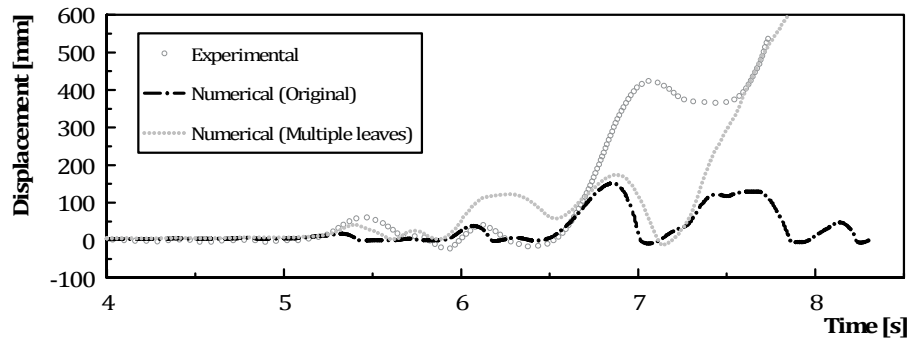
Figure 6.10. Displacement time histories of experimental and numerical data, considering both numerical models (original and multiple leaves)

From the numerical analyses performed within this section, it is possible to infer that numerical modelling of the out-of-plane behaviour of the masonry façade through kinematic chains (rigid bodies), with nonlinearity at the contacts/impacts, allow simulating adequately the dynamic behaviour, bearing in mind that the instability of a *sacco* masonry façade may occur by the instability of the outer leaf, which, if properly modelled, may allow to correctly simulate the façade's collapse.

6.4.1.4. Comparison with simplified mechanisms

A comparison between the full mechanism model (MAi) and simplified models (Figure 6.5, presented in section 6.4.1.2) was made, aiming at assessing the ability of simplified mechanisms to simulate the complex mechanism observed in the experimental test. The results obtained with simplified mechanisms are presented in Figure 6.11, for L4-60% and L5-80% stages.

Figure 6.11 shows that the numerical results, obtained with the simplified models, do not match neither the experimental nor the numerical findings obtained with a realistic reproduction of the formed mechanism. Regarding the L4-60% level, while simplified model M1 overestimates the displacements of the masonry façade probably due to the sliding interface between the top and bottom elements, the simplified model M2 underestimates the façade displacements. On the other hand, both models proved to be non-conservative for simulating the façade

collapse (L5-80% test level), mainly due to the influence of the multiple leaves which are not considered in these simplifications. Indeed, the simplified model M2 conveys a simple over-turning mechanism which could be accepted as representative of the façade overturning when analysed by simplified force-based approaches, but, as observed in Figure 6.11, the results are non-conservative for seismic assessment performed by time-history analysis.
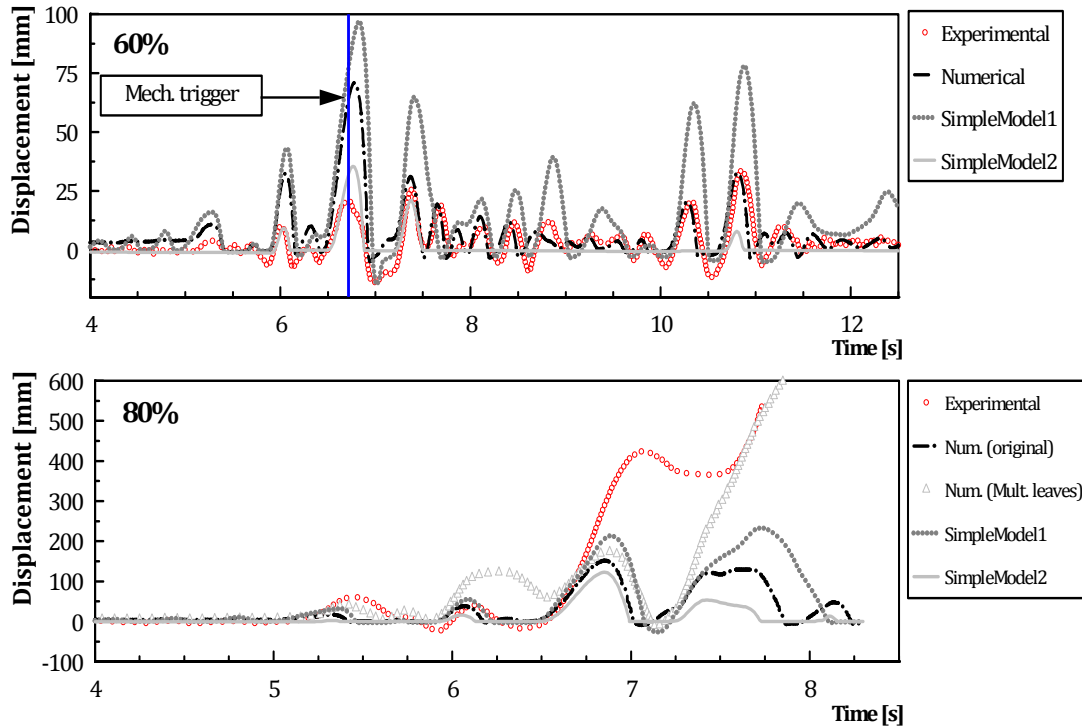

Figure 6.11. Influence of the mechanism geometry in the final results (top, L4-60%; bottom, L5-80%).

6.4.1.5.   Summary of the obtained results

Table 6.2 summarizes the numerical results in terms of peak displacement ratio Δ_{num} /Δ_{exp} (for T=10.8 s), achieved during L4-60% stage after mechanism activation, where Δ_{num} is the numerical peak displacement while Δ_{exp} is the experimental one (Δ_{exp} = 33.6 mm). The peak displacement reached by the specimen was only correctly reproduced by the "As Is" model, considering the window accelerometer input motion ("Window"). Without simulating the structure's dynamic properties (i.e. using the "Foundation" input motion), a non-conservative difference of 19% was obtained. The results obtained with simple models were definitely not satisfactory.

Table 6.2. Summary of the results for peak displacement (L4-60% level, PGA = 0.35g, T = 10.8 s)

	NWH360	ST	Foundation	Window	Simplified M1	Simplified M2
$\delta_{max}/\Delta_{exp}$	0.46	0.64	0.81	0.97	2.33	0.24

As a preliminary conclusion, it can be stated that multibody systems can be used to simulate the rocking behaviour of masonry façades but their results are strongly affected by the geometry adopted for the mechanism, at least for multi-leaf stone masonry walls. More studies should be performed, by means of comparisons with out-of-plane shaking table tests on *sacco* stone masonry façades, in order to reduce the response uncertainty associated with the collapse mechanism definitions as well as masonry façade assemblages.

6.4.2. EUCENTRE two storey masonry building simulation

The proposed numerical technique to simulate the out-of-plane behaviour of masonry façades was validated with a more complex structure. The two-storey double leaf stone masonry house tested at the EUCENTRE (Pavia, Italy) unidirectional shaking table (Magenes *et al.* 2010a), was used as another benchmark test, where the activation of an out-of-plane overturning mechanism was observed.

The tested structure was a two-storey double leaf stone masonry house (Figure 6.12) with 0.32 meter thick load bearing walls (more information available in Magenes *et al.* (2010b); Magenes *et al.* (2010c)), with plan dimensions of 5.8 x 4.4 m² and a total height of 6.0 m (5.0 m to the top of the main walls and a gable with 1.0 m height). The first floor was constituted by timber floor joists (12 x 16 cm²) supporting a wooden floor (3 cm thick), spanning between the main façades, perpendicularly to the motion direction during the shaking tests. At the top, a timber roof was placed (with 8 x 12 cm² rafters and clay tiles), supported by the main façades (with a timber spreader beam at the top) and by a 20 x 32 cm² timber ridge beam. More information regarding the specimen properties and experimental data is available in Magenes *et al.* (2010a).

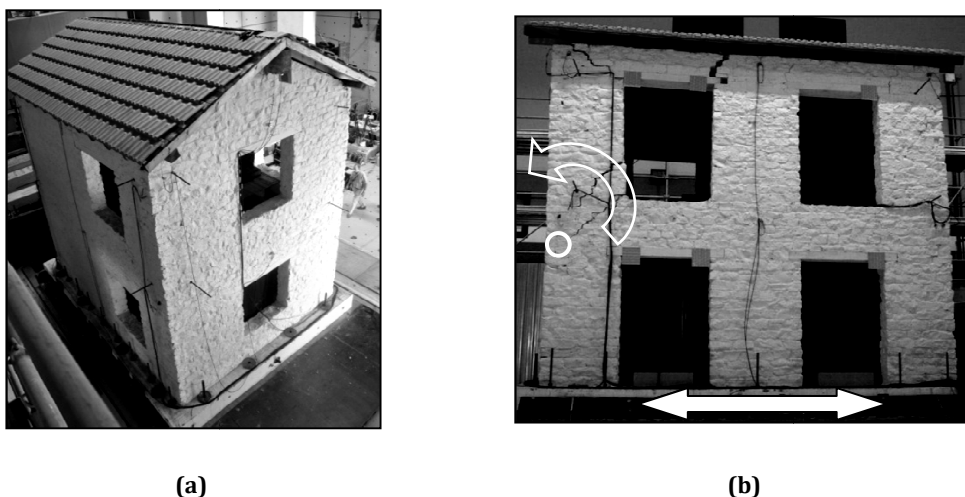(a)   (b)

Figure 6.12. Shaking table test photos: a) general view; b) activation of out-of-plane mechanism at main façade: photo taken at peak displacement

Regarding the observed behaviour of the specimen during the shaking table tests, the out-of-plane mechanism activation of the transversal wall was attained with the 0.30g (nominal PGA) scaled 1979 Montenegro earthquake record (Ulcinj-Hotel Albatros station); subsequently the out-of-plane response was clearly observed for 0.40g (Figure 6.12 b), which allowed identifying the overturning rotation point according to Magenes *et al.* (2010a). For this reason, the results obtained with the numerical model presented in the next subsection will be compared to the experimental values for 0.40g.

6.4.2.1. Description of the numerical model

The numerical model adopted to simulate the experimental shaking table test was based on the same assumptions as the for LNEC model (section 6.4). However, this model revealed to be much more complex than the first one because numerous different rigid bodies were needed to simulate the overall behaviour of the tested specimen. Since the observed out-of-plane response involved the in-plane behaviour of the main façades, all masonry portions involved in the local mechanisms had to be simulated.

For the simulation of the EUCENTRE shaking table test, this technique was found quite suitable because different elements contributed to the out-of-plane behaviour of the transversal wall. Accordingly, resorting to the cracking pattern observed during the experimental tests (Figure 6.13 a) and b)), several masonry portions were defined leading to the numerical model presented in Figure 6.13 c), d) and e), with the general characteristics described next.

(a)   **(b)**

(c) **(d)** **(e)**
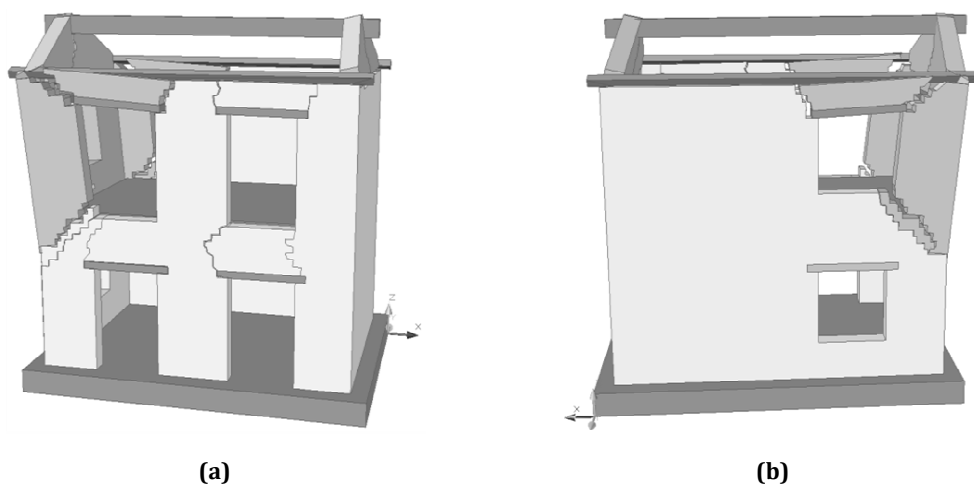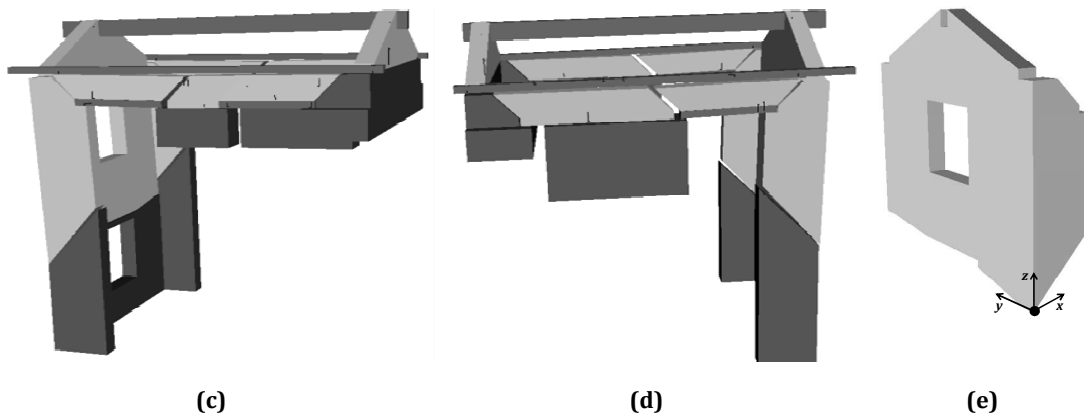
Figure 6.13. Definition of the numerical model: a) and b), collapse mechanism observed; c) and d), numerical model at peak displacement (dark gray elements - displacement input; grey elements – masonry and wood portions); e) detail of transversal wall's rigid body

The element most prone to overturn out-of-plane is the transversal wall, as observed in the experimental test. Considering that element as illustrated in Figure 6.13 e), i.e. the transversal wall part above the upper level of the ground floor window, including parts of the returning wall, the centre of mass position is defined by the coordinates listed in Table 6.3. It allows computing the theoretical ultimate displacement capacity of the wall by rigid body overturning (as evident from the experimental results, in this case the ultimate condition was governed by the maximum displacement compatible with the stability conditions of the lintels supporting the spandrels in the two main façades at the top storey). The centre of mass of the element in the longitudinal direction (x_{cm}), computed directly by MSC Adams based on element's geometry and according to the orthogonal axes presented in Figure 6.13 e), is not positioned at half thickness of the wall ($t/2$ = 0.16 m) but it is shifted inward the house (x_{cm} = 0.25 m), thus contributing to the transversal wall stability.

Table 6.3. Transversal wall mechanism: centre of mass position

x_{cm} [m]	y_{cm} [m]	z_{cm} [m]
0.25	2.10	2.09

Figure 6.13 shows that the numerical model includes the transversal wall and all the elements involved in the out-of-plane behaviour, such as façades' portions and the roof elements (top ridge beam, roof in-plane stiffness and spreader beam). The main characteristics of the EUCENTRE numerical model are presented in Table 6.4, where the number of elements used is shown as well as the different type of contact interfaces.

Table 6.4. Characteristics of the EUCENTRE numerical model

Number of rigid bodies	**Masonry**	13
	Wood	7
Contacts	**masonry-masonry**	15
	masonry-wood	21
Springs		4
Connection joints		6

Rigid bodies simulated the masonry as well as the wood elements, such as the window lintels or top ridge beams. At the interfaces between different elements, contacts were created depending on the type of elements (masonry-masonry or masonry-wood; no wood-wood contact was necessary in the model). Springs were placed at the roof to simulate the in-plane stiffness of each roof pitch, while the roof mass was lumped at the ridge and top spreader beams. Translational connection joints were used for displacement input, as well as a cylindrical joint located in the transversal wall which only allows rocking.

The mechanical characteristics needed to the numerical model refer only to the material unit weight ($\gamma_{masonry}$ = 23 kN/m³), defined according to a preliminary characterization (Magenes *et al.* 2010c). The friction coefficient (μ = 0.7) for the masonry-masonry interface and total roof weight (2310 kg) were also defined based on the cited work. The roof springs' stiffness (1.49 MN/m) was defined so as to provide an equivalent shear modulus (G) of 15 MPa, according to the results obtained from Brignola *et al.* (2008).

Concerning the contact parameters (Table 6.5), no information was available regarding the restitution coefficient and some indicative values were taken from literature for the masonry-wood friction coefficient (0.5 and 0.6, respectively, parallel and perpendicularly to wood fibres (Correia dos Reis *et al.* 2005)).

Thus, simple parametric analyses were made, within the range of assumed realistic values, in order to assess the influence of these parameters on the final response. The static friction velocity was defined with a small value to keep the friction coefficient constant and quasi-independent on the velocity value.

Table 6.5. Contact parameters used in EUCENTRE numerical model

Contact	Friction coefficient		Friction transition velocities [m/s]		Coefficient of restitution (r)	Penalty
	Static (μ_s)	Dynamic (μ_d)	Static (v_s)	Dynamic (v_d)		
Masonry masonry	0.7	0.7	0.001	0.01	0.0 - 0.3	1×10^8
Masonry wood	0.4 - 0.7	0.4 - 0.7	0.001	0.01		

A schematic 2D representation of the numerical model (main façade view) is shown in Figure 6.14, where it is possible to observe the defined masonry portions and the different contact interfaces.
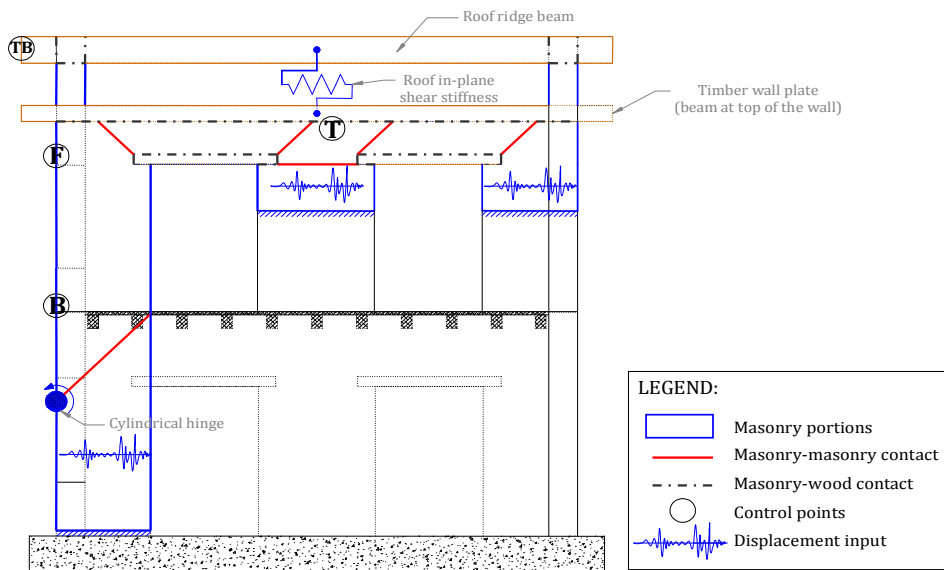
Figure 6.14. Schematic representation of the EUCENTRE numerical model (main façade view)

The input motion used in the numerical model, as demonstrated and used in the LNEC case (section 6.4), should convey the dynamic characteristics of the structure. For this reason, displacements measured during the shaking table test in elements exterior to the defined mechanism were used, as schematically represented in Figure 6.14 by the blue graphs. Unlike in the case of the LNEC numerical model, absolute displacements were used here instead of accelerations because the former input led to consistent results; conversely, the latter yield problems of convergence and "lock-up" (higher number of restrains than DOFs).

The numerical results compared to the experimental data were obtained from four predefined control points corresponding to the positions of some accelerometers and optic sensors for displacement measurement (Magenes *et al.* 2010a). According to Figure 6.14, the points are denoted as: B (for the first floor level); F (mandatory displacement for out-of-plane overturning, due to its position in the transversal wall); T (intermediate mechanism point); TB (for the top ridge beam).

6.4.2.2.   Comparison between experimental and numerical results

The comparison between experimental and numerical results is presented for the 0.40 g scaled Montenegro shaking table test, as mentioned before. The evaluation of results is shown in terms of relative displacements for the four control points (B, F, T and TB) within the time interval where significant displacements were observed (2.5 ≤ t ≤ 15 s). In order to clarify the importance of the dynamic behaviour of the model in the final results, the relative displacements were computed against the input displacement below the activated mechanism, rather than those computed against the shaking table displacements, which may also show an overestimation of the fit between numerical and experimental results.

Figure 6.15 presents the comparison between the experimental and numerical results, obtained with a restitution coefficient of 0.1 (r = 0.1) and friction coefficients (static and dynamic, $\mu_s = \mu_d$) of 0.7 in masonry-masonry interface (i.e., $\mu_{m\text{-}w}$=0.7) and 0.4 to 0.7 for the masonry-wood interface ($\mu_{m\text{-}w}$) coefficient. Some missing points are observed in the experimental data (points F, T and TB) due to acquisition problems (because optic sensors' reference was lost in some time intervals). For this reason, the experimental data for the top beam (TB) is presented for both extremities, where "Exp." refers to the position in the analyzed transversal wall and "Exp. back" refers to the position at the other transversal wall.

Results show negligible influence of the masonry-wood interface friction coefficient in the numerical response of the overturning mechanism (see time histories for points B and F). The main difference is observable at the peak displacement (for t = 12 s), where the error between numerical and experimental results decreases with the increase of the friction coefficient. Therefore, in line with the conclusions for the numerical results of the LNEC tests (section 6.4.1.3), if realistic values of the friction coefficient are provided, adequate numerical results may be obtained with the procedure proposed in this work.

The detailed observation of results for the transversal wall (point B and F) shows good agreement between numerical and experimental evidence, both for displacement peaks and for the remaining displacement time histories. However, residual displacements are not accurately captured by the numerical model due to its geometry construction because the presence of a

cylindrical hinge (shown in Figure 6.14) does not allow sliding at the masonry-masonry interface.
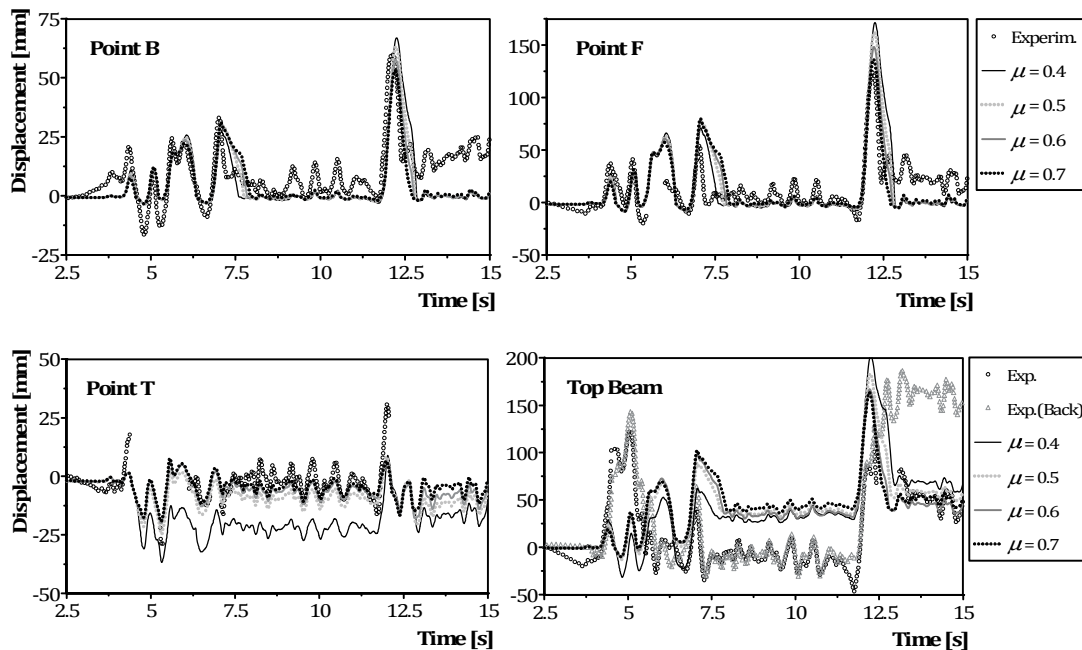
Figure 6.15. Relative displacement time histories for the EUCENTRE specimen test: comparison between experimental and numerical results (r = 0.1; $\mu_{m\text{-}m}$ = 0.7; 0.4 ≤ $\mu_{m\text{-}w}$ ≤ 0.7)

Regarding points T and TB, and due to the importance of the masonry-wood interface in these locations (see Figure 6.14), a visible influence of the friction coefficient is observed; in fact, considering $\mu_{m\text{-}w}$ = 0.4 (the lower bound of sensitivity analysis range) leads to different displacement time histories comparatively to simulations for other $\mu_{m\text{-}w}$ values and clearly not in accordance with the experimental data. Although the recorded residual displacements were captured at the main transversal wall, the in-plane roof stiffness may have played an important role in the final result of the top ridge beam because there is no agreement with the experimental data. Moreover, the amplification of the seismic effects at the gable due to its flexibility is not captured by the numerical model which may also contribute to this disagreement.

However, it seems that the overburden action of the ridge beam is more important to the simulation of the transversal wall out-of-plane response than the correct in-plane roof stiffness estimation. Good agreement between numerical and experimental data was obtained for the out-of-plane behaviour of the wall, even with significant disagreement at the top ridge displacements.

Finally, the influence of the restitution coefficient in the final results was assessed by performing a sensitivity analysis (Figure 6.16) within the range 0 ≤ r ≤ 0.3. The friction coefficient between masonry and wood ($\mu_{m\text{-}w}$) was set to 0.6, taking into account the literature values and the agreement observed in Figure 6.15.

As evident from Figure 6.16, the influence of the restitution coefficient in the final results is negligible for small values of that coefficient, which are quite acceptable because the modelled elements are expected to behave in one-sided rocking. Anyhow, some differences are observed only in the top beam displacement time histories which may be explained by the same reasons previously mentioned.

It is worth noting that, despite being involved in a complex out-of-plane mechanism where the in-plane behaviour of the façade played an important role, the transversal wall out-of-plane behaviour is not significantly affected by the restitution coefficient value (within a reasonable range of small values). Again, this conclusion is in line with what was observed in the numerical results for the LNEC tests (section 6.4.1.3).
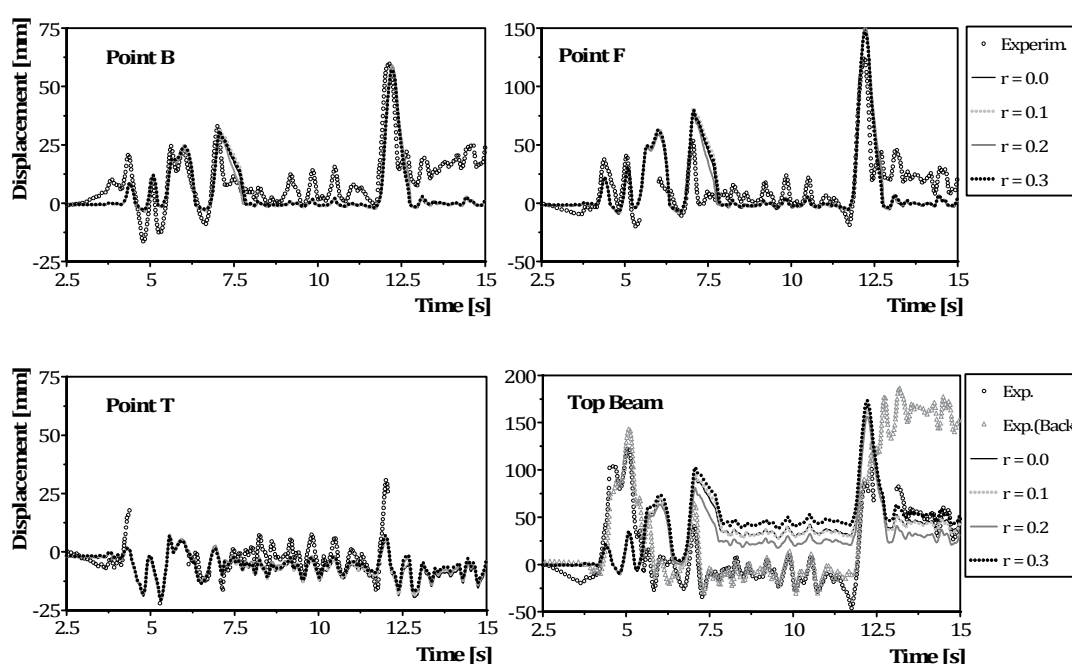
Figure 6.16. Relative displacement time histories for the EUCENTRE specimen test: comparison between experimental and numerical results ($0.0 \leq r \leq 0.3$; $\mu_{m\text{-}m}$ = 0.7; $\mu_{m\text{-}w}$ = 0.6)

Finally, Table 6.6 and Table 6.7 include the deviation between the numerical and experimental data for the peak displacement (δ_{max}) of point F, i.e. the most important output concerning the out-of-plane behaviour of the transversal wall. Taking into account the position of point F in the wall (h_F = 2.95 m, above the cylindrical hinge) and considering the values of Table 6.3, the in-stability displacement (Δ_u) is 0.353 m (obtained by $\Delta_u = (x_{cm} \ h_F)/z_{cm}$, for point F), which allows expressing the peak displacement results in terms of the ratios (δ_{max}/Δ_u) listed in Table 6.6 and Table 6.7.

The recommendation stated in the Italian Code (NTC 2008) for maximum displacement at ultimate limit state (ULS) is given as the lower of: *i*) δ_{max}/Δ_u = 0.40, where Δ_u is the displacement which leads to the instability of the kinematism; *ii*) maximum displacement compatible with

local stability of the individual elements (e.g. unseating of lintel/spandrel beam). From the shaking table data, the experimental ratio reached δ_{max}/Δ_u = 0.40 and no instability of individual elements was observed. Indeed, the out-of-plane behaviour of the transversal wall was one of the reasons to stop the experimental campaign, which contributes for supporting the reasonability of the code-standard recommended value δ_{max}/Δ_u = 0.40.

Table 6.6. Summary of the sensitivity analysis performed to the friction coefficient ($\mu_{m\text{-}w}$)

	$\mu_{m\text{-}w}$			
	0.4	**0.5**	**0.6**	**0.7**
δ_{max}/Δ_u	0.51	0.49	0.46	0.43
Deviation to experimental [%]	27.9	23.2	15.1	8.3

Table 6.7. Summary of the sensitivity analysis performed to the restitution coefficient (r)

	r			
	0.0	**0.1**	**0.2**	**0.3**
δ_{max}/Δ_u	0.46	0.46	0.46	0.45
Deviation to experimental [%]	15.5	15.1	17.3	14.3

When experimental and numerical results are compared, the latter are consistently higher (conservative values), with decreasing deviation as the $\mu_{m\text{-}w}$ value is increased. A considerable approximation to the experimental response is obtained for $\mu_{m\text{-}w}$ = 0.7. Finally, it is worth stressing that, for the presented analyses, the friction coefficient influence is more important than the restitution coefficient effect in the final dynamic response of the structure; indeed, negligible differences were obtained for peak displacement of point F with different values of r (Table 6.7), differently from what happens with the $\mu_{m\text{-}w}$ variation (Table 6.6).

6.4.2.3.   Influence of model simplifications in the dynamic response simulation

The numerical model definition may influence strongly the dynamic response if the properties of the structure are not correctly considered. Since simplified models are currently used for the assessment of the out-of-plane behaviour of masonry façades, it is worth evaluating the impact of some modelling simplifications which can be done. This evaluation was made in a two step
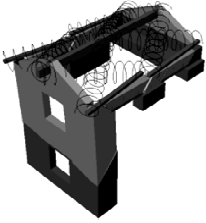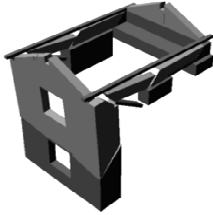
scheme: *i*) first the complex structure was modelled resorting to multibody dynamics but simplifications on the numerical model were made (leading to the hereafter denoted M# models); *ii*) then, a simplified representation of the masonry façade as a single element (corresponding to the so-called SM# models) was considered to evaluate its performance and results' quality.
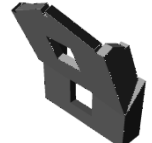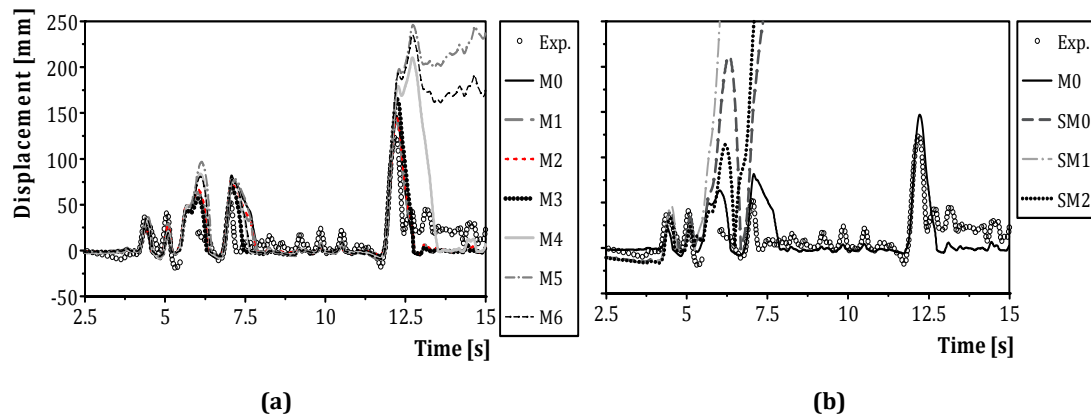
Concerning the first stage, six different models were considered, for which the main properties, simplifications made and observed behaviour are presented in Table 6.8. It should be pointed out that in model M1, similar to the original model used in the previous analyses (M0), the top timber spreader beams were divided in two separate bodies in order to reproduce exactly the tested specimen and to assess the roof modelling influence in the final response. The other remaining models consist of simplifications from the original one (M0).

In the second stage, a simple study was made with simplified models, correlated to recent proposals for assessing the dynamic behaviour of masonry walls through rigid body analysis where the complete structure is not taken into account (e.g., D'Ayala and Shi (2011)), and compared to both the M0 simulation and the experimental results. The influence of lumped masses instead of forces in the numerical results was also assessed and interesting results were obtained.

Figure 6.17 shows the numerical results in terms of readings on point F, in order to compare the final results obtained with different models.

Table 6.8. Influence of model definitions in the dynamic behaviour

	M1	M2	M3	M4	M5	M6	SM0	SM1	SM2
Model properties	Full model	Full model	No ridge beam	No ridge beam	No ridge beam nor timber plate	No roof elements	-	-	-
Simplification	2 timber plate beams (exact specimens' reproduction)	No roof stiffness	Concentrated forces, due to ridge beam mass, at transversal and gable walls	Lumped masses from ridge beam loads, placed at transversal and gable walls	Lumped masses from the ridge beam loads, placed at transversal and gable walls	No overburden masses nor forces	No overburden masses nor forces	Lumped mass from ridge beam, placed at the top of the wall	Concentrated force from ridge beam
Deformed shape									
Deformed shape time [s]	12.8	12.1	12.1	12.9	12.9	12.9	9.0	7.6	8.0
Observed behaviour	Correct failure mode. Motion of timber plate beams.	Correct failure mode	Correct failure mode	Correct failure mode. Imminent collapse	Correct failure mode. Imminent collapse	Correct failure mode. Imminent collapse	Collapse	Collapse	Collapse

(a)   **(b)**

Figure 6.17. Numerical results obtained with: a) different definitions of multibody numerical models; b) simplified models

From Figure 6.17 a), it is clear that common modelling simplifications may lead to substantially different results, with peak displacements achieving almost twice the experimental ones.

Amongst several considerations about these results, three main conclusions can be drawn from Table 6.8 and Figure 6.17: *i*) the presence of physical restraining elements, such as the ridge beam and the masonry spandrel beams which provide friction and overburden forces, contribute significantly to the structural stability, as evidenced by the difference between M1 and M2 to the other subsequent models; *ii*) the introduction of forces instead of masses, where the latter contributes to the rotational inertia of the wall, is non-conservative as shown by the comparison of numerical results and deformed shapes of M3 and M4); *iii*) simplified models may be over-conservative.

These last two conclusions gain more relevance if the single element models' (SM#) results are analyzed (Figure 6.17 b)). In fact, these simple models are too conservative because all the three different versions collapsed with the same ground motion which is not in accordance with the experimental results or numerical data (i.e., the M# models). Moreover, by comparing the results among the SM# models, it is clearly identified that the influence of lumped mass (SM1) in the dynamic response is crucial for the analysis, because, while SM1 collapses at the third rocking movement, the other two models (SM0 and SM2) only collapse at the subsequent pulse of the seismic motion.

Therefore, as a preliminary conclusion, the adopted numerical approach (using multibody dynamics) allowed simulating the out-of-plane dynamic response of the EUCENTRE masonry specimen. Moreover, the modelling simplifications were found to influence significantly the final results, being observed that too over-conservative analyses are obtained if simplified models are used. However, further studies similar to the herein presented should be pursued in order to obtain an adequate and suitable method for the simulation of the out-of-plane behaviour of masonry walls.

Computational cost

An important parameter always involved in numerical nonlinear time history analyses (NTHA) is the computational cost. For a NTHA of 15 seconds long, with time step of 0.01 seconds and a penalty value of $1x10^8$, an average value of 5780 seconds (1 hour 36 min 20 s) per analysis was obtained, using an Intel® Core™2 Quad 2.66Hz CPU running under 64-bit Windows 7© operating system. If multithread processing is taken into account, it allows reducing significantly the computational time to average value of 2206 seconds or 36 min 46 s, which further encourages the use of multibody dynamics. Moreover, if sliding friction is not considered at contact regions, the analyses can be performed in a few minutes.

In conclusion, the assessment of the out-of-plane performance of masonry façades resorting to multibody dynamics seems to be a powerful tool, providing important outputs of the dynamic behaviour of complex structures. Moreover, simple mechanical models and low knowledge level of the masonry mechanical characteristics increase the interest in this approach, which provides an important cost – effective solution.

6.5. PROPOSED METHODOLOGY FOR OUT-OF-PLANE ASSESSMENT OF MA-SONRY FAÇADES

The promising results obtained in the previous sections allow suggesting a methodology for the seismic assessment of the out-of-plane performance of masonry façades. Differently from current force-based approaches focused on the definition of a seismic multiplier and a corresponding rigid body overturning capacity curve, the proposed methodology permits performing NTHA where the out-of-plane dynamic response is obtained with limited time consumption.

For that purpose, an adequate input motion should be provided which takes into account the dynamic properties of the structure. As mentioned before, future work should be done for the definition of adequate out-of-plane seismic excitations. At present time, and for future studies' purposes, a connection between Tremuri (Galasco *et al.* 2006) and MSC Adams was developed in MATLAB® (MathWorks 2009). Tremuri, an equivalent frame-based type program for nonlinear seismic analysis of masonry buildings, can be considered as a time efficient solution which simulates the in-plane nonlinear behaviour of the structure in reduced time and provides the necessary input data (where the structural dynamic characteristics are taken into account) to feed the out-of-plane model in MSC Adams.

A real-time interaction for NLTHA between both models should be established because the out-of-plane response of the walls may locally influence the in-plane behaviour. However, a two step procedure (which should be improved) is currently implemented: Tremuri runs the in-

plane model, where displacements and accelerations are obtained at the end of in-plane analysis; after that, those results are read by MSC Adams as input motions for predefined positions and the out-of-plane analysis is performed.

A summary flowchart is presented in Figure 6.18 where the processes and their relations can be observed.
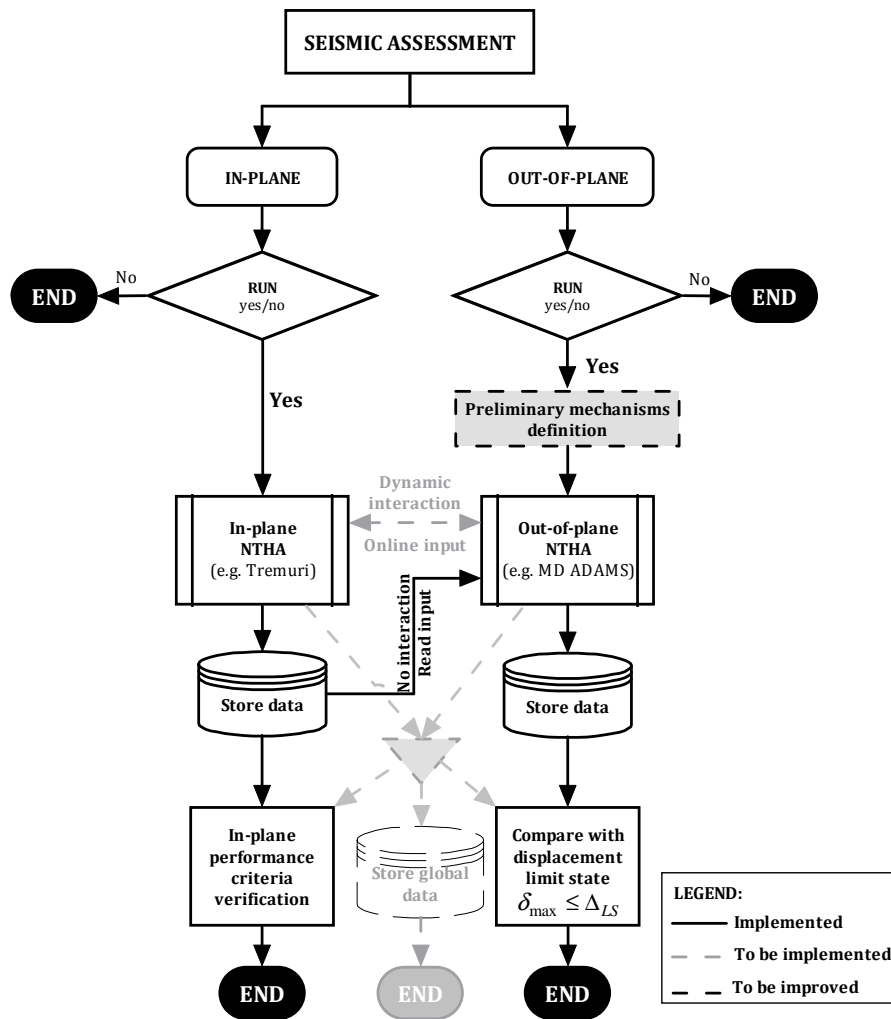

Figure 6.18. Summary of the proposed methodology for seismic assessment

The main drawback of the proposed methodology relies on the definition of the local mechanisms. Since the out-of-plane model is not able to define the most likely failure mechanism, the local mechanism(s) should be defined *a priori* by the user, which may lead to erroneous definitions and misunderstanding of the out-of-plane behaviour of the analyzed masonry structure. Clearly, further work should be made in this topic.

Finally, the out-of-plane procedure can be performed independently on the in-plane analysis if adequate input motions, which simulate the characteristics of the analyzed structure, are provided to the multibody dynamics numerical model.

6.6. CONCLUSIONS

In this chapter, the simulation of the out-of-plane dynamic behaviour of local mechanisms based on multibody dynamics was proposed. Local mechanisms were constituted by several masonry portions simulated through rigid bodies, representing kinematic chains where nonlinearity is concentrated at contact regions.

Nonlinear time history analyses were performed in the MSC Adams™ software and compared with experimental results from two full scale shaking table tests, where good agreement between numerical and experimental data was found. Modelling details have shown to be important for the correct simulation of the out-of-plane behaviour, where the simulation of the multiple leaves on a *sacco* masonry wall was mandatory for the reproduction of wall's collapse.

Moreover, for the performed analyses, reasonable values of the friction and restitution coefficients were found to have reduced influence on the final results. Conversely, dynamic amplification and filtering effects of the structure affected significantly the simulation of the tests, highlighting the importance of providing correct input data. Finally, some comparisons with the dynamic behaviour of simplified overturning mechanisms were done. For the one storey masonry façade, no consistency was obtained between the results obtained with the simplified models and the experimental ones. Concerning the two storey EUCENTRE building specimen, simplified models consistently led to the overturning of the façade but possibly in an overconservative way. More analyses should be performed following the method herein proposed.

For the correct simulation of the out-of-plane behaviour of local mechanisms, appropriate inertia and mass data proved to be necessary, as well as other elements adjacent to the main overturning mechanism and corresponding restraining forces (such as overburden and sliding). Elements' mass simulated through equivalent forces may be under-conservative for seismic assessment.

Finally, a simple proposal for the seismic assessment of local mechanisms was presented, where the in-plane and out-of-plane numerical models are connected, contributing in this manner for a more accurate simulation of the response. The main drawback of the presented proposal remains in the correct definition of the local mechanism, which should be carefully studied in future researches.

Nevertheless, the numerical simulation of the out-of-plane collapse of masonry local mechanisms through kinematic chains of masonry portions, with nonlinearity concentrated at the contact regions, proved to be a powerful, time efficient and adequate tool for the out-of-plane simulation of masonry façades, if a realistic reproduction of the overturning mechanism is provided.

Chapter 7.

FINAL REMARKS

The overall vision within this Thesis work encompassed the static and dynamic assessment of the out-of-plane behaviour of masonry walls, more precisely *sacco* stone masonry façades of existing constructions. The extent of the performed work allowed characterizing, experimentally and numerically, the behaviour of such walls through robust experimental tests along with simplified numerical simulations of the dynamics results. The main conclusions and pertinent major remarks are pointed out in the next subsection, while possible future developments and research lines (devised with the present work) are presented at the end of this chapter.

7.1. CONCLUSIONS

In-Situ Experimental Tests

The development of an experimental test setup to be applied for *in-situ* testing was made and validated with nine out-of-plane experiments and one in-plane test, all of them carried out on existing constructions. As one of the main objectives was to design a portable and light system, use was made of aluminium double acting actuators to apply the desired loads in the specimens, resorting to a self-equilibrated system within the tested structure.

The influence of the flexibility of the reaction wall may not permit the applicability of this test setup for all type of experiments. Indeed, the developed test setup should be used only for flexible specimens with reduced strength when compared to the reaction wall and always focused on quasi-static tests. Despite not being addressed during this Thesis work, the possibility of using the proposed test setup for dynamic tests seems not to be feasible because the reaction structure flexibility may influence significantly the dynamic properties of the system (reaction

wall + actuators + specimen) which may be rather complex. Moreover, extra control difficulties are likely to arise from the interaction of different system components when sudden actions occur, with problems on the release of accumulated energy and on pursuing adequately the post-peak behaviour.

Regarding the behaviour of the three unreinforced specimens tested (S01 and CN – Chapter 2, CS01 - Chapter 3), the maximum strength was achieved for a similar drift of 1.0%, while the maximum displacement was achieved for values of Δ/t close to 10% (9% for CS01 and CN and 10% for CS01), where Δ is the top displacement and t is the wall thickness. Therefore, some consistency can be found on the values obtained for the unreinforced specimens but no agreement can be found with the three specimens regarding the ultimate displacement (assumed as the displacement associated with a maximum strength decrease of 20%) mainly due to the earlier stop of CS01 test. However, the presented values may be seen as preliminary attempts to define drift limits for significant damage (SD) and near collapse (NC) limit state of masonry walls under out-of-plane loads. Finally, the linear envelope of the response obtained through limit equilibrium analysis showed to be a conservative assumption for estimating the response resorting to the strength envelope.

The test setup also proved to be adequate to perform experiments on strengthened specimens, where the maximum walls' capacity was achieved and both strength and stiffness degradations were observed, with the exception for tests stopped earlier due to safety problems.

Concerning the behaviour of strengthened specimens, a significant overall improvement was achieved with all the tested techniques when compared to the unreinforced specimens. The strength and energy dissipation capacities increased twice for specimens with top connections and three times when used together with reinforced connected plaster. These ratios were obtained for similar or higher displacement capacities when compared with the response for unreinforced specimens. The efficiency of different strengthening techniques was validated and it was found that other techniques for connecting horizontal and vertical elements (less intrusive than reinforced connected plaster) are also efficient and may be applied alternatively or complementary to the use of reinforced connected plaster. As a final remark, the drift corresponding to the maximum strength achieved for tests with reinforced connected plaster was approximately equal to 3% in all the three similar tested specimens.

As a conclusion regarding the *in-situ* experimental tests, good agreement with force-based analysis was found between the experimental data and simple analytical calculation of maximum strength, thus highlighting its applicability to existing constructions for predicting the maximum capacity of masonry walls strengthened with similar techniques.

Experimental evaluation of the dynamic behaviour of masonry façades

The out-of-plane shaking table tests performed on full scale models, representative of an existing construction, permitted concluding that the masonry façade mainly behaved as a rigid body and is influenced by the presence of multiple leaves. Moreover, with the adopted monitoring instrumentation, it was possible to determine the position of the façade rotation axis, which moved between the expected zones (base, bottom and top of window level). The energy dissipation in the masonry façade was found to take place at the impacts between the façade and the returning walls, although some flexural response was also observed.

The most interesting conclusions drawn from the shaking table tests are related to the formation of the overturning mechanism and collapse. The mechanism was formed due to insufficient interlocking between the façade and the returning walls (which in fact was expected to have been ensured during specimens' construction); in the horizontal direction it was affected by the window opening, while in the vertical direction the main façade detached from the returning walls. Moreover, the presence of vertical continuous head joints above the window level led to the existence of a more vulnerable line and the window frame position, more precisely the orientation of window jambs (located at the outer leaf), increased the façade vulnerability and potentiated its collapse.

Multi-leaf masonry walls may be analysed with the full thickness of the walls but bearing in mind that collapse occurs by instability of the outer leaf. The ultimate displacement capacity should be defined as a function of this leaf and not by the instability of the entire wall in future out-of-plane seismic assessments of *sacco* stone masonry façades.

Free rocking tests and the Equivalent Block Approach (EBA)

A new method for experimental determination of the restitution coefficient was proposed and validated, making use of a novel proposal herein named as Equivalent Block Approach (EBA), where a masonry wall or façade is experimentally simulated through an equivalent structure conveying the geometrical and dynamic properties of the original element.

Despite being a simple concept, this approach may turn out possible to analyze complex structure, as masonry façades with complex geometries difficult to reproduce experimentally, or other type of elements.

Regarding the behaviour of the masonry façade reproduced in the free rocking tests, the influence of joints' flexibility was found to be important in the correct reproduction of the experiments. For this reason, flexibility should be considered in the analysis of *sacco* masonry walls when free rocking behaviour governs the response.

The restitution coefficients obtained with the experimental tests were close or even higher than the theoretical maximum value (r_{max}). If conservative values are desired, as in the case of assessment of existing structures, the maximum theoretical value should be considered. However, higher values should not be neglected because it was experimentally evident that they may occur. More experiments for this type of masonry should be carried out to confirm such considerations.

It was also found an interesting conclusion which is in the opposite sense to previous experiments made by other authors in this research topic. The effects of repetitions in the restitution coefficient were found important and inversely proportional to the increasing number of tests in the analysed walls (*sacco* masonry), contrarily to the observations by Sorrentino *et al.* (2011). However, for a large number of repetitions, this effects seems to diminish (as in the case of FR1 specimen), being found a ratio of r/r_{max} = 0.95, as the recent proposal by Sorrentino *et al.* (2011).

The numerical simulation of the free rocking tests reproducing masonry façades was made resorting to a simple rigid block numerical model developed in MATLAB. The consideration of the foundation's flexibility was found to be important for the correct simulation of the experiments, and good compromise between efficiency and simplicity was found with the so-called semi-rigid model. This model takes into account the foundation's flexibility at the initial rotation of the block (θ_0), for which the geometrical parameter α is determined based on the corresponding displaced position, and the so-obtained numerical results contributed for validating the experimental evidence.

Finally, one of the possible applications of the EBA approach to other areas is, for example, on museum statues, where the complex geometry and mass distribution may be simplified by an equivalent block with similar geometrical properties (R and α) and dynamic characteristics (p), turning out possible to make numerical analyses for assessing the vulnerability of such masterpiece. The EBA approach may be also applicable for 3D simulation of existing elements, if the inertia properties along the principal axes (x, y and z) can be computed.

Multibody dynamics as a tool for simulation of the behaviour of local mechanisms

A novel strategy was proposed for simulating the dynamic behaviour of local mechanisms, resorting to multibody systems' dynamics. Previous suggestions from literature for the assessment of local mechanisms rely on force-based (and also more recently on displacement-based) procedures, taking into account static loads. Concerning the dynamic behaviour simulation of local mechanisms, only models for single elements were used in the past.

In this Thesis work, the dynamic behaviour of complex local mechanisms were simulated, where the characteristics of the ground motion were duly taken into account and the dynamic

behaviour of several masonry portions were modelled through kinematic chains of rigid bodies with concentrated nonlinearity at contact regions. Simple energy based criteria were adopted to define the dynamic behaviour, and it was found that reasonable friction and restitution coefficient values may lead to consistent numerical data. This proposal was validated with two shaking table tests' results and the particularities of the modelled specimens, such as the presence of multiple leaves, were found to contribute significantly for a proper simulation of the dynamic response. Finally, it was found that models simulating simple mechanisms, where local conditions of the surrounding elements are not taken into account (such as ridge beams, overburden mass and inertia from other elements), may lead to conservative or non-conservative results.

7.2. FUTURE DEVELOPMENTS

As a result of the research work performed, new research lines can be defined, either for validation of the main results and conclusions achieved or for assessing the behaviour of existing masonry structures.

The first future development or work that should be done with the developed *in-situ* test setup is the experimental characterization of similar walls with different slenderness ratios and dimensions, in order to increase the amount of acquired data and to check whether the obtained displacement values are similar to those presented in this work. Numerical simulations calibrated with experimental results should also be done to provide better insight and consistency on the available data for this type of walls. Such increase of data is mandatory for the seismic assessment of masonry façades resorting to displacement-based procedures taking into account the quasi-static results, which is a rather important research output to be achieved in the near future.

Regarding the dynamic behaviour of masonry façades, more free rocking tests should be performed on *sacco* masonry walls under two and one-sided rocking, in order to infer the restitution coefficient for impacts in vertical interfaces, somehow similar to the experiments recently performed by Sorrentino *et al.* (2011). In addition to the calibration of restitution coefficient for *sacco* masonry walls, the importance of such new experiments is related to the role of joint's flexibility and the effect of repetitions. Further experimental evidence is required to sustain the test results presented in this Thesis.

Another interesting research line to develop in the future is related to the EBA method. The simplicity of the method, based on the rotational inertia and mass properties of a complex system, can be used to simulate complex local mechanisms likely to be represented as single rigid elements. Since this method allows computing the dynamic response in a very short time pe-

riod, it may be applied to assess the dynamic behaviour of single local mechanism and/or to derive fragility curves.

As mentioned before, the application of this method in other areas is also possible, as the research of the vulnerability of art statues and sculptures. The research in this field may turn out possible to safely decrease their vulnerability with simple modifications of their dynamic properties, such as the mass at the base or other small interventions. At least, it will be possible to simulate the dynamic behaviour of these elements, thus increasing the knowledge of their dynamic performance under earthquake or accidental actions.

Finally, the novel proposal to simulate the behaviour of numerous and complex local mechanisms, resorting to multibody dynamics (MBD), should be improved. Three main developments should be made in the future for this topic, namely: *i*) the correct prediction of the local mechanism likely to form, considering also the characteristics of the seismic action (such as near-fault effects); *ii*) the development of an integrated procedure for real time in-plane and out-of-plane simulation of the dynamic behaviour; *iii*) the inclusion of interface flexibility at the contact regions (as observed in the free rocking tests).

Existing displacement-based procedures for the assessment of masonry local mechanisms may be improved at this stage with the use of multibody dynamics. However, since MBD simulates the dynamic behaviour within energy conservation rules and energy-based assumptions, the development of velocity-based or even energy-based assessment procedures could be a major future research topic, in the framework of the assessment of existing masonry buildings.

References

ABK (1981). Methodology for the mitigation of seismic hazards in existing unreinforced masonry buildings: wall testing, out-of-plane. Topical Report 04. El Segundo, California, United States of America.

Abrams D., Smith T., Lynch J. and Franklin S. (2007). Effectiveness of rehabilitation on seismic behavior of masonry piers. *Structural Engineering*, Volume 133, Issue 1, pp: 32-44. DOI: 10.1061/(ASCE)0733-9445(2007)133:1(32)

Al Shawa O., de Felice G., Mauro A. and Sorrentino L. (2011). Out-of-plane seismic behaviour of rocking masonry walls. *Earthquake Engineering & Structural Dynamics*, Volume, Issue, pp: IN PRESS. DOI: 10.1002/eqe.1168

Almeida C. (2000). Análise do comportamento da igreja do Mosteiro da Serra do Pilar sob a acção dos sismos. *MSc. Thesis*, *Faculdade de Engenharia da Universidade do Porto*. Porto, Portugal.

Andreaus U. and Casini P. (1999). On the rocking-uplifting motion of a rigid block in free and forced motion: influence of sliding and bouncing. *Acta mechanica*, Volume 381, Issue 138, pp: 219-241. DOI: 10.1007/BF01291846

Anthoine A., Magonette G. and Magenes G. (1995). Shear-compression testing and analysis of brick masonry walls. *Proceedings of the 10th European Conference on Earthquake Engineering*, Rotterdam, Holland.

Aslam M., Godden W.G. and Scalise D.T. (1978). Rocking and overturning response of rigid bodies to earthquake motions, *University of California - Berkeley*.

Aslam M., Godden W.G. and Scalise D.T. (1980). Earthquake rocking response of rigid bodies. *Journal of the Structural Division*, Volume 106, Issue 2, pp: 377-392.

Bendat J.S. and Piersol A.G. (2000). *Random data: analysis and measurement procedures*, Wiley Interscience. ISBN: 0471317330.

Benedetti D., Carydis P. and Pezzoli P. (1998). Shaking table tests on 24 simple masonry buildings. *Earthquake Engineering and Structural Dynamics*, Volume 27, Issue 1, pp: 67-90. DOI: 10.1002/(SICI)1096-9845(199801)27:1<67::AID-EQE719>3.0.CO;2-K

Binda L., Modena C., Baronio G. and Abbaneo S. (1997). Repair and investigation techniques for stone masonry walls. *Construction and Building Materials*, Volume 11, Issue 3, pp: 133-142. DOI: 10.1016/S0950-0618(97)00031-7

Binda L., Penazzi D. and Saisi A. (2003). Historic masonry buildings: necessity of a classification of structures and masonries for the adequate choice of analytical models. *Proceedings of the 6th International symposium on computer methods in Structural Masonry (STRUMAS VI)*, Roma, Italy, Computers & Geotechnics Ltd.

Binda L., Saisi A. and Tedeschi C. (2006). Compatibility of materials used for repair of masonry buildings: research and applications. *Fracture and Failure of Natural Building Stones*. S. K. Kourkoulis, Springer Netherlands, Part I, pp: 167-182. DOI: 10.1007/978-1-4020-5077-0_11.

Bothara J.K., Dhakal R.P. and Mander J.B. (2010). Seismic performance of an unreinforced masonry building: An experimental investigation. *Earthquake Engineering & Structural Dynamics*, Volume 39, Issue 1, pp: 45-68. DOI: 10.1002/eqe.932

Brignola A., Podesta S. and Pampanin S. (2008). In-plane stiffness of wooden floor. *Proceedings of the 2008 New Zealand Society for Earthquake Engineering Conference*, Wairakei, New Zealand.

Candeias P. (2008). Avaliação da vulnerabilidade sísmica de edifícios de alvenaria. *Ph.D. thesis Thesis, School of Engineering - University of Minho*. Guimarães, Portugal.

Carvalho A. (1996). *Madeiras portuguesas - Estrutura anatómica, propriedades, utilizações*, Direcção Geral de Florestas. ISBN.

Carvalho E., Oliveira C.S., Fragoso M. and Miranda V. (1998). Regras gerais de reabilitação e reconstrução de edifícios correntes afectados pela crise sísmica do Faial, Pico e S. Jorge iniciada pelo sismo de 9 de Julho de 1998. LNEC. Lisbon, *Laboratório Nacional de Engenharia Civil (LNEC)*.

CEN (1999). Methods of test for mortar for masonry. Part 11: Determination of flexural and compressive strength oh hardened mortar. EN 1015-11. CEN. Brussels, Belgium.

CEN (2004). Eurocode 5: Design of timber structures - Part 1-1: General - Common rules and rules for buildings. EN 1995 -1. CEN. Brussels, Belgium.

CEN (2005a). Eurocode 8: Design of structures for earthquake resistance, Part 3: Assessment and retrofitting of buildings. prEN 1998 -3. CEN. Brussels, Belgium.

CEN (2005b). Eurocode 8: Design of structures for rarthquake resistance, Part 1: General rules, seismic actions and rules for buildings. prEN 1998 -1. CEN. Brussels, Belgium.

Corradi M., Borri A. and Vignoli A. (2002). Strengthening techniques tested on masonry structures struck by the Umbria-Marche earthquake of 1997-1998. *Construction and Building Materials*, Volume 16, Issue 4, pp: 229-239. DOI: 10.1016/S0950-0618(02)00014-4

Corradi M., Borri A. and Vignoli A. (2003). Experimental study on the determination of strength of masonry walls. *Construction and Building Materials*, Volume 17, Issue 5, pp: 325-337. DOI: 10.1016/S0950-0618(03)00007-2

Correia dos Reis A., Farinha M.B. and Farinha J.P.B. (2005). *Tabelas técnicas*. Lisbon, Edições Técnicas Lisboa Lda. ISBN: 9789729973154.

Costa A. (2002). Determination of mechanical properties of traditional masonry walls in dwellings of Faial island, Azores. *Earthquake Engineering and Structural Dynamics*, Volume 37, Issue 7, pp: 1361-1382. DOI: 10.1002/eqe.167

Costa A. and Arêde A. (2006). Strengthening of structures damaged by the Azores earthquake of 1998. *Construction and Building Materials*, Volume 20, Issue 4, pp: 252–268. DOI: 10.1016/j.conbuildmat.2005.08.029

Costley A.C. and Abrams D. (1995). Dynamic response of unreinforced masonry buildings with flexible diaphragms. NCEER Technical Report, *Urbana-Champaign*.

D'Ayala D. and Shi Y. (2011). Modeling masonry historic buildings by multi-body dynamics. *International Journal of Architectural Heritage*, Volume 5, Issue 4-5, pp: 483-512. DOI: 10.1080/15583058.2011.557138

D'Ayala D. and Speranza E. (2000). An integrated procedure for the assessment of seismic vulnerability of historic buildings. *Proceedings of the 12th World Conference on Earthquake Engineering*, Auckland, New Zealand.

D'Ayala D. and Speranza E. (2002). An integrated procedure for the assessment of seismic vulnerability of historic buildings. *Proceedings of the 12th European Conference on Earthquake Engineering*, London, Elsevier Science.

D'Ayala D. and Speranza E. (2003). Definition of collapse mechanisms and seismic vulnerability of historic masonry buildings. *Earthquake Spectra*, Volume 19, Issue 3, pp: 479-509. DOI: 10.1193/1.1599896

de Felice G. (2011). Out-of-plane seismic capacity of masonry depending on wall section morphology. *International Journal of Architectural Heritage*, Volume 5, Issue 4-5, pp: 466-482. DOI: 10.1080/15583058.2010.530339

de Felice G. and Giannini R. (2001). Out-of-plane seismic resistance of masonry walls. *Journal of Earthquake Engineering*, Volume 5, Issue 2, pp: 253-271. DOI: 10.1080/13632460109350394

Decanini L., Masiani R., Sorrentino L. and Tocci C. (2006). Allegato 1.2-UR15-1: Risposta fuori del piano di pareti murarie, libere e vincolate in sommità, a settanta segnali naturali. Valutazione e riduzione della vulnerabilità di edifici in muratura. RELUIS. (in italian).

Derakhshan H. (2011). Seismic assessment of out-of-plane loaded unreinforced masonry walls. *Ph.D. Thesis*, *University of Auckland*. Auckland, New Zealand.

Doherty K., Griffith M.C., Lam N. and Wilson J. (2002). Displacement-based seismic analysis for out-of-plane bending of unreinforced masonry walls. *Earthquake Engineering and Structural Dynamics*, Volume 31, Issue 4, pp: 833 - 851. DOI: 10.1002/eqe.126

Dolce M., Nigro D., Ponzo F.C. and Marnetto R. (2001). The cam system for the retrofit of masonry structures. *Proceedings of the 7th International Seminar of Seismic Isolation, Passive Energy Dissipation and Active Control of Vibrations of Structures*, Assissi, Italy.

Dolce M., Ponzo F.C., Goretti A., Moroni C. and Nigro D. (2008). 3D dynamic tests on 2/3 scale masonry buildings upgraded with different systems. 14th World Conference on Earthquake Engineering. Beijing, China.

Dormand J.R. and Prince P.J. (1980). A family of embedded Runge-Kutta formulae. *Journal of Computational and Applied Mathematics*, Volume 6, Issue 1, pp: 19-26. DOI: 10.1016/0771-050X(80)90013-3

Dusi A., Mezzi M., Manzoni E. and Dusi C. (2007). The use of polymeric grids for the seismic enhancement of brick masonry buildings. *Proceedings of the 7º Congresso de Sismologia e Engenharia Sísmica*, Porto, Portugal.

ElGawady M., Lestuzzi P. and Badoux. M. (2004). A review of conventional seismic retrofitting techniques for URM. 13th International Brick and Block Masonry Conference. Amsterdam, Netherlands.

Frumento S., Magenes G., Morandi P. and Calvi G.M., Eds. (2009). Interpretation of experimental shear tests on clay brick masonry walls and evaluation of q-factors for seismic design. Pavia, EUCENTRE.

Galasco A., Lagomarsino S. and Penna A. (2006). TREMURI Program: Seismic Analyser of 3D Masonry Buildings. Genova, Italy, *University of Genova*.

Gear C.W. (1971). Simultaneous numerical solution of differential-algebraic equations. *IEEE transactions on circuit theory*, Volume CT-18, Issue 1, pp: 89-95.

Giannini R. (1984). Analisi dinamica di un sistema di blocchi sovrapposti. *Proceedings of the 2° Convegno Nazionale "L'Ingegneria Sismica in Italia"*, Rapallo, Italy.

Giuffrè A. (1993). *Sicurezza e conservazione dei centri storici: Il caso Ortigia*. Bari, Italy, Laterza. ISBN: 88-420-4250-1.

Giuffrè A. and Carocci C. (1996). Vulnerability and mitigation in historical centres in seismic areas. *Proceedings of the 11thWorld Conference on Earthquake Engineering*, Acapulco, Mexico.

Griffith M.C., Lam N., Wilson J. and Doherty K. (2004). Experimental Investigation of Unreinforced Brick Masonry Walls in Flexure. *Journal of Structural Engineering*, Volume 130, Issue 3, pp: 423-432. DOI: 10.1061/(ASCE)0733-9445(2004)130:3(423)

Griffith M.C., Magenes G., Melis G. and Picchi L. (2003). Evaluation of out-of-plane stability of unreinforced masonry walls subjected to seismic excitation. *Journal of Earthquake Engineering*, Volume 7, Issue Special Issue 1, pp: 141-169. DOI: 10.1080/13632460309350476

Griffith M.C., Vaculik J., Lam N.T.K., Wilson J. and Lumantarna E. (2007). Cyclic testing of unreinforced masonry walls in two-way bending. *Earthquake Engineering and Structural Dynamics*, Volume 36, Issue 6, pp: 801 - 822. DOI: 10.1002/eqe.654

Grigore G. (2005). Mobility of mechanisms: a critical review. *Mechanism and Machine Theory*, Volume 40, Issue 9, pp: 1068-1097. DOI: 10.1016/j.mechmachtheory.2004.12.014

Grübler M. (1883). Allgemeine Eigenschaften der Zwangläufigen ebenen kinematischen Ketten, Part I. *Zivilingenieur*, Volume 29, Issue, pp: 167-200.

Hamed E. and Rabinovitch O. (2008). Nonlinear dynamic behavior of unreinforced masonry walls subjected to out-of-plane loads. *Journal of Structural Engineering*, Volume 134, Issue 11, pp: 1743-1753. DOI: 10.1061/(ASCE)0733-9445(2008)134:11(1743)

Heyman J. (1966). The stone skeleton. *International Journal of Solids and Structures*, Volume 2, Issue 2, pp: 249-279. DOI: 10.1016/0020-7683(66)90018-7

Hogan S.J. (1990). The many steady state responses of a rigid block under harmonic forcing. *Earthquake Engineering & Structural Dynamics*, Volume 19, Issue 7, pp: 1057-1071. DOI: 10.1002/eqe.4290190709

Housner G.W. (1963). The behaviour of the inverted pendulum structures during earthquakes. *Bulletin of the Seismological Society of America*, Volume 53, Issue 2, pp: 403-417.

Juhásová E., Sofronie R. and Bairrão R. (2007). Stone masonry in historical buildings - Ways to increase their resistance and durability. *Engineering Structures*, Volume 30, Issue 8, pp: 2194-2205. DOI: 10.1016/j.engstruct.2007.07.008

Konstantinidis D. and Makris N. (2005). Seismic response analysis of multidrum classical columns. *Earthquake Engineering & Structural Dynamics*, Volume 34, Issue 10, pp: 1243-1270. DOI: 10.1002/eqe.478

Lagomarsino S. (1998). A new methodology for the post-earthquake investigation of ancient churches. *Proceedings of the 11th European Conference on Earthquake Engineering*, Paris, France, Balkema.

Lagomarsino S. (2006). On the vulnerability assessment of monumental buildings. *Bulletin of Earthquake Engineering*, Volume 4, Issue 4, pp: 445-463. DOI: DOI 10.1007/s10518-006-9025-y

Lagomarsino S. and Resemini S. (2009). The assessment of damage limitation state in the seismic analysis of monumental buildings. *Earthquake Spectra*, Volume 25, Issue 2, pp: 323-346. DOI: Doi 10.1193/1.3110242

Lam N.T.K., Wilson J.L. and Hutchinson G.L. (1995). The seismic resistance of unreinforced masonry cantilever walls in low seismicity areas. *Bulletin of the New Zealand National Society for Earthquake Engineering*, Volume 28, Issue 3, pp: 179-195.

Liberatore D. and Santansiero D. (2009). Oscillazioni di blocchi snelli sotto azione sismica: effeti del coefficiente di restituzione e della monolateralità. *Proceedings of the ANIDIS 2009 - XIII Convegno di Ingegneria Sismica in Italia*, Bologna, Italy.

Liberatore D. and Spera G. (2001). Oscillazioni di blocchi snelli: valutazione sperimentale della dissipazione di energia durante gli urti. *Proceedings of the 10º Convegno Nazionale "L'ingegneria Sismica in Italia"*, Potenza-Matera.

Lipscombe P.R. and Pellegrino S. (1993). Free rocking of prismatic blocks. *Journal of Structural Engineering*, Volume 119, Issue 7, pp: 1387-1410. DOI: 10.1061/(ASCE)0733-9399(1993)119:7(1387)

LNEC (2009). LNEC-SPA (Signal Processing and Analysis Tool for Civil Engineers). Lisbon, Portugal, *LNEC - Laboratório Nacional de Engenharia Civil*.

M.I.T. (2009). Istruzioni per l'applicazione delle nuove norme tecniche per le costruzioni di cui al D.M. 14 gennaio 2008, Ministero delle infrastrutture e dei trasporti approvata dal Consiglio Superiore dei Lavori Pubblici. Circolare, n.617, 2 febbraio 2009. (in italian).

Magenes G., Galasco A. and Penna A. (2009). Caratterizzazione meccanica di una muratura in pietra. *Proceedings of the ANIDIS 2009 - XIII Convegno di Ingegneria Sismica in Italia*, Bologna, Italy.

Magenes G., Kingsley G.R. and Calvi G.M. (1995). Static testing of a full scale, two-story masonry building: test procedure and measured experimental response. Experimental and numerical investigation on a brick masonry building prototype, Report 3.0 CNR-GNDT Numerical prediction of the experiment: 1.1 – 1.41, *University of Pavia*.

Magenes G. and Penna A. (2011). Seismic design and assessment of masonry buildings in Europe: recent research and code development issues. 9th Australasian Masonry Conference. Queenstown, New Zealand.

Magenes G., Penna A. and Galasco A. (2010a). A full-scale shaking table test on a two-storey stone masonry building. *Proceedings of the 14th European Conference on Earthquake Engineering*, Ohrid, Macedonia.

Magenes G., Penna A., Galasco A. and Da Pare M. (2010b). In-plane cyclic shear tests of undressed double-leaf stone masonry panels. *Proceedings of the 8th International Masonry Conference*, Dresden, Germany.

Magenes G., Penna A., Galasco A. and Rota M. (2010c). Experimental characterisation of stone masonry mechanical properties. *Proceedings of the 8th International Masonry Conference*, Dresden, Germany.

Maheri M.R., Najafgholipour M.A. and Rajabi A.R. (2008). The influence of mortar head joints on the in-plane and out-of-plane seismic strength of brick masonry walls. *Proceedings of the 14th World Conference on Earthquake Engineering*, Beijing, China.

Makris N. and Konstantinidis D. (2003). The rocking spectrum and the limitations of practical design methodologies. *Earthquake Engineering & Structural Dynamics*, Volume 32, Issue 2, pp: 265-289. DOI: 10.1002/eqe.223

Makris N. and Roussos Y. (2000). Rocking response of rigid blocks under near-source ground motions. *Géotechnique*, Volume 50, Issue 3, pp: 243-262. DOI: 10.1680/geot.2000.50.3.243

MathWorks (2009). MATLAB - The language of technical computing, *The MathWorks Inc.*

Menon A. and Magenes G. (2008). *Out-of-plane seismic response of unreinforced masonry. Definition of seismic input*. Pavia, Italy, IUSS - Istituto Universitario di Studi Superiori. ISBN: 978-88-6198-021-1.

Menon A. and Magenes G. (2011a). Definition of seismic input for out-of-plane response of masonry walls: I. Parametric study. *Journal of Earthquake Engineering*, Volume 15, Issue 2, pp: 165-194. DOI: 10.1080/13632460903456981

Menon A. and Magenes G. (2011b). Definition of seismic input for out-of-plane response of masonry walls: II. Formulation. *Journal of Earthquake Engineering*, Volume 15, Issue 2, pp: 195-213. DOI: 10.1080/13632460903494446

Milano L., Beolchini G.C., Mannella A., Martinelli A. and Morisi C. (2009). C.I.N.E. - Condizioni d'Instabilità Negli Edifici, *Rete dei Laboratori Universitari di Ingegneria Sismica (ReLUIS)*.

Milizia (1554). Principij di architettura. Venezia, Italy.

Modena C., Valluzzi M.R. and Zenere M. (2009). c-Sisma, *Università degli Studi di Padova*.

Morandi P. (2006). New proposals for simplified seismic design of masonry buildings. *Ph.D. Thesis*, *University of Pavia*. Pavia, Italy.

Mosallam A.S. (2007). Out-of-plane flexural behavior of unreinforced red brick walls strengthened with FRP composites. *Composites: Part B*, Volume 38, Issue 5-6, pp: 559–574. DOI: 10.1016/j.compositesb.2006.07.019

Mosele F., da Porto F. and Modena C. (2008). Out-of-plane behaviour of tall reinforced masonry walls. *Proceedings of the 14th World conference on Earthquake Engineering*, Beijing, China.

Mouzakis H.P., Psycharis I.N., Papastamatiou D.Y., Carydis P.G., Papantonopoulos C. and Zambas C. (2002). Experimental investigation of the earthquake response of a model of a marble classical column. *Earthquake Engineering & Structural Dynamics*, Volume 31, Issue 9, pp: 1681-1698. DOI: 10.1002/eqe.184

MSC (2012a). ADAMS - Automatic Dynamic Analysis of Mechanical Systems, *MSC Software Corporation*.

MSC (2012b). Adams/Solver Manual, *MSC Software Corporation*.

MSC (2012c). An Overview of How to Use ADAMS/Solver, *MSC Software Corporation*.

Neves F., Costa A. and Oliveira C.S. (2007). Vulnerabilidade Sísmica do Parque Habitacional das Ilhas do Faial e Pico (Parte 1 - Danos Exteriores). *Proceedings of the 7º Congresso de Sismologia e Engenharia Sísmica*, Porto, Portugal.

Neves F., Costa A., Vicente R., Oliveira C. and Varum H. (2012). Seismic vulnerability assessment and characterisation of the buildings on Faial Island, Azores. *Bulletin of Earthquake Engineering*, Volume 10, Issue 1, pp: 27-44. DOI: 10.1007/s10518-011-9276-0

NI (2010a). DIAdem. Austin, USA, *National Instruments*.

NI (2010b). LabVIEW. Austin, USA, *National Instruments*.

NTC (2008). Norme Tecniche per le Costruzioni, D. M. 14 gennaio 2008, Suppl. ord. n° 30 alla G.U. n. 29 del 4/02/2008, *Consiglio Superiore dei Lavori Pubblici (in italian)*.

Oliveira C.S., Costa A. and Nunes J.C. (2008). *Sismo 1998 - Uma Década Depois*. ISBN: 978-989-20-1223-4.

Oliveira C.S., Lemos J.V. and Sincraian G. (2002). Modelling large displacements of structures damaged by earthquake motions. *European Earthquake Engineering*, Volume 3, Issue, pp: 56-71.

Oliveira C.S. and Malheiro A.M. (1999). The Faial, Pico, Sao Jorge Azores earthquake of July 9, 1998. *Proceedings of the Earthquake geotechnical engineering*, Lisbon, Portugal.

OPCM no. 3274 (2005). Primi elementi in materiali di criteri generali per la classificazione sismica del territorio nazionale e di normative tecniche per le costruzioni in zona sísmica, come modificato dall'OPCM 3431 del 3/5/05 (in Italian).

Papanicolaou C.G., Triantafillou T.C., Papathanasiou M. and Karlos K. (2008). Textile reinforced mortar (TRM) versus FRP as strengthening material of URM walls: out-of-plane cyclic loading. *Materials and Structures*, Volume 41, Issue 1, pp: 143-157. DOI: 10.1617/s11527-006-9207-8

Peña F., Prieto F., Lourenço P.B., Campos Costa A. and Lemos J.V. (2007). On the dynamics of rocking motion of single rigid-block structures. *Earthquake Engineering & Structural Dynamics*, Volume 36, Issue 15, pp: 2383-2399. DOI: 10.1002/eqe.739

Penazzi D., Valluzzi M.R., Cardani G., Binda L., Baronio G. and Modena C. (2000). Behaviour of historic masonry buildings in seisimic areas: lessons learned from the Umbria-Marche earthquake. *Proceedings of the 12th International brick/block masonry conference*, Madrid, Spain.

Penazzi D., Valluzzi M.R., Saisi A., Binda L. and Modena C. (2001). Repair and strengthening of historic masonry buildings in seismic areas. *Proceedings of the Archi 2000*, Paris, France.

Peng C.Y. and Iwan W.D. (1992). An identification methodology for a class of hysteretic structures. *Earthquake Engineering & Structural Dynamics*, Volume 21, Issue 8, pp: 695-712. DOI: 10.1002/eqe.4290210804

Penna A., Calvi G.M. and Costa A.A. (2007). Prestazioni sismiche del calcestruzzo cellulare. *Proceedings of the ANIDIS 2007 - XII Convengo Nazionale L'Ingegneria Sismica in Italia*, Pisa, Italy.

Priestley M.J.N., Evison R.J. and Carr A.J. (1978). Seismic response of structures free to rock on their foundations. *Bulletin of the New Zealand National Society for Earthquake Engineering*, Volume 11, Issue 3, pp: 141-150.

Quintela C. (2009). Seismic vulnerability of historical structures. Damage state of the Abruzzo churches, in the sequence of the 2009 earthquake. *MSc. Thesis*, *University of Padova, Italy*.

Resemini S., Lagomarsino S. and Cauzzi C. (2008). Dynamic response of rocking masonry elements to long period strong ground motion. *Proceedings of the 14th World Conference on Earthquake Engineering*, Beijing, China.

Restrepo-Vélez L.F. and Magenes G. (2009). *Static tests on dry stone masonry and evaluation of static collapse multipliers*, IUSS Press. ISBN: 9788861980426.

Rondelet J.B. (1802). *Traité théorique et pratique de l'art du batir*. Paris, France. ISBN.

Shabana A.A. (2005). *Dynamics of multibody systems*. New York, Cambridge University Press. ISBN: 978-0521850117.

Sharif I., Meisl C.S. and Elwood K.J. (2007). Assessment of ASCE 41 height-to-thickness ratio limits for URM walls. *Earthquake Spectra*, Volume 23, Issue 4, pp: 893-908. DOI: 10.1193/1.2790488

Shenton H.W. (1996). Criteria for initiation of slide, rock, and slide-rock rigid-body modes. *Journal of Engineering Mechanics*, Volume 122, Issue 7, pp: 690-693. DOI: 10.1061/(ASCE)0733-9399(1996)122:7(690)

Shibata A. and Sozen M.A. (1976). Substitute-structure method for seismic design in R/C. *Journal of the Structural Division, ASCE*, Volume 102, Issue 1, pp: 1–18.

Sorrentino L., AlShawa O. and Decanini L. (2011). The relevance of energy damping in unreinforced masonry rocking mechanisms. Experimental and analytic investigations. *Bulletin of Earthquake Engineering*, Volume 9, Issue 5, pp: 1-26. DOI: 10.1007/s10518-011-9291-1

Sorrentino L., Kunnath S., Monti G. and Scalora G. (2008a). Seismically induced one-sided rocking response of unreinforced masonry façades. *Engineering Structures*, Volume 30, Issue 8, pp: 2140-2153. DOI: 10.1016/j.engstruct.2007.02.021

Sorrentino L. and Masiani R. (2007). Influenza delle caratteristiche del moto del suolo sulla risposta di un corpo rigido. *Proceedings of the XII National Conference "L'ingegneria sismica in Italia"*, Pisa, Italy.

Sorrentino L., Masiani R. and Decanini L.D. (2006). Overturning of rocking rigid bodies under transient ground motions. *Structural Engineering and Mechanics*, Volume 22, Issue 3, pp: 293-310.

Sorrentino L., Masiani R. and Griffith M.C. (2008b). The vertical spanning strip wall as a coupled rocking rigid body assembly. *Structural Engineering and Mechanics*, Volume 29, Issue 4, pp: 433-453.

Tomazevic M., Lutman M. and Petkovic L. (1996a). Seismic behavior of masonry walls: experimental simulation. *Journal of Structural Engineering*, Volume 122, Issue 9, pp: 1040-1047. DOI: 10.1061/(ASCE)0733-9445(1996)122:9(1040)

Tomazevic M., Lutman M. and Weiss P. (1996b). Seismic upgrading of old brick-masonry urban houses: tying of walls with steel ties. *Earthquake Spectra*, Volume 12, Issue 3, pp: 599-622. DOI: 10.1193/1.1585898

Tomaževič M. and Weiss P. (2010). Displacement capacity of masonry buildings as a basis for the assessment of behavior factor: an experimental study. *Bulletin of Earthquake Engineering*, Volume 8, Issue 6, pp: 1267-1294. DOI: 10.1007/s10518-010-9181-y

Tumialan J.G., Galati N. and Nanni A. (2003). Field assessment of unreinforced masonry walls strengthened with fiber reinforced polymer laminates. *Journal of Structural Engineering*, Volume 129, Issue 8, pp: 1047-1056. DOI: 10.1061/(ASCE)0733-9445(2003)129:8(1047)

Vaculik J., Griffith M.C. and Magenes G. (2010). Collapse load predictions for masonry walls in bending. *Proceedings of the 8th International Masonry Conference*, Dresden, Germany.

Valluzzi M.R., da Porto F. and Modena C. (2004). Behavior and modeling of strengthened three-leaf stone masonry walls. *Materials and Structures*, Volume 37, Issue 3, pp: 184-192. DOI: 10.1007/BF02481618

Vasconcelos G. and Lourenço P.B. (2009). Experimental characterization of stone masonry in shear and compression. *Construction and Building Materials*, Volume 23, Issue 11, pp: 3337-3345. DOI: 10.1016/j.conbuildmat.2009.06.045

Willis C.R., Griffith M.C. and Lawrence S.J. (2004). Horizontal bending of unreinforced clay brick masonry. *Masonry International*, Volume 17, Issue 3, pp: 109-122.

Winkler T., Meguro K. and Yamazaki F. (1995). Response of rigid body assemblies to dynamic excitation. *Earthquake Engineering and Structural Dynamics*, Volume 24, Issue 10, pp: 1389-1408. DOI: 10.1002/eqe.4290241008

Wong C.M. and Tso W.K. (1989). Steady state rocking response of rigid blocks. Part 2: Experiment. *Earthquake Engineering and Structural Dynamics*, Volume 18, Issue 1, pp: 107-120. DOI: 10.1002/eqe.4290180110

Yi T., Moon F.L., Leon R.T. and Kahn L.F. (2006). Analyses of a two-story unreinforced masonry building. *Journal of Structural Engineering*, Volume 132, Issue 5, pp: 653-662.

Yim C.S., Chopra A.K. and Penzien J. (1980). Rocking response of rigid blocks to earthquakes. *Earthquake Engineering & Structural Dynamics*, Volume 8, Issue 6, pp: 565-587. DOI: 10.1002/eqe.4290080606

Zhang J. and Makris N. (2001). Rocking response of free-standing blocks under cycloidal pulses. *Journal of Engineering Mechanics*, Volume 127, Issue 5, pp: 473-483. DOI: 10.1061/(ASCE)0733-9399(2001)127:5(473)

Appendix A.

LNEC SHAKING TABLE TESTS: GROUND MOTION

SELECTION DETAILS AND MONITORING SYSTEM

This appendix presents the information relative to the selection of the ground motion used on the shaking table tests presented in Chapter 4 of the thesis as well as to the monitoring system.

First, the characteristics of the 74 ground motions (Table A.1, adapted from Decanini *et al.* (2006)) used in the accelerogram selection are presented in section A.1, in terms of pseudo-acceleration and displacement response spectra, for 5% damping ratio. Afterwards, for the three different simplified mechanisms (MEC0, MEC1 and MEC2) defined to simulate the out-of-plane dynamic response of the masonry façade, the dynamic response is presented in section A.3 in terms of displacement time histories. In order to clarify each individual result, numerical data is presented in several different bins, while displacements are presented as the ratio δ/Δ_u, where δ is the numerically obtained top displacement and Δ_u is the instability displacement for each façade mechanism, computed directly from Adams/View geometry (for displacements measured at the top of the wall, $\Delta_{u,MEC1} = 0.674$ m, $\Delta_{u,MEC2} = 0.716$ m and $\Delta_{u,MEC1} = 1.122$ m).

It should be referred that all records were scaled to 0.6g, i.e. 75% of the peak acceleration of LNEC shaking table test (taking into account the tested specimen), as presented in Chapter 4, and they are listed in this appendix sorted by decreasing values of peak ground velocity (PGV), with the exception of Azores and L'Aquila earthquake data which are placed at the end.

The end of this appendix presents scaled drawings of the monitoring system used in the shaking table tests.

A.1. LIST OF ACCELEROGRAMS AND DETAILS

Table A.1. Ground motion characteristics (adapted from Decanini *et al.* (2006))

No.	Earthquake	Year Station	Name	M_w	Df (km)	Soil type EC8-USGS	PGA (g)	PGV (cm/s)
1	Northridge	1994 Sylmar - Olive View Med FF#	SYL360	6.7	1.7	C	0.84	129.4
2	Kobe	1995 Takatori	TAK000	6.9	1.8	D	0.61	127.1
3	Cape Mendocino	1992 Cape Mendocino #	CPM000	7.0	0.1	A	1.50	125.1
4	Northridge	1994 Sylmar - Converter Sta East #	SCSEN18E	6.7	0.3	B	0.82	116.5
5	Northridge	1994 Newhall - W. Pico Canyon Rd.	56SCN46E	6.7	7.1	C	0.41	115.4
6	San Fernando	1971 Pacoima Dam, abutment	PAC164	6.6	3.2	A	1.17	114.5
7	Superstitn Hills(B)	1987 Parachute Test site	PTS225	6.7	0.7	C	0.46	112.0
8	Imperial Valley	1979 El Centro Array #6	HOU230	6.5	1.4	C	0.44	109.8
9	Northridge	1994 Sylmar - Converter Sta #	SCSS38E	6.7	0.2	C	0.75	109.6
10	Imperial Valley	1979 El Centro Array #7	IVC230	6.5	0.2	C	0.46	109.3
11	Northridge	1994 Jensen Filter Plant #	JEN022	6.7	0.1	C	0.42	105.9
12	Northridge	1994 Newhall - Fire Sta #	NWH360	6.7	4	C	0.59	96.9
13	Loma Prieta	1989 LGPC (Los Gatos)	LGPC000	6.9	0.1	B	0.56	94.6
14	Imperial Valley	1979 El Centro Array #5	JMR230	6.5	1	C	0.38	90.5
15	Imperial Valley	1979 EC Meloland Overpass FF	EMO270	6.5	0.5	D	0.30	90.5
16	Cape Mendocino	1992 Petrolia #	PET090	7.0	0.1	C	0.66	89.6
17	Kobe	1995 Takarazuka	TKZU090	6.9	3.2	D	0.69	85.2
18	Northridge	1994 Sepulveda VA #	SPV270	6.7	0.4	C	0.75	84.4
19	Erzican, Turkey	1992 Erzincan	ERZINS	6.9	0.1	B	0.51	83.9
20	Kobe	1995 KJMA	KJM000	6.9	1	B	0.82	81.3
21	San Salvador	1986 Geotech Investig Center	CIG90	5.8	1.6	C	0.69	80.6
22	Imperial Valley	1979 El Centro Array #4	ANDROA23	6.5	4.4	C	0.36	77.5
23	Parkfield	1966 Cholame #2	CHOL652	6.1	0.1	C	0.49	75.8
24	N. Palm Springs	1986 North Palm Springs	NPS210	6.0	0.1	B	0.59	73.2
25	San Salvador	1986 National Geografical Inst	IGN270	5.8	1.3	C	0.53	73.2
26	Gazli, USSR	1976 Karakyr	GAZ090	6.8	4	D	0.72	71.6
27	Imperial Valley	1979 El Centro Differential Array	HEDA270	6.5	5.2	C	0.35	71.2
28	Irpinia, Italy	1980 Sturno	STURWE	6.9	6.7	B	0.31	70.0
29	Northridge	1994 Beverly Hills - 14145 Mulhol	13SCN81W	6.7	8.4	B	0.49	69.2
30	Northridge	1994 Canoga Park - Topanga Can	53SCS16W	6.7	1.6	C	0.39	64.3

31	Northridge	1994 LA Dam	LDM064	6.7	2.6	B	0.51	63.7
32	Loma Prieta	1989 Hollister - South & Pine	HOLL0	6.9	33	C	0.37	63.0
33	Loma Prieta	1989 Saratoga - W Valley Coll.	WVC270	6.9	12	B	0.33	61.5
34	Northridge	1994 Northridge - 17645 Saticoy St	03SCS00E	6.7	0.2	C	0.45	60.7
35	Northridge	1994 Newhall - W. Pico Canyon Rd.	56SCN44W	6.7	7.1	C	0.35	59.2
36	Loma Prieta	1989 Corralitos	CORRAL0	6.9	1	B	0.63	55.1
37	Kobe	1995 Kobe University	KBU000	6.9	2	A	0.29	54.8
38	Imperial Valley	1979 El Centro Array #8	CRU140	6.5	3.5	C	0.60	54.3
39	Loma Prieta	1989 APEEL 2 - Redwood City	A02043	6.9	47.4	D	0.27	53.6
40	Northridge	1994 Simi Valley - Katherine Rd	55SCN00E	6.7	1.5	B	0.73	52.3
41	Northridge	1994 Castaic - Old Ridge Route #	CASTA360	6.7	20.8	B	0.51	52.1
42	Montenegro (YU)	1979 Bar-Skupstina Opstine	BARSKUEW	6.9	12	D	0.36	52.0
43	Northridge	1994 PacoimaKagelCanyon#	PKAG360	6.7	8.1	B	0.43	50.8
44	Imperial Valley	1979 BondsCorner	BCR230	6.5	2.8	C	0.78	45.9
45	Nahanni, Canada	1985 Site1	1ST010	6.8	0.1	A	0.98	45.9
46	Loma Prieta	1989 HollisterCityHall	HCH180	6.9	27.8	C	0.21	45.0
47	Northridge	1994 CanyonCountry-WLostCan	LOS270	6.7	11.4	C	0.48	44.9
48	Imperial Valley	1979 HoltvillePostOffice	HOLTN225	6.5	7.5	C	0.25	44.0
49	Cape Mendocino	1992 RioDellOverpass-FF#	RIO270	7.0	12.3	B	0.39	43.8
50	Northridge	1994 LA-SaturnSt	91SCS70E	6.7	22.3	C	0.43	43.4
51	Superstitn Hills(B)	1987 SuperstitionMtn.	SUP135	6.7	4.3	B	0.89	42.2
52	Loma Prieta	1989 Saratoga–AlohaAve	SARATO0	6.9	11.7	B	0.50	41.5
53	Dinar	1995 Dinar	DIN090	6.2	0.6	D	0.35	40.2
54	Loma Prieta	1989 GilroyArray#4	YSIDRO0	6.9	15.8	C	0.42	39.4
55	Montenegro (YU)	1979 Petrovac-HotelOliva	PETROVNS	6.9	12	C	0.45	38.9
56	Montenegro (YU)	1979 Ulcinj-HotelOlimpic	ULCHOLNS	6.9	9	C	0.29	38.6
57	Imperial Valley	1940 ElCentroArray#9	40ELC180	7.0	6.4	C	0.35	38.1
58	Irpinia, Italy	1980 BagnoliIrpino	BAGNIRWE	6.9	8	A	0.17	37.7
59	Loma Prieta	1989 Capitola	CAPIT0	6.9	8.6	C	0.47	36.4
60	Loma Prieta	1989 GilroyArray#1	GAVTOW90	6.9	10.5	A	0.44	33.9
61	Loma Prieta	1989 GilroyArray#2	MISTRA0	6.9	12.1	C	0.35	33.6
62	N. Palm Sptrings	1986 DesertHotSprings	DSP000	6.0	8.8	C	0.30	33.5
63	Nahanni, Canada	1985 Site2	2ST330	6.8	0.2	A	0.32	33.1
64	Kalamata (Greece)	1986 Kalamata-Prefecture	KALAPREW	5.9	5	B	0.30	32.2
65	Friuli, Italy	1976 Tolmezzo	TOLMEZWE	6.5	16	B	0.35	32.1

66	Irpinia, Italy	1980 Calitri	CALITWE	6.9	20.5	B	0.18	31.7
67	Northridge	1994 LA–ObregonPark#	OBRE360	6.7	35.9	B	0.41	30.9
68	Imperial Valley	1979 Chihuahua	CHH282	6.5	17.6	C	0.25	30.1
69	Umbria-Marche	1997 NoceraUmbra	R1168EW	6.0	4.7	A	0.49	28.0
70	Umbria-Marche	1997 Colfiorito	R1139EW	5.7	2.5	D	0.44	24.6
71	Azores, Portugal	1998 Observ Prínc Alb Món, HOR NS	AZXX	6.0	14.9	D	0.40	29.4
72	Azores, Portugal	1998 Observ Prínc Alb Món, HOR WE	AZYY	6.0	14.9	D	0.40	29.4
73	L'Aquila, Italy	2009 V Aterno–Colle Grilli, FA030 NS	AQGNS	5.8	4.3	B	0.49	35.7
74	L'Aquila, Italy	2009 V Aterno–Colle Grilli, FA030 WE	AQGWE	5.8	4.3	B	0.49	35.7

A.2. RESPONSE SPECTRA
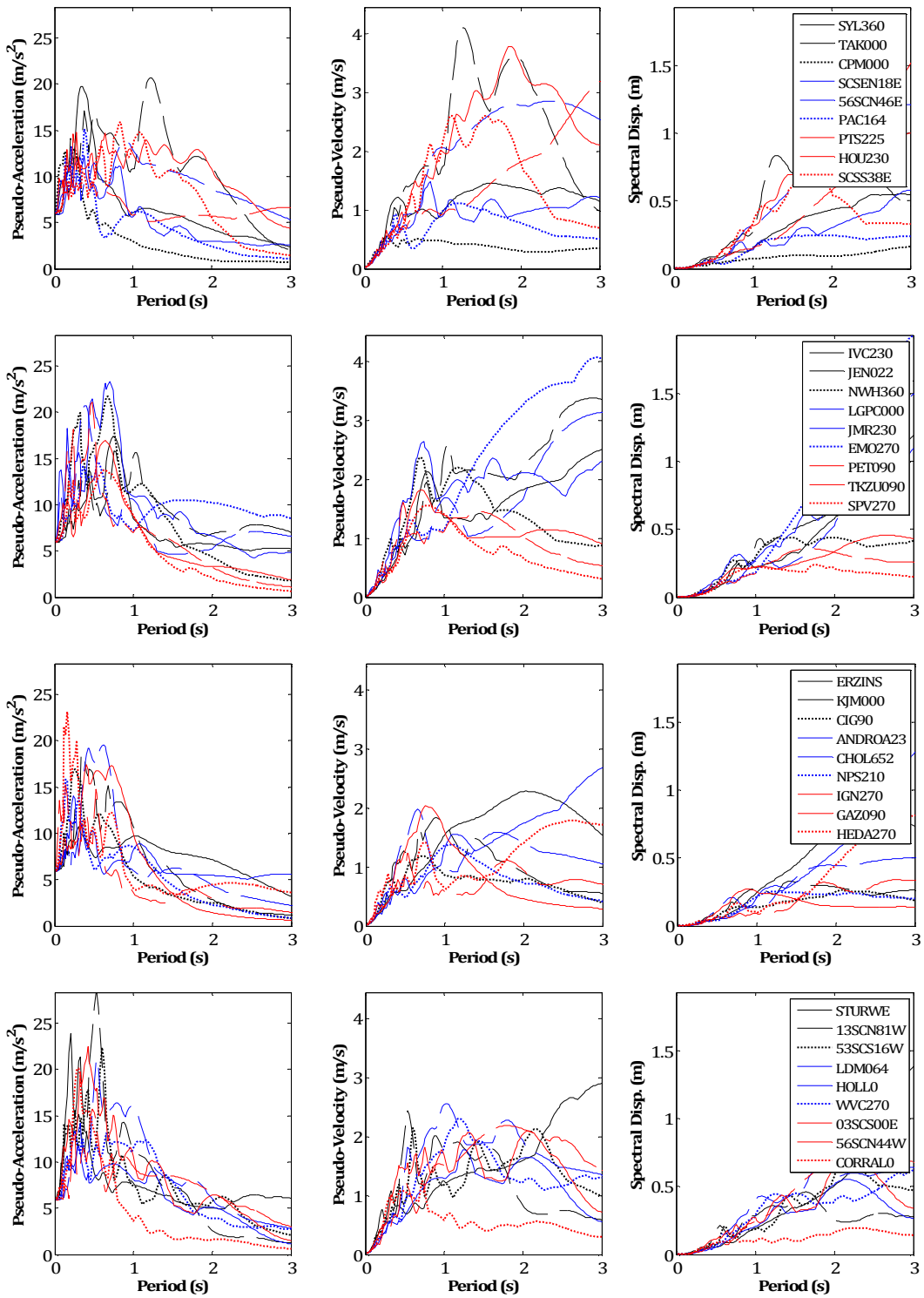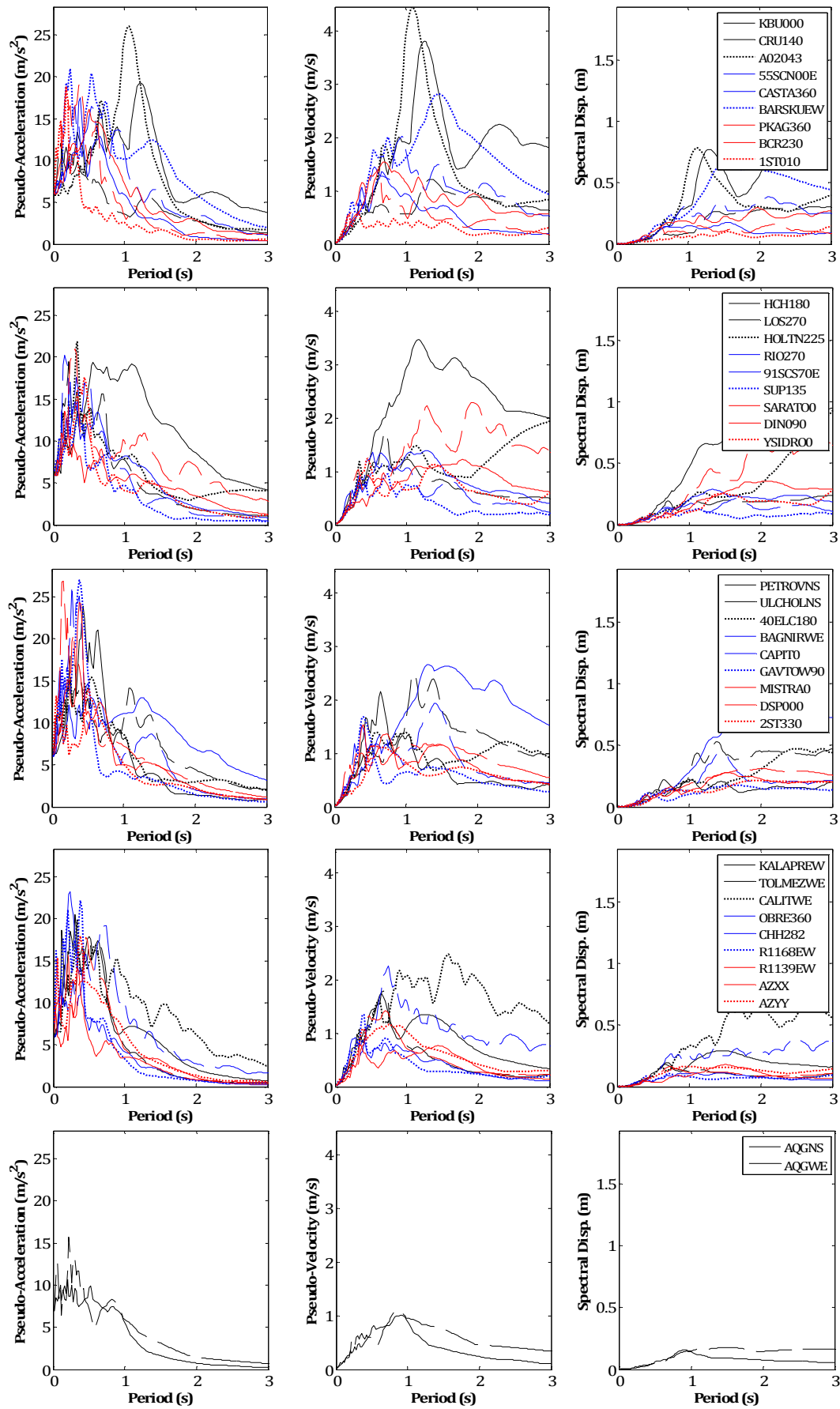
A.3. NONLINEAR TIME HISTORY ANALYSES RESULTS

A.3.1. *Overturning mechanism: gable (MEC0)*
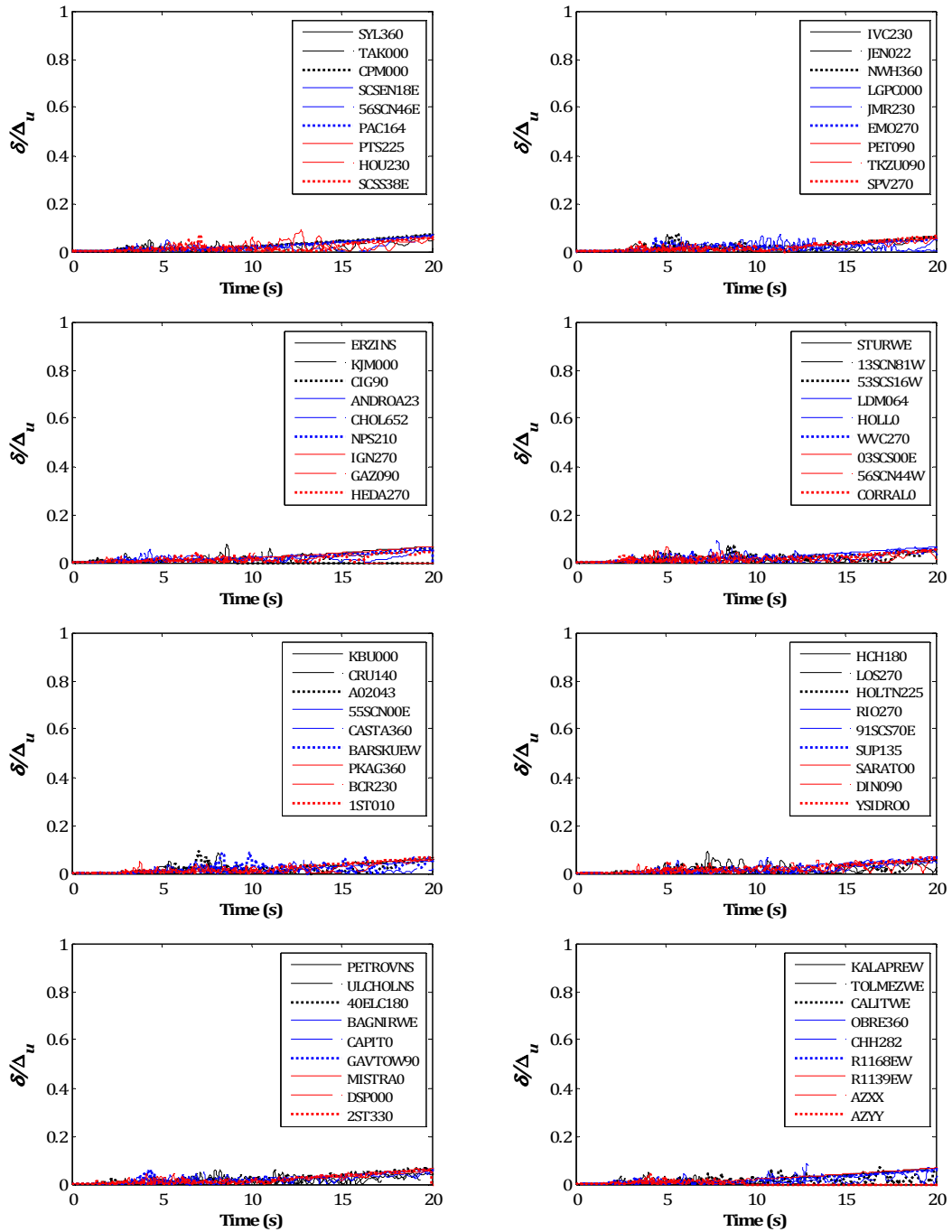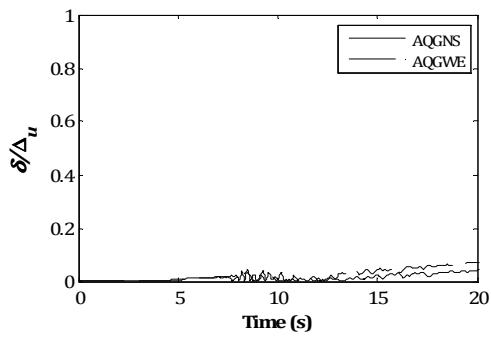
A.3.2. Overturning mechanism: façade (MEC1)
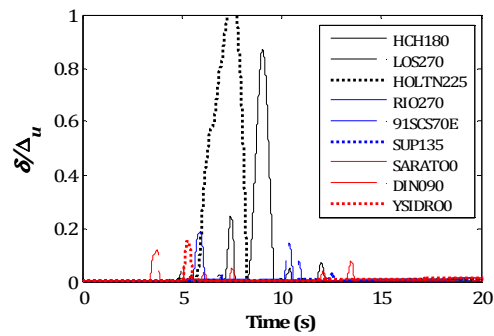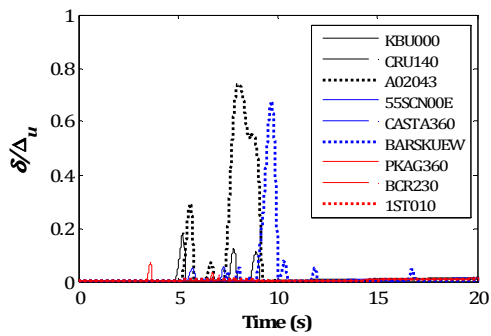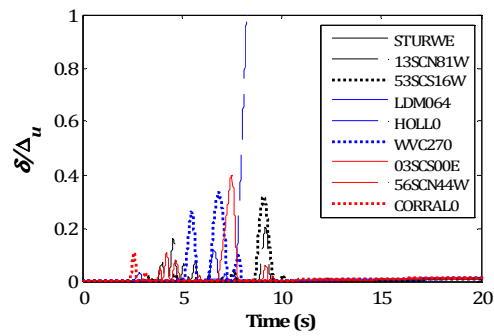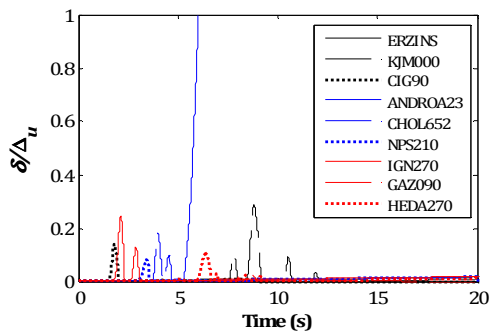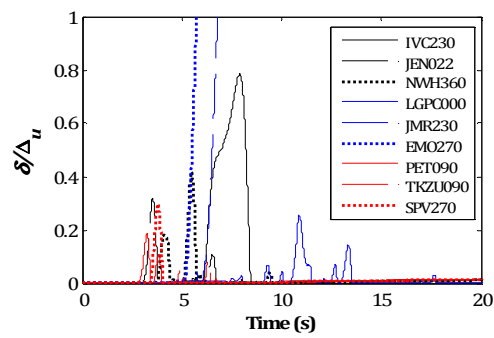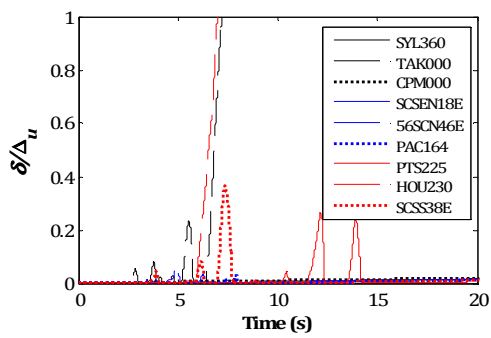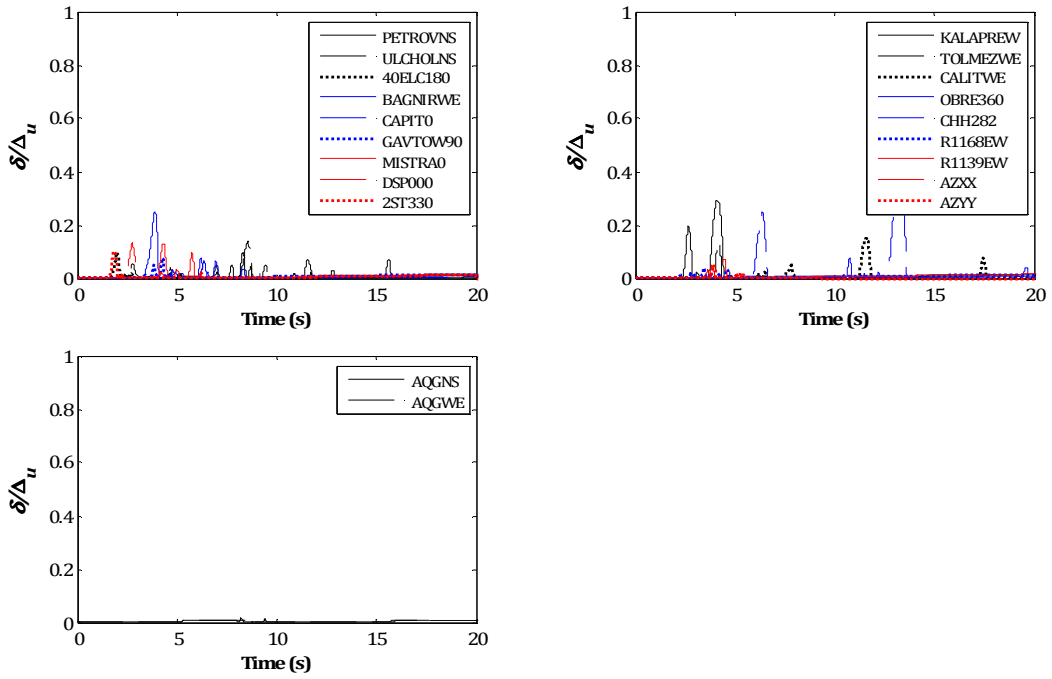
A.3.3. Overturning mechanism: façade with returning walls (MEC2)
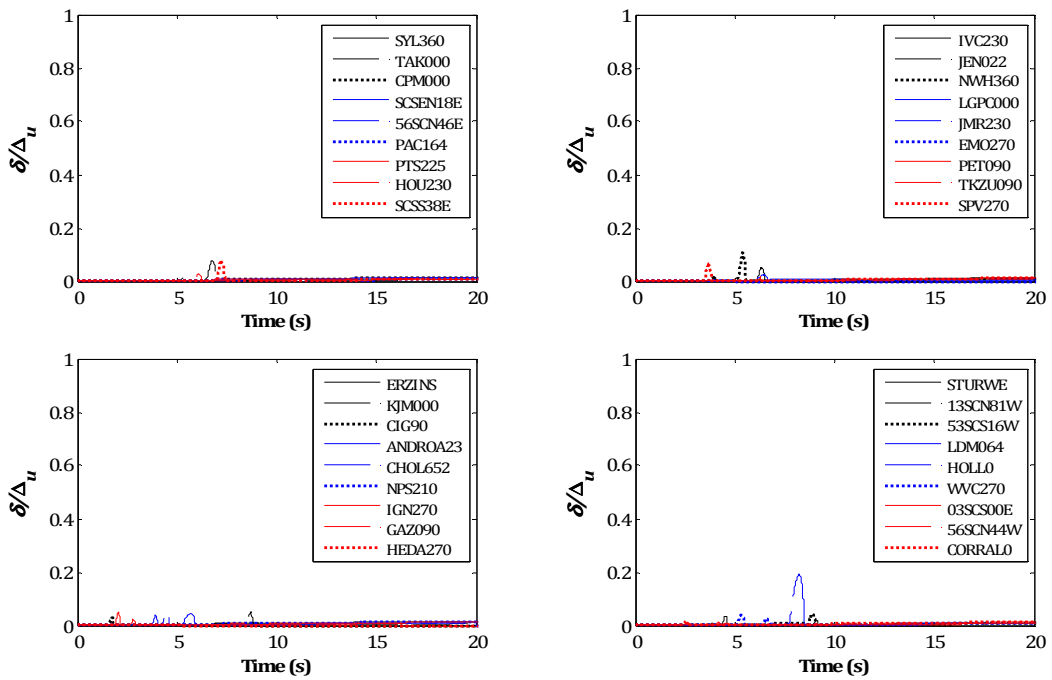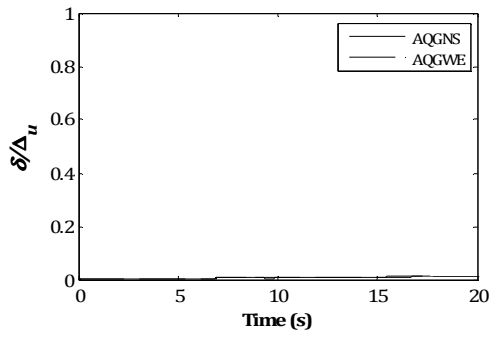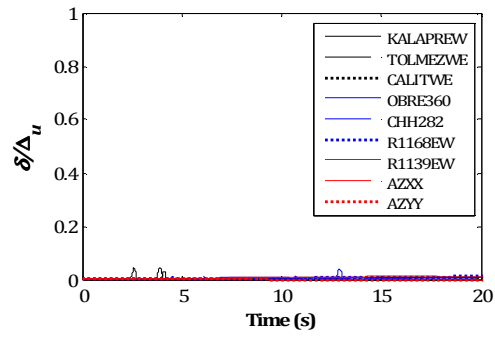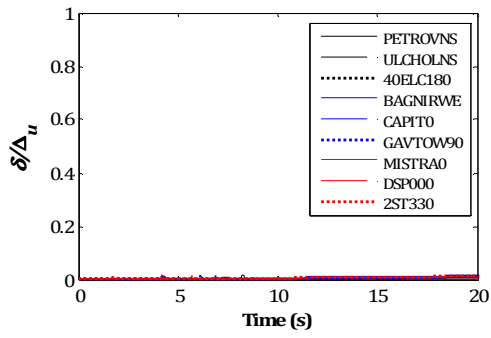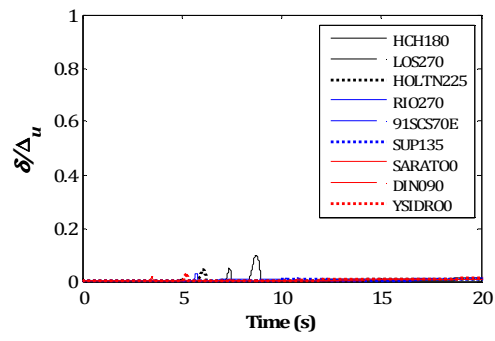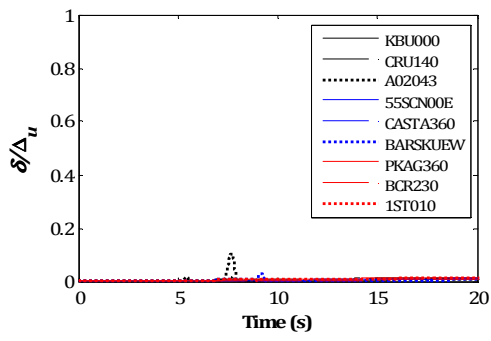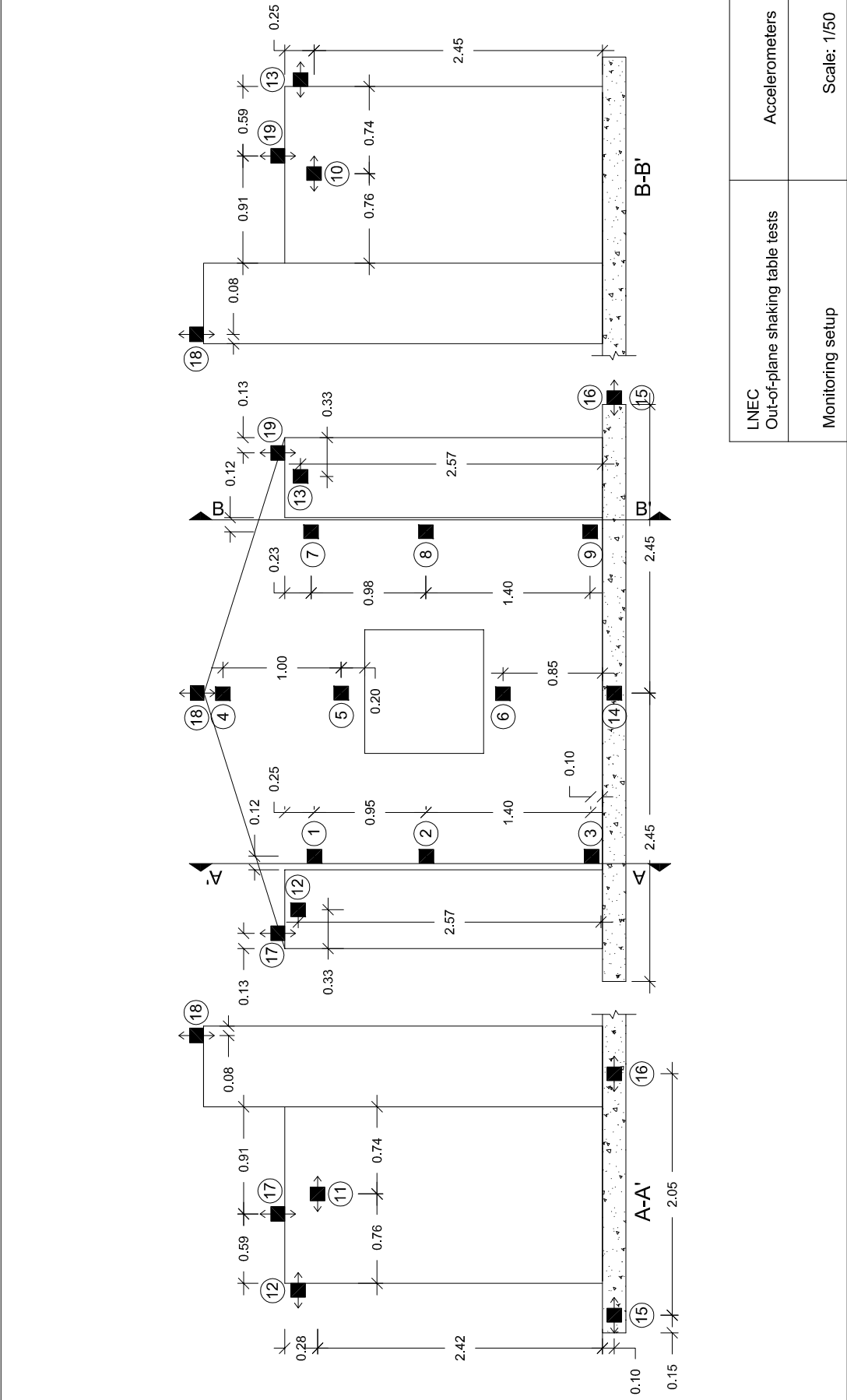
A-A'

B-B'

B-B'

A-A'

LNEC
Out-of-plane shaking table tests

Monitoring setup

LVDTs and draw wire
position transducers

Scale: 1/50

Appendix B.

FREE ROCKING TESTS RESULTS

The procedure to compute the rotations experienced by the masonry wallettes is herein presented, as well as the experimental results obtained in the free rocking tests and not presented in Chapter 5 of the main document, in order to help on supporting the findings.

B.1. COMPUTATION OF EXPERIMENTAL ROTATIONS

The complete procedure to compute the angular terms of the masonry wallette rocking at a masonry joint level should be done, for each time step *i*, as follows:

i)   Calculate $R_{1,i}$ and $R_{2,i}$ from the transducers readings and compute th*e* coordinates of P_i by intersecting the two circles in the same vertical plane, using Eq. (1) and selecting the correct solution (there are two intersecting points between the two circles), to obtain the new measured point position relative to the initial one P_0 (x_0, y_0). In order to simplify the calculation, the rotations can be in the same vertical plane coincident with the vertical axis, leading to $a_1 = a_2 = 0$.

$$P_i\left(x_i, y_i\right) = \begin{cases} \left(x_i - a_1\right)^2 + \left(y_i - b_1\right)^2 = R_{1,i}^{\;2} \\ \left(x_i - a_2\right)^2 + \left(y_i - b_2\right)^2 = R_{2,i}^{\;2} \end{cases} \tag{1}$$

$$y_i = \frac{R_{2,i}^{\;2} - R_{1,i}^{\;2} + b_1^{\;2} - b_2^{\;2}}{2 \cdot b_1 - 2 \cdot b_2} \quad \text{and} \quad x_i = \pm\sqrt{R_{1,i}^{\;2} - \left(y_i - b_1\right)^2} \tag{2}$$

ii)   Determine the displacement components (dx_i, dy_i) and magnitude (δ_i) since time t_0.

$$dx_i = x_i - x_0 \;;\; dy_i = y_i - y_0 \quad \text{and} \quad \delta_i = \sqrt{\left(x_i - x_0\right)^2 + \left(y_i - y_0\right)^2} \tag{3}$$

iii)   Calculate the rotation from the dy_i values of both North and South face monitoring points (respectively, $dy_i[N]$ and $dy_i[S]$) using Eq. (4), which can be linearized for small rotation angles,

$$\theta_i = \tan^{-1}\left(\frac{dy_i[S] - dy_i[N]}{l_{mon}}\right) \qquad (4)$$

where l_{mon} is the distance between the monitoring points (North and South), equal to the thickness of the wall in the present case. The positive signal is given for rotations in the South-North sense. Angular velocity time histories $\dot{\theta}(t)$ are obtained by differentiating the rotation time history signal.

B.2. TIME HISTORIES OF MEASURED ROTATIONS

Table B.1. Experimental rotation time histories for different initial rotation obtained for both specimens
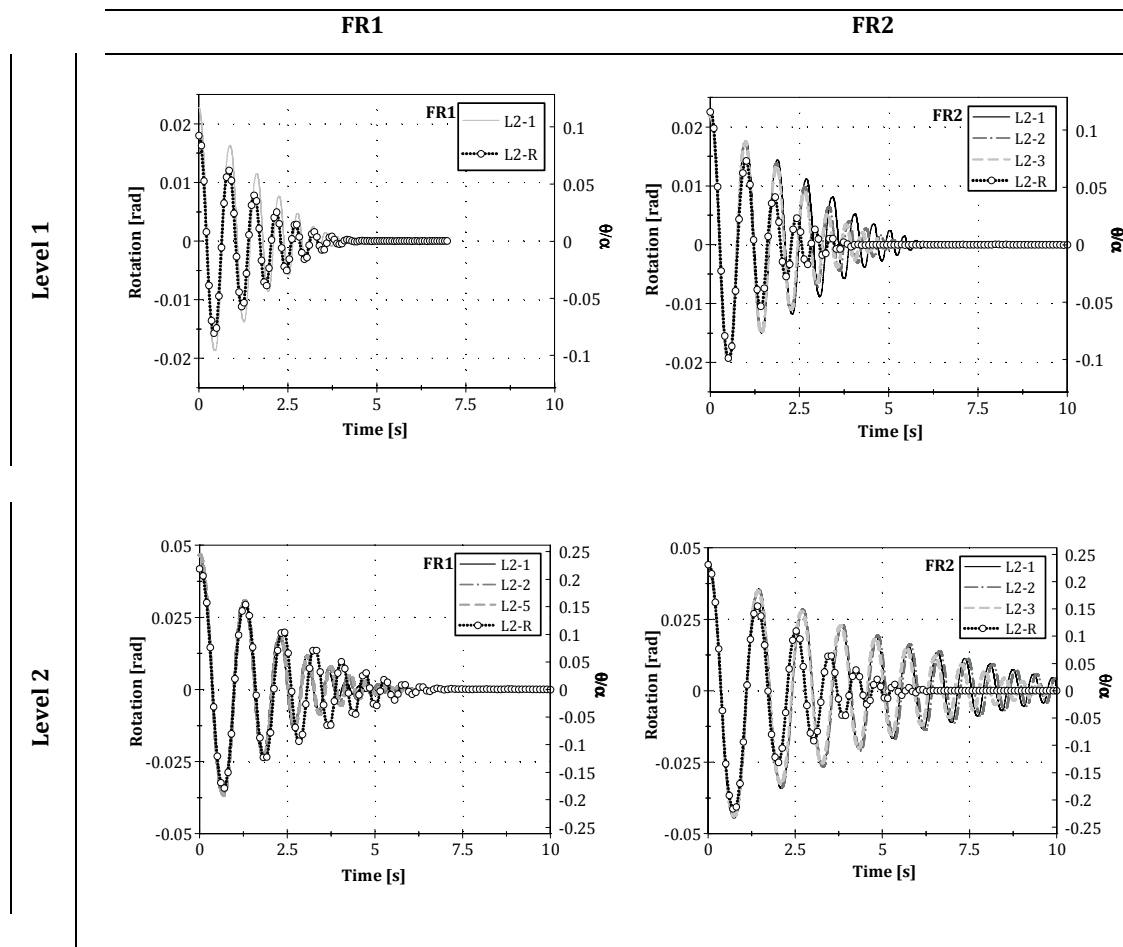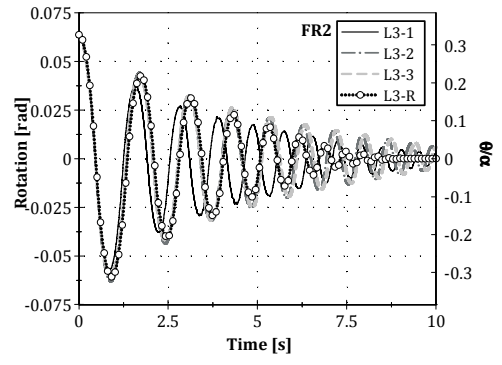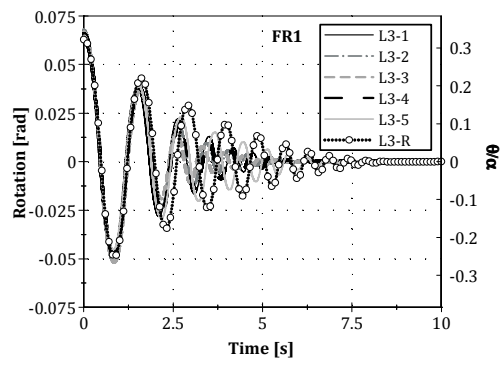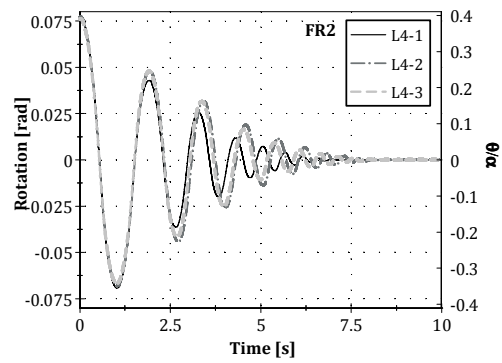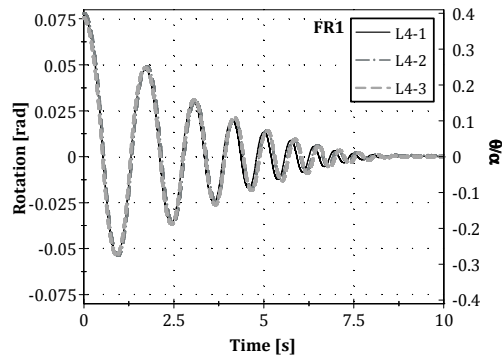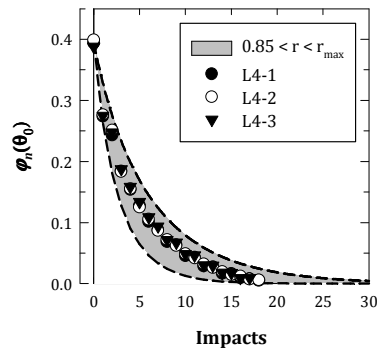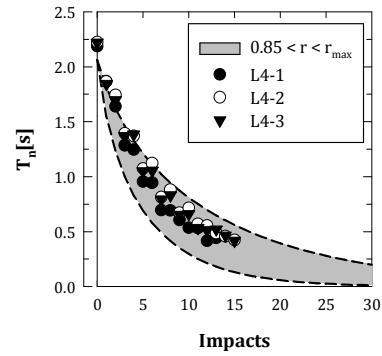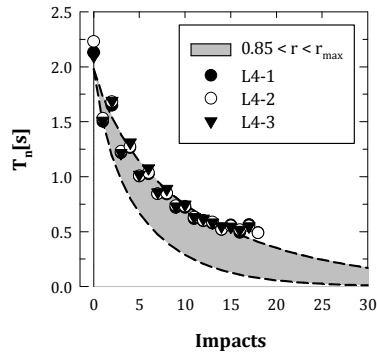
B.3. EXPERIMENTAL VS. THEORETICAL CURVES

Table B.2. Experimental vs theoretical curves, for different initial rotations and for both specimens
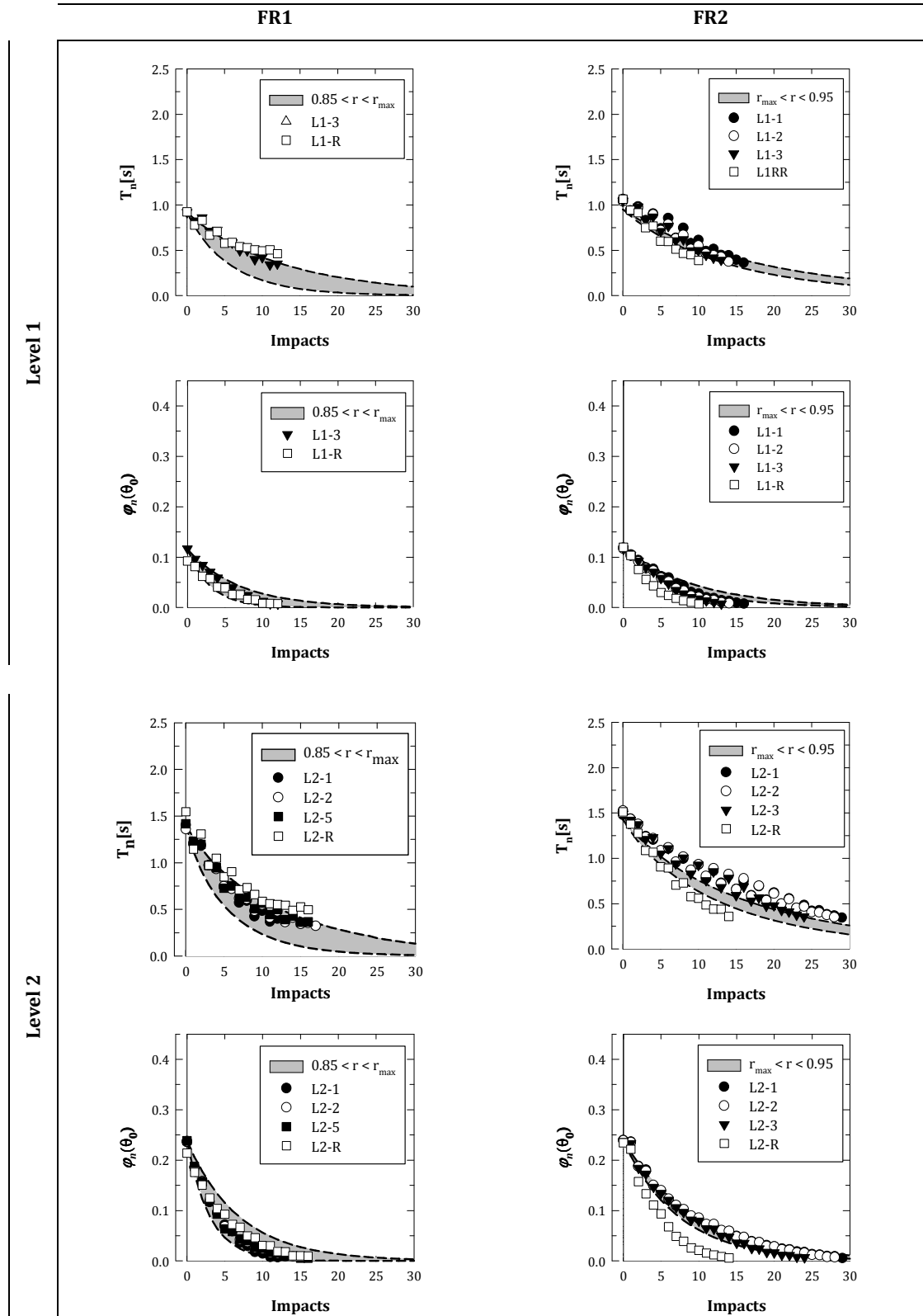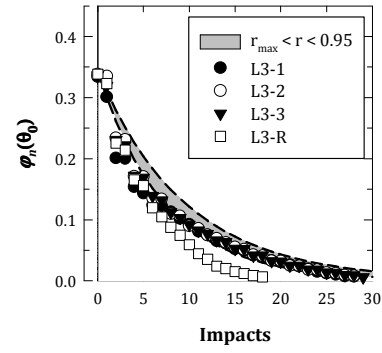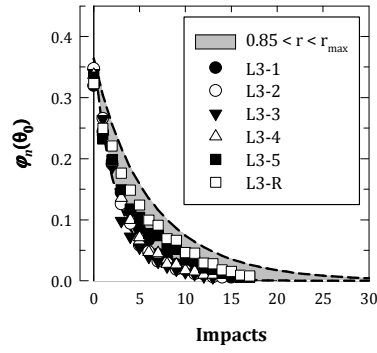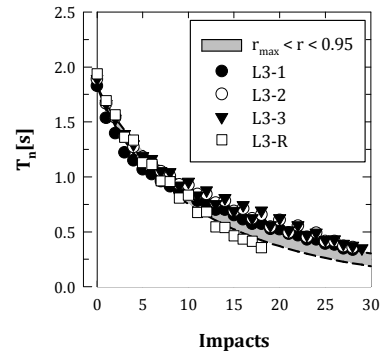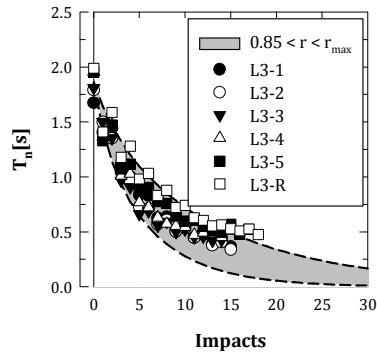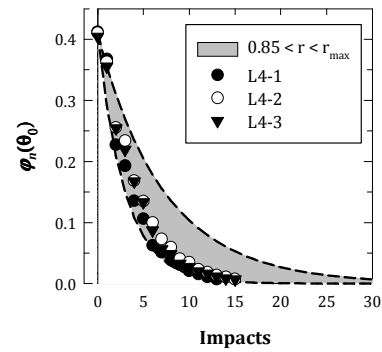
Appendix C.

NUMERICAL SIMULATIONS

In this appendix section, more details regarding MSC Adams™ software (MSC 2012a) are presented, aiming at helping on understanding results interpretation and numerical issues. Moreover, the evaluation of MSC Adams capabilities to reproduce the desired behaviour is presented, comparing the Adams' results with theoretical exact solution. At the end, a sensitivity study is presented, which aimed at understanding the governing parameters in the final behaviour of the LNEC shaking table model.

C.1. BRIEF DESCRIPTION OF ADAMS

MSC Adams software involves various distinct subjects, where several different analysis moduli are available for the numerical simulation of mechanical systems. For the purposes of this Thesis, three main moduli were used, namely: Adams/View, Adams/Solver, Adams/PostProcessor.

The first modulus is used for the numerical model definition resorting to a friendly graphical user interface (GUI). Once the model is defined, including the type of analysis and restraining conditions, Adams/View launches Adams/Solver in order to obtain the desired solution (nonlinear time history analysis, in the present case). It allows real-time observation of the deformed shape, position and magnitude of forces, measurable quantities (displacements, velocities, accelerations, kinetic energy, etc.) at predefined monitoring points, among other issues.

At the end, the evolution of the deformed shape as well as measured quantities is possible to be observed in Adams/View. However, for output purposes, Adams/PostProcessor permits plotting and exporting several information, such as measured quantities or even deformed shapes. It also delivers high quality videos of the dynamic analyses performed in a friendly GUI.

Regarding the dynamic simulation, the nonlinear behaviour of the modelled structure is concentrated at the contact regions. These contacts, detected by a geometry engine which locates the points of contact and applies the contact forces at the intersecting bodies, are modelled as a unilateral constraint.

Two major types of contacts are considered: *i*) intermittent contact; *ii*) persistent contact.

The intermittent contact, the most adequate for the analysis performed in the current numerical analyses, is characterized by two distinct phases. The first phase is compression, where the bodies continue to approach each other even after contact occurs. The kinetic energy of the bodies is converted to potential and dissipation energy of the compressing contact material. When the entire kinetic energy is transformed, the potential energy stored in the material reverses the motion of the contacting bodies. Potential energy is transformed again to dissipation and kinetic energy. This is known as the decompression phase. It is important to note that energy losses due to dissipation occur in both phases and may be represented in the value of the restitution coefficient.

On the other hand, the persistent contact is characterized by contact for relatively long periods of time. External forces acting between the two bodies serve to maintain continuous contact. Two bodies are said to be in persistent contact when the separation velocity, after a collision event, is close to zero. The bodies, therefore, cannot separate after the contact.

The unilateral constraint associated with a given contact is a force that is null when no penetration exists between the specified geometries, and a force with a positive value when penetration exists between two geometries and supporting multiple contacts (MSC 2012b).

The contact conditions and constraints can be summarized as follows (MSC 2012b):

i) **Impenetrability constraint**: $g \geq 0$, where g is a gap function, where positive values indicates penetration;

ii) **Separating, normal force constraint**: $F_n \geq 0$, normal contact force magnitude, where a positive value indicates a separation force between two bodies;

iii) **Normal force non-zero, when contact occurs***: $F_n\, g$ = 0;

iv) **Persistency condition**: $F_n \cdot \dfrac{dg}{dt} = 0$, specifies that the normal force is nonzero only when the rate of separation between the bodies is zero.

This last condition (persistency), in addition to the definition of intermittent or persistent contact, was found to be important for the correct definition of the rocking behaviour of masonry portions, as presented in section C.2.

For the performed analyses, the normal force calculation is made through the restitution coefficient of the *Poisson* model, resulting from a penalty regularization of the normal contact constraints and computed according to Eq. (C.1), where p is a penalty parameter (the penalization is exact for $p \to \infty$) and ε is a restitution coefficient (energy based).

$$F_n = p(\varepsilon - 1)\left(\frac{dg}{dt}\right) \tag{C.1}$$

More information is available in MSC (2012b) but it is worth mentioning here that this coefficient can be correlated to the coefficient of restitution (r) firstly presented by Housner (1963), already discussed in Chapter 5. If the restitution coefficient is defined as the ratio of total energy before and after the impacts, it is possible to simulate the behaviour of a rigid body moving in the three-dimensional space where impacts can occur.

Regarding the contact prediction, it must be taken into account that a contact is fundamentally a discontinuous event occurring when two geometries come into contact, for which: *i*) a large normal force or an impulse is generated; *ii*) the bodies' velocities change sign; *iii*) the accelerations are almost discontinuous and show a large spike. This spike represents the impulse that was generated due to the contact. The bodies usually separate because of the contact forces or impulses. ADAMS/Solver contains a contact predictor that predicts the onset of contact and controls the integrator step size accordingly.

When ADAMS/Solver detects a new contact, it calculates the penetration effects and depth. Furthermore, the integrator order is set to one, so that ADAMS/Solver does not use the time history of the system to predict the future behaviour of the system. The algorithm essentially ensures that: *i*) the penetration for a new contact is small; *ii*) the integrator is at first order when the contact event occurs; *iii*) the integrator is taking small time steps.

C.2. EVALUATION AND VALIDATION OF THE ROCKING RESPONSE

C.2.1. Free rocking

The free rocking behaviour of a single element was evaluated with ADAMS software against the exact solution (Eq. (5.27), of Chapter 5), for which two common situations were considered: *i*) 1-sided rocking, simulating impacts on vertical interfaces (e.g., façade with returning walls); *ii*) 2-sided rocking, simulating impacts at the horizontal surfaces (e.g., church frontispiece, free standing walls). For these analyses, a theoretical block with dimensions b x t x h equal to 1.0 x 0.6 x 3.0 m³ was considered (leading to $\alpha_0 = 0.197$ rad, where $\alpha_0 = \tan^{-1}(t/h)$), with a restitution

coefficient (r) of 0.6 and an initial rotation $\theta_0/\alpha_0 = 0.9$. The obtained results are shown in Figure C.1.
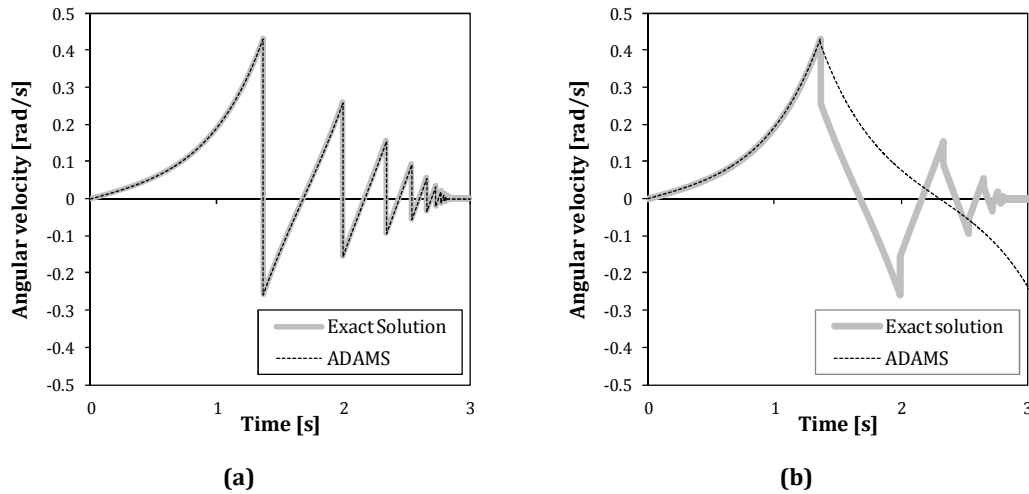

Figure C.1. Comparison between theoretical and numerical response of a rocking block (b = 0.60 m, h = 3.0 m, r = 0.6) for θ_0/α_0 = 0.9: a) 1-sided rocking; b) 2-sided rocking.

As it is possible to observe in Figure C.1, vertical interface impacts are correctly simulated with ADAMS because the separation of the two colliding bodies occurs, which yields energy dissipation at the impact by the numerical solver. On the other hand, the 2-sided rocking behaviour of a block is correctly simulated until the first impact at the base (point of maximum angular velocity). Since no separation of the two colliding bodies is detected after the impact (persistency condition) because the block is still rotating around the edge, the numerical solver assumes the contact as a permanent one where no dissipation occurs, contrarily to an intermittent contact where energy is dissipated at impacts according to the defined restitution coefficient.

Despite the limitation of the numerical solver to detect and correctly simulate 2-sided rocking, the major source of energy dissipation in the performed experimental tests reported in this thesis occurs by one-sided rocking (vertical interface impacts against the returning walls), which is well reproduced by the ADAMS solver. For this reason, the numerical simulations were performed with ADAMS software, making use of 3D dynamic modelling and contacts for multi-body systems.

C.2.2. Influence of penalty parameter and time step

An important parameter for the contact definition, using the *Poisson* model available in MSC Adams, is the penalty parameter, used for normal contact force computation. For this reason, a sensitivity analysis of this parameter was made, whose results are presented in Figure C.2 a), while Figure C.2 b) shows the influence of the time step definition.
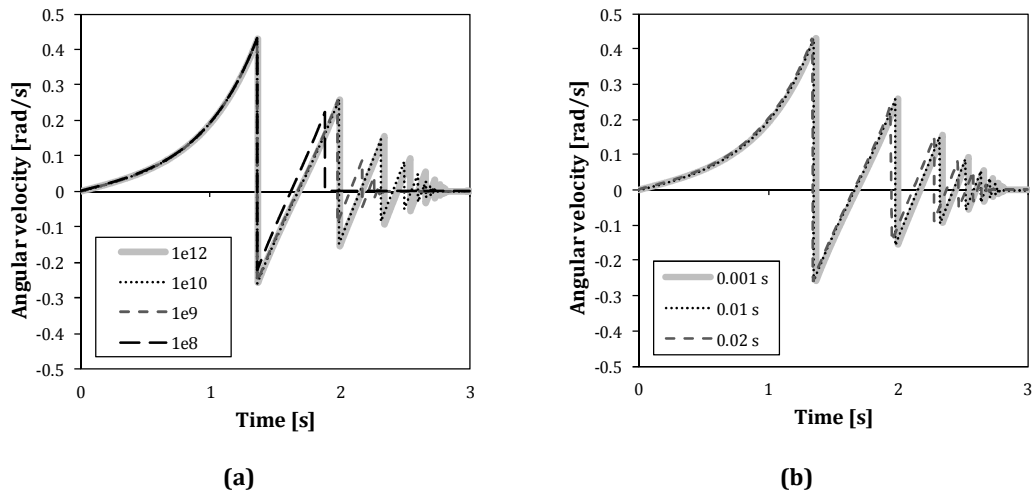
Figure C.2. Influence of numerical parameters in the final solution (θ_0/α_0 = 0.9, r = 0.6): a) penalty parameter (for time step = 0.001 s); b) time step (for penalty = 1x10^{12}).

As shown in these figures, for increasing penalty (p) values, the approximation to the exact solution (coincident with the "1e12" curve) is evident. However, concerning only the first impact, penalty values of 10^8 provide satisfactory simulations of the dynamic response.

As expected, the importance of the time step definition in the main program (Adams/View and Adams/Solver) for the numerical analyses does not influence the response. Since the GSTIFF is a variable order, multi-step integrator, the step is internally adjusted by the integrator leading to the best response with minor errors.

C.3. LNEC NUMERICAL MODEL: SENSITIVITY ANALYSES

The influence of the restitution and friction coefficients in the final results was analyzed by performing a sensitivity analysis, considering the three different mechanisms used: "As is" model; simplified mechanism 1 (SM1); simplified mechanism 2 (SM2). For this analysis, the restitution coefficient values (r) for vertical interface impacts were contained within the interval [0.0; 0.3] with increments of 0.1, while the static and dynamic coefficient of friction (μ) were the same, ranging in the interval [0.2; 1.0] with 0.1 as increments. The restitution coefficient for horizontal interface impacts (rocking) were kept at 0.533 (i.e., the theoretical maximum value for the gable) but, as mentioned previously, the model is not able to simulate this type of behaviour and therefore its influence in the final results should not be significant. The major source of energy dissipation during the experimental tests was due to vertical interface impacts at the returning walls.

The experimental results are also presented in the dashed red line in order to observe the correlation or discrepancy between the numerical and experimental data. All the results correspond to a penalty value of 10^8 and the response curves for the different r values are plotted in the same graph, considering each friction coefficient level.
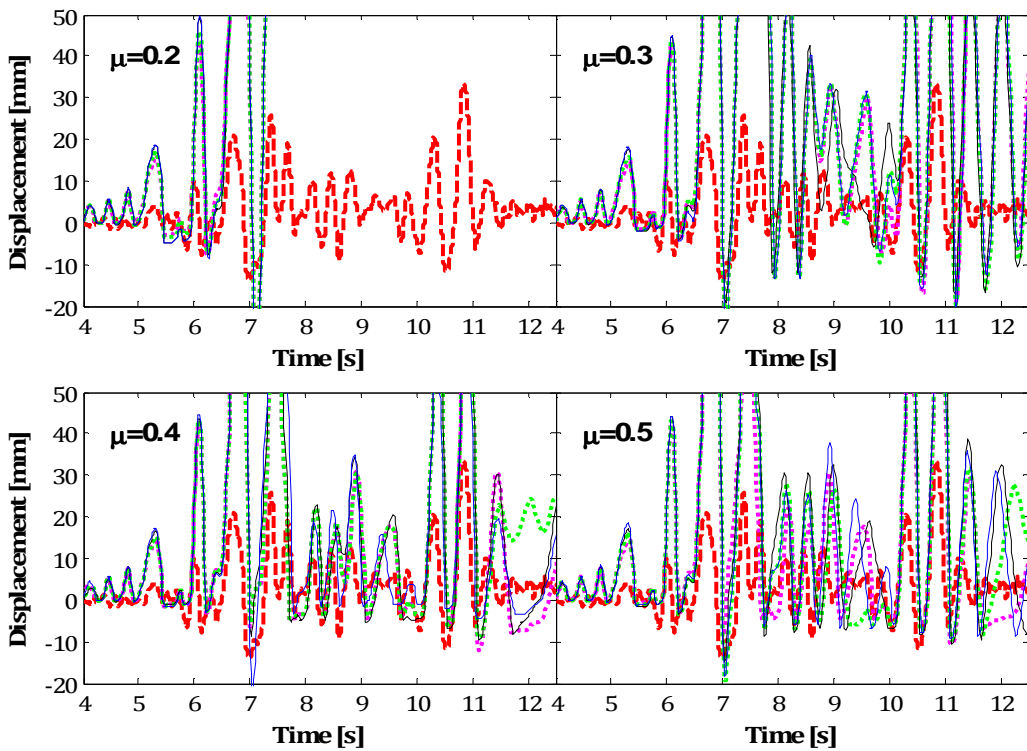
Finally, it should be referred that it was noticed some influence of the penalty parameter value in the final results, in the same line as the observed in Figure C.2.
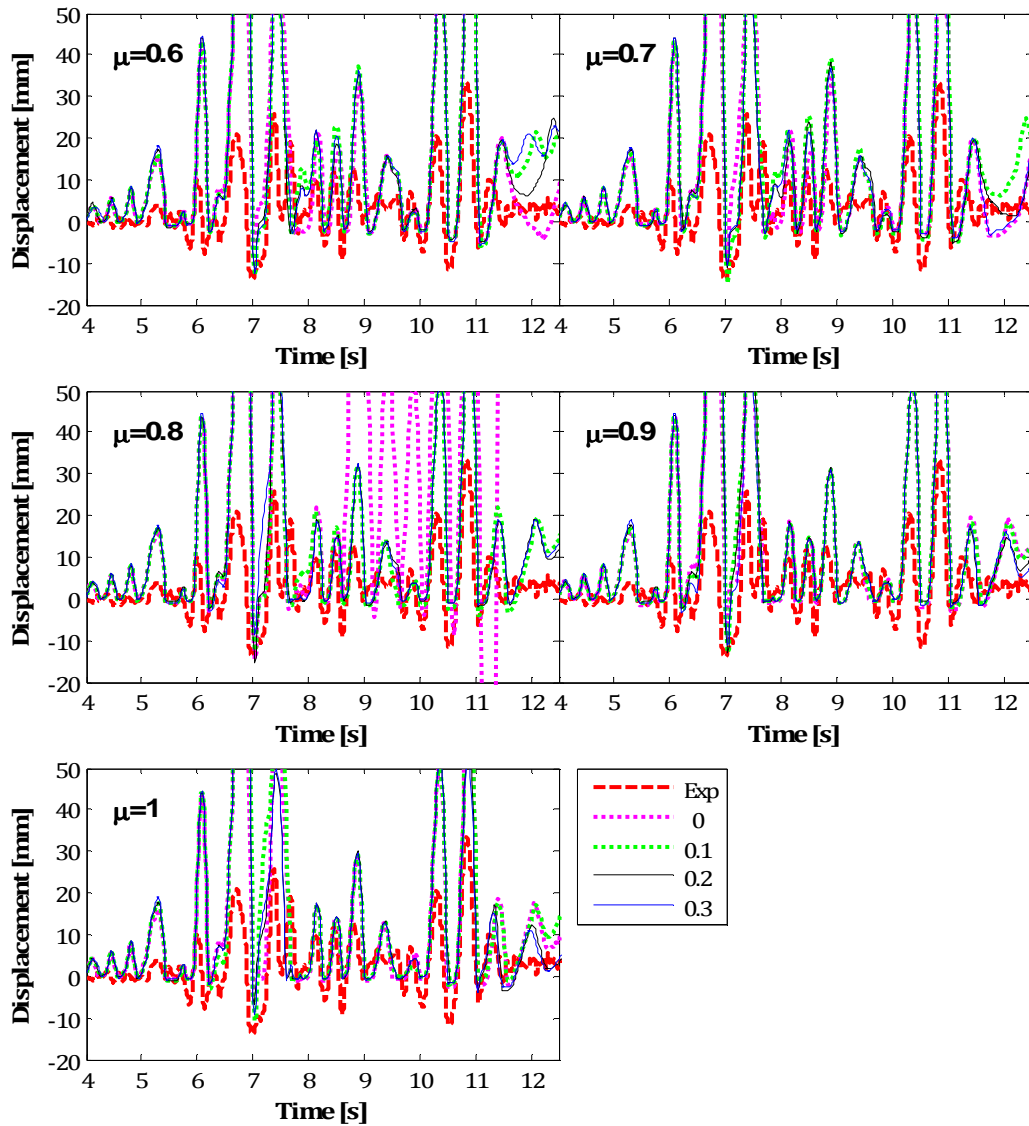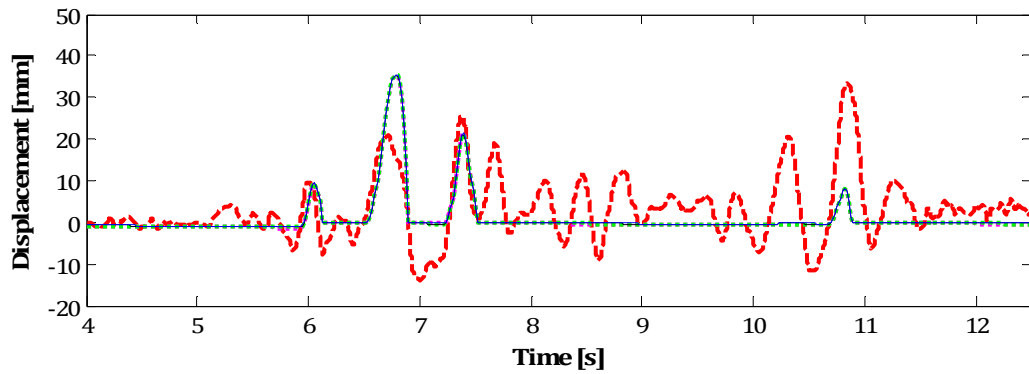
C.3.1. As Is model (AIm)
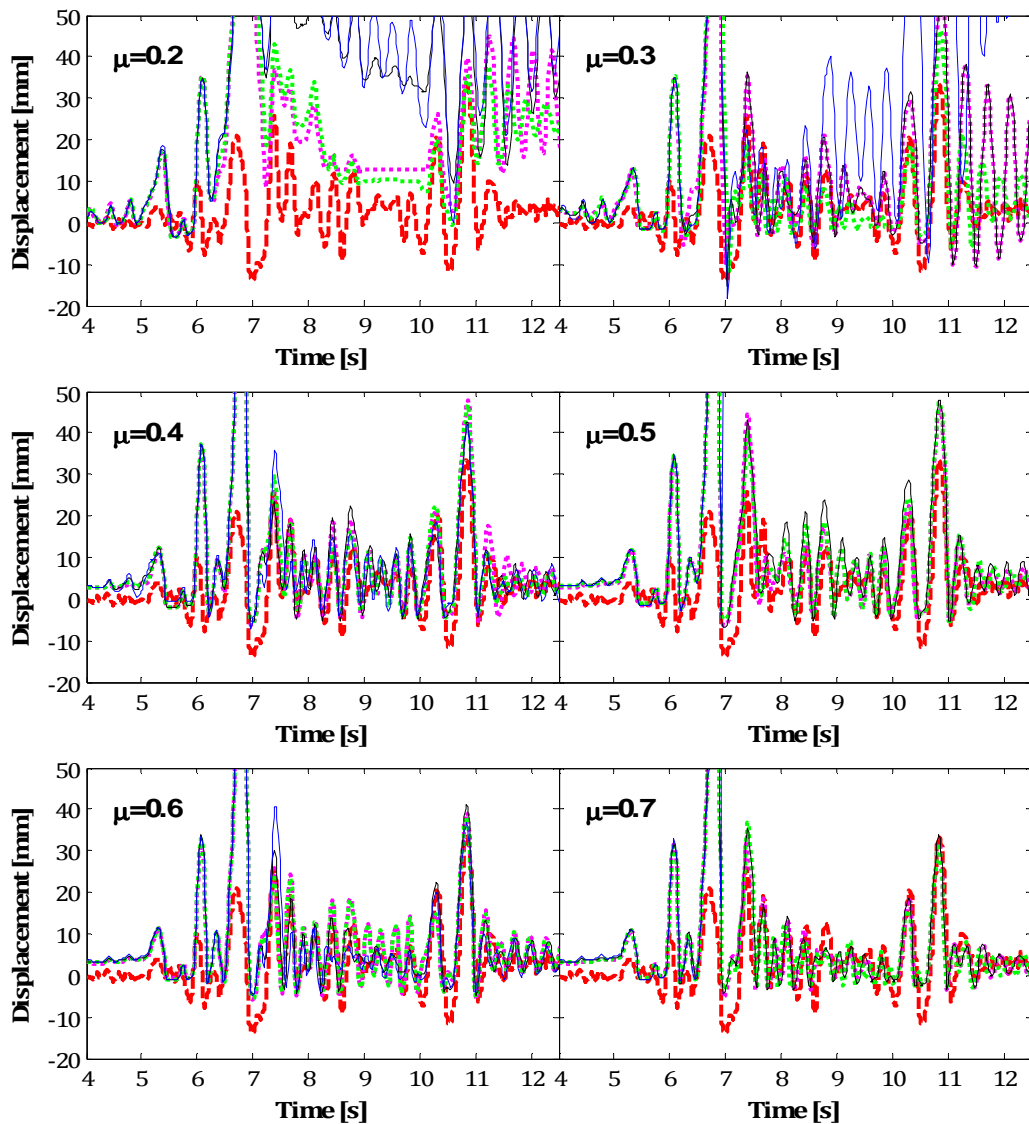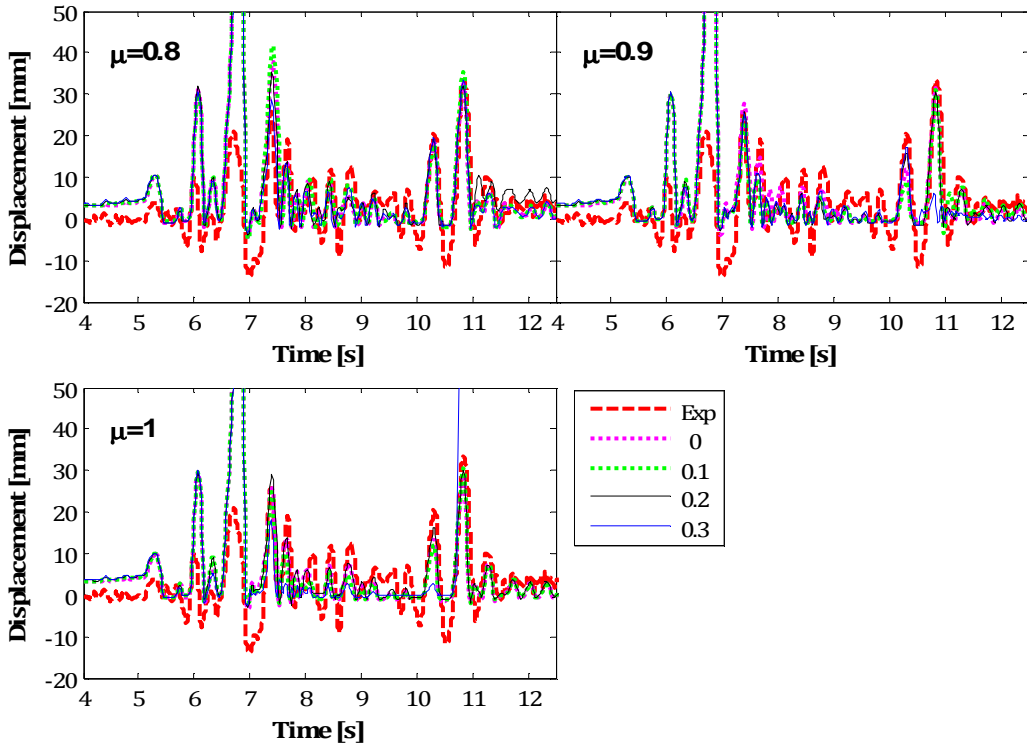
C.3.2. Simplified Model M1

C.3.3. Simplified model M2

The responses are quasi-coincident within the range of the restitution coefficients analysed.